DERIVING ATMOSPHERIC DENSITY ESTIMATES USING SATELLITE PRECISION ORBIT EPHEMERIDES

BY

Andrew Timothy Hiatt

Submitted to the graduate degree program in Aerospace Engineering and the Graduate Faculty of the University of Kansas in partial fulfillment of the requirements for the degree of Master's of Science.

Chairperson: Dr. Craig McLaughlin

Committee members

Dr. Ray Taghavi

Dr. Shahriar Keshmiri

Date defended:

The Thesis Committee for Andrew Timothy Hiatt certifies that this is the approved Version of the following thesis:

DERIVING ATMOSPHERIC DENSITY ESTIMATES USING SATELLITE PRECISION ORBIT EPHEMERIDES

Committee:

Chairperson: Dr. Craig McLaughlin

Dr. Ray Taghavi

Dr. Shahriar Keshmiri

Date approved:

ABSTRACT

The atmospheric models in use today are incapable of properly modeling all of the density variations in the Earth's upper atmosphere. This research utilized precision orbit ephemerides (POE) in an orbit determination process to generate improved atmospheric density estimates. Based on their correlation to the accelerometer density, the resulting POE density estimates were demonstrated to be an improvement over existing atmospheric models regardless of solar and geomagnetic activity levels. Also, the POE density estimates were somewhat better in terms of their correlation with the accelerometer density than the improved density estimates obtained by the High Accuracy Satellite Drag Model (HASDM). The results showed that the POE density estimates were obtained with the desired accuracy for a ±10% variation in the nominal ballistic coefficient used to initialize the orbit determination process. Also, the length of the fit span showed little influence on the accuracy of the POE density estimates. Overlap regions of POE density estimates demonstrated a method of determining the consistency of the solutions. Finally, Gravity Recovery and Climate Experiment (GRACE) POE density estimates showed consistent results with the Challenging Mini-Satellite Payload (CHAMP) POE density estimates.

Modeling the atmospheric density has always been and continues to be one of the greatest uncertainties related to the dynamics of satellites in low Earth orbit. The unmodeled density variations directly influence a satellite's motion thereby causing difficulty in determining the satellite's orbit resulting in possibly large errors in orbit prediction. Many factors influence the variations observed in the Earth's atmospheric density with many of the processes responsible for these variations not modeled at all or not modeled completely. The Earth's atmospheric density is affected to the greatest extent by direct heating from the Sun

and through the influence of geomagnetic storms. Deficiencies in existing atmospheric models require corrections be made to improve satellite orbit determination and prediction.

This research used precision orbit ephemerides in an orbit determination process to generate density corrections to existing atmospheric models, including Jacchia 1971, Jacchia-Roberts, CIRA-1972, MSISE-1990, and NRLMSISE-2000. This work examined dates consisting of days from every year ranging from 2001 to 2007 covering the complete range of solar and geomagnetic activity. The density and ballistic coefficient correlated half-lives were considered and are a user controlled parameter in the orbit determination process affecting the way the unmodeled or inaccurately modeled drag forces influence a satellite's motion. The values primarily used in this work for both the density and ballistic coefficient correlated half-lives were 1.8, 18, and 180 minutes. The POE density estimates were evaluated by examining the position and velocity consistency test graphs, residuals, and most importantly the cross correlation coefficients from comparison with accelerometer density.

The POE density estimates were demonstrated to have significant improvements over existing atmospheric models. Also, the POE density estimates were found to have comparable and often superior results compared with the HASDM density. For the overall summary, the best choice was the CIRA-1972 baseline model with a density and ballistic coefficient correlated half-life of 18 and 1.8 minutes, respectively. The best choice refers to the baseline atmospheric model and half-life combination used to obtain the POE density estimate having the best correlation with the accelerometer density.

During periods of low solar activity, the best choice was the CIRA-1972 baseline model with a density and ballistic coefficient correlated half-life of 180 and 18 minutes, respectively. When considering days with moderate solar activity, using a density correlated half-life of 180 minutes and a ballistic coefficient correlated half-life of 1.8 minutes for the

Jacchia 1971 baseline model was the best combination or choice. During periods of elevated and high solar activity, the best combination was the CIRA-1972 baseline atmospheric model with a density and ballistic coefficient correlated half-life of 18 and 1.8 minutes, respectively. When considering times of quiet geomagnetic activity, the best choice was the Jacchia 1971 baseline model with a density and ballistic coefficient correlated half-life of 1.8 and 18 minutes, respectively. During times of moderate and active geomagnetic activity, the CIRA-1972 baseline atmospheric model with a density correlated half-life of 18 minutes and a ballistic coefficient correlated half-life of 1.8 minutes was the best combination. The conclusions found for the overall and binned results did not hold true for every solution. However, using CIRA-1972 as the baseline atmospheric model with a density and ballistic coefficient correlated half-life of 18 and 1.8 minutes, respectively, is the recommended combination for generating the most accurate POE density estimates.

Variations of ±10% in the nominal ballistic coefficient used to initialize the orbit determination process provided sufficiently accurate POE density estimates as compared with the accelerometer density. The extent of this sensitivity remains unclear and requires additional study. The dependence of the POE density estimate on the solution fit span length was shown to be very low. Six hour fit span lengths considered to be the worst case scenario were shown to provide good agreement with the accelerometer density and POE density estimates with longer fit span lengths. Also, regions of overlap between successive solutions demonstrated good agreement between the individual POE density estimates indicating consistent solutions were obtained from the orbit determination process. The GRACE-A POE density estimates demonstrated consistent results compared with the CHAMP POE density estimates. Additional research is required that utilizes GRACE-A POE data to generate POE density estimates to confirm the CHAMP POE density estimate results.

ACKNOWLEDGEMENTS

I would like to take this opportunity to express my appreciation to Dr. McLaughlin who provided a great opportunity to learn and gain experience with this research. His patience, insight, and guidance throughout this process have been invaluable. I would also like to thank Dr. Taghavi and Dr. Keshmiri for their willingness to serve on my thesis committee. Their comments and input regarding this work are very much appreciated.

This research was made possible by a grant provided by the National Science Foundation awarded to Dr. McLaughlin. Also, I would like to thank Travis Lechtenberg who developed the Orbit Determination Tool Kit (ODTK) script used to generate much of the data. David Vallado also provided a script that was necessary for orbit data conversion. Jim Wright, Jim Woodburn, John Seago, and Jens Ramrath provided valuable information regarding this research and the operation of ODTK. Chris Sabol, Matt Wilkins, and Paul Cefola have also provided helpful discussions related to this work. Sean Bruinsma of the Centre National d'Études Spatiales (CNES) supplied all of the accelerometer density data and Bruce Bowman of the U.S. Space Command provided all of the High Accuracy Satellite Drag Model (HASDM) density data used in this work.

Most importantly I am so grateful that God loves me unconditionally and has always provided for me and seen me through every situation, including this process. Words can not express how thankful I am for the life I have in Jesus Christ. Also, I am so blessed to have a mother and father who have always encouraged me, a constantly supportive sister and brother-in-law, and a wonderful niece and nephew. Finally, I am so appreciative of my amazing wife whose love, compassion, understanding, and support has been such a blessing and encouragement to me.

TABLE OF CONTENTS

NOMENCLATURE

Symbol	Definition	Units
$\vec{a}_{drag}$	acceleration vector due to atmospheric drag	m/s^2
a_p	geomagnetic 3-hourly planetary equivalent amplitude index	gamma, Telsa, or kg s m^{-1}
A	satellite cross-sectional area	m^2
A_p	geomagnetic daily planetary amplitude index	gamma, Telsa, or kg s m^{-1}
$\Delta B/B$	estimated ballistic coefficient correction	~
BC	ballistic coefficient	m^2/kg
c_D	satellite drag coefficient	~
d	cross correlation delay	
$F_{10.7}$	daily solar radio flux measured at 10.7 cm wavelength	SFU
$\overline{F}_{10.7}$	$F_{10.7}$ running 81-day centered smoothed data set	SFU
$\overline{F}_S$	Jacchia-Bowman 2008 new solar index	SFU
g_o	gravitational acceleration	m/s^2
Δh	altitude change	m
i	cross correlation series index	
j	user defined Gauss-Markov correlated half-life time series index	
k	Gauss-Markov sequence index	
K_p	geomagnetic planetary index	~
$M_{10.7}$	solar proxy for far ultra-violet radiation	SFU

$\bar{M}_{10.7}$	$M_{10.7}$ running 81-day centered smoothed data set	SFU
m	satellite mass	kg
mx	mean of series x	
my	mean of series y	
M	mean molecular mass	amu
N	number of elements	
Δp	atmospheric pressure change	N/m^2
p_o	absolute pressure	N/m^2
$\hat{P}$	filter covariance matrix	
$\tilde{P}$	smoother covariance matrix	
$\bar{P}$	differenced covariance matrix	
r	cross correlation coefficient	
$\vec{r}$	satellite position vector	m
R	universal gas constant	$J\ K^{-1}\ mol^{-1}$
$\vec{R}$	McReynold's consistency test ratio	
$S_{10.7}$	solar extreme ultra-violet radiation at 26-34 nm wavelength	SFU
$\bar{S}_{10.7}$	$S_{10.7}$ running 81-day centered smoothed data set	SFU
t	time	S
T	temperature	K
v_{rel}	satellite velocity magnitude relative to Earth's atmosphere	m/s
$\vec{v}_{rel}$	satellite velocity vector relative to Earth's atmosphere	m/s

$w(t)$	Gaussian white random variable	
x	x component of satellite position vector	m
x	Gauss-Markov process dynamic scalar random variable	
x	cross correlation series	
ΔX	state error	
$\Delta\hat{X}$	optimal state error estimate	
$\boldsymbol{X}$	satellite state vector	
$\overline{X}$	difference state vector	
$\vec{X}_{filter}$	filter state estimate	
$\vec{X}_{smoother}$	smoother state estimate	
Δy	measurement residual	
y	y component of satellite position vector	m
y	cross correlation series	
Y_{10}	mixed solar index	SFU
z	z component of satellite position vector	m

Greek Letters	Definition	Units
α	Gauss-Markov process variable	
$\Delta\rho/\rho$	estimated atmospheric density correction	~
ρ	atmospheric density	kg/m^3
$\bar{\sigma}$	denominator for McReynold's consistency test ratio	
σ_w^2	variance of Gaussian white random variable	
τ	user defined correlated half-life	
ω_{Earth}	Earth's angular velocity magnitude	rad/s
$\vec{\omega}_{Earth}$	Earth's angular velocity vector	rad/s
Φ	transition function	

Abbreviations	Definition
CHAMP	Challenging Minisatellite Payload
CIRA	COSPAR International Reference Atmosphere
COSPAR	Committee on Space Research
CNES	Centre National d'Études Spatiales
DCA	Dynamic Calibration of the Atmosphere
DORIS	Doppler Orbitography by Radiopositioning Integrated on Satellite
DRAO	Dominion Radio Astrophysical Observatory

Dst	Disturbance Storm Time index
DTM	Drag Temperature Model
ESA	European Space Agency
EUV	Extreme Ultra-Violet
FUV	Far Ultra-Violet
GEOSAT	Geodetic Satellite
GFO	GEOSAT Follow-On
GOES	Geostationary Operational Environmental Satellites
GPS	Global Positioning System
GRACE	Gravity Recovery And Climate Experiment
GSFC	Goddard Space Flight Center
HASDM	High Accuracy Satellite Drag Model
ICESat	Ice, Cloud, and Land Elevation Satellite
MSISE	Mass Spectrometer Incoherent Scatter Extending from ground to space
MUV	Middle Ultra-Violet
NASA	National Aeronautics and Space Administration
NOAA	National Oceanic and Atmospheric Administration
NORAD	North American Aerospace Defense Command
NRLMSISE	Naval Research Laboratory Mass Spectrometer Incoherent Scatter Extending from ground to space
ODTK	Orbit Determination Tool Kit
POE	Precision Orbit Ephemerides

PSO	Precision Science Orbit
RSO	Rapid Science Orbit
SBUV	Solar Backscatter Ultraviolet
SEE	Solar Extreme ultraviolet Experiment
SEM	Solar Extreme-ultraviolet Monitor
SETA	Satellite Electrostatic Triaxial Accelerometer
SFU	Solar Flux Units
SLR	Satellite Laser Ranging
SOHO	Solar and Heliospheric Observatory
SOLSTICE	Solar/Stellar Irradiance Comparison Experiment
SORCE	Solar Radiation and Climate Experiment
STAR	Spatial Triaxial Accelerometer for Research
TAD	Traveling Atmospheric Disturbance
TIMED	Thermosphere Ionosphere Mesosphere Energetics and Dynamics
TLE	Two Line Element
UARS	Upper Atmosphere Research Satellite
XRS	X-Ray Spectrometer

LIST OF FIGURES

LIST OF TABLES

1 INTRODUCTION

1.1 Objective

The goal of this research is to show the potential for utilizing precision orbit data from a satellite in order to generate corrections to a given density model thus yielding a more accurate density necessary for enhanced atmospheric drag calculations, improved orbit determination and prediction, and an increased understanding and measurement of the density and its variations in the thermosphere and exosphere. Emphasis in this research is placed on atmospheric density variations occurring with shorter time scales than those of empirical models typically used for calculations of atmospheric drag.

1.2 Motivation

The extreme upper atmosphere including the thermosphere and exosphere is more variable than predicted by current density models. The variations not modeled in atmospheric density have a significant effect on the ability to determine a satellite's orbit resulting in potentially large errors in orbit predictions.

Atmospheric density modeling is one of the greatest uncertainties in the dynamics of satellites in low Earth orbit. Accurate density calculations are required to generate meaningful estimates of the atmospheric drag perturbing satellite motion. The effects of atmospheric drag increase with lower satellite mass, higher effective area, and lower altitude orbits.

The Earth's atmospheric density including any variations is influenced by many factors with the largest influence being the Sun. The Sun affects atmospheric density primarily by direct heating through extreme ultra-violet (EUV) radiation and the release of charged particles into the upper atmosphere, which interact with the Earth's magnetic field.

The data for the Earth's magnetic field and solar flux used in current density models are measured and reported as either averaged daily or three hour values and daily, global values, respectively. These time scales are too large when improvements in orbit determination and prediction are desired in time scales smaller than those available in the magnetic field and solar flux data.

Therefore, current density models require corrections in order to achieve more accurate orbit determination and prediction as well as a better understanding and measurement of the thermospheric and exospheric densities and density variations. These corrections will be estimated using precision orbit determination to examine the behavior of the total density through varying the density and ballistic coefficient correlated half-lives for multiple density models. The resulting estimated density data will be compared with density data obtained from the Spatial Triaxial Accelerometer for Research (STAR) on board the Challenging Minisatellite Payload (CHAMP) satellite as derived by Sean Bruinsma at the Centre National d'Études Spatiales (CNES). Estimated atmospheric density for the dual satellite Gravity Recovery and Climate Experiment (GRACE) project will also be compared with GRACE accelerometer derived density data. Select CHAMP and GRACE POE density estimates will be compared with density data from the High Accuracy Satellite Drag Model (HASDM) as obtained by Bruce Bowman of the U.S. Air Force Space Command. A large selection of time periods encompassing all levels of solar and geomagnetic activity will be examined because of the varying effects observed in the atmospheric density.

The improved density estimates can be directly applied to drag equations resulting in an improved drag force representation. Determining drag forces on a spacecraft is directly related to the accuracy of the density estimate. Therefore, the better the estimate of atmospheric density, the better the drag calculation will be. Because drag forces are a major

part of the perturbing forces on low Earth orbiting satellites, orbit determination and prediction will also benefit from increased accuracy density estimates. If the drag force is represented more accurately, then the orbit determination and prediction process will be capable of generating solutions of increased accuracy. This has direct applicability to determining a satellite's lifetime, time of reentry, and the ability to predict with higher confidence the satellite's future state. Also, improved density estimates facilitate a way of better understanding how the space environment and weather influence the atmospheric density. The full impact of the Sun on the density variations observed in the thermosphere and exosphere is not fully understood so a better measurement of the density and its variations allow for further study of the interaction between the Sun and the Earth's atmosphere.

1.3 Satellite Drag

The information contained in this section is summarized from Reference 1. The two main sources of satellite perturbations in low-Earth orbit are accelerations due to an oblate or nonspherical Earth and atmospheric drag. In particular, the drag effects for a satellite are the largest perturbing factor during the final orbits. Minor effects for low-Earth orbit satellites include solar radiation pressure and third body effects. For satellites in higher orbits, the solar radiation pressure and third body effects take dominance over perturbations caused by atmospheric drag and effects caused by the Earth's oblateness. Atmospheric drag can be used for desired applications such as aerobraking and satellite tethers. However, most satellites experience drag as an unwanted perturbation. Because of the great importance atmospheric drag has on low-Earth orbiting satellites, a large amount of research has been directed toward understanding the upper atmosphere and creating the most accurate atmospheric models possible. These models must possess sufficiently accurate estimates of atmospheric density

while modeling the effects of drag on a satellite's orbit. As mentioned previously, the Sun's interaction with the Earth's atmosphere and magnetic field is the greatest influence on drag variations and uncertainty. There are three main categories for studying drag as described in Reference 1. They are determining the orbit of satellites influenced by drag, estimating the lifetime of a satellite, and determining the upper atmosphere's physical properties.

A satellite's motion is slowed by the presence of atmospheric particles thereby inducing drag. Calculating the density of the atmospheric particles is a complicated task. On orbit determination of the density is difficult and the atmospheric models that currently exist are incomplete. Neither approach is capable of exactly calculating the atmospheric density. Satellite drag is a nonconservative force or perturbation because the satellite's total energy changes. The total energy changes because of energy losses due to momentum transfers from collisions with atmospheric particles. Atmospheric drag lowers the semimajor axis and eccentricity of a satellite's orbit while periodic effects are observed in the other orbital elements [Ref. 1]. Also, there are some coupling effects with the aspherical potential associated with drag [Ref. 1].

Vallado [Ref. 1] states that a complete model of the atmospheric perturbations must include knowledge of molecular chemistry, thermodynamics, aerodynamics, hypersonics, meteorology, electromagnetics, planetary sciences, and orbital mechanics. Studying astrodynamics in the atmosphere is extremely complex and difficult. Therefore, any study of satellite drag calls for an accurate determination and understanding of the atmospheric properties. A very useful way to examine drag is to consider a satellite's acceleration induced by the drag forces experienced. The following equation describes the relationship between acceleration caused by drag and atmospheric density.

$$\vec{a}_{drag} = -\frac{1}{2}\frac{c_D A}{m}\rho v_{rel}^2 \frac{\vec{v}_{rel}}{\left|\vec{v}_{rel}\right|} \tag{1.1}$$

The coefficient of drag, c_D, is a dimensionless quantity describing the level of influence drag forces have on a satellite. The higher the number the more susceptible a satellite is to the effects of drag. The coefficient of drag is typically approximated for satellites because its dependence on satellite configuration and atmospheric composition makes precise determination difficult. Satellite drag coefficients for satellites in the upper atmosphere are usually approximated to no more than three significant figures as 2.2 for a flat plate model and ~2.0 to 2.1 for a spherical model [Ref. 1]. Because satellite drag coefficients are typically approximated due to the complexity associated with calculating an actual value, this remains an area of satellite dynamics where more research is needed.

The atmospheric density, ρ, is the density of the atmospheric particles at the satellite's position. Density is often the most difficult parameter to calculate. The cross-sectional area, A, is the area normal to the satellite's velocity vector. The cross-sectional area is another parameter that is difficult to calculate because the attitude of the satellite often changes continually. Therefore, an accurate determination of the cross-sectional area necessitates the attitude data for a given satellite or an attitude determination process. The satellite's mass, m, may or may not stay constant so the mass must be carefully considered. The relative velocity vector, $\vec{v}_{rel}$, is the velocity relative to the Earth's atmosphere and can be represented as follows assuming the atmosphere rotates with the Earth.

$$\vec{v}_{rel} = \frac{d\vec{r}}{dt} - \vec{\omega}_{Earth} \times \vec{r} = \left[\frac{dx}{dt} + \omega_{Earth} y \quad \frac{dy}{dt} - \omega_{Earth} x \quad \frac{dz}{dt}\right]^T \tag{1.2}$$

The rotating atmosphere has a velocity profile due to the Earth's rotation causing the atmosphere closest to the surface to rotate the fastest and a decreasing speed as a function of altitude. However, the atmosphere possesses a mean motion with the winds superimposed on this mean motion. Nonspherical satellites experience aerodynamic lift and side forces that must be carefully considered. The observed drag forces always act in the opposite direction of the velocity vector.

Another important satellite parameter present in the equation describing the satellite's acceleration due to drag is the ballistic coefficient, *BC*. The ballistic coefficient is another way to describe the satellite's susceptibility to the effects of drag. However, the ballistic coefficient can be defined in many different ways so knowing which definition is in use becomes extremely important. The ballistic coefficient is typically defined as follows.

$$\text{Usual Definition: } BC = \frac{m}{c_D A} \tag{1.3}$$

However, this work uses the inverse of this relationship, which is stated below, to be consistent with the nominal ballistic coefficients supplied by Bruce Bowman and Orbit Determination Tool Kit (ODTK) software used in this research. The ballistic coefficient values obtained from Bruce Bowman are defined and briefly discussed in a subsequent section.

$$\text{Definition Used in this Work: } BC = \frac{c_D A}{m} \tag{1.4}$$

With the definition being used in this work, a lower value for the ballistic coefficient means that drag will have a lesser influence on a satellite compared with a higher value.

As mentioned previously, an accurate determination and understanding of the atmospheric properties is essential to accurately calculating drag. Therefore, determining atmospheric density accurately is particularly important for use in calculating drag. The

upper atmospheric density changes because of the complex interactions between three basic parameters. They are the nature of the molecular structure in the atmosphere, the incident solar flux, and the geomagnetic or auroral interactions [Ref. 1]. Solar flux and geomagnetic interactions are discussed in greater detail in subsequent sections. Generally speaking, these parameters influence the atmospheric density by increasing the number of particle collisions, especially at higher altitudes.

The pressure and density of the atmosphere are primarily determined by the gravitational attraction of the atmospheric constituents [Ref. 1]. Static and time-varying atmospheric models rely on two hydrostatic relationships that model atmospheric effects [Ref. 1]. The first is the ideal gas law as given below.

$$\rho = \frac{p_o M}{g_o R T} \tag{1.5}$$

The relationship displays the interconnection of the absolute pressure, p_o, the mean molecular mass of the atmospheric constituents, M, the gravitational acceleration, g_o, the universal gas constant, R, and the absolute temperature, T, in Kelvin. Atmospheric temperature is a parameter to consider carefully, because as the Earth rotates, the atmosphere is exposed to the Sun's heating, which greatly influences the density. The Sun's heating of the atmosphere is the main contributing factor causing difficulty in determining an accurate model for the atmospheric density. Therefore, the connection between temperature and density is of great importance.

The second relationship is the hydrostatic equation relating a specific change in pressure to the atmospheric density and gravitational acceleration for a given change in altitude [Ref. 1]. The hydrostatic equation is defined as follows.

$$\Delta p = -\rho g \Delta h \tag{1.6}$$

These equations are crucial for the understanding and determination of drag. The Earth's atmosphere is very complex and constantly changing making modeling of the atmosphere difficult. A more in depth discussion of the Earth's atmosphere and the time-varying effects and parameters are given in subsequent sections. Atmospheric models are defined as being either static or time-varying. Static models are the easiest to use but are the least accurate because of the assumption that none of the atmospheric parameters change. Time-varying models are the most difficult and require the most resources but are the most accurate. These considerations directly influence the determination of satellite drag, because as the accuracy increases for the estimates of the atmospheric parameters, the better the drag estimation will be.

1.4 Neutral Atmosphere

Information regarding the neutral atmosphere, the time-varying effects on the thermospheric and exospheric density, basic variations in density, drivers of density variations, and the space environment can be found in References 1-5. The summary in this subsection is derived from these references, especially Reference 3.

1.4.1 Neutral Atmosphere Structure

The Earth's atmosphere is typically divided into five layers classified according to their temperature profiles. The boundary between each layer is often times not well defined and varies over tens of kilometers. The lowest layer ranging from 0-12 km is the troposphere and demonstrates decreasing temperature with increasing altitude. The stratosphere ranges from 12-50 km and is characterized by increasing temperature with increasing altitude, which is due to the absorption of ultraviolet radiation by ozone. The stratosphere also contains nearly isothermal regions at higher altitudes. The mesosphere is the next layer ranging from

50-85 km and also shows decreasing temperature with increasing altitude. At the boundary of each of these layers is a transition region of nearly constant temperature and are defined as the tropopause, stratopause, and mesopause. None of these three layers directly apply to the problem of orbit determination, but the coupling of the lower and upper atmosphere is of great interest because disturbances in the lower atmosphere may propagate upwards through the mesosphere and into the upper atmosphere.

The final two layers of the Earth's atmosphere are the thermosphere and exosphere, which are of interest for orbit determination. The thermosphere ranges from 85-600 km and is characterized by increasing temperature with increasing altitude. The thermosphere may sometimes be described as encompassing all altitudes above 85 km. The increase in temperature in the thermosphere is primarily due to the absorption of ultraviolet radiation by the ambient constituents. The exosphere is the outer most layer of the atmosphere extending above 600 km where temperature is nearly constant with altitude. The density of particles in the exosphere is so low and collisions between them so infrequent that the particles essentially possess ballistic trajectories influenced primarily by the Earth's gravitational field. Therefore, the exosphere can no longer be regarded as a fluid but must be approached as a collection of individual particles. However, the exosphere may be approximated as a fluid provided that a large number of particles do not reach escape velocity.

The chemical composition of the atmosphere changes as a function of altitude because gravitational effects tend to keep the heavier molecules closest to the Earth's surface while chemical reactions and ultraviolet radiation at higher altitudes tend to break molecular bonds. Nitrogen (N_2) is the dominant molecule up to altitudes of approximately 175 km. Between 175 and 650 km, atomic oxygen is the predominate species. Helium becomes the

most prevalent at altitudes ranging 650-2500 km. Atomic hydrogen is the most abundant at altitudes greater than 2500 km.

1.4.2 Variations Affecting Static Atmospheric Models

While static atmospheric models are the easiest to use, latitudinal and longitudinal variations affect these models. Latitudinal variations can be easily visualized by considering a satellite in a circular, inclined orbit. These variations occur when a satellite passes over the Earth's equatorial bulge effectually changing the altitude and therefore the atmospheric density. Accordingly, this change in density alters the drag at practically every point in the orbit [Ref. 1].

Longitudinal variations are primarily considered for time-varying models, especially for diurnal or daily effects, but they also have the potential to impact static models. The Earth possesses many terrain features such as mountain ranges and large oceans. The differences in the wind, density, and temperature between these two distinct terrains will be significant for constant latitude but different longitude [Ref. 1]. Therefore, determining a completely symmetric atmosphere capable of fitting all the varying features of the Earth becomes quite difficult if not impossible.

1.4.3 Time-Varying Effects on the Thermospheric and Exospheric Density

The Earth's atmospheric density, including any variations, is influenced by many factors with the largest influence being the Sun. The Sun affects atmospheric density by direct heating primarily through EUV radiation. The Sun also heats the atmosphere by releasing charged particles into the upper atmosphere, which interact with the Earth's magnetic field. In addition to the variations affecting static atmospheric models as discussed

previously, the time-varying effects on the thermospheric and exospheric density include the following for real-world effects.

- Solar rotation
- Solar cycle
- Cyclical variations
- Semi-annual and seasonal variations
- Diurnal variations
- Rotating atmosphere
- Magnetic storms and substorms
- Gravity waves
- Winds
- Tides
- Long-term climate change
- Irregular short-periodic variations

A better understanding of the variations in neutral density caused by these time-varying effects will hopefully be achieved through this research.

Solar Rotation. The Sun rotates on its axis about once every 27 days. The implication of this rotation is that any active regions on the Sun will return in approximately 27 days. Such a pattern is readily observable in the measurements of $F_{10.7}$, which is explained in subsequent sections. However, predicting this pattern proves to be extremely difficult given that the active regions will change over the course of the rotation.

Solar Cycle. Because the Sun's magnetic field reverses approximately every 11 years, a full cycle takes 22 years to return to the original state. During a period of approximately 11 years, sunspots and solar flux go through a period of minimum to maximum and back to minimum activity levels. Around periods of solar maximum, the upper atmosphere becomes orders of magnitude denser and more variable making predictions more difficult.

Cyclic Variations. The Sun has an additional 11-year cycle lagging a few years behind the sunspot cycle. The magnitude of this cycle's maximum varies between the cycles. The minimum of the cycle is less than halfway between the maxima due to the recovery time from a maximum being between six and seven years. While the exact cause is unknown, this cyclic variation is likely related to the sunspot cycle.

Semi-Annual and Seasonal Variations. The varying distance of the Earth to the Sun and the Sun's declination throughout the year introduce variations lasting about six months.

Diurnal Variations. Daily variations occur in the atmospheric density due to the rotation of the Earth and direct heating of the Sun resulting in a density maximum or bulge. This density bulge lags the general direction of the Sun and is centered on the meridians with a local time of 2-2:30 p.m. The bulge centers on the equator at the equinoxes and occurs at higher latitudes according to Sun's varying declination. Due to the diurnal variations, the atmospheric density is a function of latitude, local time, and time of year. The daily atmospheric density minimum occurs at about 0400 local time each day.

Rotating Atmosphere. The atmosphere rotates with the Earth to a certain extent with the velocity typically being larger closer to the surface because of increased friction. This atmospheric rotation produces time-varying effects in the density.

Magnetic Storms and Substorms. Fluctuations in the Earth's magnetic field will introduce slight variations in the atmospheric density during quiet or normal periods of geomagnetic activity. However, these density variations will become substantially larger during active geomagnetic periods. Magnetic storms are caused by variations in the solar wind and typically follow solar flares or coronal mass ejections. Substorms are large, transient changes in the magnetosphere that deposit large amounts of energy into the atmosphere at high latitudes and are usually visible as auroral activity. When geomagnetic activity is high, a density bulge will form at each pole and propagate to lower latitudes and toward the opposite pole.

Gravity Waves. Gravity waves are a mechanism by which a fluid displacement, whether vertical or horizontal, is forced by gravity to return to an equilibrium position. For instance, when a rock is dropped into a lake, waves or ripples emanate outwards from the source of the disturbance. When the water is above the equilibrium point, gravity will pull the water back toward the original undisturbed level. The water will undershoot the equilibrium position and be forced upwards again resulting in an oscillatory behavior. Ultimately, these ripples are dampened as they move farther away causing the displacement to approach the equilibrium position.

For gravity waves in the atmosphere affecting orbiting satellites, a disturbance in the lower atmosphere causes a vertical displacement that will attempt to return to an equilibrium

position because of gravitational influences. The displaced air mass will undershoot the equilibrium point and rebound upwards and overshoot the original undisturbed level. These vertical atmospheric displacements generate vertical waves that propagate upwards into the upper atmosphere.

These gravity waves transfer energy from the lower atmosphere to the upper atmosphere and primarily affect the mesosphere and lower thermosphere. The gravity waves grow in magnitude as the density decreases as they propagate upwards into the upper atmosphere. At altitudes of 75 km or potentially higher, the waves are dissipated by viscous damping and are a source of heat as they break in the upper atmosphere.

Winds. Intensity and direction of the winds in the upper atmosphere are difficult to predict and can be influenced by geomagnetic storms and substorms. However, these winds still have an impact on the orbit of satellites and some general observations can be made. Around the equinoxes the winds generally flow eastward in the evening and westward in the morning. During the day the winds flow from the equator to the poles and in reverse at night. A wind component from the summer to the winter hemisphere is added to the above effects for periods around the solstices. Additionally, as these winds flow, they create temperature variations therefore resulting in variations in density.

Tides. Ocean and atmospheric tides result in very small variations in the atmospheric density. The diurnal tidal component driven by solar heating is the dominant tidal component in the thermosphere. The velocity can reach up to 200 m/s with a day time velocity of about 40 m/s and a night time velocity of approximately 120 m/s. The interaction with the ionosphere creates the observed differences between the day and night velocities

Long-Term Climate Change. Recent satellite orbital data suggests a long-term secular decrease in the total mass density and temperature in the thermosphere [Ref. 6]. Such a predicted effect on global change is caused by an increase in carbon dioxide in the troposphere. Such findings demonstrate the applicability of orbit determination to examining long-term climate change.

Irregular Short-Periodic Variations. Random solar flares, variations in hydrogen currents in the atmosphere, and other small effects are often associated with transient geomagnetic disturbances. Their influence on atmospheric density and density variations is small.

1.5 Atmospheric Density Models

An introduction to the most commonly used atmospheric models in orbit determination can be found in Ref. 1. The summary in this subsection is derived from this reference. A vast number of density models have been developed since the 1960s using two main approaches. The first approach produces a physical model from the combination of conservation laws and atmospheric constituent models. The second provides a density model from simplified physical concepts based on in-situ measurements and satellite tracking data. Choosing the appropriate density model is not a trivial task and no model is best for all applications. Modeling the various physical processes in the atmosphere is a difficult undertaking resulting in errors in the model.

Time-varying models, such as the Jacchia 1971 atmosphere, provide the best accuracy and are the most complete, but require accurate data and large computational resources. In contrast, the exponential model requires far less resources but the results may

be too inaccurate for the needs of a given application. Selection of the appropriate model is often based on trade-offs between performance and speed.

The atmospheric models used in this research include Jacchia 1971 [Ref. 7], Jacchia-Roberts [Ref. 8], Committee on Space Research (COSPAR) International Reference Atmosphere (CIRA-1972) [Ref. 9], Mass Spectrometer Incoherent Scatter (MSISE-1990) [Ref. 10], and Naval Research Laboratory Mass Spectrometer Incoherent Scatter (NRLMSISE-2000) [Ref. 11]. The "E" in the MSISE 1990 and NRLMSISE 2000 atmospheric models indicates that the model extends from the ground to space.

1.5.1 Jacchia 1971 Atmospheric Model

The Jacchia 1971 atmospheric model was reformulated from the Jacchia 1970 model using newer and often times more complete data. The Jacchia 1971 model is defined empirically and utilizes exospheric temperature and altitude ranging from 110-2000 km to represent atmospheric density. The upper atmosphere is divided into two separate regions of 90-125 km and above 125 km. The distinction is made by Jacchia's assumption of a fixed-boundary atmospheric condition at 90 km, that mixing dominates between the altitude of 90 and 100 km, and diffusive equilibrium above 100 km. These assumptions led to diffusion differential equations containing a low-altitude temperature profile between 100 km and 125 km and a high-altitude temperature profile above 125 km. These differential equations were solved by numerical integration over various constant exospheric temperature values. The model also uses an 81-day average of solar parameters intended to average out any differences introduced by the 27-day solar rotation cycle.

1.5.2 Jacchia-Roberts Atmospheric Model

The Jacchia-Roberts atmospheric model is based on the Jacchia 1970 model. The Jacchia-Roberts model analytically determines exospheric temperature as a function of position, time, and solar and geomagnetic activity. The corresponding atmospheric density is obtained using the computed temperature with empirically determined temperature profiles or the diffusion equation. In 1971, Charles Roberts realized that determining tabulated atmospheric density and numerically integrating partial derivatives for drag required a large amount of computational resources. The Jacchia 1970 model was analytically evaluated using partial fractions to integrate values between the altitudes of 90 and 125 km. An asymptotic function was introduced for altitudes above 125 km, which is different than the function used to obtain an integrable form in the Jacchia 1970 model. The Jacchia-Roberts model deviates very little from the Jacchia values and the Roberts corrections can be used with Jacchia's later models. Oza and Friertag [Ref. 12] suggest that the Jacchia-Roberts model responds well to variations in geomagnetic activity.

1.5.3 CIRA 1972 Atmospheric Model

The Committee on Space Research (COSPAR) of the International Council of Scientific Unions in 1965 began to periodically adopt atmospheric models. CIRA 1972 is the Jacchia 1971 atmospheric model adopted by COSPAR including mean values from 25-500 km altitude. The CIRA models are semi-theoretical techniques possessing some free variables with the data primarily coming from satellite drag measurements and ground-based measurements.

1.5.4 MSISE 1990 and NRLMSISE 2000 Atmospheric Models

This family of models incorporates mass spectrometer data from satellites and incoherent radar scatter data from the ground to develop an atmospheric model. They also are derived from the Drag Temperature Model (DTM) based on air-glow temperatures. DTM uses spherical harmonics to incorporate satellite drag data from two complete solar cycles and a large amount of observational data based on a model of global exospheric temperature. The MSISE family of models has proven to be quite accurate and applicable to some difficult problems. The MSISE models are able to successfully model the atmosphere for a satellite that is traveling very quickly at perigee and therefore crossing several bands of the atmosphere in a single integration step. The newest release, NRLMSISE 2000, is very popular and widely used for a variety of applications. Complete source code for the 1986, 1990, and 2000 models is readily available. Comparison of the MSISE family of models with the Jacchia models shows that a slightly slower speed for the MSISE models.

1.5.5 Jacchia-Bowman Atmospheric Models

The Jacchia-Bowman family of atmospheric models is based on Jacchia's diffusion equations and is intended to reduce the density model errors by incorporating new solar proxies and indices, an improved semiannual density variation function, and a geomagnetic index algorithm [Ref. 13]. These atmospheric models utilize a combination of on orbit satellite and ground based measurements of solar activity to calculate exospheric temperatures. The solar flux data is also used in an improved semiannual density variation function that provides better estimates of the major semiannual density changes associated with changing long-term EUV heating of the atmosphere. The geomagnetic activity data collected are used to calculate the exospheric temperature and the subsequent thermospheric

density distribution during a geomagnetic storm. Jacchia-Bowman 2008 is the most recent atmospheric model in the Jacchia-Bowman family and builds upon previous work done for the Jacchia-Bowman 2006 model.

The Jacchia-Bowman 2008 model uses four solar indices to account for the solar activity responsible for the observed atmospheric density variations. The first solar index is the solar flux as observed for 10.7 cm length radio waves, $F_{10.7}$, which is discussed in greater detail in a subsequent section. This data is also reported as a running 81-day centered smoothed set of $F_{10.7}$ values represented by $\overline{F}_{10.7}$. This solar index is widely used in many atmospheric models as a proxy to the flux of EUV radiation that provides direct heating of the upper atmosphere. EUV radiation is not directly measurable on the ground due to the absorption of such radiation by the atmosphere whereas the atmosphere is transparent to $F_{10.7}$ permitting ground-based measurements to be made as a substitute. However, $F_{10.7}$ does not fully account for all of the energy delivered into the upper atmosphere so additional parameters are required for a more complete model.

In December 1995, the NASA/ESA Solar and Heliospheric Observatory (SOHO) satellite was launched equipped with the Solar Extreme-ultraviolet Monitor (SEM) capable of measuring 26-34 nm solar EUV radiation. The data produced by this satellite is extremely valuable because a portion of EUV spectrum responsible for direct heating of the upper atmosphere can now be measured directly. This solar activity is represented by the solar index, S_{10} or $S_{10.7}$. This data is also reported as a running 81-day centered smoothed set of $S_{10.7}$ values represented by $\overline{S}_{10.7}$. Even with this additional information and direct measurement of a key solar index, more solar activity data is necessary to obtain a more complete atmospheric model.

Far Ultra-Violet (FUV) radiation also contributes to the observed thermospheric density variations making knowledge of FUV solar flux of great importance for modeling density. As is the case with EUV radiation, FUV radiation is absorbed by the upper atmosphere and is represented in the Jacchia-Bowman 2008 model by a solar proxy, M_{10} or $M_{10.7}$. This data is also reported as a running 81-day centered smoothed set of $M_{10.7}$ values represented by $\bar{M}_{10.7}$. The National Oceanic and Atmospheric Administration has a series of operational satellites carrying the Solar Backscatter Ultraviolet (SBUV) spectrometer capable of measuring solar Middle Ultra-Violet (MUV) radiation near 280 nm. This directly measured solar index is used as the proxy for the FUV solar flux in the atmospheric model.

The last solar index utilized by the Jacchia-Bowman 2008 atmospheric model accounts for X-rays in the 0.1-0.8 nm range and hydrogen (H) Lyman-α wavelength at 121 nm. The GOES X-Ray Spectrometer (XRS) instrument observes the X-rays. The UARS and SORCE NASA satellites equipped with the SOLSTICE instrument and the SEE instrument on the NASA TIMED satellite have observed the Lyman-α emissions. X-rays and Lyman-α solar emissions are competing drivers of the mesosphere and lower thermosphere. The X-rays provide a large amount of energy primarily to the mesosphere and lower thermosphere during periods of high solar activity. The Lyman-α emissions also influence the same region of the atmosphere as X-rays but are most dominant during moderate and low periods of solar activity. Because of the competing influence of these two solar emissions, a mixed solar index, Y_{10}, was created. Y_{10} is weighted such that it represents mostly X-rays during solar maximum and predominately Lyman-α emissions during periods of moderate and low solar activity levels. The weighting function is the normalized, running 81-day centered smoothed set of $\bar{F}_{10.7}$ values.

Use of $\overline{F}_{10.7}$ data often will not fully represent the heating experienced in the thermosphere particularly during periods of solar minima. However, this data does better represent the changes in the Sun's 11-year cycle compared with the other indices used in the Jacchia-Bowman models. Therefore, these models utilize $\overline{F}_{10.7}$ data augmented with $\overline{S}_{10.7}$ data during periods of solar minima to create a new solar index $\overline{F}_S$. This new solar index is used in conjunction with all the previously mentioned solar indices to generate an equation for the best nighttime minimum exospheric temperature, which is in turn used to calculate atmospheric density. The Jacchia-Bowman models use the difference between the daily and 81-day centered values for each solar index as input variables into the exospheric temperature equation. The Jacchia-Bowman 2008 atmospheric model introduced the Y_{10} solar index not present in the Jacchia-Bowman 2006 model. Therefore, the exospheric temperature equation is different between these two models with the results showing differences as a consequence of this alteration.

The semiannual density variation has been observed for many decades and has been historically difficult to accurately model. The Jacchia-Bowman family of models attempts to provide better estimates of this variation by including a more complete consideration of the upper atmospheric heating by incorporating new solar indices. As previously discussed, the inclusion of these new solar indices are meant to account for a more complete range of the solar spectrum responsible for heating of the upper atmosphere and the resulting density variations. The Jacchia-Bowman models use a previously determined semiannual density variation function that describes the atmospheric density as a function of the average density as a function of time and a relationship between the amplitude and the height. The process of obtaining the semiannual density variation function used in the models entails utilization of

the solar indices previously described and an analysis of the density observed for several satellites over a range of years.

Geomagnetic storm modeling in the Jacchia-Bowman models uses a Disturbance Storm Time (Dst) index primarily indicating the strength of the ring current in the magnetosphere during geomagnetic storms. The index is compiled from hourly measurements of the magnetic field taken at four points lying on the Earth's equator. The Jacchia-Bowman models contain an algorithm that integrates a differential equation for the exospheric temperature based on the storm's development as observed in the Dst index. The algorithm also attempts to eliminate large erroneous density increases during periods where the three-hourly geomagnetic planetary amplitude, which is discussed in greater detail in a subsequent section, is high but no magnetic storm exists as defined by the Dst index. These periods where no storms exists, as defined by the algorithm, use Jacchia's 1970 exospheric temperature equation and are set to a constant value when the three-hourly geomagnetic planetary amplitude exceeds a predetermined threshold.

1.5.6 Solar and Geomagnetic Indices

A discussion of some of the difficulties connected with the temporal resolution of various proxies utilized by the empirical density models is given in Ref. 5. An overview of the research addressing the inaccuracies in modeling satellite drag is available in Ref. 14.

The majority of effects on the Earth's atmosphere are caused by the Sun's output or overall activity. The Sun's variable output can have drastically different effects on a satellite's orbit depending on whether the current period is one of solar minima or maxima. When the Sun is at its minimum output, only slight differences may be observed in most satellites' orbits because of the less than normal amount of incoming radiation. However,

during periods of solar maxima, the relatively large amounts of incoming radiation may produce perturbations in a satellite's orbit that are large and unpredictable.

Atmospheric density is most influenced by EUV radiation absorbed by the upper atmosphere. Due to the atmosphere blocking EUV radiation from reaching the ground, measuring the amount of EUV radiation at the Earth's surface is impossible. While a few satellites currently exist that directly measure EUV flux, there are few atmospheric models, such as Jacchia-Bowman, specifically designed to use such measurements. However, scientists have determined that EUV and 10.7 cm wavelength solar radiation come from the same layers of the Sun's chromosphere and corona. Fortunately, the Earth's atmosphere allows the 10.7 cm wavelength radiation to pass through to the ground so that the relative strength of EUV radiation can be inferred. The observed solar flux measured at the 10.7 cm wavelength is used as a proxy for EUV in most atmospheric models. These 10.7 cm length radio waves, $F_{10.7}$, have been regularly measured since about 1940 and are measured in Solar Flux Units (SFU) with the following relationship.

$$1 \text{ SFU} = 1\text{x}10^{-22} \frac{watt}{m^2/Hz}$$

A typical range of values for $F_{10.7}$ is less than 70 to more than 300. The National Oceanic and Atmospheric Administration (NOAA) at the National Geophysical Data Center in Boulder, Colorado distributes the most commonly accepted daily measurement values of $F_{10.7}$ [Ref. 15]. From 1947 until 1991 these measurements were made at 1700 UT at the Algonquin Radio Observatory in Ottawa, Ontario, Canada. From 1991 to the present, the Dominion Radio Astrophysical Observatory (DRAO) in Penticton, British Columbia, Canada now takes these measurements at 2000 UT.

The daily solar flux values are reported as daily observed (at the true distance between the Sun and the Earth), daily adjusted (to a distance of 1.0 AU), and as 81-day averaged values (either centered or trailing about the date of interest). Because the $F_{10.7}$ data are daily values, discontinuities exist in the orbit determination process where the values change from one day to the next. Additionally, an orbit determination process that relies on daily solar flux values may suffer from poor temporal resolution because of the changes that can occur so quickly in the Sun's output.

The atmospheric density can also be greatly influenced by the level of geomagnetic activity. As the charged particles emitted by the Sun interact with the Earth's magnetic field and ultimately with the upper atmosphere, ionization occurs resulting in geomagnetic heating of the upper atmosphere. This heating directly affects the density and accompanying drag forces and so must be measured. In fact, satellites at altitudes ranging from 300-1000 km experience noticeable impacts of drag caused by magnetic disturbances. The geomagnetic planetary index, K_p, is a commonly used quasi-logarithmic, worldwide average of the geomagnetic activity that takes place below the auroral zones. K_p is quasi-logarithmic because the values range from low activity ($K_p = 0.0$) to extreme geomagnetic activity ($K_p = 9.0$) with intermediate values given to the nearest third of an integer. The average K_p is found from twelve stations that record values of K_p every three hours corrected for latitude.

Because some atmospheric models, such as the Jacchia-Roberts model, use geomagnetic activity as an input, the geomagnetic planetary amplitude, a_p, is utilized as a linear equivalent of the K_p index and is intended to minimize differences seen at 50 degrees latitude. An alternate name for a_p is the 3-hourly index due to eight values of a_p averaged to form a daily planetary amplitude, A_p. The values for A_p range from 0-400 with a value

greater than 100 being rare and values of 11-20 being average. The unit for the daily planetary amplitude is in gamma units shown below.

$$\text{one gamma} = 10^{-9}\ \text{Tesla} = 10^{-9}\ \text{kg} \cdot \text{s}/\text{m}$$

The planetary geomagnetic indices (K_p and a_p) are measured by observatories in United Kingdom, Canada, United States, New Zealand, Australia, Sweden, and Denmark all lying between 48 degrees north and 63 degrees south latitude. The compilation of these indices is most commonly obtained from the Institut für Geophysik at Göttingen University, Germany [Ref. 1]. The National Oceanic and Atmospheric Administration (NOAA) at the National Geophysical Data Center in Boulder, Colorado makes these daily measurement values of K_p and a_p available [Ref. 16].

Trends in the daily planetary amplitude follow the 11-year sunspot cycle with large values consistently occurring as the sunspot activity enters a declining phase in each $F_{10.7}$ 11-year cycle. Also, there is a secondary semi-annual cycle of the solar wind's position to the Earth's magnetosphere that is variable and difficult to predict. Variations in the daily planetary amplitude are attributed to solar flares, coronal holes, disappearing solar filaments, and the solar-wind environment around the Earth. Additionally, because the shape of the atmosphere is influenced by intense geomagnetic activity in the auroral zones, the atmospheric density becomes a function of latitude.

As mentioned with the solar flux, a deficiency arises when using any of the geomagnetic indices in an orbit determination process because of the fact that the indices are either averaged three-hourly values or are averaged daily values. Any orbit determination process that utilizes these indices will demonstrate effects of the discontinuities present in the data and may have poor temporal resolution [Refs. 5 and 17].

1.6 Previous Research on Atmospheric Density Model Corrections

Two primary categories of research exist to address the problems of modeling atmospheric density for satellite drag. The first category is dynamic calibration of the atmosphere (DCA) and the second is using accelerometers onboard satellites to measure non-conservative accelerations, which includes drag.

1.6.1 Dynamic Calibration of the Atmosphere

Dynamic calibration of the atmosphere is not an atmospheric model but a technique available for improving or correcting current atmospheric models and the corresponding atmospheric density. This approach provides basic scientific information concerning observed density variations with their associated statistics [Ref. 1]. The initial work was conducted in the 1980's and has continued to be a vibrant area of research with applicability to current operational orbit determination [Ref. 1]. The general idea behind dynamic calibration of the atmosphere is to generate corrections to the atmospheric density obtained from an existing atmospheric model.

Measurement data such as observations and two-line element sets are used in an orbit estimation process to generate orbital elements and satellite drag data as one part of a solution for applied problems. Simultaneous to the creation of the orbital elements and drag data, the DCA approach will accumulate data in order to construct a model for the atmospheric variations including an estimate of the true ballistic factors [Ref. 1]. The atmospheric variation model is used to calculate a summary of the density that is included as the second part of a solution for applied problems.

Dynamic calibration of the atmosphere requires a set of calibration satellites to create the density corrections. These corrections are often reported every three hours but recent

DCA approaches generate only a single daily density correction. These corrections require a "true" ballistic coefficient as an input to an existing atmospheric density model, typically Jacchia 1971, Jacchia-Roberts, or one of the MSISE models. The "true" ballistic coefficient input into a DCA approach is the basis for changing the atmospheric densities from an existing model.

Dynamic calibration of the atmosphere utilizes the observed motions of a large number of satellites in order to estimate large-scale density corrections to a given atmospheric density model. Examples of the DCA approach of making large-scale corrections to existing atmospheric density models can be found in References 18-26. In particular, Bowman and Storz [Ref. 18] used the observed motions of 75-80 calibration satellites to compute density variations in the upper atmosphere. The calibration satellites covered a wide range of orbit inclinations and perigee heights extending from 200 to 800 km. This allowed a set of global density correction parameters to be made to an existing atmospheric model every three hours as specified by the HASDM program. These density correction parameters were then predicted forward in time three days by a time series filter as a function of the predicted $F_{10.7}$ solar flux and a_p geomagnetic indices. The resulting estimated and predicted density fields are utilized to provide differential corrections for all of the drag influenced orbits contained within the North American Aerospace Defense Command (NORAD) catalog, which the authors state as over 6,000. Finally, the predicted orbits for all satellites were projected forward in time for three days. Improvement was achieved for the epoch accuracy, ballistic coefficient consistency, and predicted satellite positions [Ref. 18]. Ultimately, the HASDM program provided a significant reduction of atmospheric density model errors, compared with existing atmospheric models, for low-perigee satellites with an altitude less than 600 km [Ref. 18].

Reference 19 describes a method developed for calculating daily density values based on satellite drag as observed by radar and visual observations. A standard 6-element state vector and ballistic coefficient value are obtained from a differential orbit correction program that utilizes the modified Jacchia 1970 atmospheric model developed for use in the HASDM program. The differential orbit correction program applies the modified Jacchia 1970 model and the fitted ballistic coefficient in a special perturbations orbit integration technique to compute energy dissipation rates over the period of observations, which ranges from three to eight days. The process outlined in Reference 19 calculates temperature and density from daily energy dissipation rates using a "true" ballistic coefficient and additional related parameters provided by the HASDM model. Validation of the daily temperature values for satellites in 2001 were conducted by comparison with results from the HASDM dynamic calibration of the atmosphere program. Historical daily density values calculated for over 25 satellites spanning the previous 30 years was used to validate the daily density values obtained from the differential orbit correction program. Geographical regions of overlapping perigee location data were compared against the resulting density values to determine their accuracy.

Reference 20 looked at characterizing the semiannual thermospheric density variation in the Earth's upper atmosphere for a wide range of heights. Historical radar observations for 13 satellites with special perturbations were examined within this range of heights. A differential orbit correction program fit these observations resulting in a 6-element state vector and a ballistic coefficient value. The process, validation techniques, and error results are similar to those in Reference 19. The differential orbit correction program was capable of observing the semiannual variation and successfully characterizing the variations according to height and solar maximum and minimum.

Two Line Element (TLE) data sets have been used to generate corrections to an atmospheric model such as the Russian GOST atmospheric model [Ref. 21]. The daily density corrections are created with a bias term and a term linear with altitude. The corrections consider the observed solar flux and geomagnetic data as inputs and the TLE data sets for a large number of drag perturbed space objects. All of the objects chosen for use in this process described in Reference 21 have a perigee height less than 600 km and their element sets are regularly updated in the U.S. Space Catalog. The process generates density corrections from ballistic coefficient factors determined along with an element set. The process aims to increase the accuracy of orbit determination and prediction of low-Earth orbiting satellites, to estimate errors in the upper atmospheric density models and provide improvement to those models, and to contribute to the analysis of the physical processes that occur in the upper atmosphere.

Reference 22 also outlines an approach for using TLE data sets to provide density corrections, which are expressed as a linear function of altitude, to a given atmospheric density model. A large number of satellites are routinely observed and cataloged a few times a day. These drag perturbed space objects provide drag data that can provide information useful for creating density corrections with limited additional costs. This particular approach emphasizes and demonstrates monitoring the density variations for drag perturbed satellites in near-real time. Any improvements with this approach would be enhanced if real observations were used compared with the use of TLE data sets.

Atmospheric density corrections can also be used to improve predictions of reentry time for a satellite as described in Reference 23. TLE data sets are used in conjunction with solar flux and geomagnetic index data. This reference relies on a large number of observations from a large number of space objects to create atmospheric density corrections

to the NRLMSISE-2000 model resulting in improved density estimates along with ballistic coefficient estimates. The study considers both spherical and arbitrarily shaped objects to observe the associated impact of shape on reentry time predictions. Reentry prediction times are improved for both classes of objects but the improvement for nonspherical objects is not as good due to their ballistic coefficient varying with time [Ref. 23].

Reference 24 recognizes the need for improvements in the dynamic calibration of the atmosphere technique. In a typical DCA approach, global optimal correction coefficients are generated that are directly related to the basis function chosen. This reference describes successive refinements to density corrections where a series of vanishing coefficients is introduced into the procedure for determining atmospheric density model corrections. The successive refinements use the previous set of corrections as the basis for starting the next refinement. This approach ultimately attempts to greatly reduce solution error, particularly errors observed in the residuals.

Reference 25 provides a comparison of the results obtained from using dynamic calibration of the atmosphere corrections for the NRLMSISE-2000 with the well established Russian DCA density correction method during two four year periods with relative differences in solar and geomagnetic activity levels. A large number of satellites are again used in this study. This reference also attempts to observe, as a function of the number and kind of space objects used, the global density correction coefficients associated with a DCA approach. The study verifies the usefulness of a DCA approach while acknowledging the need for additional investigation.

Reference 26 discusses the complexity associated with applying DCA corrections to an existing atmospheric model such as NRLMSISE-2000. The ultimate goal of the work in this reference is to provide atmospheric corrections for increased accuracy in orbit prediction

and determination. Increased accuracy can be achieved when using the DCA corrections but the accuracy depends on agreement between the way the corrections were produced and the way they are applied. Specific information is required when using the density corrections including the time system used, input and output test cases, input parameters used, and any subroutines or model parameters utilized to generate the corrections. The atmospheric model used to generate the atmospheric density corrections must be the exact same as the model used for estimating density for a particular application. Significant variations can be observed in the orbit determination process, including estimated density and prediction, if any of the information concerning how the density corrections were generated is missing.

Dynamic calibration of the atmosphere provides a significant improvement to existing atmospheric density models but with several disadvantages. First, a DCA approach is designed to run internal to a particular orbit determination scheme with the resulting atmospheric density corrections only applying to a specific time period. Therefore, those using a different orbit determination scheme must rely on that particular system for updates to atmospheric density corrections as well as requiring a complete archive of density corrections for a given problem. The second limitation of DCA approaches is the limited spatial and temporal resolution of the atmospheric density corrections. The corrections allow the baseline density model to characterize atmospheric density variations in terms of several hours to days but not in shorter time scales. A temporal limitation is introduced by the use of a daily solar flux and averaged 3-hour geomagnetic indices as input values into a DCA scheme so as to address solar and geomagnetic activity. The use of this input data does not permit the baseline atmospheric density model to properly represent variations that occur within the averaging interval of these indices. Further difficulty arises in DCA approaches because of the predominate use of two-line element sets of a large number of low Earth orbit

objects as observational inputs for a given DCA approach. Reliance on two-line elements results in reduced accuracy density corrections with restricted temporal resolution. References 18-20 describe an approach that utilizes radar observations of low Earth orbit objects, but the accuracy of radar observations is still less than those obtained by precision orbit ephemerides (POE) or satellite laser ranging (SLR). In addition, the radar observation data are not readily accessible.

Current research being conducted using dynamic calibration of the atmosphere includes applying a DCA approach to GEODYN, which is the NASA GSFC Precision Orbit Determination and Geodetic Parameter Estimation Program [Ref. 27]. The density corrections are applied to the NRLMSISE-2000 atmospheric model with the intent of improving the orbit precision of the GEOSAT Follow-On (GFO). The results obtained from this process were compared with the MSIS-86 atmospheric model over a range of solar and geomagnetic activity levels. This particular paper examined altitudes up to 600 km and will eventually extend up to GFO's orbit at 800 km. The results showed little difference with the MSIS-86 results for all levels of solar and geomagnetic activity. However, once the density corrections are extended up to 800 km, significant improvement in the results should be realized [Ref. 27].

Current research also includes using TLE data to calibrate thermospheric density models [Ref. 28]. TLE data can be converted to satellite drag data that is in turn used to generate a daily adjustment to the density model calibration parameters. The calibration parameters are applied to an existing atmospheric model with the ultimate goal of improving its accuracy. The reference describes two different calibration schemes. The first involves height-dependent scale factors and the second incorporates corrections to the CIRA-1972 atmospheric model temperatures and therefore the density. The reference demonstrates

varying improvement using this approach based on the number of daily parameters used to calibrate the thermospheric model.

1.6.2 Accelerometers

The second category of research for improving atmospheric density knowledge is using accelerometers onboard satellites to measure non-conservative accelerations, which can be utilized to estimate density. The accelerometer data allows the separation of gravitational forces from non-conservative forces including Earth radiation pressure, solar radiation pressure, and drag. Use of accurate radiation pressure models permits the drag acceleration and resulting estimated density to be accurately calculated with precise temporal resolution. The accelerometer data are extremely precise but only available for a few satellites. This represents an extreme opposite in terms of accuracy and data availability compared with the use of two-line element sets. The availability of accelerometer measurements is currently limited to the CHAMP and GRACE satellites. Other satellites with accelerometers have flown in the past. Reference 29 is an example of where the accelerometer data from the Satellite Electrostatic Triaxial Accelerometer (SETA) experiment flown at an altitude of about 200 km was used to examine thermospheric density and confirmed that energy from magnetic storms deposited at high latitudes created a "density bulge" that propagated toward the equator and then toward the opposite poles.

Some of the early results for estimating density using CHAMP accelerometer data are published in References 30 and 31 with additional atmospheric density values derived using CHAMP accelerometer data found in References 32-34. Reference 30 demonstrates that the accelerometer onboard CHAMP is capable of measuring thermospheric density variations caused by substantial events such as large solar mass eruptions that intersect with the Earth. Accelerometer data can be used in place of nonconservative force models in

precise orbit determination processes. However, while the accelerometer measurements are more precise than the nonconservative force model estimates, the calibration parameters are of great importance in the accuracy and subsequent use of accelerometer data. The reference recommends an external check, such as SLR data, to determine if the expected orbit improvements from using accelerometer data really exist.

The total atmospheric density retrieved from the accelerometer proves to be more accurate than those obtained from an atmospheric model provided accurate force models are used for the radiation forces [Ref. 31]. Also, the reference indicates that the accuracy of the accelerometer derived densities depends primarily on the performance and calibration of the instrument and the magnitude of the unmodeled winds. A potential for a systematic bias exists for accelerometer derived densities because of uncertainties in the drag coefficient model. However, the accuracy attainable from accelerometer data is very promising and only looks to improve as accelerometers become more sensitive.

Reference 32 describes the density retrieval system for the accelerometer onboard CHAMP. The CHAMP satellite possesses good geographical and altitude coverage over a long range of time, originally set for five years but having surpassed that lifetime by almost four years at the current time. The accelerometer measurements must be corrected for maneuvers, specific events, and instrumental bias. Determining the accuracy of the total density observed by satellite requires a model for the aerodynamic coefficient and uncertainties of the estimated accelerometer calibration parameters of the aerodynamic coefficient and geomagnetic activity. This reference examines the high precision achieved by the data and the shortcomings of the aerodynamic coefficient model.

The operational requirements and attainable accuracy of the accelerometer onboard the CHAMP satellite are given in Reference 33. In addition to the accelerometer, CHAMP is

equipped with GPS and SLR tracking systems allowing accurate orbit positions to be calculated. This reference details the comparison made between the accelerometer data and several atmospheric models in terms of the estimated density. Also, the results were obtained for periods of high solar activity so certain effects, such as seasonal effects, were most likely not estimated correctly. Information regarding CHAMP, including the accelerometer and the spacecraft as a whole, and the mission profile are discussed in this resource. The bias and scale factors, various modeling approaches, variations in the numerous aspects of the atmospheric model, and density retrieval methods are also given significant consideration.

Reference 34 provides additional information concerning atmospheric density obtained from the STAR accelerometer onboard CHAMP. As with Reference 33, modeling of the atmosphere, the various force models, and the density retrieval system is discussed in this reference. The GPS receiver onboard CHAMP allows the satellite to be tracked continuously permitting the accelerometer bias and scale factors, including their time variations, to be calibrated. Because the density is derived assuming negligible upper atmospheric winds, the accuracy of the accelerometer measurements is a function of the latitude and geomagnetic activity and therefore large wind amplitudes. This reference focuses on time periods surrounding three geomagnetic storms that occurred in 2002 where the derived densities are compared with semi-empirical thermospheric density models. The resulting comparison demonstrates some of the deficiencies associated with the atmospheric models. Additional consideration is given to the variations in density influenced by seasonal, latitude, local time, and solar activity effects. The opportunity of using the accelerometers onboard the twin GRACE satellites is also mentioned.

CHAMP accelerometer data has also been used to examine polar region density structures [Ref. 35]. The accelerometer derived densities showed significant density

structures in the thermosphere at high latitudes particularly around the magnetic cusp region. Energetic particles from the Sun trapped in the Earth's magnetic field collide in the cusp region with the Earth's upper atmosphere. These density structures are observed in a limited fashion by existing atmospheric models but not to the extent or altitude as observed by the accelerometer. Such an occurrence demonstrates the superiority of accelerometers over current atmospheric models in detecting rapid changes in the upper atmospheric density.

Several papers involving joint work between researchers at the University of Colorado and the Centre National d'Études Spatiales (CNES) utilized CHAMP and GRACE accelerometer data to examine density variations created during solar and geomagnetic events [Ref. 36-41]. The accelerometers are able to observe variations in the density that the atmospheric models are only able to broadly account for at best. The accelerometers are capable of resolving density bulges that exist at the polar cusp regions during periods of geomagnetic activity when large amounts of energy are deposited into the upper atmosphere. A resulting density wave can also propagate from high latitudes down toward the equatorial regions and progress toward the opposite pole. Because of the orbits of the CHAMP and GRACE satellites, these density waves can also be observed with greater accuracy compared with the atmospheric models. The measurements obtained from the accelerometers allow the width and speed of the density waves and the width of the density bulges to be determined. These references state that the accelerometers allow the density and winds in the thermosphere to be calculated with even greater accuracy than predicted by the existing atmospheric models.

A description of a technique to estimate atmospheric density from the GRACE accelerometer data can be obtained from Reference 42. An important problem in observing thermospheric density variations is accurately characterizing the solar and geomagnetic

variability, especially for short time scales. Use of accelerometer data for increasing the accuracy of the orbit predictions of a satellite has many requirements, which are described in this reference and listed as follows. First, the biases and scale factors for accelerometer axis must be calculated with the resulting data aligned with an inertial reference frame. Secondly, any anomalies such as thrusts present in the accelerometer data must be removed or filtered. Thirdly, any surface forces besides atmospheric drag forces must be accurately modeled so that they can be removed from the total nongravitational accelerations. Finally, the drag force model representing the upper atmosphere and the spacecraft surface must be sufficiently accurate to properly determine density.

There is ongoing research that utilizes the CHAMP accelerometer to measure the medium and large-scale density variations that occur in the thermosphere [Ref. 43]. The density variations observed by CHAMP appear to have a common high-latitude wave source. The density waves typically dissipate at mid-latitudes for most waves, especially for periods of low geomagnetic activity. However, density waves tend to propagate into the equatorial region during nighttime and during periods of increased geomagnetic activity and low levels of solar activity. Gravity waves propagating upwards from the lower atmosphere into the lower thermosphere might also be contributing to the density variations observed by CHAMP. CHAMP accelerometer measurements can also be used to characterize large-scale traveling atmospheric disturbances (TADs) [Ref. 44]. The width and wind speed of these observed TADs can be inferred from the accelerometer data. Also, the differences between day side and night side TADs can be determined and compared. The TADs do not appear to be correlated to the geomagnetic index except for the generation of the TAD. Reference 45 uses the STAR accelerometer onboard CHAMP to study the global distribution of the total mass changes associated with density variations at a height of about 400 km during

geomagnetic storms. The goal is to improve current thermospheric models to better predict storm-time mass density distribution. The empirical relation allows a correction to be calculated that can be added to the NRLMSISE-2000 model reference described in the paper resulting in a more accurate prediction of the thermospheric mass density distribution during geomagnetic storms. The CHAMP and GRACE satellites have contributed vast amounts of information regarding the upper atmosphere and are capable of adding even more. Unfortunately, these three satellites only provide limited spatial coverage at any given time and only at low altitudes.

1.6.3 Additional Approaches

Several papers have examined the use of GPS receiver or SLR observations for estimating non-conservative accelerations. One such approach is where a type of differential correction was examined by using two-line element sets in a traditional DCA scheme along with a small number of satellites with precision orbit data [Ref. 46]. Thermospheric density models contribute the majority of the error in orbit determination and prediction of satellites in low-Earth orbit. The error is associated with the way the models are formulated, especially the connection between density and the space weather affecting Earth. Calibrating the atmospheric model using correction parameters obtained from observations of satellite should allow for increased accuracy of the atmospheric density estimate. A density calibration uses TLE data for a large number of satellites to improve the accuracy of an existing atmospheric density model. These density calibrations can be further augmented by the addition of density data derived from accelerometer measurements or from precise satellite tracking. These additional parameters can be used for purposes of validation or for inputs into the calibration process. A calibrated model should have increased accuracy and enhanced spatial and temporal resolution.

Another approach described as GPS accelerometry utilizes GPS receiver data to estimate non-conservative forces as empirical accelerations [Refs. 47, 48, and 49]. Through this method the in-track and cross-track accelerations derived from the CHAMP accelerometer may be reasonably determined with a temporal resolution of 20 minutes or greater according to the authors of these references. GPS accelerometry requires accurate gravity models to function properly. Fortunately, with the recent launch of the GRACE satellites, such an enhanced gravity model exists. The largest remaining errors appear to originate with the GPS receiver carrier-phase noise and GPS ephemeris errors. This technique is most sensitive in the along-track direction of a satellite's orbit, which is where the majority of the non-conservative forces are experienced. The cross-track and radial directions are not nearly as sensitive and provide less information than the along-track direction. GPS accelerometry is able to determine longer wavelengths but has difficulty recovering high-frequency accelerations, which are caused by geomagnetic storms. The technique may not be as sensitive as accelerometers but the potential does seem to exist for its application to recent and upcoming missions as the number of satellites equipped with GPS receivers increases. GPS accelerometry utilizes precision orbit data to infer the accelerations experienced by a satellite due to drag. This acceleration can then be used to determine the atmospheric density. Therefore, GPS accelerometry is another way of using precision orbit data to estimate the atmospheric density.

Batch and Kalman filter estimation techniques have been utilized to investigate the reconstruction of empirical accelerations of the GRACE-B satellite [Ref. 50]. The extended Kalman filter/smoother is more efficient in terms of required computer memory and processing time. The batch least-squares method provides smoother trajectories and exhibits a more robust behavior, especially when dealing with gaps in the data. Both the batch and

Kalman techniques demonstrated similar overall variations in the empirical accelerations but with a sizeable scale difference between the acceleration magnitudes obtained from the two methods. Position accuracies of 4 to 7 cm have been achieved with this process and the resulting estimation of empirical accelerations included in the orbit determination scheme produced a highly accurate trajectory. These results hold true even during periods of high solar activity where the conditions in the upper atmosphere are quite dynamic.

Additional research being conducted includes using Doppler Orbitography and Radio positioning Integrated by Satellite (DORIS) and SLR data to observe the effects thermospheric density perturbations have on low-Earth orbiting satellites during periods of active geomagnetic activity [Ref. 51]. The satellites used in this study are at varying altitudes and so experience the effects of the density perturbations differently. In particular, determining how to get the best quality geodetic products during periods of active geomagnetic levels is of great interest. The authors of this reference demonstrated that results obtained from a precision orbit determination process were improved during active geomagnetic periods with the performance of the process very similar to those obtained for quieter periods. As expected, significant errors in the thermospheric models exist during these periods but the models can be improved through the use of a more sophisticated data processing regime. DORIS is another form of precision orbit data that can be used to estimate atmospheric density in an orbit determination process and increase the understanding of the thermospheric and exospheric density and density variations.

1.7 Current Research on Atmospheric Density Model Corrections

This research presents another step toward the goal of combining accurate data with good spatial coverage obtained from a large number of satellites. Many satellites currently possess Global Positioning System (GPS) receivers that when combined with an optimal orbit

determination process provide position accuracies of a few centimeters to within a few meters. This research estimates atmospheric density by using the precision orbit data of these satellites in an optimal orbit determination scheme. For this research CHAMP POEs during several periods with solar and geomagnetic activity of varying levels were used to estimate atmospheric density. Some of those results are displayed with particular attention given to the performance of the process as the perturbing effects increase. Use of POE data results in increased accuracy from a smaller number of satellites as compared with two-line element sets. When compared with accelerometer data, POE data provide a larger number of available satellites with reduced accuracy.

Some of the initial results and work relevant to the current research are presented in References 52-54. In particular, the consistency of the derived densities obtained from the CHAMP POEs was investigated by comparing the estimated densities obtained as density corrections to several models for the same time period and comparison of the estimated densities in orbit overlap solutions [Ref. 52]. The results of the two comparisons yielded consistencies of at worst about 10% of the estimated density. The POE derived atmospheric densities were compared to those derived from the accelerometer data resulting in a similar range for the errors [Ref. 53].

Reference 55 describes how precision orbit data from the CHAMP satellite was utilized as measurements in an optimal orbit determination process to generate density estimates during periods of increased solar activity. The density estimates are compared with CHAMP accelerometer derived density for determining the accuracy of the density estimates derived from precision orbit data. The reference studied multiple days and covered a wide range of solar and geomagnetic activity. The input parameters for an orbit determination scheme were systematically varied to study their effects on estimated density. The results

were correlated to the accelerometer derived densities for each solution and organized into solar and geomagnetic activity bins and in an overall summary. The cross correlation results provide a quantitative means by which to choose the best parameters for use in an optimal orbit determination scheme. The precision orbit derived densities show improved accuracy over the existing atmospheric models.

1.8 Gauss-Markov Process

Orbit determination problems often possess unmodeled or inaccurately modeled accelerations that act on a spacecraft. In order to resolve this difficulty, a first-order Gauss-Markov process is typically used as a dynamic model compensating for these misrepresented or missing accelerations. A Gauss-Markov process is one that satisfies the requirements for both the Gaussian and Markovian processes. A Gaussian process obeys a Gaussian probability density function and is defined by a series that is normally distributed. A Markov process displays the Markov property defined as having a future state that depends only on the current state and not a past state. In other words, "The Markov property means that the probability density function at t_n given its past history at t_{n-1},t_{n-2},… is equal to its probability density function at t_n given its value at t_{n-1} [Ref. 56]."

A Gauss-Markov process consists of a deterministic part and a random part. The deterministic part is estimated, along with any associated time constants, as part of the state vector and the random part contributes to the process noise covariance matrix. This research utilizes a Gauss-Markov model to account for unmodeled or inaccurately modeled drag forces in an optimal orbit determination scheme to generate a state vector containing an atmospheric density correction based on a given baseline atmospheric density model.

1.9 Estimating Density and Ballistic Coefficient Separately

When dealing with acceleration, density and ballistic coefficient are directly related to each other. Therefore, being able to separately and simultaneously estimate the density and ballistic coefficient in an orbit determination process becomes increasingly difficult if possible at all. However, a technique has been outlined suggesting the feasibility of simultaneously estimating both the density and ballistic coefficient in real-time [Refs. 57 and 58].

Historically, the ballistic coefficient estimate has absorbed any errors in the atmospheric density model and ballistic coefficient model and possibly geopotential errors. However, the current approach taken to simultaneously estimate the density and ballistic coefficient requires an exponential half-life for the ballistic coefficient errors to be significantly different than the exponential half-life for the atmospheric density errors. An exponential half-life in the Gauss-Markov model states how much of the previous state to consider for calculation in the current state. The user may specify a density and ballistic coefficient correlated half-life, which is the time necessary for the respective estimated correction to decay to half its original value without any measurements. These correlated half-lives are associated with the exponential half-lives. Exponential half-lives will be discussed in greater detail in a subsequent section. Even though the density and ballistic coefficient estimates are correlated, they have been shown to be observable and separable.

2 METHODOLOGY

The results obtained from this research were generated by processing the positions and velocities from the CHAMP and GRACE POE data as observations in an optimal orbit determination process in order to estimate density and ballistic coefficient. The atmospheric density was estimated for six distinct approaches including variation of the baseline density model, solution fit span length variation, examination of the solutions during periods of solution overlap, variation of the density and ballistic coefficient correlated half-lives, examination of the estimated density as a function of solar and geomagnetic activity levels, and the solution's sensitivity to the nominal ballistic coefficient used to initialize the orbit determination process.

2.1 Precision Orbit Ephemerides

The CHAMP POE data are available as either precision science orbits (PSO) or rapid science orbits (RSO). The GRACE POE data can be obtained only as RSOs. CHAMP and GRACE POE data may be downloaded from the website http://isdc.gfz-potsdam.de. Processing and accuracy of the RSOs are discussed in References 59-62. These papers also mention the PSOs, which were found as part of the gravity field solutions acquired from CHAMP data, but no publication concerning their accuracies is available. The published accuracy of the RSOs compared to SLR data is approximately 5-10 cm for the majority of the mission life with the exception of early in the mission when the accuracy was as poor as 25 cm. Published accuracies of the PSOs are not available, but their accuracies are assumed at least as accurate as the RSOs and are likely slightly better. PSO data is preferred and used when available, but no published PSOs are available after 2003.

2.2 Optimal Orbit Determination

Optimal orbit determination is used to estimate atmospheric density and ballistic coefficient in this work. Information regarding orbit determination as discussed in this section was obtained from Reference 56. Additional information regarding orbit determination can be found in References 1 and 63. Orbit determination refers to estimating the orbits of spacecraft, natural satellites, or any orbiting satellite relative to a central celestial body provided applicable measurements are available. Because orbiting spacecraft possess size, mass, and orbit characteristics that are significantly different from natural satellites, the nongravitational forces play a significant role in determining and predicting their orbits. Also, most spacecraft are in orbits relatively close to the Earth causing the gravitational forces to no longer act strictly as a central force [Ref. 56]. Accordingly, an accurate gravitational model is required for a good determination and prediction of a satellite's orbit.

The state of a dynamical system is defined as being the set of parameters necessary for prediction of the future motion of a system. Satellite orbit determination problems require the position and velocity vectors for a given epoch as the minimal set of parameters. Additional parameters, such as dynamic and measurement model parameters, can be included with the minimal set of parameters to increase the accuracy of the predictions.

A general orbit determination problem consists of a general state vector $\boldsymbol{X}(t)$ as a function of time, t. The state vector of the vehicle at any time can be determined provided that the initial state and the differential equations governing the vehicle's motion along a ballistic trajectory are known. These equations can be integrated to yield the desired state vector values for a specified time. Unfortunately, the initial state vector of a satellite is not known exactly and the mathematical models and physical constants of the forces used to define the differential equations of motion are only approximated. The consequence of these

errors is a deviation of the predicted motion from the true motion of the object. The deviation will increase over time as the orbit determination process progresses. However, using observations of the spacecraft's trajectory from tracking stations whose positions are accurately known will generate an estimate with increased accuracy by providing updates to the satellite's state vector. Even with the improved trajectory, the estimate will not be exact due to random and systematic errors. Typically, the observational data consists of observable quantities such as range, range rate, azimuth, elevation, and other parameters that are usually nonlinear functions of the state variables [Ref. 56].

Orbit determination can therefore be described as determining the best estimate of a spacecraft's state vector by using a process that typically includes starting with an unknown initial state, using incomplete or inaccurate mathematical force models, and employing observations that are subject to random and systematic errors [Ref. 56]. The question of what is meant by the "best" estimate is sometimes difficult to answer. One approach to defining what the best estimate is for a satellite's state vector is discussed in greater detail a little later in this section. Additional errors in any orbit determination process include errors in the computational procedure used in generating a solution and errors in the numerical integration procedure introduced by errors inherent in the dynamical model and errors attributed to computer truncation and roundoff. Because of these various sources of error, continually observing and estimating a satellite's state vector becomes important and must be done to keep the desired accuracy in the state estimate.

For this research, precise orbit ephemerides are used as measurements to determine the orbit of a satellite in low-Earth orbit. The position and velocity in these ephemerides provide accurate measurements as inputs for a sequential Kalman filter/smoother approach utilizing a Gauss-Markov process, which is discussed in a subsequent section. The observations are

used in each time step to update the state estimate providing increased accuracy as the process progresses forward in time.

As mentioned previously, defining what is meant by "best" when discussing a state estimate for a given satellite is difficult. The approach taken in this research to define a "best" state estimate is optimal orbit determination. Optimal is defined as the best, most desirable, or most satisfactory. However, a difficulty arises when defining exactly what optimal is given a specific situation. Many orbit determination methods exist with varying results. Therefore, there are many considerations to keep in mind when conducting orbit determination. Some methods are faster than others but with reduced accuracy. Selecting a sequential or batch method, knowing whether to minimize measurement residuals or orbit errors, and correctly modeling measurement residuals and orbit errors are important aspects of an orbit determination scheme. Additionally, while all orbit determination processes are nonlinear, multidimensional problems, the question exists whether to directly attempt a nonlinear, multidimensional solution or linearize the problem first. If a problem must be linearized prior to obtaining a solution, then another question arises in terms of which linearization method is best. Wright [Ref. 64] has developed a definition for optimal orbit determination that is not necessarily generally accepted nor has been proven to be true, but the author has used his definitions for a long period of time with overall satisfactory results. Any orbit determination method used to calculate the state estimate, including the orbit estimate, is optimal provided the following eight attributes are satisfied [Ref. 64].

1. "*Sequential processing is used to account for force modeling errors and measurement information in the time order in which they are realized.*

2. *The optimal state error estimate $\Delta\hat{X}$ is the expectation of the state error ΔX given the measurement residual Δy. That is: $\Delta\hat{X} = E\{\Delta X \mid \Delta y\}$. This is Sherman's Theorem.*
3. *Linearization of state estimate time transition and state to measurement representation is local in time, not global.*
4. *The state estimate structure is complete.*
5. *All state estimate models and state estimate error model approximations are derived from appropriate force modeling physics, and measurement sensor performance.*
6. *All measurement models and measurement error model approximations are derived from appropriate sensor hardware definition and associated physics, and measurement sensor performance.*
7. *Necessary conditions for real data:*
    - *Measurement residuals approximate Gaussian white noise.*
    - *McReynolds' filter-smoother consistency test is satisfied with probability 0.99.*
8. *Sufficient conditions for simulated data: The state estimate errors agree with the state estimate error covariance function.*

The first six requirements defined standards for optimal algorithm design, and the creation of a realistic state estimate error covariance function. The last two requirements enable validation: They define realizable test criteria for optimality. The last requirement implies the development and use of a physically realistic measurement simulator."

2.3 Gauss-Markov Process Half-Lives

Within the Orbit Determination Tool Kit (ODTK) software package there are two parameters called the density correlated half-life and the ballistic coefficient correlated half-life that can be adjusted by the user to affect the orbit determination process and in particular affect the estimated density and ballistic coefficient. These parameters are part of the force model and are directly applied to modeling the air drag on the spacecraft. The atmospheric density is denoted by ρ and the estimated correction to the atmospheric density generated in ODTK is denoted by $\Delta\rho/\rho$. The atmospheric density and estimated density correction are determined by the user defined baseline atmospheric model. Also, ODTK represents the ballistic coefficient as B and the estimated correction to the ballistic coefficient as $\Delta B/B$. The density correlated half-life is specified in units of time and represents the time necessary for the estimated correction to the atmospheric drag to decay to half its value in the absence of measurement data. The ballistic coefficient correlated half-life also has units of time and is the time required for the estimated correction to the ballistic coefficient to decay to half its value in the absence of measurement data. The density and ballistic coefficient correlated half-life values are represented by τ and are associated with the exponential half-life in the Gauss-Markov processes used by ODTK [Refs. 65 and 66]. The estimated density correction, $\Delta\rho/\rho$, and the ballistic coefficient correction, $\Delta B/B$, are assumed to behave as Gauss-Markov processes but this assumption has yet to be validated as true.

ODTK technical documents provide information regarding the use of the density and ballistic coefficient correlated half-lives [Refs. 65 and 66]. Let $x = x(t_k)$ denote a dynamic scalar random variable that satisfies the following scalar exponential Gauss-Markov sequence.

$$x(t_{k+1}) = \Phi(t_{k+1}, t_k)\, x(t_k) + \sqrt{1 - \Phi^2(t_{k+1}, t_k)}\, w(t_k),\ k \in \{0,1,2,...\} \tag{2.1}$$

The $w(t)$ variable is a Gaussian white random variable with zero mean and a constant variance, σ_w^2. Also, the initial values of the dynamic scalar random variable and the Gaussian white random variable are equal as shown in the first of the two following equations. The transition function, Φ, is defined in the second of the two following equations.

$$x(t_0) = w(t_0) \tag{2.2}$$

$$\Phi(t_{k+1}, t_k) = e^{\alpha |t_{k+1} - t_k|} \tag{2.3}$$

For the transition function, the constant in the exponential is defined as follows. This constant is where the user defined value of the density and ballistic coefficient correlated half-lives is used by the Gauss-Markov processes in ODTK. The value of τ is associated with the exponential half-life on the transition function.

$$\alpha = (\ln 0.5)/\tau \tag{2.4}$$

$$\tau = |t_{j+1} - t_j| \tag{2.5}$$

All information in this section comes from References 65 and 66.

2.4 Filter-Smoother Description

Precision orbit ephemerides were input as measurements into a sequential filter resulting in a state estimate containing multiple parameters. The state estimate includes six parameters for position and velocity components, one parameter for relative atmospheric density, one parameter for relative spacecraft ballistic coefficient, and additional parameters

associated with the process including station biases and other forces, measurements, and model parameters. The filter inputs and processes the measurements sequentially forward in time. The filter output consists of a complete state estimate and error covariance, which are used as the initial conditions for their forward propagation.

The smoother inputs and processes the stored filtered data sequentially backward in time. The smoother is initialized using the last filter state estimate, error covariance matrix, and associated epoch. As the smoother progresses backwards in time, the input into the smoother is defined by the stored filter output and the recursively created smoother output. The smoother does not reprocess the measurement data that was input into the filter. The state estimate generated by the smoother is superior to the state estimate created by the filter because the smoother takes into account all available data to improve the accuracy of the state estimate. All information in this section comes from References 17 and 65. Additional information regarding filters and smoothers, including extended Kalman filters and general orbit determination processes, can be found in References 1, 56, 63, 64, 66.

2.5 McReynolds' Filter-Smoother Consistency Test

A unitless ratio, $\vec{R}$, can be formed for each of the parameters in the state estimate and can be graphed as a function of time. The numerator is obtained by differencing the filter and smoother state estimates for a common time. The denominator, $\vec{\sigma}$, consists of the square roots of the main diagonal elements of a matrix formed by differencing the filter covariance matrix, $\hat{P}$, and the smoother covariance matrix, $\tilde{P}$. This difference covariance is defined as $\overline{P} = \hat{P} - \tilde{P}$. The denominator is composed of a root-variance or sigma on the numerator as derived from the state estimate error covariance function for the filter and smoother. A basic equation representing this ratio is given as follows.

$$\vec{R} = \frac{\vec{X}_{filter} - \vec{X}_{smoother}}{\vec{\sigma}} \tag{2.6}$$

The McReynolds' Filter-Smoother Consistency Test compares the unitless ratio to ±3. A successful test is defined for the situation where at least 99% of the ratios have values between -3 and +3 as given in the first of the following two equations. A failed test occurs when less than 99% of the ratios fall between -3 and +3 as stated in the second of the two following equations.

Initializing the sequential filter requires that the measurement data be processed across the filter initialization time interval. Because realistic covariance elements require filter initialization, the McReynolds' Filter-Smoother Consistency Test is ignored during initialization. All information in this section can be found in References 17 and 64-66.

2.6 Using Orbit Determination to Estimate Atmospheric Density

The estimated orbit is optimal in the least squares or minimum variance sense. The POE data are input as measurements into a sequential measurement processing and filtering scheme. This sequential filtering scheme estimates corrections to atmospheric density and ballistic coefficient, calculates residuals, conducts position and velocity consistency tests, generates an estimated state vector including position and velocity, and estimates other state parameters including those related to solar radiation pressure. A smoother is then applied to the filtered solution to account for all available solution data to increase the accuracy over the whole solution span. The filter and smoother combination estimates the time variable density and ballistic coefficient including realistic covariance matrices established by the physics associated with the problem. Earth gravity, solar radiation pressure, Earth infrared and albedo radiation pressure, luni-solar point masses, general relativity, and solid Earth and ocean tides are additional force models included in the optimal orbit determination process.

Techniques for estimating density available in the Orbit Determination Tool Kit (ODTK) software package are outlined in References 57-58. The technique developed by Wright [Ref. 57] permits the local atmospheric density to be estimated in real-time in conjunction with the orbit determination process. Wright's technique provides a significant improvement over the standard technique of estimating the ballistic coefficient (BC) or drag coefficient because BC estimates absorb the errors generated by the model for atmospheric density and BC. Additionally, BC estimates will often include geopotential model errors. Wright demonstrates the feasibility of simultaneously observing both the atmospheric density and ballistic coefficient in a filtering scheme [Ref. 58]. Wright also shows that the use of 3-hourly step functions of geomagnetic indices fails the McReynold's filter/smoother consistency tests [Ref. 17]. However, if a polynomial spline is used to fit the 3-hourly data then the McReynold's consistency tests are satisfied. These results illustrate the necessity of smooth data over shorter time scales than what is currently available. Tanygin and Wright present the polynomial spline fit technique for geomagnetic data utilized by Wright's atmospheric density estimation scheme [Ref. 17].

The estimated atmospheric density is obtained as a correction to an atmospheric model. The models currently available in ODTK are Jacchia 1971, Jacchia-Roberts, CIRA 1972, MSISE-1990, and NRLMSISE-2000. The Jacchia-Roberts and CIRA 1972 density models were derived from the Jacchia 1971 model so the results from these three models should be similar. Once a baseline atmospheric density model is selected, two different types of corrections are applied to the model as part of the optimal orbit determination process. The first is a baseline correction derived from historical $F_{10.7}$ and a_p measurements obtained over several solar cycles. The baseline density correction propagates from perigee height

through the use of an exponential Gauss-Markov sequence. A transformation exists such that the error in the atmospheric density at perigee is related to the current point in the orbit.

The second type of atmospheric density correction utilizes the observations and current conditions to yield a dynamic correction. The use of a sequential process allows a correction to be estimated at each time step in the filter as opposed to a single correction applied to the complete time span of data as for a batch least squares process. Exponentially correlated Gauss-Markov processes describing the modeling errors also exist for dynamic corrections as observed for the baseline corrections. The user of the optimal orbit determination process may specify the values of the density and ballistic coefficient exponential Gauss-Markov process half-lives, which determines the effect of past data on the individual density correction at each time step. While the ballistic coefficient is estimated as part of the filter/smoother process, the ballistic coefficient was initialized using yearly averages of 0.00444 m^2/kg for 2002-2003 and 0.00436 m^2/kg for 2004-2005 [Ref. 67].

The initial ballistic coefficient values for 2001 and 2006-2007 were estimated based on the 2002-2003 and 2004-2005 yearly averages and changes in satellite mass. Three maneuvers were made for CHAMP resulting in the orbit being raised and a change in satellite mass. The orbit raising maneuvers occurred on June 10-11, 2002, December 9-10, 2002, and March 27-28, 2006. Satellite mass data can be downloaded from the website http://isdc.gfz-potsdam.de. In order to estimate the ballistic coefficient yearly average values, the assumption was made that the ballistic coefficient changed primarily as a function of the satellite mass. Accordingly, the change in the yearly average ballistic coefficient from 2002-2003 to 2004-2005 was assumed to depend on the change in satellite mass associated with the December 2002 orbit maneuver. Using this information, the change in yearly average ballistic coefficient from 2002-2003 to 2001 was linearly interpolated using the satellite mass

change associated with the June 2002 orbit maneuver. A similar approach was taken to determine the change in ballistic coefficient from 2004-2005 to 2006-2007 utilizing the satellite mass change associated with the March 2006 orbit maneuver. Therefore, an initial ballistic coefficient yearly average value of 0.004501 m^2/kg was used for 2001. The 2006-2007 initial ballistic coefficient yearly average value was 0.004261 m^2/kg.

The atmospheric density was estimated for six distinct approaches. Those approaches are varying the baseline density model, varying solution fit span length, examining solutions during periods of solution overlap, varying the density and ballistic coefficient correlated half-lives, examining the estimated density as a function of solar and geomagnetic activity levels, and the solution's sensitivity to the nominal ballistic coefficient used to initialize the orbit determination process.

2.6.1 Varying Baseline Density Model

There are many atmospheric density models currently available. Only five of those models are used in ODTK. Yet an important consideration is what baseline atmospheric density model should be used to offer the best performance. The models available in ODTK were discussed in the previous chapter and all possess different characteristics. Determining which baseline density model works best for given situations becomes extremely important. Thus, special consideration is given to the baseline density model chosen and in fact is a constant thread throughout the entire research endeavor.

2.6.2 Varying Density and Ballistic Coefficient Correlated Half-Lives

Solutions for the dates shown in Table 1 were generated using all combinations of the ballistic coefficient and density Gauss-Markov process half-lives at order of magnitude increments of 1.8 min, 18 min, and 180 min for all available baseline density models in

ODTK. Additionally, some solutions were created using all combinations of density and ballistic coefficient correlated half-lives at order of magnitude increments of 1.8 min, 18 min, 180 min, 1,800, 18,000 min, and 180,000 min. The dates displayed in the following table consist of days from every year ranging from 2001 to 2007 sampling all twelve calendar months and all four seasons. The dates were distributed so that the various solar and geomagnetic bins were covered and sufficiently sampled. For the dates examined in this work, the orbit of CHAMP was near circular with an inclination of 87 degrees and an altitude ranging from about 452 km in June 2001 to approximately 346 km in September 2007.

Table 2.1 Solar and Geomagnetic Indices.

Date	3 Hour Planetary Equivalent Amplitude Indices, a_p	Daily Planetary Amplitude, A_p	Observed 10.7 cm Daily Solar Radio Flux, $F_{10.7}$
June 18, 2001	7 32 48 48 56 32 22 39	36	221.3
June 19, 2001	22 9 4 5 5 15 18 18	12	195.4
June 20, 2001	9 12 18 18 12 12 3 6	11	198.5
July 28, 2001	4 2 2 2 4 2 2 3	3	115.5
July 29, 2001	5 7 7 5 6 6 4 3	5	116.9
July 30, 2001	5 4 5 5 5 6 12 15	7	114.5
February 17, 2002	12 18 27 9 9 7 4 7	12	196.6
February 18, 2002	4 7 7 5 6 12 22 22	11	192.8
February 19, 2002	15 4 6 3 3 4 7 5	6	189.4
February 20, 2002	6 3 7 6 12 9 7 12	8	193.4
February 21, 2002	5 7 9 6 7 6 7 15	8	201.1
April 15, 2002	7 4 2 2 6 7 7 9	6	203.3
April 16, 2002	7 12 12 3 5 3 6 5	7	195.7
April 17, 2002	15 15 12 80 111 154 94 15	62	193.5
April 19, 2002	22 22 32 80 80 94 111 56	62	179.7
April 20, 2002	132 154 67 32 48 80 39 12	70	177.3
April 23, 2002	4 39 80 18 18 32 9 18	27	175.3
October 29, 2003	39 27 400 207 179 179 300 300	204	279.1
October 30, 2003	300 154 56 39 48 132 400 400	191	271.4

October 31, 2003	5 2 5 2 15 12 27 32	12	221.1
November 1, 2003	48 39 27 12 15 18 18 27	26	210.4
November 20, 2003	4 22 94 94 179 300 300 207	150	175.2
November 21, 2003	111 80 80 22 7 15 12 12	42	177.0
January 16, 2004	39 18 9 32 22 39 39 32	29	120.3
January 17, 2004	15 18 15 18 12 15 27 27	18	122.6
January 18, 2004	9 22 22 12 12 6 32 32	18	119.5
March 10, 2005	22 18 15 12 12 22 9 5	14	101.6
March 11, 2005	9 9 6 4 4 3 0 5	5	104.9
March 12, 2005	6 3 4 0 2 3 2 6	3	110.1
March 13, 2005	5 0 0 3 3 5 9 18	5	113.8
March 14, 2005	32 27 12 15 39 12 7 9	19	111.5
March 15, 2005	7 4 4 3 3 0 2 7	4	108.2
March 16, 2005	3 2 3 6 15 7 7 7	6	104.6
March 17, 2005	15 22 9 9 6 32 7 5	13	101.4
March 18, 2005	3 4 5 6 3 6 27 27	10	96.5
March 19, 2005	39 27 6 6 5 0 2 4	11	93.0
March 20, 2005	2 7 4 4 4 2 4 2	4	89.0
May 13, 2005	39 27 27 12 18 27 12 7	21	125.9
May 14, 2005	6 5 7 5 5 6 9 3	6	99.5
May 15, 2005	67 67 236 179 27 27 48 48	87	103.0
August 2, 2006	12 12 7 9 7 6 5 15	9	72.1
August 3, 2006	12 5 3 4 3 3 5 5	5	71.3
August 4, 2006	2 4 2 0 0 0 3 3	2	69.6
December 22, 2006	18 18 22 32 15 12 12 18	18	73.2
December 23, 2006	12 12 22 9 18 27 18 9	16	72.7
December 24, 2006	12 9 9 7 15 18 15 7	12	73.5
September 9, 2007	0 0 2 3 3 3 0 3	2	66.7
September 10, 2007	3 2 3 3 2 2 2 2	2	66.9
September 11, 2007	0 0 3 3 3 3 3 3	2	66.1

Table 2 visually demonstrates the 36 possible combinations of the density and ballistic coefficient correlated half-lives at order of magnitude increments over the given

range and increment value for a given date. The baseline atmospheric density model, date, initial time, and time span used for each variation listed in the table is displayed in the upper left gray box with the density and ballistic coefficient correlated half-lives shown in the upper light blue and left light orange boxes, respectively. The light green boxes, Cases 1, 8, 15, 22, 29, and 36, depict variations where the density and ballistic coefficient correlated half-lives are equal. The light yellow boxes, Cases 6 and 31, represent variations where the density and ballistic coefficient correlated half-lives are at their maximum/minimum values. A total of nine cases including Cases 1-3, 7-9, and 13-15 were investigated for all days examined in this work. Some of the initial work used all 36 cases for February 17-21, 2002 and March 17, 2005 but the initial results demonstrated that solutions with smaller half-lives typically generated better results. Therefore, the research was refined to focus on solutions utilizing the half-life combinations shown for the aforementioned nine cases.

Table 2.2 Density and Ballistic Coefficient Correlated Half-Life Variation Map.

NRLMSISE 2000 March 17, 2005 00:00:00.000 UTC 24 Hour Fit Span		Density Correlated Half-Life (min)					
		1.8	18	180	1,800	18,000	180,000
Ballistic Coefficient Correlated Half-Life (min)	1.8	Case 1	Case 2	Case 3	Case 4	Case 5	Case 6
	18	Case 7	Case 8	Case 9	Case 10	Case 11	Case 12
	180	Case 13	Case 14	Case 15	Case 16	Case 17	Case 18
	1,800	Case 19	Case 20	Case 21	Case 22	Case 23	Case 24
	18,000	Case 25	Case 26	Case 27	Case 28	Case 29	Case 30
	180,000	Case 31	Case 32	Case 33	Case 34	Case 35	Case 36

2.6.3 Solar and Geomagnetic Activity Level Bins

POE derived density solutions were developed for multiple time periods with varying levels of solar and geomagnetic activity as shown in Table 1. Categories for the level of solar and geomagnetic activity as represented by the daily solar radio flux ($F_{10.7}$) and daily planetary amplitude (A_p), respectively, are loosely defined in Reference 11. Based on the definitions given in Reference 11, low solar activity is defined by $F_{10.7} < 75$, moderate solar

activity for $75 \leq F_{10.7} < 150$, elevated solar activity for $150 \leq F_{10.7} < 190$, and high solar activity by $F_{10.7} \geq 190$. Additionally, quiet geomagnetic periods are defined for $A_p \leq 10$, moderate geomagnetic activity for $10 < A_p < 50$, and active geomagnetic periods by $A_p \geq 50$. These definitions are applied to the solar and geomagnetic indices given in Table 1 to separate the POE derived density solutions into the appropriate categories.

This cataloging of solutions facilitates the analysis of the POE derived density solutions as a function of solar and geomagnetic activity. Particular attention is paid to those periods of increased solar and geomagnetic activity and the resulting estimated atmospheric density. Creating bins according to activity levels allows a more detailed investigation of the results because atmospheric density is highly affected by the solar flux and geomagnetic activity. As the solar flux increases, the atmospheric density should exhibit more variations. Therefore, examining solutions as a function of solar and geomagnetic activity levels should provide an increased understanding of the upper atmosphere and better insight into how well the orbit determination process is estimating density according to activity levels.

2.6.4 Solution Sensitivity to Nominal Ballistic Coefficient Initialization Value

While the orbit determination process does estimate the ballistic coefficient, the process requires an initial value for the ballistic coefficient. Selecting a value that is at least close to the actual value is important to keep the process behaving properly and converging to a good estimate. The question remains of how close is close enough and what are the effects on the estimated density and ballistic coefficient of varying the initial value of the ballistic coefficient. An initial value is specified and subsequent scenarios are considered where the initial value is changed by a prescribed percentage.

2.6.5 Varying Solution Fit Span Length

The question of whether or not the length of the solution fit span has any affect on the estimated density must be considered. The more data available the better the solution should be. However, the minimum amount of data required for a good solution and how much data is sufficient for a solution must be determined. Conducting orbit determination with too few data points may result in a poor solution. However, an orbit determination process with too many data points might be inefficient, wasteful of time and computational resources, and not offer much if any improvement in accuracy. Knowing what is needed without going into wasteful excess becomes an important aspect of orbit determination not simply for efficiency but more importantly for accuracy and confidence in the results.

Also, for all solutions regardless of fit span length, end effects are always present and are an important consideration. End effects are a common occurrence in any orbit determination process and result from the small amount of data that exists at the beginning and end of a solution. As a solution progresses in time either forward or backward away from the beginning or end of a solution, more data is available before and after the current time increasing the accuracy of the solution. The end effects will be minimized for orbit determination processes that are well defined.

2.6.6 Solution Overlaps

Regions where solutions overlap one another provide insight into how well the orbit determination process is working. If the orbit determination process is well determined, then the solutions should overlap with very little if any difference between the two. However, comparison of solutions during overlap periods does not offer any evaluation of the solutions in regards to their accuracy. The solutions must be compared with a benchmark such as

accelerometer density data to quantify the results. In other words, the solutions might be consistent with each other but a bias might exist within the orbit determination process causing the solutions to be consistently wrong when compared with the accelerometer density. Therefore, the solution overlap regions provide a valuable check on the consistency of the process and the associated solutions without determining the accuracy of the results.

2.7 Validation of the Estimated Atmospheric Density

The derived densities obtained from the POE data are compared against those derived from the CHAMP and GRACE accelerometers as calculated by Sean Bruinsma of CNES. Bruinsma's density values are averaged to 10-second intervals. Bruinsma's method of data processing is described in References 31-34. The accelerometer derived densities were taken as truth for comparison purposes. The POE derived density data sets are compared with the CHAMP and GRACE density data sets from the High Accuracy Satellite Drag Model (HASDM) [Ref. 18] obtained from Bruce Bowman of the Air Force Space Command.

The February 17-21, 2002 solutions are 36 hour fit spans starting at 0 hr UTC February 17, 2002 with no solution overlap periods. The April 2002 solutions are 24 hour fit spans beginning at 0 hr UTC for each day with no solution overlap periods. The November 20-21, 2003 solution is a 48 hour fit span with a start time of 0 hr UTC November 20, 2003. All other solutions are 14 hour fit spans with start times at 10 hr UTC and 22 hr UTC yielding solution overlap periods of two hours at the beginning and end of each solution. All of the solution spans generated during this work have fit span lengths that stem from the POE data spans. In other words, if the POE data spans a period of 14 hours, then the solution will also span the same 14 hour period. The results are given in the following chapters.

2.8 Cross Correlation

For all cases examined the zero delay cross correlation coefficient was calculated for the POE estimated density compared with the accelerometer derived density, which was taken as truth for comparison purposes. The cross correlation coefficient quantifies the degree of correlation between the POE derived densities and accelerometer derived densities. The cross correlation coefficients in this paper have been normalized yielding values ranging from -1 to 1. The bounds indicate maximum correlation. If a high negative correlation is obtained, a maximum correlation is indicated but of the inverse of one of the series. If a value of zero is obtained, then no correlation is indicated.

When considering two series *x(i)* and *y(i)* where *i*=0, 1, 2, …, N-1 and N is the number of elements in each series, the cross correlation between these two series is defined as follows [Ref. 68].

$$r(d) = \frac{\sum_i \left[\left(x(i) - mx \right) * \left(y(i-d) - my \right) \right]}{\sqrt{\sum_i \left(x(i) - mx \right)^2} \sqrt{\sum_i \left(y(i-d) - my \right)^2}} \tag{2.7}$$

In the above equation, *mx* and *my* are the means for each respective series and the delay is defined as d=0, 1, 2, …, N-1. A difficulty arises when the index in the y series is less than zero or greater than or equal to the number of elements. These out-of-bounds indices can either be ignored or wrapped back around so that they become in-bounds again. For the purposes of this research, any out-of-bounds indices were ignored in computation of the cross correlation coefficient. The denominator in the cross correlation equation normalizes the coefficient to be between -1 and 1 as previously discussed. In essence, one series is held at a constant position or index while the other series is incrementally adjusted to determine the full range of cross correlation coefficients for a range of delays.

The accelerometer data and the resulting solution data are slightly offset from one another and often times have a different number of elements. Therefore, the accelerometer is chosen as the basis for comparison in terms of setting the time indices as the reference. The two data sets must then be made to have equal lengths in terms of time duration and number of elements. The estimated density data sets are interpolated to the accelerometer data using linear or Hermite interpolation. No significant difference is realized between these two interpolation techniques because the time interval between the data points is typically very small. A select few scenarios were examined to investigate the effect of the two interpolation methods with Hermite interpolation selected for use with this data. The results from this data formatting are two series with an equal number of elements with identical indices between the two series. The cross correlation is computed for a user-specified delay with the cross correlation coefficient at zero delay, the maximum cross correlation coefficient, and the delay at which the maximum cross correlation coefficient occurs reported back to the user.

3 OVERALL EFFECTS OF VARYING SELECT ORBIT DETERMINATION PARAMETERS

The overall effects of varying select parameters in the orbit determination process on the estimated density are examined in this chapter. Particular attention is given to varying the baseline atmospheric model and the density and ballistic coefficient correlated half-lives. The baseline atmospheric model used in the orbit determination process is the existing atmospheric model used to generate a baseline atmospheric density value. This baseline atmospheric density value is then corrected with a density correction factor in the orbit determination process resulting in an improved atmospheric density estimate. The baseline atmospheric model is not modified or changed in any way but is used as a starting point for the atmospheric density estimates generated by the orbit determination process. In other words, the POE density estimates are obtained by adding a density correction determined by the orbit determination process to the atmospheric density determined by the existing or baseline atmospheric model used within the orbit determination process. Cross correlation coefficients relating the POE density estimates to the accelerometer density are calculated for all baseline models and half-life combinations to draw overall conclusions. The residuals and position and velocity consistency tests are provided as a check on the orbit determination process. The POE estimated density is compared with other methods of density estimation to determine if any improvement is achieved over existing atmospheric models and if the results are competitive with HASDM density data sets. Also, an important note is that HASDM uses CHAMP as a calibration satellite meaning the accuracy of the HASDM density obtained for the CHAMP solution will be higher than for most other satellites.

The normalized zero delay and maximum cross correlation coefficients were calculated for all examined combinations of the Gauss-Markov process density and ballistic

coefficient correlated half-lives used to generate POE estimated atmospheric density. This includes applying the density and ballistic coefficient correlated half-life combinations for all baseline atmospheric models currently available within the orbit determination software ODTK. Normalized zero delay and maximum cross correlation coefficients were also calculated for the Jacchia 1971 empirical model and the HASDM density. The accelerometer derived density data was taken as truth for comparison purposes and was used as the basis of comparison for calculating the cross correlation coefficients. This quantifiable, systematic approach helps in determining which baseline density model and Gauss-Markov half-life combination yields the best density estimate for each solution. The cross correlation coefficients obtained for each solution were then used to calculate the time averaged zero delay and maximum cross correlation coefficients in an overall summary.

Density and ballistic coefficient correlated half-life values of 1.8, 18, and 180 minutes are the prime consideration for this work. However, as mentioned in the Methodology chapter, the density and ballistic coefficient correlated half-lives were originally considered in order of magnitude increments starting at 1.8 minutes and ending at 180,000 minutes. These larger half-life values were considered for February 17-21, 2002 and March 17, 2005 but were not used for later days because of poor results. In particular, the POE density estimates had poor agreement with the accelerometer density, showed consistent failure of the consistency tests, and occasionally rejected measurement data. The initial results indicated that the smaller half-life values had better POE density estimates compared with the accelerometer density and the orbit determination process performed better for these smaller half-life values.

Table 3.1 Time Averaged Zero Delay Cross Correlation Coefficients for All Solutions. *The columns of density models are the baseline models used for the POE estimated density and not the actual models themselves. Yellow (or light gray) highlighted numbers indicate the largest value for the baseline model. The orange (or darker gray) highlighted number indicates the largest overall number. The cross correlation coefficient for the Jacchia 1971 empirical model is 0.8717. The cross correlation coefficient for the HASDM density is 0.9218.*

Half-Life Combinations, Density/Ballistic Coefficient (min)	*CIRA-1972*	*Jacchia 1971*	*Jacchia-Roberts*	*MSISE-1990*	*NRLMSISE-2000*
Case 1 1.8/1.8	0.9251	0.9242	0.9244	0.9011	0.9034
Case 2 18/1.8	0.9286	0.9278	0.9282	0.8998	0.9043
Case 3 180/1.8	0.9263	0.9260	0.9261	0.9059	0.9081
Case 7 1.8/18	0.9229	0.9224	0.9226	0.8997	0.9017
Case 8 18/18	0.9276	0.9270	0.9273	0.8983	0.9023
Case 9 180/18	0.9247	0.9244	0.9245	0.9038	0.9053
Case 13 1.8/180	0.9114	0.9109	0.9113	0.8909	0.8939
Case 14 18/180	0.9144	0.9140	0.9144	0.8863	0.8905
Case 15 180/180	0.8849	0.8990	0.8992	0.8847	0.8853

Table 3.1 shows the overall summary for the time averaged zero delay cross correlation coefficients for all solutions. Examination of these results reveals two specific trends. First, the CIRA-1972, Jacchia 1971, and Jacchia-Roberts based POE density estimates all have very similar results with very slight differences between them. Secondly, the MSISE-1990 and NRLMSISE-2000 baseline atmospheric models used to generate POE estimate densities also have very similar results with only very slight differences between them. These trends should be expected given that the CIRA-1972, Jacchia 1971, and Jacchia-Roberts models are derived from or very closely related to a common prior atmospheric model. The same applies for the MSISE-1990 and the NRLMSISE-2000 models in that they too share a common atmospheric model heritage.

The next result immediately visible is the higher degree of correlation of the POE estimated densities obtained using the Jacchia family of baseline models over the MSIS

family of baseline atmospheric models. All of the Jacchia based POE density estimates have their greatest correlation with the accelerometer derived density at the same Gauss-Markov process density and ballistic coefficient correlated half-life values of 18 and 1.8 minutes, respectively. A similar result is obtained for the POE density estimates using the MSIS family of baseline models but for a density correlated half-life of 180 minutes and a ballistic coefficient correlated half-life of 1.8 minutes. A conclusion based on these results is that the POE density estimates correlate best to the accelerometer density when the Jacchia family of atmospheric models is used as the baseline model in an orbit determination scheme using precision orbit ephemerides. Also, the results demonstrate that there is little difference in the POE estimated densities whether the CIRA-1972, Jacchia 1971, or Jacchia-Roberts atmospheric model is used as the baseline model. The POE density estimates obtained from using the Jacchia based models show the best correlation with the accelerometer density. Also, there is a noticeable small difference in the cross correlation coefficients for the POE estimated densities using either the Jacchia or MSIS based models. Therefore, choosing a preference between the two families of atmospheric models is not necessarily clear cut.

The time averaged zero delay cross correlations coefficients for all solutions are also given for the Jacchia 1971 empirical model and HASDM density. The Jacchia 1971 empirical model has the lowest cross correlation coefficient compared with all of the results. Therefore, the Jacchia 1971 empirical model has the lowest degree of correlation with the accelerometer derived density. This result is expected because all other results correspond to a process where density corrections of some kind are added to a baseline density model. Therefore, the density corrections should generally result in an estimated density that has an increased degree of correlation. Also, the existing atmospheric models, including the Jacchia

1971 empirical model, are well known to possess deficiencies in their capabilities in estimating density.

The cross correlation coefficient for the HASDM density is included for the sake of comparison. HASDM densities are generated as a correction to an existing density model so the resulting densities should correlate better with accelerometer density compared with existing atmospheric models. The cross correlation coefficient shown for the HASDM density shows that such an improvement is achieved. The HASDM density correlates better with the accelerometer density compared with the POE density estimates obtained from using all of the density and ballistic coefficient correlated half-life combinations for the MSIS baseline models. The HASDM density also has a higher degree of correlation with the accelerometer density than some of the POE density estimates found using certain half-life combinations for the Jacchia baseline models. However, the highest degree of correlation with the accelerometer density remains with the POE derived densities obtained from using the CIRA-1972, Jacchia 1971, or Jacchia-Roberts baseline atmospheric models in an orbit determination scheme. In particular, the POE density estimate generated using the CIRA-1972 baseline atmospheric model with a density correlated half-life of 18 minutes and a ballistic coefficient correlated half-life of 1.8 minutes has the highest degree of correlation with the accelerometer derived density.

Table 3.2 Time Averaged Maximum Cross Correlation Coefficients for All Solutions. *The columns of density models are the baseline models used for the POE estimated density and not the actual models themselves. Yellow (or light gray) highlighted numbers indicate the largest value for the baseline model. The orange (or darker gray) highlighted number indicates the largest overall number. The cross correlation coefficient for the Jacchia 1971 empirical model is 0.8748. The cross correlation coefficient for the HASDM density is 0.9262.*

Half-Life Combinations, Density/Ballistic Coefficient (min)	*CIRA-1972*	*Jacchia 1971*	*Jacchia-Roberts*	*MSISE-1990*	*NRLMSISE-2000*
Case 1 1.8/1.8	0.9300	0.9291	0.9294	0.9054	0.9076
Case 2 18/1.8	0.9328	0.9321	0.9324	0.9042	0.9082
Case 3 180/1.8	0.9296	0.9292	0.9293	0.9094	0.9114
Case 7 1.8/18	0.9265	0.9261	0.9262	0.9031	0.9050
Case 8 18/18	0.9317	0.9311	0.9313	0.9026	0.9061
Case 9 180/18	0.9278	0.9276	0.9276	0.9072	0.9085
Case 13 1.8/180	0.9145	0.9141	0.9144	0.8940	0.8968
Case 14 18/180	0.9182	0.9178	0.9181	0.8905	0.8940
Case 15 180/180	0.9025	0.9022	0.9024	0.8882	0.8885

Table 3.2 shows the overall summary for the time averaged maximum cross correlation coefficients for all solutions. The same trends, relationships, discussion, and conclusions can be made for these results as for those displayed for the time averaged zero delay cross correlation coefficients and will not be repeated here.

Table 3.3 Zero Delay Cross Correlation Coefficients for 1000-2400 Hours January 16, 2004. *The columns of density models are the baseline models used for the POE estimated density and not the actual models themselves. Yellow (or light gray) highlighted numbers indicate the largest value for the baseline model. The orange (or darker gray) highlighted number indicates the largest overall number. The cross correlation coefficient for the Jacchia 1971 empirical model is 0.8592. The cross correlation coefficient for the HASDM density is 0.8370.*

Half-Life Combinations, Density/Ballistic Coefficient (min)	*CIRA-1972*	*Jacchia 1971*	*Jacchia-Roberts*	*MSISE-1990*	*NRLMSISE-2000*
Case 1 1.8/1.8	0.8905	0.8906	0.8906	0.8783	0.8802
Case 2 18/1.8	0.8948	0.8951	0.8950	0.8801	0.8835
Case 3 180/1.8	0.8845	0.8847	0.8846	0.8677	0.8711
Case 7 1.8/18	0.8887	0.8888	0.8888	0.8775	0.8790
Case 8 18/18	0.8962	0.8965	0.8963	0.8815	0.8841
Case 9 180/18	0.8862	0.8864	0.8863	0.8699	0.8721
Case 13 1.8/180	0.8880	0.8881	0.8881	0.8770	0.8783
Case 14 18/180	0.8866	0.8869	0.8868	0.8761	0.8779
Case 15 180/180	0.8667	0.8667	0.8668	0.8635	0.8633

Table 3.3 shows the zero delay cross correlation coefficients for January 16, 2004. This particular day was chosen as a representative example for the overall summary of the cross correlation coefficients. The solution corresponding to these results is a 14 hour fit span beginning at 1000 hours and ending at 2400 hours that day. This day has geomagnetic activity classified as moderate with a daily planetary amplitude value of 29 and solar activity categorized as moderate with a 10.7 cm daily solar radio flux value of 120.3 SFUs. This particular day was selected because the solar and geomagnetic activity levels correspond to middle range values. At 10 a.m. January 16, 2004 CHAMP was in a near circular orbit with an inclination of 87 degrees and an altitude of about 374 km.

The zero delay cross correlation coefficients calculated for this day do not have their highest degree of correlation with accelerometer density for the same half-life combinations compared with the time averaged values calculated for the overall summary. Instead, the

highest degree of correlation now occurs for density and ballistic coefficient correlated half-lives of 18 minutes each for all the baseline density models displayed. However, the POE density estimates obtained using the Jacchia family of baseline models again shows similar results with each other as do the POE density estimates using the baseline MSIS models. Also, the difference between the cross correlation coefficients for the POE density estimates using the Jacchia and MSIS based models is diminished compared with the time averaged coefficients displayed in the overall summary. The Jacchia 1971 empirical model still displays a lower degree of correlation with accelerometer density compared with the POE derived densities for all baseline models and half-life combinations. One notable change from the overall summary observed in the results for this day is that the HASDM density now possesses the lowest degree of correlation with the accelerometer density compared with all coefficients for this day. This is a marked departure from the results seen in the overall summary. Also, the POE density estimates using the Jacchia 1971 baseline model now possess the highest degree of correlation with the accelerometer density compared with the POE density estimates obtained from using the CIRA-1972 baseline model as seen in the overall summary. However, because the cross correlation coefficients for the POE density estimates using the Jacchia family of baseline models are all very similar, selection of one baseline model over the other from this family shows little effect on the results. Even selecting between baseline models in the Jacchia and MSIS families demonstrates a reduced impact on the cross correlation coefficients for the POE density estimates compared with the overall summary.

Table 3.4 Maximum Cross Correlation Coefficients for 1000-2400 Hours January 16, 2004. *The columns of density models are the baseline models used for the POE estimated density and not the actual models themselves. Yellow (or light gray) highlighted numbers indicate the largest value for the baseline model. The orange (or darker gray) highlighted number indicates the largest overall number. The cross correlation coefficient for the Jacchia 1971 empirical model is 0.8630 with a -70 second delay. The cross correlation coefficient for the HASDM density is 0.8680 with a delay of -180 seconds. The values in parenthesis are the corresponding delays in seconds.*

Half-Life Combinations, Density/Ballistic Coefficient (min)	*CIRA 1972*	*Jacchia 1971*	*Jacchia-Roberts*	*MSISE 1990*	*NRLMSISE 2000*
Case 1 1.8/1.8	0.8915 (-30)	0.8916 (-30)	0.8916 (-30)	0.8787 (-20)	0.8806 (-20)
Case 2 18/1.8	0.8965 (-40)	0.8965 (-40)	0.8965 (-40)	0.8814 (-40)	0.8842 (-30)
Case 3 180/1.8	0.8882 (-70)	0.8883 (-60)	0.8882 (-70)	0.8709 (-60)	0.8739 (-60)
Case 7 1.8/18	0.8896 (-30)	0.8897 (-30)	0.8896 (-30)	0.8782 (-30)	0.8795 (-20)
Case 8 18/18	0.8976 (-40)	0.8977 (-40)	0.8976 (-40)	0.8826 (-40)	0.8848 (-30)
Case 9 180/18	0.8889 (-60)	0.8890 (-50)	0.8890 (-60)	0.8721 (-50)	0.8740 (-50)
Case 13 1.8/180	0.8890 (-30)	0.8890 (-30)	0.8890 (-30)	0.8779 (-30)	0.8789 (-30)
Case 14 18/180	0.8879 (-40)	0.8879 (-30)	0.8880 (-40)	0.8774 (-40)	0.8786 (-30)
Case 15 180/180	0.8693 (-60)	0.8692 (-50)	0.8694 (-60)	0.8658 (-50)	0.8654 (-50)

Table 3.4 shows the overall summary for the maximum cross correlation coefficients for January 16, 2004. Some of the same trends, relationships, discussion, and conclusions can be made for these results as for those displayed for the zero delay cross correlation coefficients. A noticeable difference in these results compared with the zero delay coefficients is that the HASDM density now shows a higher degree of correlation with the

accelerometer data compared with some of the POE density estimates using certain half-life combinations for the MSIS family of baseline atmospheric models. The HASDM density has a delay of -180 seconds, which is quite large compared with a delay of -70 seconds for the Jacchia 1971 empirical model and delays ranging from -20 to -50 seconds for the POE density estimates. This large delay for the HASDM density shows why the HASDM zero delay cross correlation coefficient is so low compared with the zero delay cross correlation coefficients for the Jacchia 1971 empirical model and the POE density estimates. Also, the Jacchia 1971 empirical model now has the lowest degree of correlation with the accelerometer derived density. However, the POE density estimate obtained from using the Jacchia 1971 baseline atmospheric model with density and ballistic coefficient correlated half-lives of 18 minutes each has the highest degree of correlation with the accelerometer density.

The tables showing the zero delay and maximum cross correlation coefficients for January 16, 2004 demonstrate that the conclusions drawn from the results for the overall summary of the coefficients do not hold true for all solutions. The results also help in determining the performance of the orbit determination scheme particularly in terms of selecting the best combination of half-lives and an appropriate baseline atmospheric model. The following graphs show results specific to the POE density estimate using the Jacchia 1971 baseline atmospheric model and a density and ballistic coefficient correlated half-life of 18 minutes each as determined by the cross correlation coefficient tables.

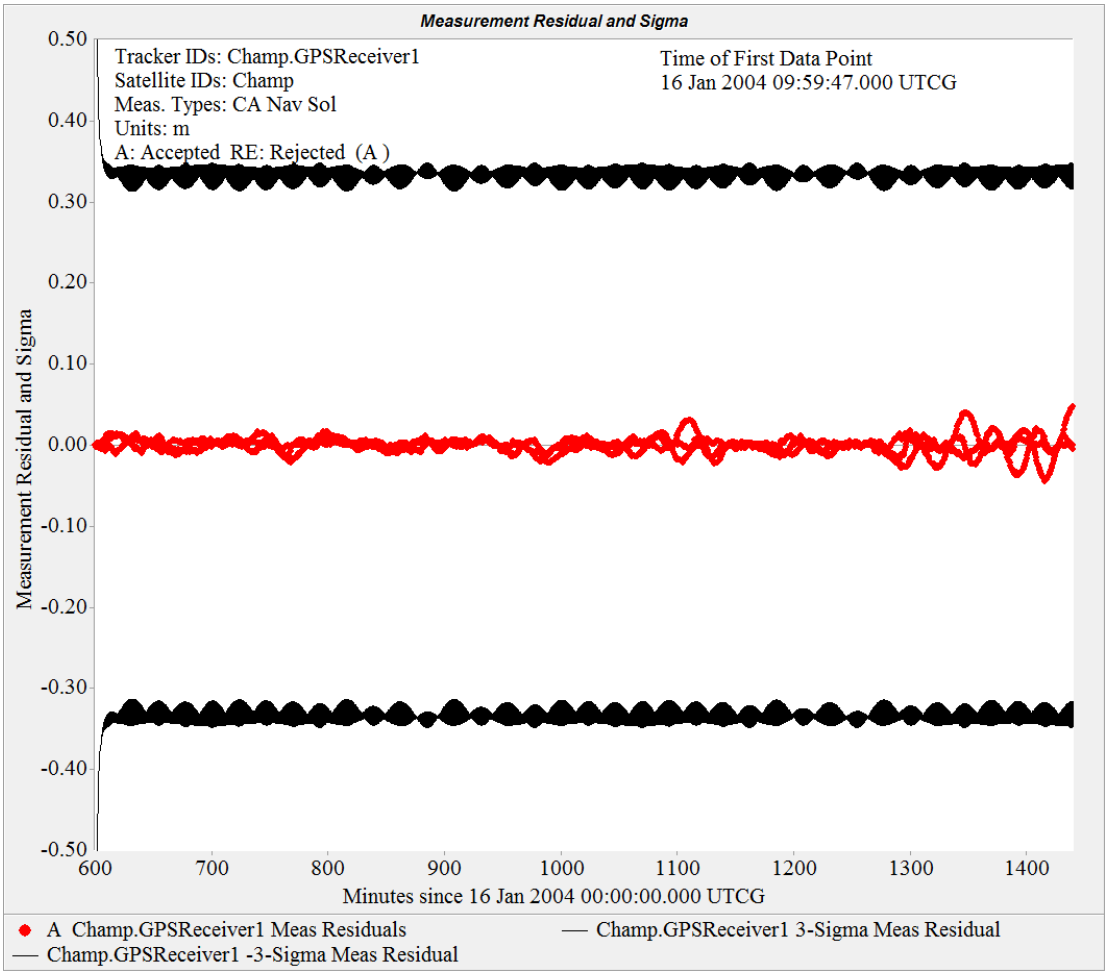

Figure 3.1 Filter Residuals for 1000-2400 Hours January 16, 2004. *Density and ballistic coefficient correlated half-lives are 18 minutes and the baseline density model is Jacchia 1971.*

Figure 3.1 shows the residuals for the January 16, 2004 solution as previously defined. The 3σ boundary values are approximately 33 cm with the majority of residuals falling within a few centimeters. There are a few areas where the residuals have worst values of 5-7 cm, which are within the range of the errors associated with the POE data. This is a typical residuals plot for most days with similar solar and geomagnetic activity levels. Also, the residuals for most solutions examined in this work do not have values far exceeding the worst case values observed for this day.

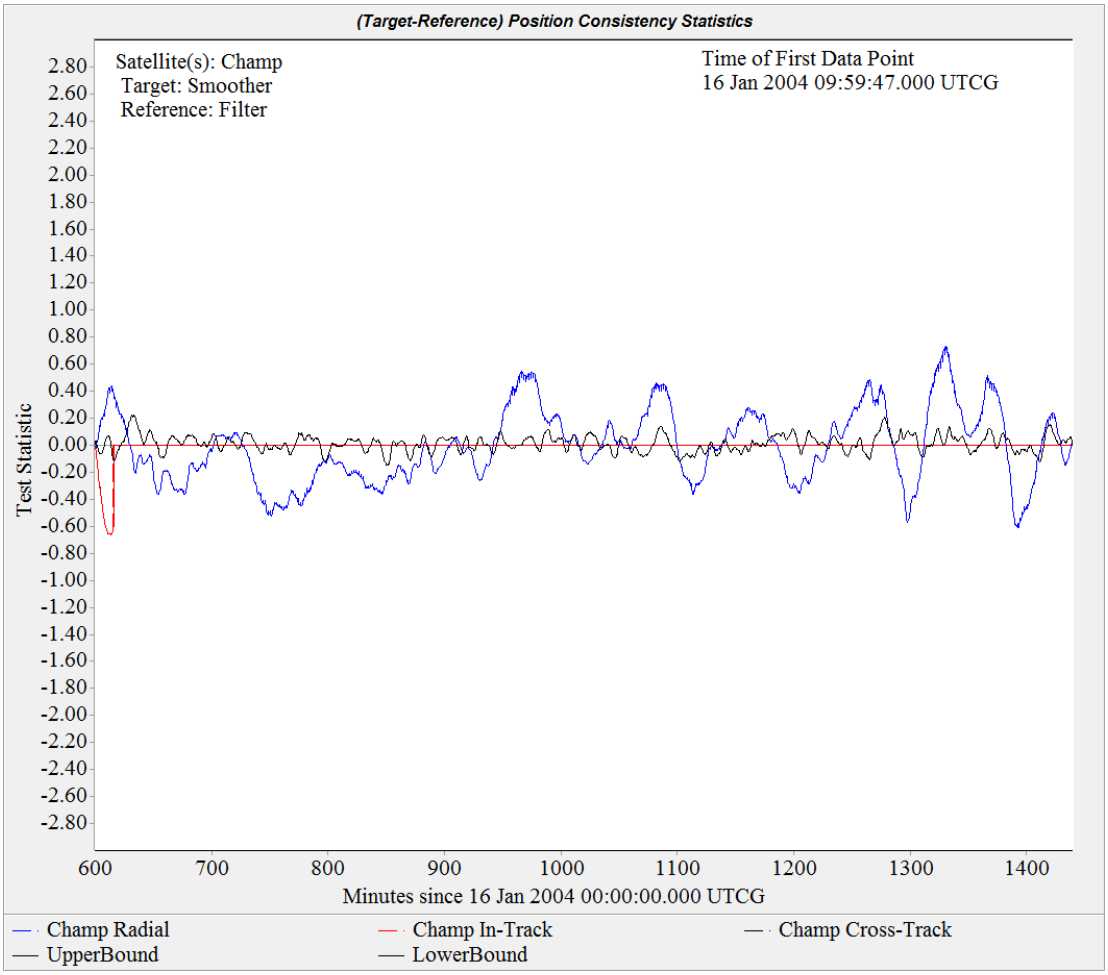

Figure 3.2 Position Consistency Test for 1000-2400 Hours January 16, 2004. *Density and ballistic coefficient correlated half-lives are 18 minutes and the baseline density model is Jacchia 1971.*

Figure 3.2 displays a graph of the position consistency test for January 16, 2004. The position consistency test is well satisfied for this day. This is a typical graph of a position consistency test for days with similar solar and geomagnetic activity levels. The magnitude of the test statistic is related to the solar and geomagnetic activity levels with increasing magnitudes as the activity levels increase.

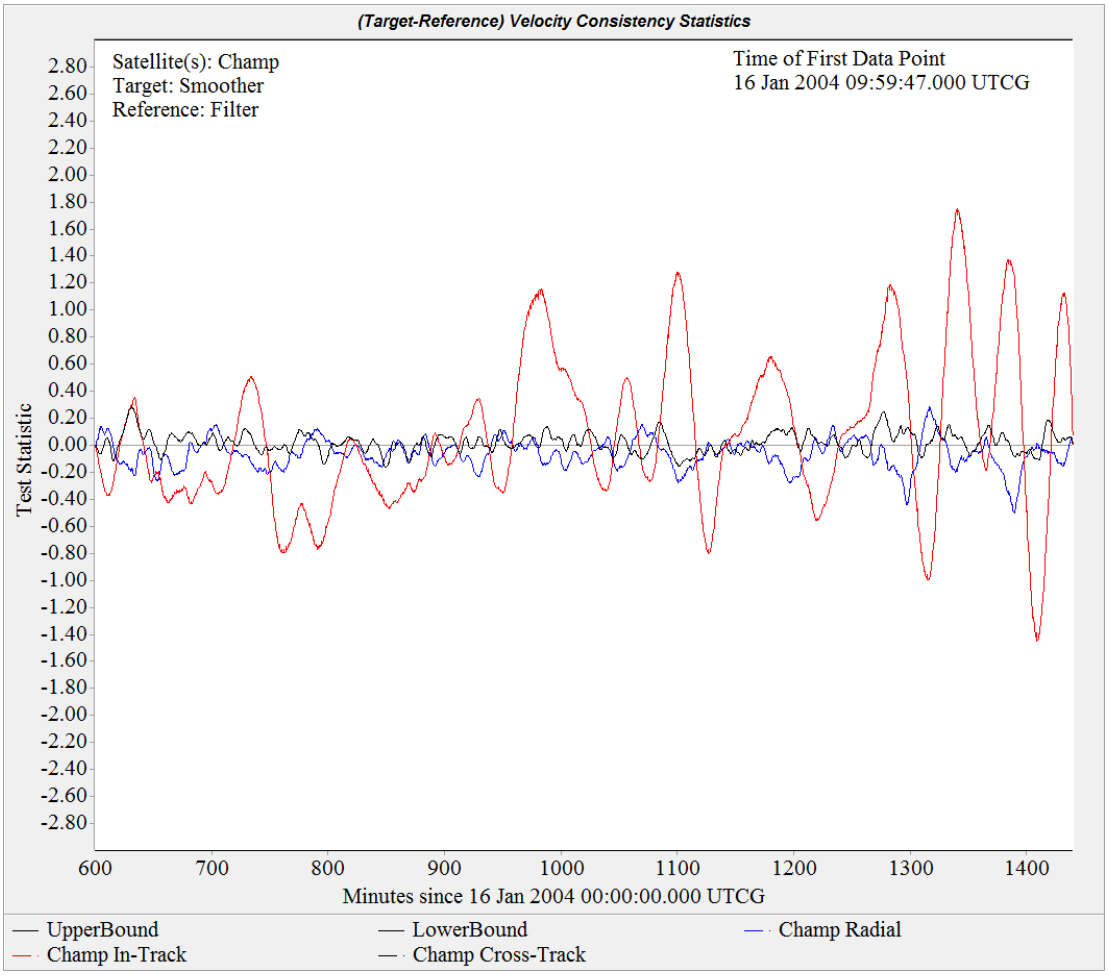

Figure 3.3 Velocity Consistency Test for 1000-2400 Hours January 16, 2004. *Density and ballistic coefficient correlated half-lives are 18 minutes and the baseline density model is Jacchia 1971.*

Figure 3.3 displays a graph of the velocity consistency test for January 16, 2004. The velocity consistency test is well satisfied for this day. This is a typical graph of a velocity consistency test for days with similar solar and geomagnetic activity levels. As with the position consistency test, the magnitude of the test statistic is related to the solar and geomagnetic activity levels with increasing magnitudes as the activity levels increase.

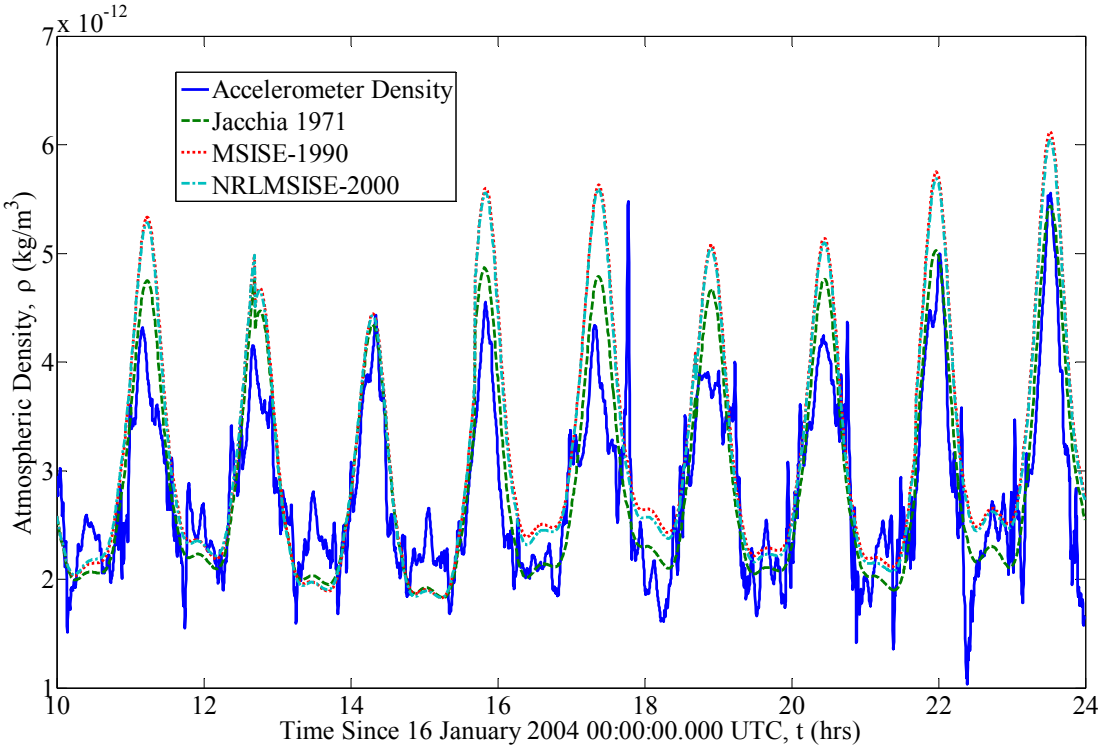

Figure 3.4 Effect of Varying the Baseline Atmospheric Model on the Estimated Density for 1000-2400 hours January 16, 2004. *The models displayed are the POE estimated density obtained from the baseline models and not the actual models themselves. Density and ballistic coefficient correlated half-lives are 18 minutes and the baseline density model is Jacchia 1971.*

Figure 3.4 demonstrates the effects of varying the baseline atmospheric model on the estimated density for January 16, 2004 as previously defined. The zero delay and maximum cross correlation coefficients gave general trends and conclusions regarding the correlation of the estimated density with accelerometer derived density. In particular, the POE density estimate using the Jacchia 1971 baseline model showed the highest degree of correlation with the accelerometer density. Therefore, the accelerometer derived density and the POE estimated density obtained from using the Jacchia 1971 baseline model along with the MSISE-1990 and NRLMSISE-2000 baseline models for a density and ballistic coefficient correlated half-life of 18 minutes each are displayed in this figure.

The POE density estimates using the MSIS family of baseline models show very similar estimated density values. The POE density estimate using the Jacchia 1971 baseline model shows much better agreement with the accelerometer density data compared with the MSIS family of baseline models used in creating the POE estimated densities. An important result directly observable from this figure is that the orbit determination scheme used to estimate density is incapable of modeling the rapid variations in density as observed by the accelerometer. This limitation is due to the dependence of the density corrections on the underlying baseline model and the subsequent deficiencies of the baseline model to accurately model density. However, the POE estimated density is capable of showing relative agreement with the general density structure. While only Jacchia 1971 is displayed in the figure, the POE density estimates obtained for the CIRA-1972 and Jacchia-Roberts baseline models will be very similar to the POE estimated density generated using the Jacchia 1971 baseline model as the two POE density estimates using the MSIS family of baseline models showed similar results. This similarity is due to the CIRA-1972, Jacchia 1971, and Jacchia-Roberts atmospheric models belonging to the same family of models and the inherent similarity between the models themselves. These results are typical for most solutions studied in this work.

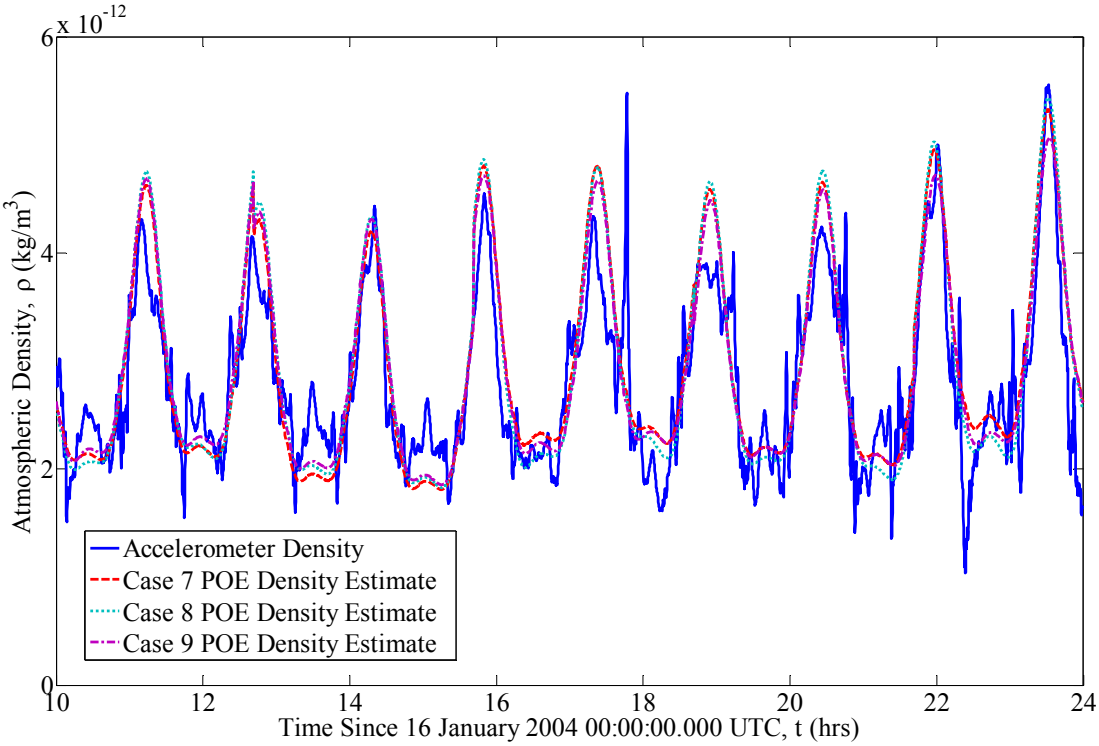

Figure 3.5 Effect of Varying the Density Correlated Half-Life on the Estimated Density for 1000-2400 hours January 16, 2004. *Ballistic coefficient correlated half-life is 18 minutes and the baseline density model is Jacchia 1971. Cases 7, 8, and 9 correspond to density correlated half-lives of 1.8, 18, and 180 minutes, respectively.*

Figure 3.5 demonstrates the effect of varying the density correlated half-life on the POE estimated density for January 16, 2004. The ballistic coefficient correlated half-life is held constant at 18 minutes while the density correlated half-life is varied by orders of magnitude from 1.8 to 18 to 180 minutes. The accelerometer density is included for comparison purposes. The figure shows that the density correlated half-life has mixed influences on the POE estimated density. In some situations, an increase in the density correlated half-life results in a decrease in the POE estimate density. However, in other situations, the opposite is true where as the density correlated half-life is decreased the estimated density increases. Also, the POE density estimates show relatively good agreement with the accelerometer derived density. While all three of the density correlated half-life

variations show similar results, the POE density estimate with density and ballistic coefficient correlated half-lives of 18 minutes each does show slightly better agreement with the accelerometer density over the other half-life combinations used for POE density estimates.

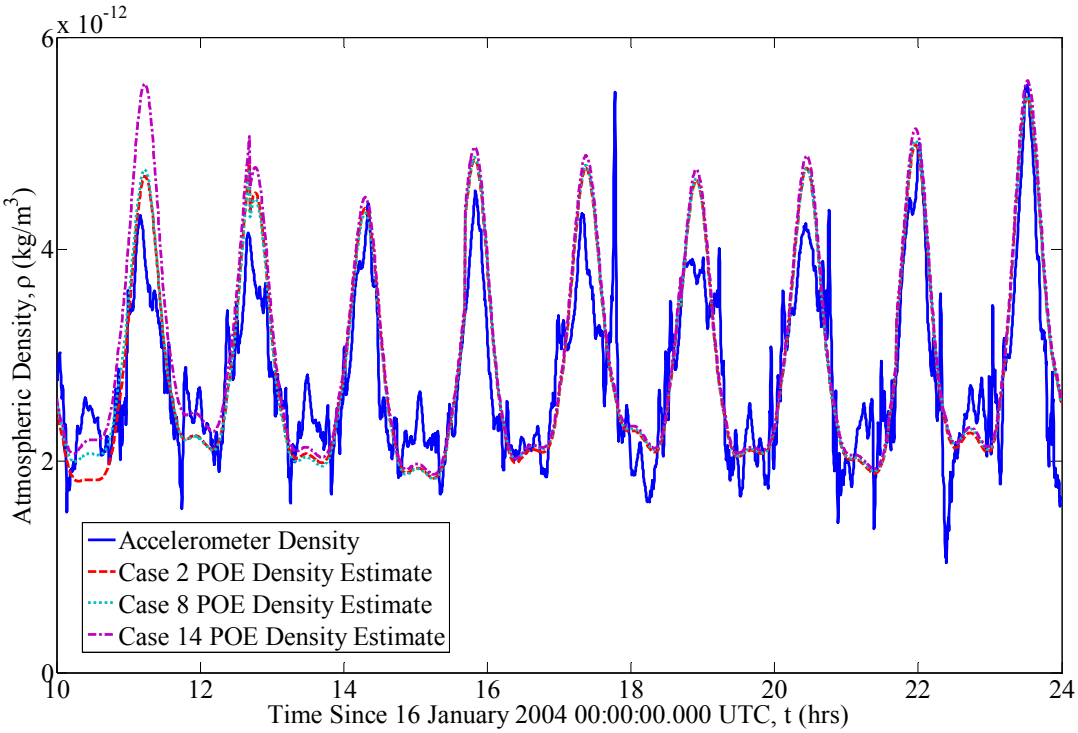

Figure 3.6 Effect of Varying the Ballistic Coefficient Correlated Half-Life on the Estimated Density for 1000-2400 hours January 16, 2004. *Density correlated half-life is 18 minutes and the baseline density model is Jacchia 1971. Cases 2, 8, and 14 correspond to ballistic coefficient correlated half-lives of 1.8, 18, and 180 minutes, respectively.*

Figure 3.6 shows the impact on the POE estimated density from varying the ballistic coefficient correlated half-life. The density correlated half-life is kept at a constant value of 18 minutes and the ballistic coefficient correlated half-life is varied by orders of magnitude starting at 1.8 minutes and ending at 180 minutes. This figure is the opposite of Figure 3.5 where the density correlated half-life was allowed to vary for a constant ballistic coefficient correlated half-life value. The accelerometer density is included for comparison purposes. This figure shows similar mixed effects of varying the ballistic coefficient correlated half-life

on the POE estimated density as seen in Figure 3.5. For this particular day, the results obtained for varying the ballistic coefficient correlated half-life are comparable with a slight preference for a density and ballistic coefficient half-life of 18 minutes each.

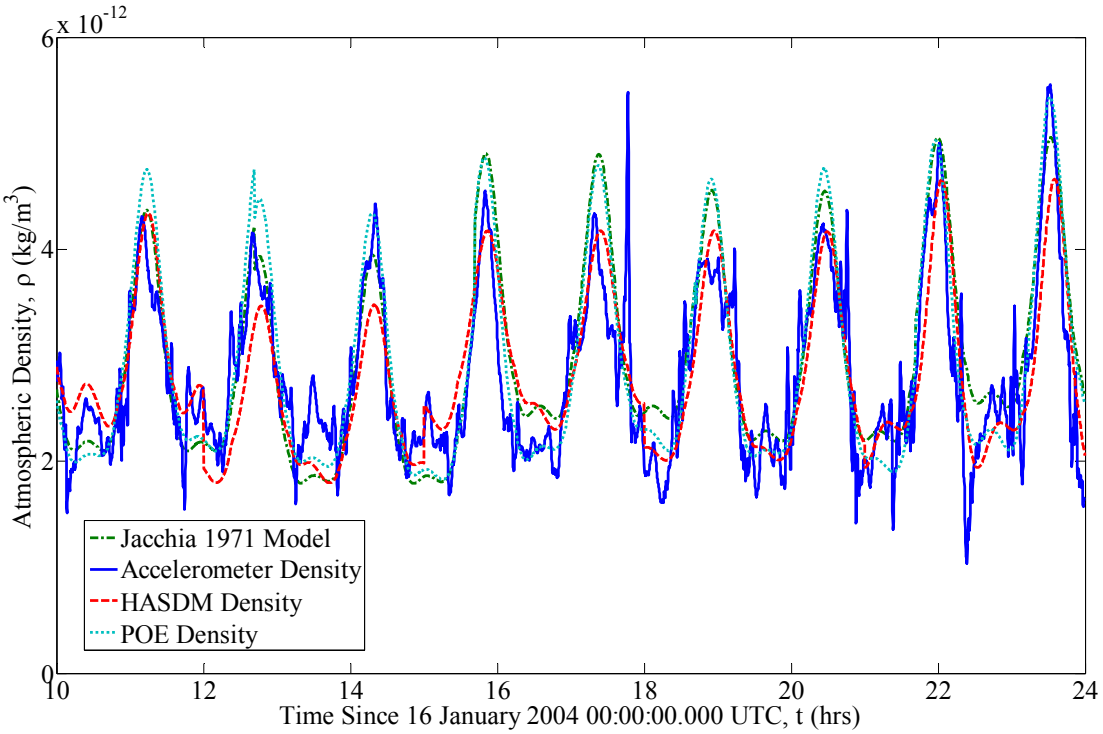

Figure 3.7 Comparison of Densities Obtained from Different Methods for 1000-2400 hours January 16, 2004. *POE density obtained using density and ballistic coefficient correlated half-lives of 18 minutes each and Jacchia 1971 as the baseline density model.*

Figure 3.7 compares the densities obtained from using four different methods for January 16, 2004. The baseline atmospheric model used for the POE density estimates is Jacchia 1971 and the density and ballistic coefficient correlated half-lives are 18 minutes each. The four methods displayed are the Jacchia 1971 empirical model density, accelerometer derived density, HASDM derived density, and POE derived density data sets. Comparing the POE estimated density with other methods is perhaps the most crucial metric used in this work. Such a comparison provides a valuable check on the POE density estimate

results to determine whether the process is offering a real improvement compared with existing methods. Again, the accelerometer density data is taken as truth as a basis for comparison with the other methods. The POE estimated density shows general improvement over the existing Jacchia 1971 atmospheric model and the HASDM density data. The HASDM density data also exhibits a general improvement over the Jacchia 1971 atmospheric model.

The cross correlation coefficients for January 16, 2004 displayed in this chapter support these conclusions. The highest degree of correlation with the accelerometer density belongs to the POE density estimate using a Jacchia 1971 baseline model and a density and ballistic coefficient correlated half-life of 18 minutes each. The maximum cross correlation coefficient table for this day also showed that the HASDM density has a lower degree of correlation with the accelerometer density than the POE density estimate, but the HASDM density is still superior to the Jacchia 1971 empirical model. The Jacchia 1971 empirical model has the lowest degree of correlation with the accelerometer density. Notice that in the zero delay cross correlation coefficient table for January 16, 2004, the Jacchia 1971 empirical model has a higher coefficient than the HASDM density.

4 DENSITY ESTIMATES BINNED ACCORDING TO SOLAR AND GEOMAGNETIC ACTIVITY LEVELS

The previous chapter examined the results as an overall summary to draw general conclusions. Another useful way of viewing the results is to group them in bins according to solar and geomagnetic activity levels. The Earth's atmosphere is directly influenced by solar and geomagnetic activity with observed density variations correlated to the input of energy from the Sun. The various dates examined can be divided into the following solar and geomagnetic activity bins.

Solar Activity Bins (units of SFU)

- Low solar flux bin for $F_{10.7} < 75$
- Moderate solar flux bin for $75 \leq F_{10.7} < 150$
- Elevated solar flux bin for $150 \leq F_{10.7} < 190$
- High solar flux bin for $F_{10.7} \geq 190$

Geomagnetic Activity Bins (units of gamma)

- Quiet geomagnetic bin for $A_p \leq 10$
- Moderate geomagnetic bin for $10 < A_p < 50$
- Active geomagnetic bin for $A_p \geq 50$

The effects of varying select parameters within an orbit determination scheme on the atmospheric density estimates are examined as a function of these bins of solar and geomagnetic activity levels. The parameters varied are the baseline atmospheric model and the density and ballistic coefficient correlated half-lives. As with the previous chapter, the POE density estimates obtained from all combinations of baseline models and both correlated half-lives are cross correlated with the accelerometer density data to generate cross correlation coefficients. These coefficients are used to make conclusions according to the

activity bins. A select number of residual and position and velocity consistency test graphs are included to demonstrate the performance of the orbit determination process as a function of solar and geomagnetic activity. Finally, the POE density estimates are compared with the results obtained from other methods of density estimation to determine if any improvement is achieved to the existing atmospheric models and if the POE estimated densities compare favorably with the HASDM density data.

The cross correlation coefficients calculated in this chapter follow the same form and results as for those calculated in the previous chapter. Also, the accelerometer density data is taken as truth for comparison purposes. This chapter describes representative results obtained from the systematic study of the variation of baseline atmospheric models and density and ballistic coefficient correlated half-lives as a function of solar and geomagnetic activity levels.

4.1 Effects of Solar Activity on Atmospheric Density Estimates

This section examines the effect of the Sun's energy on atmospheric density variations as grouped by solar activity bins. Particular attention is given to how the correlation and half-life combinations change as a function of the solar activity level.

4.1.1 Low Solar Activity Bin

Low solar activity as categorized by a $F_{10.7}$ value less than 75 is discussed in this section. The atmospheric density is typically characterized as being relatively calm with few large-scale disturbances. Periods of low solar activity are one of the easiest times to model or predict atmospheric density because the input and variability of energy from the Sun are at the lowest values of the solar cycle. A total of nine days were analyzed for the low solar activity bin.

Table 4.1 Time Averaged Zero Delay Cross Correlation Coefficients for Solutions with Low Solar Flux Activity. *The columns of density models are the baseline models used for the POE estimated density and not the actual models themselves. Yellow (or light gray) highlighted numbers indicate the largest value for the baseline model. The orange (or darker gray) highlighted number indicates the largest overall number. The cross correlation coefficient for the Jacchia 1971 empirical model is 0.9463. The cross correlation coefficient for the HASDM density is 0.9439.*

Half-Life Combinations, Density/Ballistic Coefficient (min)	*CIRA-1972*	*Jacchia 1971*	*Jacchia-Roberts*	*MSISE-1990*	*NRLMSISE-2000*
Case 1 1.8/1.8	0.9398	0.9372	0.9370	0.9360	0.9360
Case 2 18/1.8	0.9426	0.9414	0.9414	0.9402	0.9405
Case 3 180/1.8	0.9480	0.9474	0.9475	0.9450	0.9454
Case 7 1.8/18	0.9481	0.9476	0.9476	0.9445	0.9445
Case 8 18/18	0.9463	0.9455	0.9455	0.9432	0.9435
Case 9 180/18	0.9506	0.9502	0.9502	0.9470	0.9475
Case 13 1.8/180	0.9495	0.9495	0.9495	0.9472	0.9472
Case 14 18/180	0.9446	0.9445	0.9446	0.9416	0.9418
Case 15 180/180	0.9395	0.9389	0.9390	0.9371	0.9374

Table 4.1 shows the time averaged zero delay cross correlation coefficients for the low solar flux activity bin. Examination of these cross correlation coefficients yields several significant trends. First, the most important trend visible in these results is the high degree of correlation between the POE density estimates and the accelerometer density. Additionally, the Jacchia 1971 empirical model and the HASDM density also have a high degree of correlation with the accelerometer density data. Secondly, the POE density estimates obtained from using the CIRA-1972, Jacchia 1971, and Jacchia-Roberts baseline atmospheric models have comparable results and vary only slightly from one another. Thirdly, the POE density estimates generated from the MSISE-1990 and NRLMSISE-2000 baseline models also have similar coefficients with only slight differences between them. These trends are also exhibited in the previous chapter where the overall summary was examined.

Notice that the difference between the POE density estimates using the Jacchia and the MSIS families of baseline models shown in the cross correlation coefficients is very small. Therefore, for periods of low solar flux, the POE density estimates show comparable results regardless of the baseline atmospheric model used in the orbit determination process. Choosing between any of the models within either family of baseline models shows even less influence on the resulting POE estimated density.

The Jacchia 1971 empirical model and the HASDM density also show similar results, and in fact the HASDM density has the lowest degree of correlation with the accelerometer density compared with all of the results. Comparing the Jacchia 1971 empirical model with the POE density estimate results shows that only a slight improvement of correlation is achieved for the POE estimated density. These results are expected given that days with low solar flux activity occur during periods of the lowest energy output from the Sun making atmospheric modeling much easier and subsequently more accurate.

Table 4.2 Time Averaged Maximum Cross Correlation Coefficients for Solutions with Low Solar Flux Activity. *The columns of density models are the baseline models used for the POE estimated density and not the actual models themselves. Yellow (or light gray) highlighted numbers indicate the largest value for the baseline model. The orange (or darker gray) highlighted number indicates the largest overall number. The cross correlation coefficient for the Jacchia 1971 empirical model is 0.9471. The cross correlation coefficient for the HASDM density is 0.9453.*

Half-Life Combinations, Density/Ballistic Coefficient (min)	*CIRA-1972*	*Jacchia 1971*	*Jacchia-Roberts*	*MSISE-1990*	*NRLMSISE-2000*
Case 1 1.8/1.8	0.9454	0.9431	0.9431	0.9403	0.9406
Case 2 18/1.8	0.9464	0.9452	0.9452	0.9431	0.9436
Case 3 180/1.8	0.9503	0.9498	0.9498	0.9468	0.9473
Case 7 1.8/18	0.9505	0.9500	0.9500	0.9463	0.9465
Case 8 18/18	0.9496	0.9487	0.9488	0.9457	0.9461
Case 9 180/18	0.9527	0.9523	0.9524	0.9486	0.9492
Case 13 1.8/180	0.9508	0.9507	0.9507	0.9482	0.9483
Case 14 18/180	0.9468	0.9466	0.9467	0.9432	0.9435
Case 15 180/180	0.9412	0.9406	0.9407	0.9384	0.9388

Table 4.2 displays the time averaged maximum cross correlation coefficients for the low solar flux activity bin. The same general trends observed for the zero delay cross correlation coefficients are seen in this table of coefficients. The differences between the zero delay and maximum cross correlation coefficients are very small indicating a relative calm in the Earth's atmosphere. The two tables show little variation among all of the results whether considering all the half-life combinations for a particular baseline density model or all baseline models for a specific half-life combination. Such consistency in the results is evidence of the low variations in the Earth's atmosphere during periods of low solar flux.

For the time averaged zero delay cross correlation, the highest degree of correlation of the POE density for each baseline model with the accelerometer density is achieved primarily for density and ballistic coefficient correlated half-lives of 180 and 18 minutes, respectively. The only exception is the POE density estimate using the MSISE-1990 baseline model where the best correlation is achieved for a density correlated half-life of 1.8 minutes and a ballistic coefficient correlated half-life of 180 minutes. The difference in the cross correlation coefficients between this half-life combination and the density and ballistic coefficient half-life seen to have the best correlation for the other baseline models is extremely small.

The time averaged maximum cross correlation shows that the highest degree of correlation of the POE density estimates for each baseline model with the accelerometer density is obtained for a density correlated half-life of 180 minutes and a ballistic coefficient correlated half-life of 18 minutes. The overall highest degree of correlation in this bin corresponds to the POE density estimate using the CIRA-1972 baseline atmospheric model

with a density and ballistic coefficient correlated half-life of 180 and 18 minutes, respectively.

4.1.2 Moderate Solar Activity Bin

Grouping the results according to moderate solar flux activity is considered in this section. Periods of moderate solar flux are characterized by values of the observed daily solar radio flux of $75 \leq F_{10.7} < 150$. Days with such a classification are the most prevalent. There were a total of 19 days analyzed in the moderate solar activity bin.

Table 4.3 Time Averaged Zero Delay Cross Correlation Coefficients for Solutions with Moderate Solar Flux Activity. *The columns of density models are the baseline models used for the POE estimated density and not the actual models themselves. Yellow (or light gray) highlighted numbers indicate the largest value for the baseline model. The orange (or darker gray) highlighted number indicates the largest overall number. The cross correlation coefficient for the Jacchia 1971 empirical model is 0.9198. The cross correlation coefficient for the HASDM density is 0.9463.*

Half-Life Combinations, Density/Ballistic Coefficient (min)	*CIRA-1972*	*Jacchia 1971*	*Jacchia-Roberts*	*MSISE-1990*	*NRLMSISE-2000*
Case 1 1.8/1.8	0.9420	0.9419	0.9418	0.9275	0.9284
Case 2 18/1.8	0.9419	0.9417	0.9417	0.9257	0.9271
Case 3 180/1.8	0.9425	0.9426	0.9425	0.9269	0.9284
Case 7 1.8/18	0.9391	0.9390	0.9390	0.9274	0.9280
Case 8 18/18	0.9408	0.9407	0.9407	0.9245	0.9257
Case 9 180/18	0.9409	0.9410	0.9409	0.9250	0.9264
Case 13 1.8/180	0.9356	0.9355	0.9356	0.9263	0.9269
Case 14 18/180	0.9329	0.9329	0.9330	0.9185	0.9196
Case 15 180/180	0.9293	0.9292	0.9291	0.9159	0.9166

Table 4.3 displays the time averaged zero delay cross correlation coefficients for the moderate solar flux activity bin. Similar trends for the POE density estimates using the Jacchia and MSIS families of baseline density models are observed for these results. Also, many of the general trends observed for previous tables of cross correlation coefficients can be seen in these results. However, a notable difference is that the results are less consistent

compared with the results obtained for periods of low activity. There is a greater disparity between the coefficients for the range of half-life combinations for a particular baseline density model and for a specific half-life combination applied to all five baseline models. Also, the differences between the cross correlation coefficients for the POE estimated densities obtained from using the Jacchia and MSIS families of baseline density models has increased compared with the low solar activity bin. However, a general increase in the degree of correlation with the accelerometer density is observed with the POE estimate density over the Jacchia 1971 empirical model. The general magnitude of the correlation of all methods of estimating density is slightly reduced as the solar activity level increases. A final notable difference is that the HASDM density during periods of moderate solar flux activity now has the highest degree of correlation with the accelerometer density data.

Table 4.4 Time Averaged Maximum Cross Correlation Coefficients for Solutions with Moderate Solar Flux Activity. *The columns of density models are the baseline models used for the POE estimated density and not the actual models themselves. Yellow (or light gray) highlighted numbers indicate the largest value for the baseline model. The orange (or darker gray) highlighted number indicates the largest overall number. The cross correlation coefficient for the Jacchia 1971 empirical model is 0.9230. The cross correlation coefficient for the HASDM density is 0.9504.*

Half-Life Combinations, Density/Ballistic Coefficient (min)	*CIRA-1972*	*Jacchia 1971*	*Jacchia-Roberts*	*MSISE-1990*	*NRLMSISE-2000*
Case 1 1.8/1.8	0.9459	0.9458	0.9457	0.9320	0.9330
Case 2 18/1.8	0.9457	0.9456	0.9456	0.9300	0.9316
Case 3 180/1.8	0.9461	0.9461	0.9460	0.9307	0.9321
Case 7 1.8/18	0.9426	0.9426	0.9425	0.9313	0.9320
Case 8 18/18	0.9448	0.9447	0.9447	0.9288	0.9302
Case 9 180/18	0.9444	0.9445	0.9444	0.9287	0.9301
Case 13 1.8/180	0.9387	0.9387	0.9387	0.9296	0.9303
Case 14 18/180	0.9366	0.9366	0.9367	0.9223	0.9236
Case 15 180/180	0.9325	0.9324	0.9323	0.9191	0.9199

Table 4.4 displays the time averaged maximum cross correlation coefficients for the moderate solar activity bin. The same trends are observed for these results as those seen for the time-averaged zero delay cross correlation coefficients. An increase in the Sun's energy output from low to moderate has a significant impact on the POE estimate density as determined from examination of the cross correlation coefficients. The ability to accurately model or estimate the atmospheric density is greatly affected by an increase in energy received from the Sun.

The time averaged zero delay and maximum cross correlations demonstrate that as the solar activity increases from low to moderate the half-life combination giving the highest degree of correlation with the accelerometer density also changes. For moderate solar activity, the best half-life combination is a density correlated half-life of 180 minutes and a ballistic coefficient correlated half-life of 1.8 minutes for the POE density estimates using the Jacchia family of baseline models. Also, when the MSISE-1990 baseline model is used to generate POE density estimates, the best half-life corresponds to a density and ballistic coefficient correlated half-life of 1.8 and 18 minutes, respectively. The POE estimated density using the NRLMSISE-2000 baseline model has a best half-life combination of 1.8 minutes for the density and ballistic coefficient correlated half-lives. The overall highest degree of correlation of the POE density estimate with the accelerometer now corresponds to the Jacchia 1971 baseline model with a density and ballistic coefficient correlated half-life combination of 180 and 1.8 minutes, respectively.

4.1.3 Elevated Solar Activity Bin

This section examines the cross correlation coefficients calculated for the elevated solar activity bin. Days experiencing elevated solar flux are characterized by values of the observed daily solar radio flux of $150 \leq F_{10.7} < 190$. Periods of elevated solar activity can be

easily found but are not the most common. Six total days are included in the elevated solar activity bin for analysis.

Table 4.5 Time Averaged Zero Delay Cross Correlation Coefficients for Solutions with Elevated Solar Flux Activity. *The columns of density models are the baseline models used for the POE estimated density and not the actual models themselves. Yellow (or light gray) highlighted numbers indicate the largest value for the baseline model. The orange (or darker gray) highlighted number indicates the largest overall number. The cross correlation coefficient for the Jacchia 1971 empirical model is 0.7206. The cross correlation coefficient for the HASDM density is 0.8741.*

Half-Life Combinations, Density/Ballistic Coefficient (min)	*CIRA-1972*	*Jacchia 1971*	*Jacchia-Roberts*	*MSISE-1990*	*NRLMSISE-2000*
Case 1 1.8/1.8	0.8842	0.8823	0.8832	0.8162	0.8215
Case 2 18/1.8	0.8980	0.8961	0.8970	0.8246	0.8315
Case 3 180/1.8	0.8803	0.8790	0.8794	0.8356	0.8356
Case 7 1.8/18	0.8697	0.8680	0.8688	0.8029	0.8082
Case 8 18/18	0.8891	0.8873	0.8882	0.8141	0.8200
Case 9 180/18	0.8725	0.8713	0.8717	0.8232	0.8216
Case 13 1.8/180	0.8364	0.8345	0.8357	0.7771	0.7874
Case 14 18/180	0.8648	0.8629	0.8642	0.7948	0.8026
Case 15 180/180	0.8274	0.8260	0.8272	0.7993	0.7975

Table 4.5 gives the time averaged zero delay cross correlation coefficients for periods grouped according to elevated levels of solar flux activity. A major difference seen in this table of results compared with previous results is the increased range of values for the cross correlation coefficients for variations both in baseline models for a given half-life combination and for the complete range of half-lives given a particular baseline model. The differences are also larger when comparing the POE density estimates using the Jacchia and MSIS families of baseline models. Also, the HASDM density has a higher degree of correlation with the accelerometer data than most of the POE estimated density data sets but not all. In fact, the highest overall coefficient value lies with one of the POE density data sets. Notice that all of the results show an increase in the degree of correlation with the

accelerometer density compared with the Jacchia 1971 empirical model. However, the cross correlation coefficients are generally reduced in size as the Sun's energy level increases, especially for the Jacchia 1971 empirical model.

Table 4.6 Time Averaged Maximum Cross Correlation Coefficients for Solutions with Elevated Solar Flux Activity. *The columns of density models are the baseline models used for the POE estimated density and not the actual models themselves. Yellow (or light gray) highlighted numbers indicate the largest value for the baseline model. The orange (or darker gray) highlighted number indicates the largest overall number. The cross correlation coefficient for the Jacchia 1971 empirical model is 0.7213. The cross correlation coefficient for the HASDM density is 0.8784.*

Half-Life Combinations, Density/Ballistic Coefficient (min)	*CIRA-1972*	*Jacchia 1971*	*Jacchia-Roberts*	*MSISE-1990*	*NRLMSISE-2000*
Case 1 1.8/1.8	0.8871	0.8851	0.8861	0.8191	0.8240
Case 2 18/1.8	0.8993	0.8974	0.8983	0.8260	0.8328
Case 3 180/1.8	0.8813	0.8800	0.8804	0.8376	0.8376
Case 7 1.8/18	0.8723	0.8705	0.8713	0.8055	0.8106
Case 8 18/18	0.8903	0.8885	0.8894	0.8150	0.8209
Case 9 180/18	0.8736	0.8724	0.8728	0.8249	0.8232
Case 13 1.8/180	0.8387	0.8368	0.8377	0.7796	0.7900
Case 14 18/180	0.8659	0.8640	0.8652	0.7955	0.8033
Case 15 180/180	0.8284	0.8269	0.8282	0.8004	0.7985

Table 4.6 shows the time averaged maximum cross correlation coefficients for the elevated solar flux activity bin. The same general trends and conclusions are observed in this table of results as were seen in the previous table. Both tables of cross correlation coefficients for periods of elevated solar flux activity demonstrate the difficulty in modeling the Earth's atmosphere as the Sun's energy output increases.

The time averaged zero delay and maximum cross correlations show that an increase in the solar activity to an elevated level changes the half-life combinations giving the highest degree of correlation with the accelerometer density. The POE density estimates using the Jacchia family of baseline models all have the highest coefficients for a density correlated

half-life of 18 minutes and a ballistic coefficient correlated half-life of 1.8 minutes. Also, the POE density estimates using the MSIS family of baseline models all have the highest coefficients for a density correlated half-life of 180 minutes and a ballistic coefficient correlated half-life of 1.8 minutes. During elevated solar activity levels, the overall highest degree of correlation of the POE density estimate with the accelerometer now corresponds to the CIRA-1972 baseline model with a density and ballistic coefficient correlated half-life combination of 18 and 1.8 minutes, respectively.

4.1.4 High Solar Activity Bin

This section groups the calculated cross correlation coefficients for periods of high solar activity. Periods of high solar flux are characterized by values of the observed daily solar radio flux of $F_{10.7} \geq 190$. Days with high solar activity are relatively rare. A total of 14 days were included for analyzing periods of high solar activity.

Table 4.7 Time Averaged Zero Delay Cross Correlation Coefficients for Solutions with High Solar Flux Activity. *The columns of density models are the baseline models used for the POE estimated density and not the actual models themselves. Yellow (or light gray) highlighted numbers indicate the largest value for the baseline model. The orange (or darker gray) highlighted number indicates the largest overall number. The cross correlation coefficient for the Jacchia 1971 empirical model is 0.8050. The cross correlation coefficient for the HASDM density is 0.8891.*

Half-Life Combinations, Density/Ballistic Coefficient (min)	*CIRA-1972*	*Jacchia 1971*	*Jacchia-Roberts*	*MSISE-1990*	*NRLMSISE-2000*
Case 1 1.8/1.8	0.9057	0.9049	0.9056	0.8695	0.8740
Case 2 18/1.8	0.9110	0.9102	0.9109	0.8619	0.8724
Case 3 180/1.8	0.9047	0.9043	0.9045	0.8738	0.8788
Case 7 1.8/18	0.9011	0.9005	0.9009	0.8632	0.8674
Case 8 18/18	0.9094	0.9088	0.9093	0.8598	0.8694
Case 9 180/18	0.9021	0.9019	0.9019	0.8722	0.8753
Case 13 1.8/180	0.8772	0.8763	0.8772	0.8418	0.8477
Case 14 18/180	0.8851	0.8842	0.8851	0.8352	0.8449
Case 15 180/180	0.8067	0.8550	0.8553	0.8346	0.8363

Table 4.7 displays the time average zero delay cross correlation coefficients for the high solar activity bin. The cross correlation coefficients for high solar activity have the widest range of values of all the solar flux bins. However, the results do show a general improvement of the POE density estimate and HASDM density data sets over the Jacchia 1971 empirical model. The same general trends observed in the previous tables of cross correlation coefficients can also be observed for the coefficient obtained for periods of high solar activity.

Notice that the cross correlation coefficients for solutions with high solar activity are larger than those coefficients for solutions during periods of elevated solar activity. This is the opposite of what is expected and there are several possible causes for what would appear to be a backwards relationship. First, each respective bin may not have a proper representation of the distribution of total days according to the solar and geomagnetic activity levels. Secondly, the geomagnetic activity level associated with the days in the elevated and high solar activity bins may be affecting the results. In other words, a day in the high solar bin may have a moderate geomagnetic activity level causing the results for that day to be different for another day in the high solar bin with active geomagnetic activity. Thirdly, the distribution of the days in terms of the level of solar activity within each bin may also affect the results. The solar and geomagnetic activity level classification consists of a range of values for each bin. Therefore, the difference between results generated by a day on the low end of the high solar bin and those results for a day on the high end of the high solar bin may be different and consequently influence the averaged results. Fourthly, the days are categorized according to solar and geomagnetic indices that are measured daily and every three hours, respectively. The actual energy input into the Earth's atmosphere is not a

constant value as reported by the indices but rather constantly changing. Accordingly, the actual level of solar and geomagnetic activity may differ from the reported value thereby affecting the results for each day or solution and the subsequent averaged results for each bin.

Table 4.8 Time Averaged Maximum Cross Correlation Coefficients for Solutions with High Solar Flux Activity. *The columns of density models are the baseline models used for the POE estimated density and not the actual models themselves. Yellow (or light gray) highlighted numbers indicate the largest value for the baseline model. The orange (or darker gray) highlighted number indicates the largest overall number. The cross correlation coefficient for the Jacchia 1971 empirical model is 0.8105. The cross correlation coefficient for the HASDM density is 0.8961.*

Half-Life Combinations, Density/Ballistic Coefficient (min)	*CIRA-1972*	*Jacchia 1971*	*Jacchia-Roberts*	*MSISE-1990*	*NRLMSISE-2000*
Case 1 1.8/1.8	0.9120	0.9114	0.9119	0.8737	0.8779
Case 2 18/1.8	0.9170	0.9163	0.9169	0.8685	0.8771
Case 3 180/1.8	0.9088	0.9085	0.9087	0.8787	0.8829
Case 7 1.8/18	0.9061	0.9056	0.9059	0.8672	0.8709
Case 8 18/18	0.9151	0.9146	0.9150	0.8662	0.8740
Case 9 180/18	0.9061	0.9059	0.9059	0.8766	0.8794
Case 13 1.8/180	0.8817	0.8810	0.8816	0.8461	0.8512
Case 14 18/180	0.8909	0.8902	0.8909	0.8425	0.8498
Case 15 180/180	0.8597	0.8597	0.8599	0.8409	0.8413

Table 4.8 gives the time averaged maximum cross correlation coefficients for solutions with high solar activity. While the same general trends are visible, a notable difference is that the range of values for the coefficients is smaller compared with the previous table. The time averaged zero delay and maximum cross correlations show that an increase in the level of solar activity from elevated to high causes no change to the half-life combinations giving the highest degree of correlation with the accelerometer density. The POE density estimates using the Jacchia family of baseline models all have the highest coefficients for a density correlated half-life of 18 minutes and a ballistic coefficient correlated half-life of 1.8 minutes. Also, the POE density estimates using the MSIS family of

baseline models all have the highest coefficients for a density correlated half-life of 180 minutes and a ballistic coefficient correlated half-life of 1.8 minutes. During high solar activity levels, the overall highest degree of correlation of the POE density estimate with the accelerometer corresponds to the CIRA-1972 baseline model with a density and ballistic coefficient correlated half-life combination of 18 and 1.8 minutes, respectively.

4.1.5 Summary of the Solar Activity Bins

The Sun's influence on the atmospheric density can be seen in the cross correlation coefficients relating the POE density estimates to the accelerometer density. Specifically, as the level of solar activity increases, the degree of correlation between the POE density estimates and the accelerometer density generally experiences a slight reduction. Also, as the solar activity increases, the values of the density and ballistic coefficient correlated half-lives tend to generally decrease. However, no change is observed in the best combination of half-lives when moving from periods of elevated to high solar activity. Because the best half-life combination changes as a function of solar activity level, selecting a combination of half-lives that works well as an overall standard is difficult. These results would also suggest that the Jacchia family of baseline atmospheric models provides the best results in generated POE density estimates. In particular, CIRA-1972 is the most frequent best baseline model in the results.

4.2 Effects of Geomagnetic Activity on Atmospheric Density Estimates

This section examines the effect of the geomagnetic activity on atmospheric density variations as grouped by geomagnetic activity bins. Particular attention is given to how the correlation and half-life combinations change as a function of the geomagnetic activity level.

4.2.1 Quiet Geomagnetic Activity Bin

Geomagnetic activity, which is directly connected to solar activity, also influences the atmospheric density. This section groups the results according to quiet geomagnetic activity conditions. Quiet geomagnetic conditions are defined for $A_p \leq 10$. Periods of quiet geomagnetic activity are somewhat common. A total of 18 days was analyzed for the quiet geomagnetic activity bin.

Table 4.9 Time Averaged Zero Delay Cross Correlation Coefficients for Solutions with Quiet Geomagnetic Activity. *The columns of density models are the baseline models used for the POE estimated density and not the actual models themselves. Yellow (or light gray) highlighted numbers indicate the largest value for the baseline model. The orange (or darker gray) highlighted number indicates the largest overall number. The cross correlation coefficient for the Jacchia 1971 empirical model is 0.9393. The cross correlation coefficient for the HASDM density is 0.9504.*

Half-Life Combinations, Density/Ballistic Coefficient (min)	*CIRA-1972*	*Jacchia 1971*	*Jacchia-Roberts*	*MSISE-1990*	*NRLMSISE-2000*
Case 1 1.8/1.8	0.9503	0.9501	0.9496	0.9341	0.9376
Case 2 18/1.8	0.9479	0.9474	0.9475	0.9294	0.9335
Case 3 180/1.8	0.9499	0.9497	0.9497	0.9371	0.9399
Case 7 1.8/18	0.9523	0.9523	0.9523	0.9379	0.9408
Case 8 18/18	0.9485	0.9483	0.9483	0.9291	0.9333
Case 9 180/18	0.9497	0.9496	0.9496	0.9360	0.9386
Case 13 1.8/180	0.9496	0.9494	0.9496	0.9365	0.9394
Case 14 18/180	0.9382	0.9381	0.9382	0.9200	0.9237
Case 15 180/180	0.8898	0.9291	0.9289	0.9183	0.9202

Table 4.9 displays the time averaged zero delay cross correlation coefficients for periods grouped according to quiet geomagnetic activity levels. These results show that when the geomagnetic activity level is low most of the density estimates have very similar and high cross correlation coefficients. A familiar grouping of results within the POE density estimates from using the Jacchia and MSIS families of baseline density models is still observable. The differences between the POE density estimates from using these two

families of baseline models is very small so there is little preference of one baseline model over another regardless of what family of models it belongs to. Also, the HASDM density data is often better correlated with the accelerometer density than most of the POE density estimates. While the Jacchia 1971 empirical model has a higher cross correlation coefficient than some of the POE density estimates, a general improvement is achieved by HASDM density and the majority of POE densities over the Jacchia 1971 empirical model.

Table 4.10 Time Averaged Maximum Cross Correlation Coefficients for Solutions with Quiet Geomagnetic Activity. *The columns of density models are the baseline models used for the POE estimated density and not the actual models themselves. Yellow (or light gray) highlighted numbers indicate the largest value for the baseline model. The orange (or darker gray) highlighted number indicates the largest overall number. The cross correlation coefficient for the Jacchia 1971 empirical model is 0.9423. The cross correlation coefficient for the HASDM density is 0.9531.*

Half-Life Combinations, Density/Ballistic Coefficient (min)	*CIRA-1972*	*Jacchia 1971*	*Jacchia-Roberts*	*MSISE-1990*	*NRLMSISE-2000*
Case 1 1.8/1.8	0.9557	0.9555	0.9552	0.9403	0.9438
Case 2 18/1.8	0.9534	0.9529	0.9530	0.9352	0.9395
Case 3 180/1.8	0.9537	0.9535	0.9535	0.9410	0.9438
Case 7 1.8/18	0.9564	0.9565	0.9564	0.9425	0.9455
Case 8 18/18	0.9538	0.9536	0.9536	0.9347	0.9390
Case 9 180/18	0.9534	0.9533	0.9533	0.9398	0.9425
Case 13 1.8/180	0.9530	0.9529	0.9530	0.9399	0.9429
Case 14 18/180	0.9429	0.9428	0.9430	0.9248	0.9285
Case 15 180/180	0.9323	0.9324	0.9322	0.9217	0.9236

Table 4.10 displays the time average maximum cross correlation coefficients for the quiet geomagnetic activity bin. The same results observed in the previous table are also seen in these results. Periods of quiet geomagnetic activity provide the best correlation of the POE densities and HASDM density with the accelerometer density data. This is an expected result given the dependence of the POE and HASDM approaches on the underlying baseline models.

The time averaged zero delay and maximum cross correlation coefficients show that the highest degree of correlation of the POE density estimates for all of the baseline models with the accelerometer density is obtained for a density correlated half-life of 1.8 minutes and a ballistic coefficient correlated half-life of 18 minutes. The overall highest degree of correlation in this bin corresponds to the POE density estimate using the Jacchia 1971 baseline atmospheric model with a density and ballistic coefficient correlated half-life of 1.8 and 18 minutes, respectively.

4.2.2 Moderate Geomagnetic Activity Bin

This section considers the results as binned according to moderate geomagnetic activity levels. Periods of moderate geomagnetic activity are defined for $10 < A_p < 50$. Days with moderate levels of geomagnetic activity are quite common. A total of 19 days was included in the analysis of the moderate geomagnetic activity bin.

Table 4.11 Time Averaged Zero Delay Cross Correlation Coefficients for Solutions with Moderate Geomagnetic Activity. *The columns of density models are the baseline models used for the POE estimated density and not the actual models themselves. Yellow (or light gray) highlighted numbers indicate the largest value for the baseline model. The orange (or darker gray) highlighted number indicates the largest overall number. The cross correlation coefficient for the Jacchia 1971 empirical model is 0.8963. The cross correlation coefficient for the HASDM density is 0.9303.*

Half-Life Combinations, Density/Ballistic Coefficient (min)	*CIRA-1972*	*Jacchia 1971*	*Jacchia-Roberts*	*MSISE-1990*	*NRLMSISE-2000*
Case 1 1.8/1.8	0.9306	0.9291	0.9297	0.9110	0.9131
Case 2 18/1.8	0.9356	0.9350	0.9354	0.9089	0.9146
Case 3 180/1.8	0.9345	0.9343	0.9344	0.9144	0.9181
Case 7 1.8/18	0.9301	0.9297	0.9299	0.9108	0.9128
Case 8 18/18	0.9341	0.9335	0.9338	0.9079	0.9127
Case 9 180/18	0.9319	0.9318	0.9318	0.9127	0.9153
Case 13 1.8/180	0.9231	0.9227	0.9230	0.9056	0.9083
Case 14 18/180	0.9203	0.9199	0.9204	0.8962	0.9006
Case 15 180/180	0.9040	0.9036	0.9038	0.8924	0.8936

Table 4.11 displays the time averaged zero delay cross correlation coefficients for periods with moderate geomagnetic activity. Similar trends are observed in these results as seen for the previous table of cross correlation coefficients. However, a notable difference is the general reduction in magnitude of the correlation as the geomagnetic activity increases. There is also a slight increase in the range of values for the various combinations of baseline models and half-lives. Also, the differences between the POE estimated densities created from the Jacchia and MSIS family of baseline atmospheric models is more pronounced for periods of moderate geomagnetic activity compared with quiet geomagnetic activity levels. The HASDM and POE density estimates do exhibit a general improvement over the Jacchia 1971 empirical model in terms of how well their results correlate with the accelerometer density data.

Table 4.12 Time Averaged Maximum Cross Correlation Coefficients for Solutions with Moderate Geomagnetic Activity. *The columns of density models are the baseline models used for the POE estimated density and not the actual models themselves. Yellow (or light gray) highlighted numbers indicate the largest value for the baseline model. The orange (or darker gray) highlighted number indicates the largest overall number. The cross correlation coefficient for the Jacchia 1971 empirical model is 0.8998. The cross correlation coefficient for the HASDM density is 0.9352.*

Half-Life Combinations, Density/Ballistic Coefficient (min)	*CIRA-1972*	*Jacchia 1971*	*Jacchia-Roberts*	*MSISE-1990*	*NRLMSISE-2000*
Case 1 1.8/1.8	0.9359	0.9346	0.9351	0.9145	0.9165
Case 2 18/1.8	0.9397	0.9391	0.9394	0.9130	0.9178
Case 3 180/1.8	0.9381	0.9380	0.9380	0.9182	0.9214
Case 7 1.8/18	0.9340	0.9336	0.9338	0.9138	0.9156
Case 8 18/18	0.9380	0.9375	0.9377	0.9119	0.9159
Case 9 180/18	0.9354	0.9353	0.9353	0.9161	0.9184
Case 13 1.8/180	0.9264	0.9261	0.9263	0.9088	0.9111
Case 14 18/180	0.9240	0.9237	0.9240	0.9005	0.9038
Case 15 180/180	0.9074	0.9070	0.9073	0.8963	0.8970

Table 4.12 gives the time averaged maximum cross correlation coefficients during periods of moderate geomagnetic activity. Similar results are displayed in this table of coefficients compared with the previous table. The cross correlation coefficients for periods of moderate geomagnetic activity demonstrate the influence increased geomagnetic activity has on estimating density. The results become less correlated with the accelerometer density data as the geomagnetic activity level increases. As expected, the atmospheric density becomes increasingly difficult to accurately estimate as the energy input into the atmosphere increases. The resulting density variations are not adequately understood or modeled in existing atmospheric models. However, various density correction methods displayed in these results show that improvements can be achieved despite the underlying baseline model's inability to accurately model such density variations.

The time averaged zero delay and maximum cross correlations demonstrate that as the geomagnetic activity increases from quiet to moderate the half-life combination giving the highest degree of correlation with the accelerometer density also changes. For moderate geomagnetic activity, the best half-life combination is a density correlated half-life of 18 minutes and a ballistic coefficient correlated half-life of 1.8 minutes for the POE density estimates using the Jacchia family of baseline models. Also, the POE density estimates using the MSIS family of baseline models all have the highest coefficients for a density correlated half-life of 180 minutes and a ballistic coefficient correlated half-life of 1.8 minutes. During moderate geomagnetic activity levels, the overall highest degree of correlation of the POE density estimate with the accelerometer now corresponds to the CIRA-1972 baseline model with a density and ballistic coefficient correlated half-life combination of 18 and 1.8 minutes, respectively.

4.2.3 Active Geomagnetic Activity Bin

This last geomagnetic group considers the results as binned according to active geomagnetic conditions. High geomagnetic activity levels are defined for $A_p \geq 50$. Days possessing high geomagnetic activity levels are quite rare. Eight total days were analyzed for the active geomagnetic activity bin.

Table 4.13 Time Averaged Zero Delay Cross Correlation Coefficients for Solutions with Active Geomagnetic Activity. *The columns of density models are the baseline models used for the POE estimated density and not the actual models themselves. Yellow (or light gray) highlighted numbers indicate the largest value for the baseline model. The orange (or darker gray) highlighted number indicates the largest overall number. The cross correlation coefficient for the Jacchia 1971 empirical model is 0.6479. The cross correlation coefficient for the HASDM density is 0.8327.*

Half-Life Combinations, Density/Ballistic Coefficient (min)	*CIRA-1972*	*Jacchia 1971*	*Jacchia-Roberts*	*MSISE-1990*	*NRLMSISE-2000*
Case 1 1.8/1.8	0.8527	0.8515	0.8521	0.7983	0.7982
Case 2 18/1.8	0.8646	0.8631	0.8638	0.8070	0.8086
Case 3 180/1.8	0.8494	0.8484	0.8488	0.8108	0.8074
Case 7 1.8/18	0.8353	0.8340	0.8346	0.7812	0.7812
Case 8 18/18	0.8615	0.8602	0.8608	0.8012	0.8024
Case 9 180/18	0.8472	0.8464	0.8466	0.8057	0.8012
Case 13 1.8/180	0.7916	0.7900	0.7910	0.7454	0.7494
Case 14 18/180	0.8438	0.8423	0.8432	0.7820	0.7864
Case 15 180/180	0.8193	0.8182	0.8190	0.7863	0.7827

Table 4.13 displays the time average zero delay cross correlation coefficients calculated for periods of active geomagnetic activity. While general trends are observed in these results, there are a few notable differences. In particular, the cross correlation coefficients are reduced in magnitude and cover a slightly wider range of values during periods of active geomagnetic activity. Also, the differences between the POE estimated density generated from using the Jacchia and MSIS family of baseline models are more pronounced as the geomagnetic activity level increases. The HASDM density is better

correlated to the accelerometer density data to most of the POE density estimate data sets. However, some of the POE estimate densities have the highest degree of correlation with the accelerometer density.

Table 4.14 Time Averaged Maximum Cross Correlation Coefficients for Solutions with Active Geomagnetic Activity. *The columns of density models are the baseline models used for the POE estimated density and not the actual models themselves. Yellow (or light gray) highlighted numbers indicate the largest value for the baseline model. The orange (or darker gray) highlighted number indicates the largest overall number. The cross correlation coefficient for the Jacchia 1971 empirical model is 0.6507. The cross correlation coefficient for the HASDM density is 0.8394.*

Half-Life Combinations, Density/Ballistic Coefficient (min)	*CIRA-1972*	*Jacchia 1971*	*Jacchia-Roberts*	*MSISE-1990*	*NRLMSISE-2000*
Case 1 1.8/1.8	0.8551	0.8538	0.8544	0.8004	0.7999
Case 2 18/1.8	0.8666	0.8651	0.8659	0.8089	0.8099
Case 3 180/1.8	0.8503	0.8493	0.8496	0.8128	0.8093
Case 7 1.8/18	0.8372	0.8359	0.8364	0.7831	0.7829
Case 8 18/18	0.8634	0.8620	0.8627	0.8030	0.8036
Case 9 180/18	0.8481	0.8474	0.8475	0.8075	0.8030
Case 13 1.8/180	0.7933	0.7916	0.7926	0.7475	0.7514
Case 14 18/180	0.8457	0.8442	0.8451	0.7840	0.7876
Case 15 180/180	0.8209	0.8197	0.8206	0.7890	0.7847

Table 4.14 gives the time averaged maximum cross correlation coefficients for the active geomagnetic activity bin. The same general trends can be observed for these results as were seen in the previous table. The effect of geomagnetic activity on the estimated density is clearly visible in the three different bins of geomagnetic activity. As the activity level increases, the correlation of the various density estimates with the accelerometer density decreases. These results are expected given that as the energy received by the atmosphere increases, the resulting density variations will become more difficult to model and therefore estimate.

The time averaged zero delay and maximum cross correlations demonstrate that as the geomagnetic activity increases from moderate to active the half-life combination giving

the highest degree of correlation with the accelerometer density changes only for the POE density estimate using MSISE-1990 as the baseline atmospheric model. For active geomagnetic activity, the best half-life combination is a density correlated half-life of 18 minutes and a ballistic coefficient correlated half-life of 1.8 minutes for the POE density estimates using the Jacchia family of baseline models and the NRLMSISE-2000 baseline model. Also, the POE density estimates using MSISE-1990 as the baseline model has the highest degree of correlation for a density correlated half-life of 180 minutes and a ballistic coefficient correlated half-life of 1.8 minutes. During active geomagnetic activity levels, the overall highest degree of correlation of the POE density estimate with the accelerometer now corresponds to the CIRA-1972 baseline model with a density and ballistic coefficient correlated half-life combination of 18 and 1.8 minutes, respectively.

4.2.4 Summary of the Geomagnetic Activity Bins

The impact of the geomagnetic activity on the atmospheric density can be seen in the cross correlation coefficients relating the POE density estimates to the accelerometer density. Specifically, as the level of geomagnetic activity increases, the degree of correlation between the POE density estimates and the accelerometer density generally experiences a slight reduction. Also, the greatest change in the best half-life combination is observed as the geomagnetic activity increases from quiet to moderate. However, very little change is observed in the best combination of half-lives when moving from periods of moderate to active geomagnetic activity. Even though the best half-life combination does change as a function of geomagnetic activity level, the best half-life combination tend to consist of density and ballistic coefficient correlated half-lives of 1.8 to 18 minutes. These results would also suggest that the Jacchia family of baseline atmospheric models provides the best

results in generated POE density estimates. In particular, CIRA-1972 is the most frequent best baseline model in the results.

4.3 Representative Days for the Solar and Geomagnetic Activity Bins

The following days are representative examples of the results obtained for the solar and geomagnetic activity bins. The results are meant to cover the extremes and midrange values to offer general conclusions based on the solar and geomagnetic activity levels. Because each day has a solar and geomagnetic activity bin classification, specific days were selected that collectively contained all of the solar and geomagnetic bins. The days selected are April 23, 2002, October 29, 2003, January 16, 2004, and September 9, 2007. The April date covers the elevated solar and moderate geomagnetic activity bins. The October date falls in the high solar and active geomagnetic bins. The January solution is classified as a moderate solar and moderate geomagnetic activity bin. The September period goes into the low solar and quiet geomagnetic bins. The representative example for January 16, 2004 was given in chapter 3 along with a discussion of the results. A summary of the results for the January date are given later in this chapter. For all dates examined CHAMP was in a near circular orbit with an inclination of 87 degrees. At midnight April 23, 2002 CHAMP was at altitude of about 389 km. At 10 a.m. October 29, 2003 CHAMP was at an approximate altitude of 381 km. At 10 a.m. January 16, 2004 CHAMP had an altitude of about 374 km. At 10 a.m. September 9, 2007 CHAMP was at an approximate altitude of 338 km.

4.3.1 April 23, 2002 Covering Elevated Solar and Moderate Geomagnetic Activity

Table 4.15 Zero Delay Cross Correlation Coefficients for 0000-2400 Hours April 23, 2002. *The columns of density models are the baseline models used for the POE estimated density and not the actual models themselves. Yellow (or light gray) highlighted numbers indicate the largest value for the baseline model. The orange (or darker gray) highlighted number indicates the largest overall number. The cross correlation coefficient for the Jacchia 1971 empirical model is 0.7696. The cross correlation coefficient for the HASDM density is 0.9000.*

Half-Life Combinations, Density/Ballistic Coefficient (min)	*CIRA-1972*	*Jacchia 1971*	*Jacchia-Roberts*	*MSISE-1990*	*NRLMSISE-2000*
Case 1 1.8/1.8	0.9220	0.9214	0.9214	0.8454	0.8536
Case 2 18/1.8	0.9353	0.9346	0.9347	0.8519	0.8643
Case 3 180/1.8	0.9081	0.9078	0.9077	0.8378	0.8448
Case 7 1.8/18	0.9072	0.9068	0.9067	0.8347	0.8418
Case 8 18/18	0.9303	0.9296	0.9297	0.8436	0.8553
Case 9 180/18	0.9020	0.9017	0.9016	0.8234	0.8300
Case 13 1.8/180	0.8817	0.8811	0.8814	0.8271	0.8337
Case 14 18/180	0.8976	0.8963	0.8971	0.8300	0.8393
Case 15 180/180	0.8447	0.8430	0.8448	0.8143	0.8124

Table 4.16 Maximum Cross Correlation Coefficients for 0000-2400 Hours April 23, 2002. *The columns of density models are the baseline models used for the POE estimated density and not the actual models themselves. Yellow (or light gray) highlighted numbers indicate the largest value for the baseline model. The orange (or darker gray) highlighted number indicates the largest overall number. The cross correlation coefficient for the Jacchia 1971 empirical model is 0.7699 with a 20 second delay . The cross correlation coefficient for the HASDM density is 0.9022 with a delay of -50 seconds. The values in parenthesis are the corresponding delays in seconds.*

Half-Life Combinations, Density/Ballistic Coefficient (min)	*CIRA-1972*	*Jacchia 1971*	*Jacchia-Roberts*	*MSISE-1990*	*NRLMSISE-2000*
Case 1 1.8/1.8	0.9280 (80)	0.9276 (80)	0.9275 (80)	0.8474 (50)	0.8556 (50)
Case 2 18/1.8	0.9361 (30)	0.9354 (30)	0.9355 (30)	0.8529 (40)	0.8650 (30)
Case 3 180/1.8	0.9095 (40)	0.9094 (40)	0.9092 (40)	0.8405 (60)	0.8467 (50)
Case 7 1.8/18	0.9120 (70)	0.9117 (70)	0.9116 (70)	0.8362 (40)	0.8433 (40)
Case 8 18/18	0.9308 (20)	0.9302 (20)	0.9302 (20)	0.8444 (30)	0.8559 (30)
Case 9 180/18	0.9039 (50)	0.9037 (50)	0.9035 (50)	0.8262 (60)	0.8320 (50)
Case 13 1.8/180	0.8864 (70)	0.8860 (70)	0.8862 (70)	0.8294 (50)	0.8359 (50)
Case 14 18/180	0.8980 (20)	0.8967 (20)	0.8975 (20)	0.8310 (40)	0.8399 (30)
Case 15 180/180	0.8452 (20)	0.8436 (30)	0.8453 (20)	0.8165 (50)	0.8138 (40)

Tables 4.15 and 4.16 display the zero delay and maximum cross correlation coefficients, respectively, for April 23, 2002. The solution corresponding to these results is a 24 hour fit span beginning at 0000 hours and ending at 2400 hours that day. This day has solar activity classified as elevated with a $F_{10.7}$ equal to 175.3 SFUs and a moderate geomagnetic bin category with an A_p of 27. The cross correlation coefficients calculated for

this day have their highest degree of correlation with the accelerometer density for the same combination of baseline model and half-lives as the overall summary and the time averaged tables for elevated solar and moderate geomagnetic activity bins.

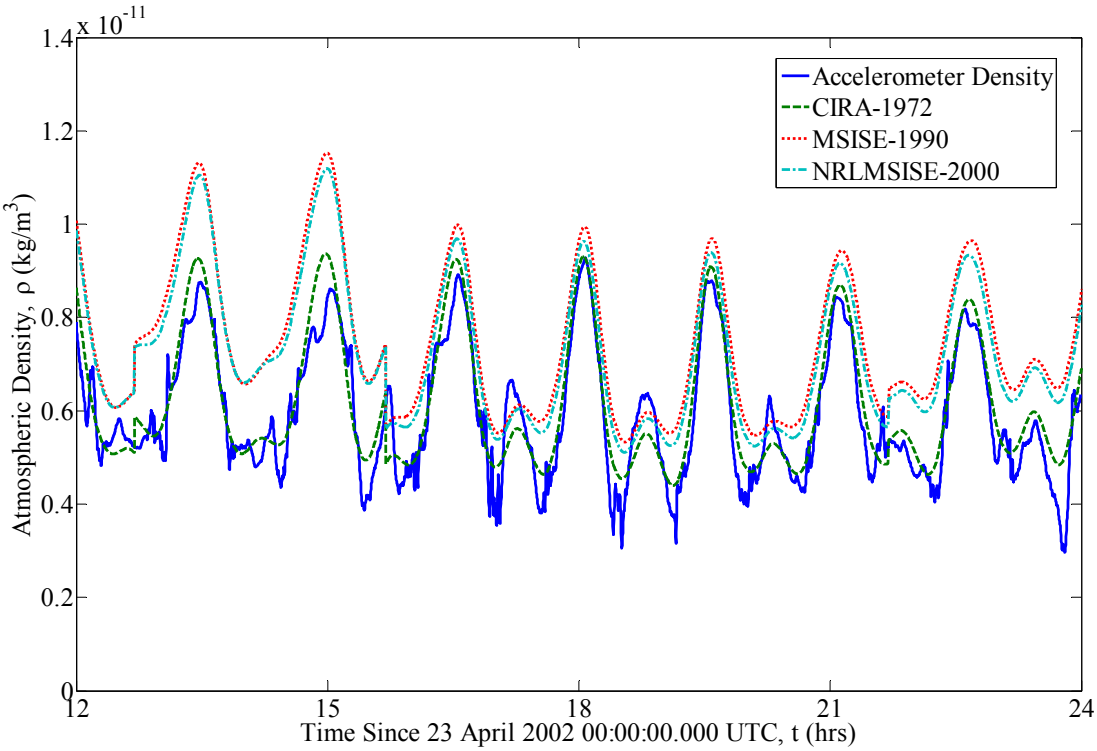

Figure 4.1 Effect of Varying the Baseline Atmospheric Model on the Estimated Density for 1200-2400 hours April 23, 2002. *Density and ballistic coefficient correlated half-lives are 18 and 1.8 minutes, respectively. The baseline density model is CIRA-1972.*

Figure 4.1 show the effect of varying the baseline atmospheric model on the POE estimated density for April 23, 2002. The MSISE-1990 and NRLMSISE-2000 baseline density models give similar results, which is expected given their common atmospheric model heritage. The CIRA-1972 baseline model provides the best agreement with the accelerometer density. All of the POE density estimates are capable of matching the general observed density structure but they fail to successfully model the rapid changes in density observed by the accelerometer. These results for varying the baseline density model are

typical for most solutions in these bins. The cross correlation coefficient results indicate that the POE density estimate using CIRA-1972 as the baseline atmospheric model is the best choice.

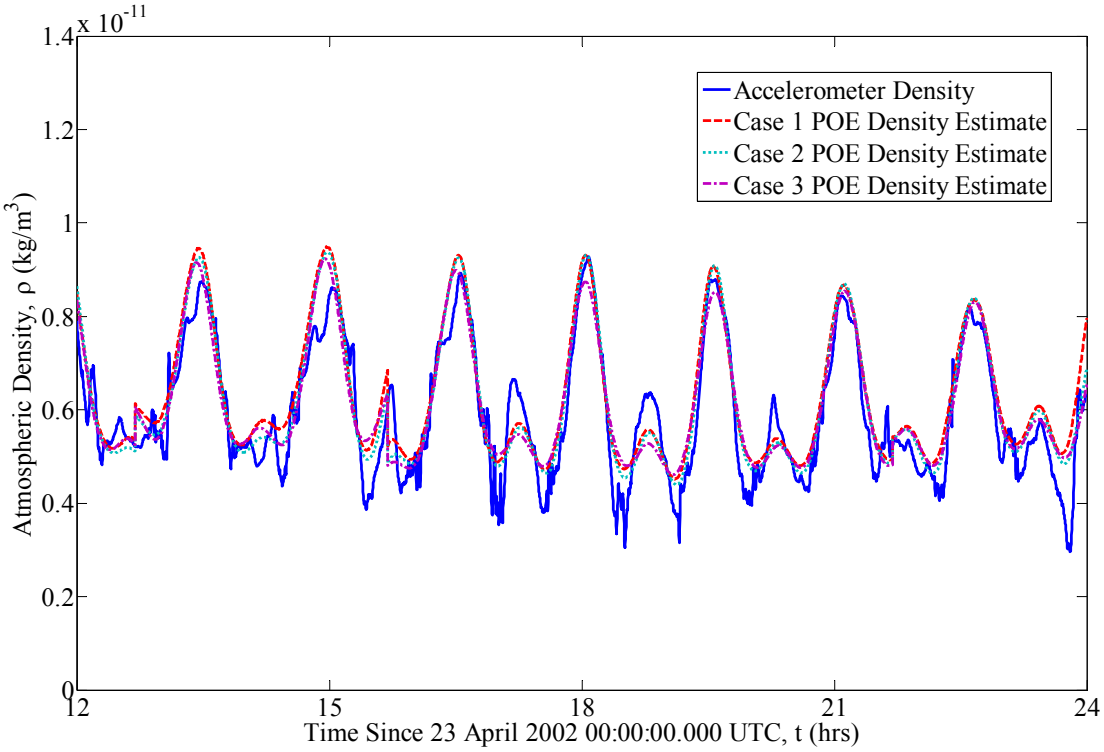

Figure 4.2 Effect of Varying the Density Correlated Half-Life on the Estimated Density for 1200-2400 hours April 23, 2002. *Ballistic coefficient correlated half-life is 1.8 minutes and the baseline density model is CIRA-1972. Cases 1, 2, and 3 have density correlated half-lives of 1.8, 18, and 180 minutes, respectively.*

Figure 4.2 demonstrates the behavior of the POE estimate density as the density correlated half-life is varied for a constant ballistic coefficient correlated half-life value. As the density correlated half-life is increased the POE density estimate is generally reduced. All of the variations still show relatively good agreement with the accelerometer density and show the ability of matching the basic density structure. The cross correlation coefficient results indicate that the best of the three POE density estimates is the one using values of 18 and 1.8 minutes for the density and ballistic coefficient correlated half-life, respectively.

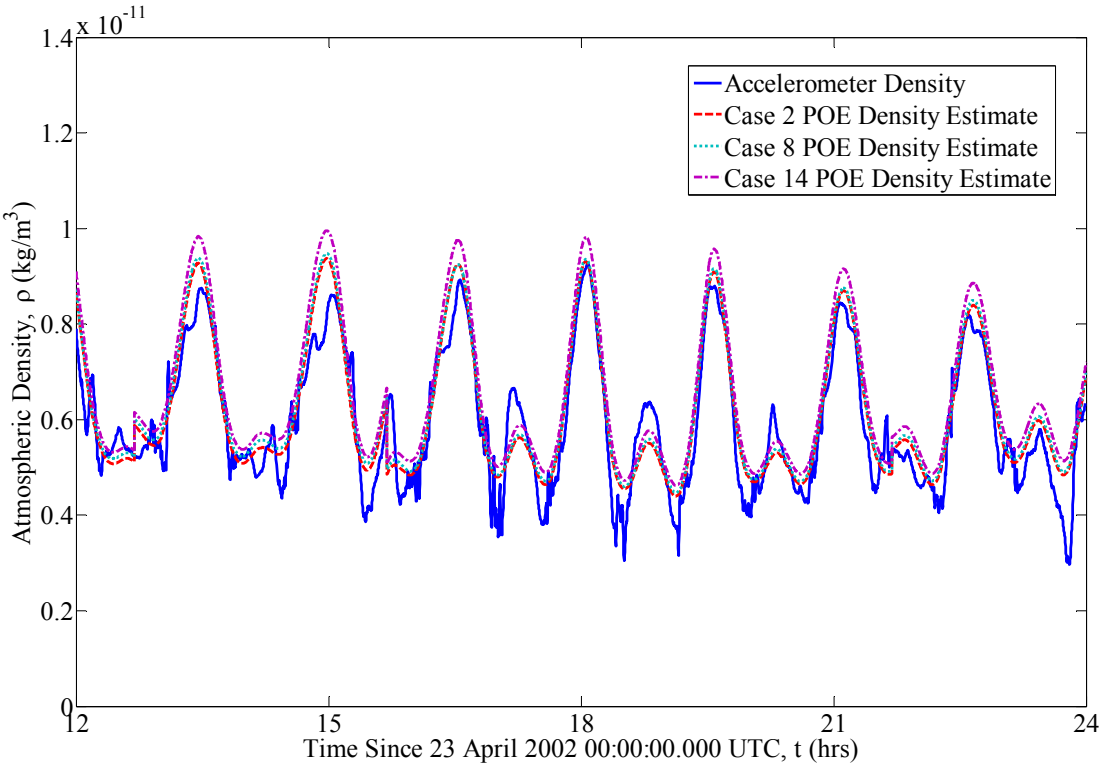

Figure 4.3 Effect of Varying the Ballistic Coefficient Correlated Half-Life on the Estimated Density for 1200-2400 hours April 23, 2002. *Density correlated half-life is 18 minutes and the baseline density model is CIRA-1972. Cases 2, 8, and 14 have ballistic coefficient correlated half-lives of 1.8, 18, and 180 minutes, respectively.*

Figure 4.3 shows how the POE density estimate is affected by variations in the ballistic coefficient correlated half-life for a constant density correlated half-life. This is the opposite consideration of the previous figure. The general effect of increasing the ballistic coefficient correlated half-life is to increase the POE estimated density. All of the variations are able to match the general structure of the accelerometer density data with primarily good agreement. Again, the cross correlation coefficient results indicate that the best of the three POE density estimates is the one using values of 18 and 1.8 minutes for the density and ballistic coefficient correlated half-life, respectively.

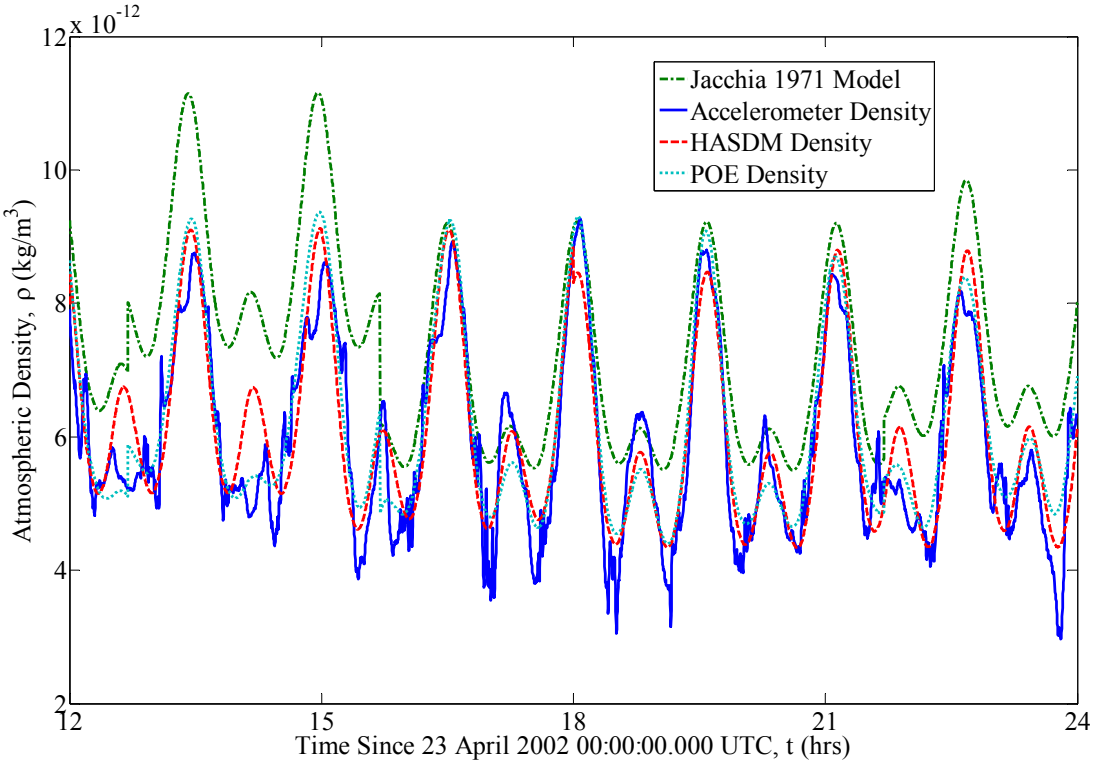

Figure 4.4 Comparison of Densities Obtained from Different Methods for 1200-2400 hours April 23, 2002. *POE density obtained using density and ballistic coefficient correlated half-lives of 18 and 1.8 minutes, respectively. CIRA-1972 is the baseline density model.*

Figure 4.4 compares the estimated densities obtained from four different approaches. The four methods used for comparison are the Jacchia 1971 empirical model, accelerometer derived density, HASDM derived density, and POE derived density data sets. This figure demonstrates the improvement achieved over the Jacchia 1971 empirical model by using either the HASDM or POE density estimates. The POE density estimate for this scenario generally has better agreement with the accelerometer density over the HASDM density. The Jacchia 1971 empirical model generally has the poorest agreement with the accelerometer density while the HASDM and POE densities offer comparable and relatively good results. These observation are also supported by the cross correlation coefficients given

previously where the coefficients for the POE and HASDM density estimates are higher than the coefficient for the Jacchia 1971 empirical model.

The residuals figure and the position and velocity consistency test graphs are not given for this day because there is little change observed in these graphs compared with those that have already been given or will be given. Please refer to these other graphs as representative of the results obtained for this particular day.

4.3.2 October 29, 2003 Covering High Solar and Active Geomagnetic Activity

Table 4.17 Zero Delay Cross Correlation Coefficients for 1000-2400 Hours October 29, 2003. *The columns of density models are the baseline models used for the POE estimated density and not the actual models themselves. Yellow (or light gray) highlighted numbers indicate the largest value for the baseline model. The orange (or darker gray) highlighted number indicates the largest overall number. The cross correlation coefficient for the Jacchia 1971 empirical model is 0.4406. The cross correlation coefficient for the HASDM density is 0.7619.*

Half-Life Combinations, Density/Ballistic Coefficient (min)	*CIRA-1972*	*Jacchia 1971*	*Jacchia-Roberts*	*MSISE-1990*	*NRLMSISE-2000*
Case 1 1.8/1.8	0.8188	0.8186	0.8187	0.7751	0.7283
Case 2 18/1.8	0.8180	0.8181	0.8185	0.7872	0.7440
Case 3 180/1.8	0.7950	0.7953	0.7955	0.7694	0.7243
Case 7 1.8/18	0.7890	0.7885	0.7885	0.7412	0.6943
Case 8 18/18	0.8377	0.8378	0.8380	0.7975	0.7559
Case 9 180/18	0.8195	0.8197	0.8198	0.7934	0.7475
Case 13 1.8/180	0.7061	0.7059	0.7067	0.6914	0.6447
Case 14 18/180	0.8317	0.8317	0.8317	0.7850	0.7391
Case 15 180/180	0.7889	0.7889	0.7898	0.7834	0.7113

Table 4.18 Maximum Cross Correlation Coefficients for 1000-2400 Hours October 29, 2003. *The columns of density models are the baseline models used for the POE estimated density and not the actual models themselves. Yellow (or light gray) highlighted numbers indicate the largest value for the baseline model. The orange (or darker gray) highlighted number indicates the largest overall number. The cross correlation coefficient for the Jacchia 1971 empirical model is 0.4432 with a -70 second delay . The cross correlation coefficient for the HASDM density is 0.7785 with a delay of -140 seconds. The values in parenthesis are the corresponding delays in seconds.*

Half-Life Combinations, Density/Ballistic Coefficient (min)	*CIRA-1972*	*Jacchia 1971*	*Jacchia-Roberts*	*MSISE-1990*	*NRLMSISE-2000*
Case 1 1.8/1.8	0.8192 (-20)	0.8190 (-30)	0.8191 (-30)	0.7800 (-80)	0.7299 (-50)
Case 2 18/1.8	0.8210 (-70)	0.8213 (-70)	0.8215 (-70)	0.7976 (-120)	0.7477 (-80)
Case 3 180/1.8	0.7992 (-80)	0.7997 (-80)	0.7997 (-80)	0.7777 (-120)	0.7297 (-90)
Case 7 1.8/18	0.7896 (-30)	0.7891 (-30)	0.7891 (-30)	0.7458 (-80)	0.6959 (-50)
Case 8 18/18	0.8409 (-60)	0.8411 (-70)	0.8412 (-60)	0.8081 (-120)	0.7597 (-70)
Case 9 180/18	0.8231 (-80)	0.8234 (-80)	0.8234 (-80)	0.7998 (-100)	0.7519 (-80)
Case 13 1.8/180	0.7076 (-40)	0.7075 (-50)	0.7082 (-40)	0.6972 (-90)	0.6465 (-50)
Case 14 18/180	0.8375 (-80)	0.8377 (-80)	0.8375 (-80)	0.7998 (-130)	0.7443 (-80)
Case 15 180/180	0.7953 (-90)	0.7955 (-90)	0.7963 (-90)	0.7971 (-140)	0.7181 (-100)

Tables 4.17 and 4.18 display the zero delay and maximum cross correlation coefficients, respectively, for October 29, 2003. The solution corresponding to these results is a 14 hour fit span beginning at 1000 hours and ending at 2400 hours that day. This day has solar activity classified as high with a $F_{10.7}$ equal to 279.1 SFUs and an active geomagnetic bin category with an A_p of 204. The cross correlation coefficients calculated for this day do

not have their highest degree of correlation with the accelerometer density for the same combination of baseline model and half-lives for the overall summary or the time averaged tables for elevated solar and moderate geomagnetic activity bins. This represents a situation where the individual solutions do not always agree even with the binned results, which is a difficult task given that both the solar and geomagnetic indices are being considered. However, while the half-life combinations of the individual day do not agree with the predicted binned combination, the POE density estimates for the stated baseline atmospheric models are very close both in terms of their cross correlation coefficients and their estimated density values.

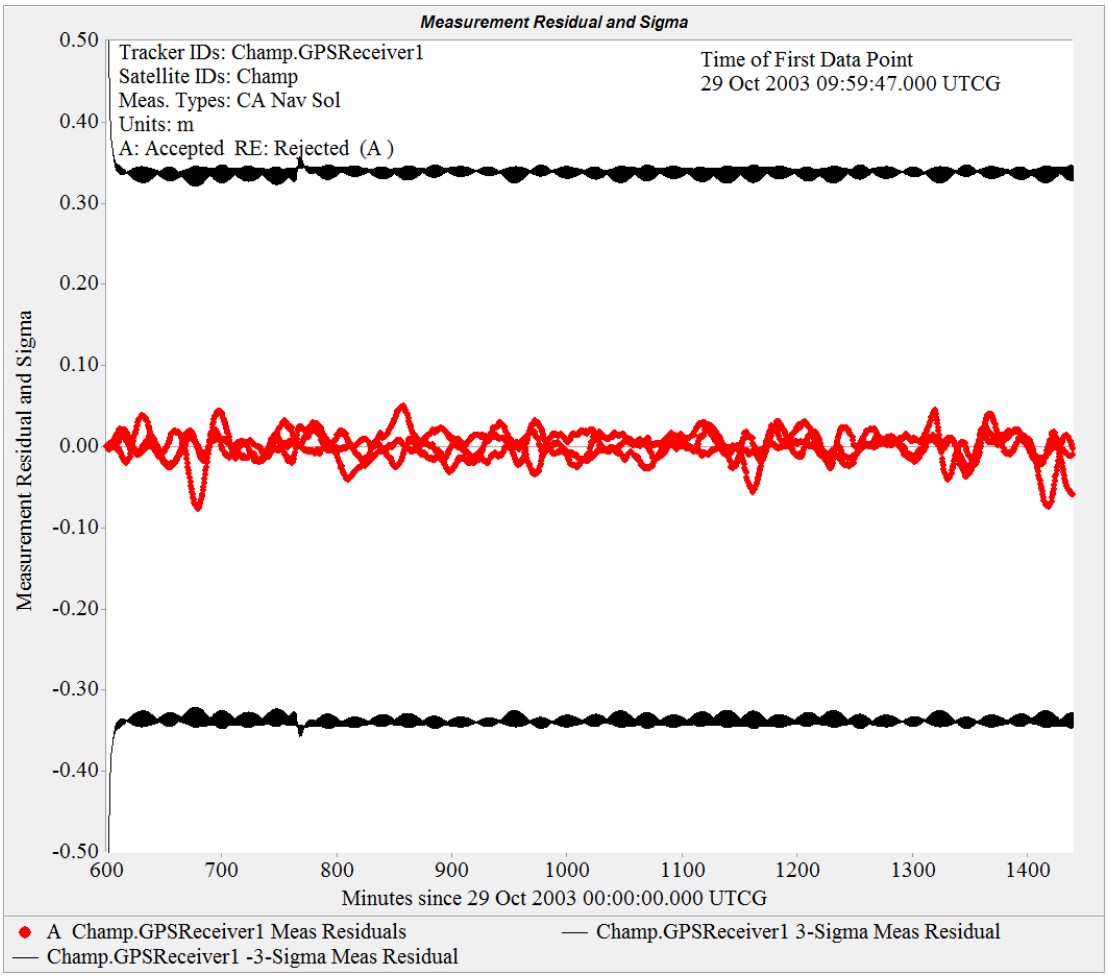

Figure 4.5 Filter Residuals for 1000-2400 Hours October 29, 2003. *Density and ballistic coefficient correlated half-lives are 18 minutes and the baseline density model is Jacchia-Roberts.*

Figure 4.5 displays the residuals for October 29, 2003. The 3σ boundary values are approximately 33 cm with the residual values falling to within about +5 to -8 cm. The residuals for this day are near the error associated with the precision orbit ephemerides used to calculate the POE estimated density. The residuals tend to increase for increasing solar or geomagnetic activity levels. These residuals are typical for most solutions that fall into the high solar or active geomagnetic bins.

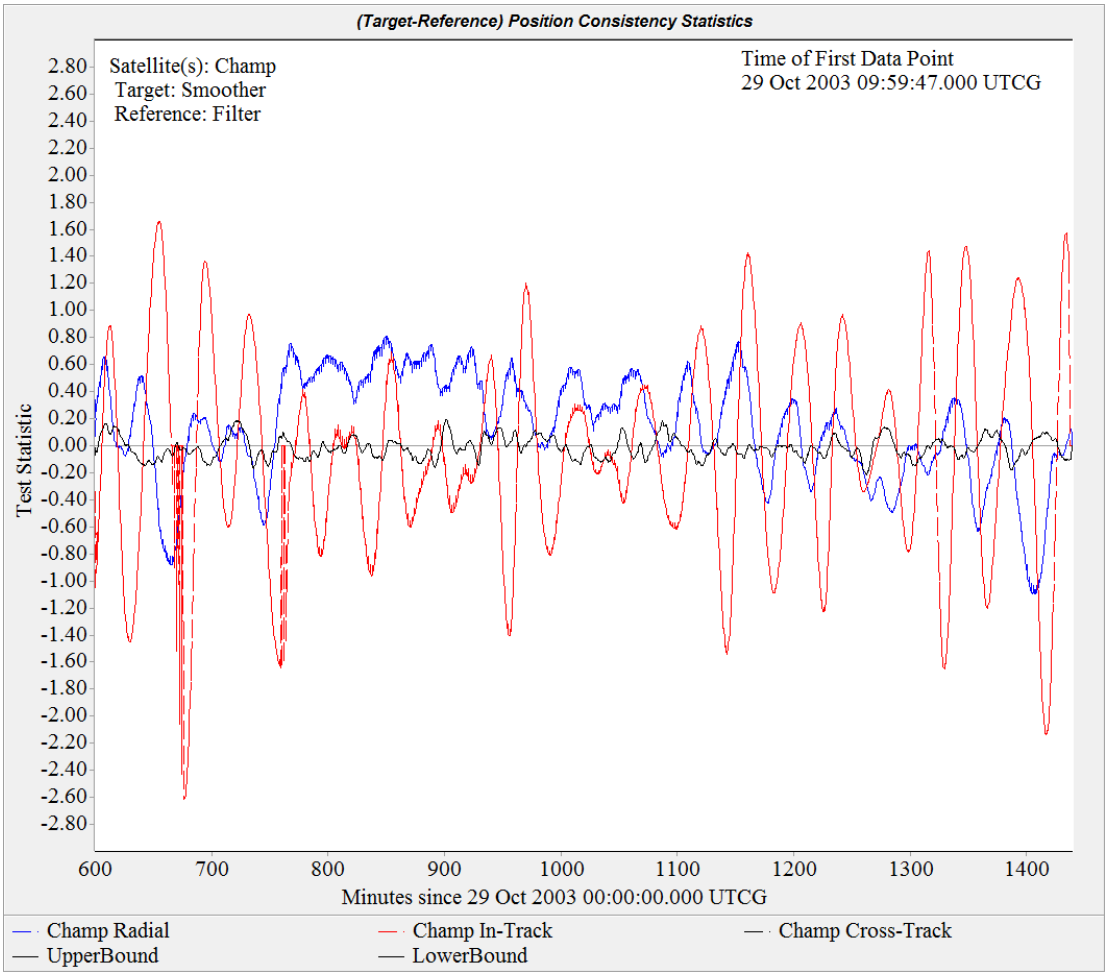

Figure 4.6 Position Consistency Test for 1000-2400 Hours October 29, 2003. *Density and ballistic coefficient correlated half-lives are 18 minutes and the baseline density model is Jacchia-Roberts.*

Figure 4.6 displays the position consistency test graph for October 29, 2003. The solution satisfies the position consistency test for all times. The position consistency test moves farther away from zero as the solar or geomagnetic activity levels increases. This is a typical graph of the position consistency test for solutions classified by high solar or active geomagnetic activity levels.

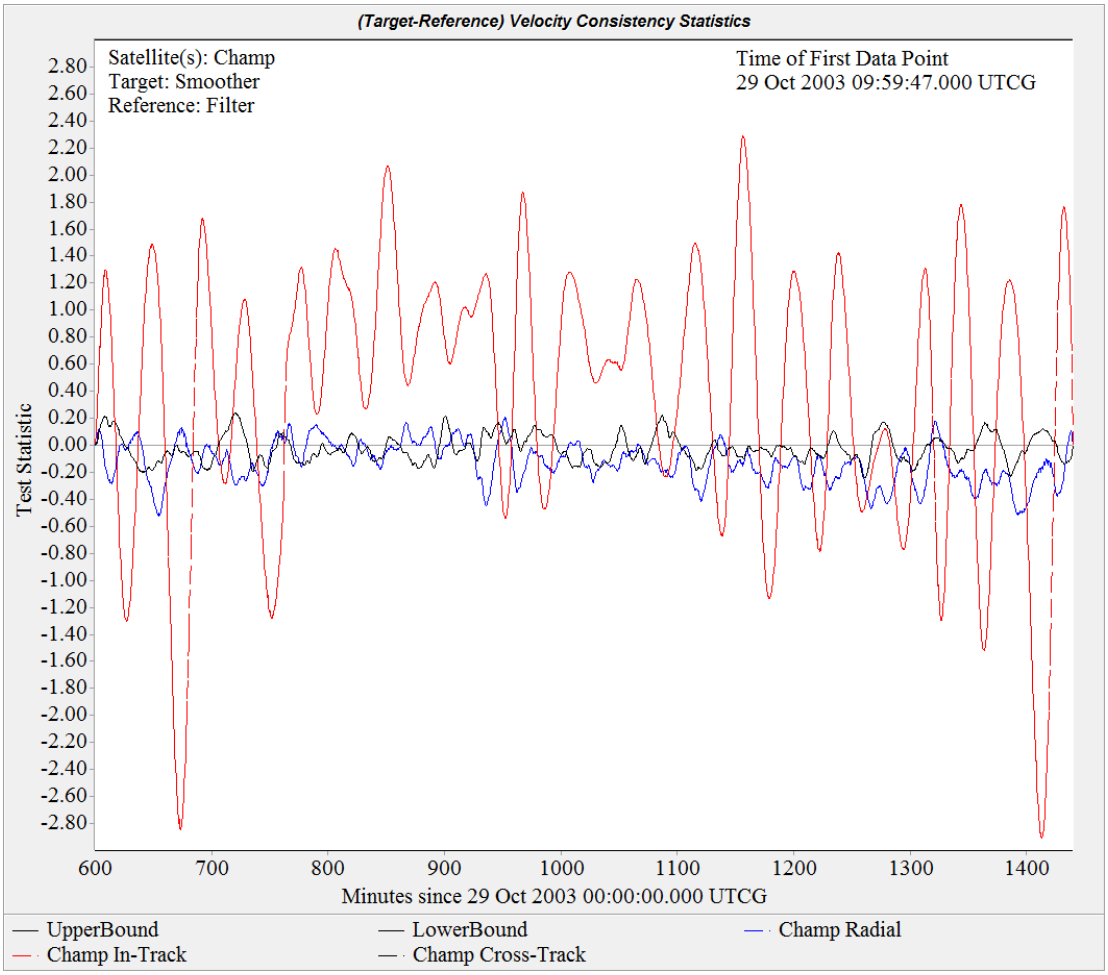

Figure 4.7 Velocity Consistency Test for 1000-2400 Hours October 29, 2003. *Density and ballistic coefficient correlated half-lives are 18 minutes and the baseline density model is Jacchia-Roberts.*

Figure 4.7 displays the velocity consistency test graph for October 29, 2003. The solution satisfies the velocity consistency test for all times. The velocity consistency test moves farther away from zero as the solar or geomagnetic activity levels increases. This is a typical graph of the velocity consistency test for solutions classified by high solar or active geomagnetic activity levels.

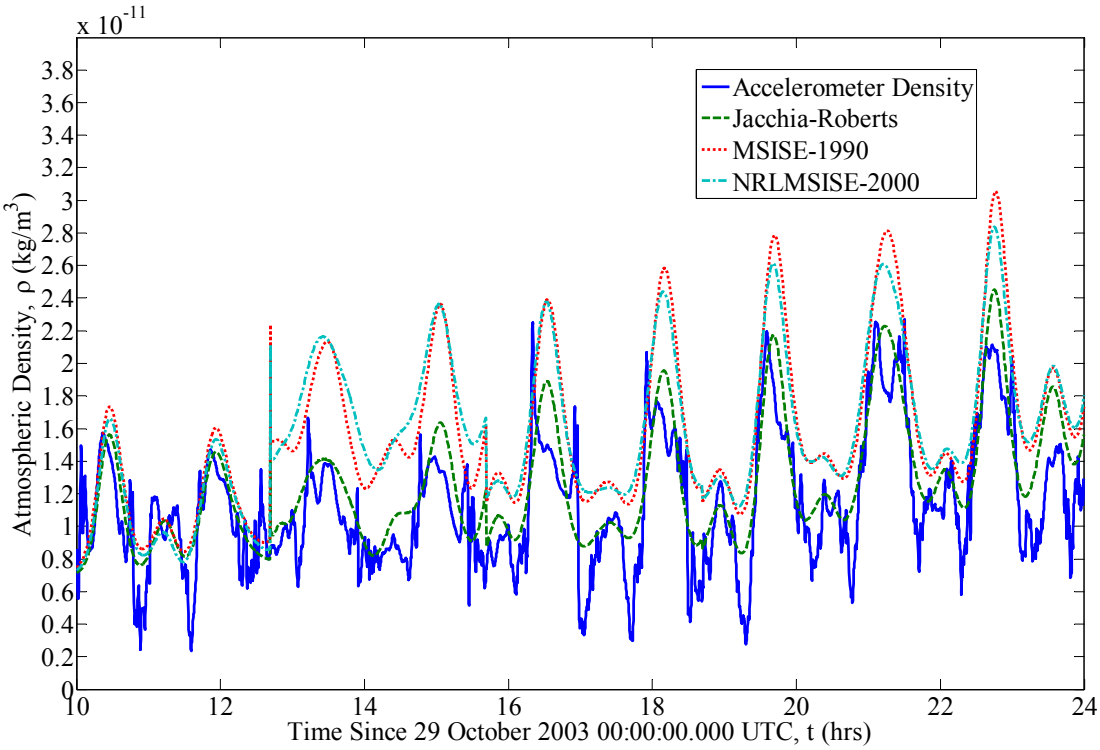

Figure 4.8 Effect of Varying the Baseline Atmospheric Model on the Estimated Density for 1000-2400 hours October 29, 2003. *Density and ballistic coefficient correlated half-lives are 18 minutes and the baseline density model is Jacchia-Roberts.*

Figure 4.8 demonstrates how changing the baseline atmospheric model influences the POE estimated density. As seen previously, the MSISE-1990 and NRLMSISE-2000 baseline models produce similar results. However, when the solar or geomagnetic activity level increases, the differences between these two baseline models also increases as observed in this figure. The Jacchia-Roberts baseline atmospheric model provides the best agreement with the accelerometer density and in particular more closely matches the peaks and valleys in the accelerometer density. All three POE density estimates are capable of matching the general density structure measured by the accelerometer but are unable to follow the rapid changes in density. The cross correlation coefficient results indicate that the POE density estimate using Jacchia-Roberts as the baseline atmospheric model is the best choice.

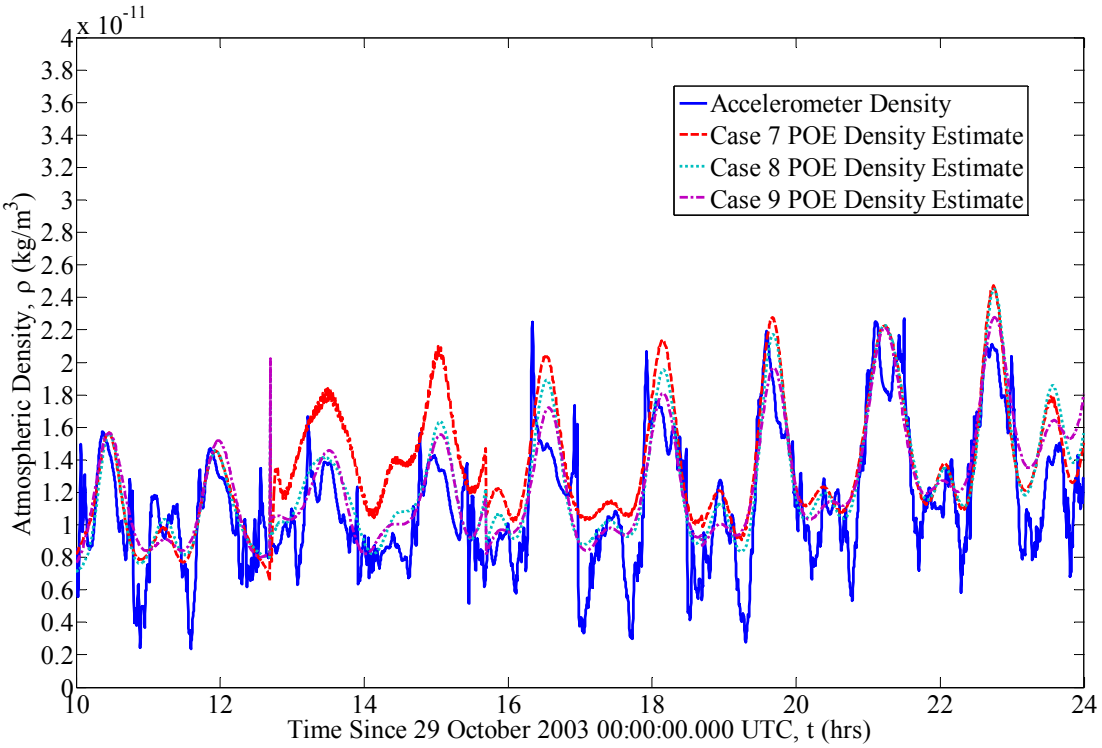

Figure 4.9 Effect of Varying the Density Correlated Half-Life on the Estimated Density for 1000-2400 hours October 29, 2003. *Ballistic coefficient correlated half-life is 18 minutes and the baseline density model is Jacchia-Roberts. Cases 7, 8, and 9 have density correlated half-lives of 1.8, 18, and 180 minutes, respectively.*

Figure 4.9 shows the effects of varying the density correlated half-life on the POE estimated density for a constant value of the ballistic coefficient correlated half-life. The general effect of increasing the density correlated half-life is a decrease in the estimated density. This result was observed for April 23, 2002 but the influence of varying the density half-life is more pronounced for October 29, 2003 where the solar and geomagnetic activity levels have increased. The cross correlation coefficient results indicate that the best of the three POE density estimates is the one with density and ballistic coefficient correlated half-lives of 18 minutes each.

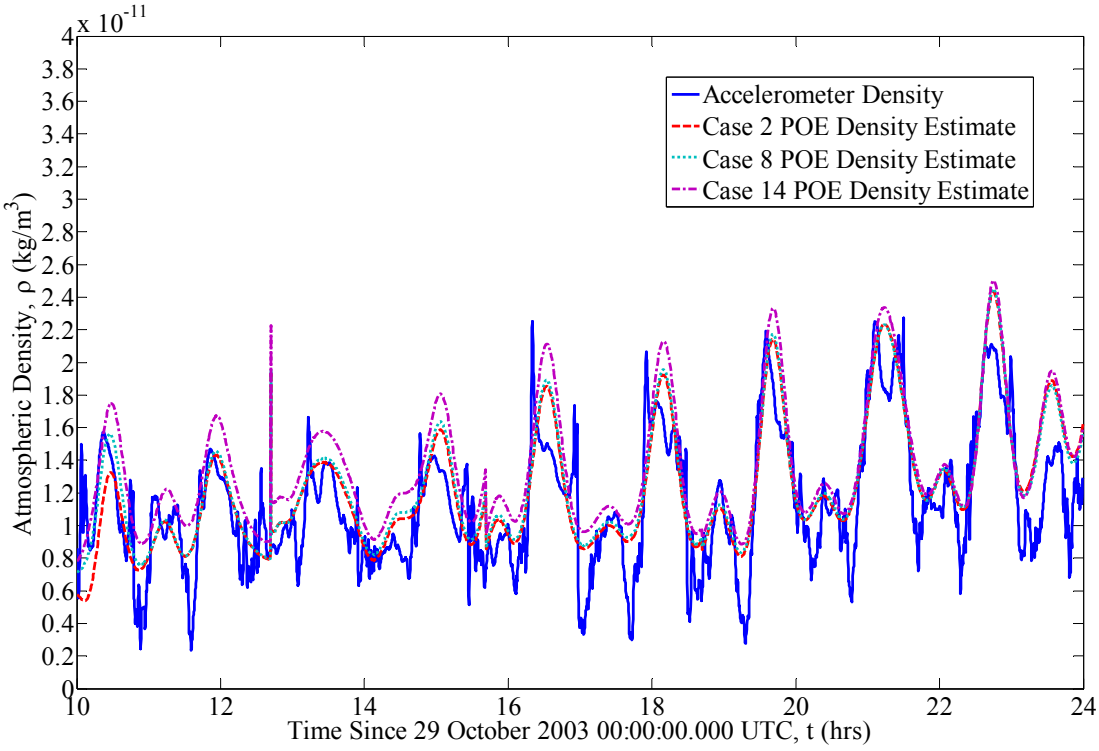

Figure 4.10 Effect of Varying the Ballistic Coefficient Correlated Half-Life on the Estimated Density for 1000-2400 hours October 29, 2003. *Density correlated half-life is 18 minutes and the baseline density model is Jacchia-Roberts. Cases 2, 8, and 14 have ballistic coefficient correlated half-lives of 1.8, 18, and 180 minutes, respectively.*

Figure 4.10 demonstrates the influence of varying the ballistic coefficient correlated half-life on the POE estimate density using a constant density correlated half-life. Variation of the ballistic coefficient half-life produces the opposite effects compared with the results seen when the density correlated half-life is varied. As the ballistic coefficient half-life is increased the estimated density is also increased. The influence of the ballistic coefficient half-life variation is slightly more pronounced for periods of high solar and active geomagnetic activity. Again, the cross correlation coefficient results indicate that the best of the three POE density estimates is the one with density and ballistic coefficient correlated half-lives of 18 minutes each.

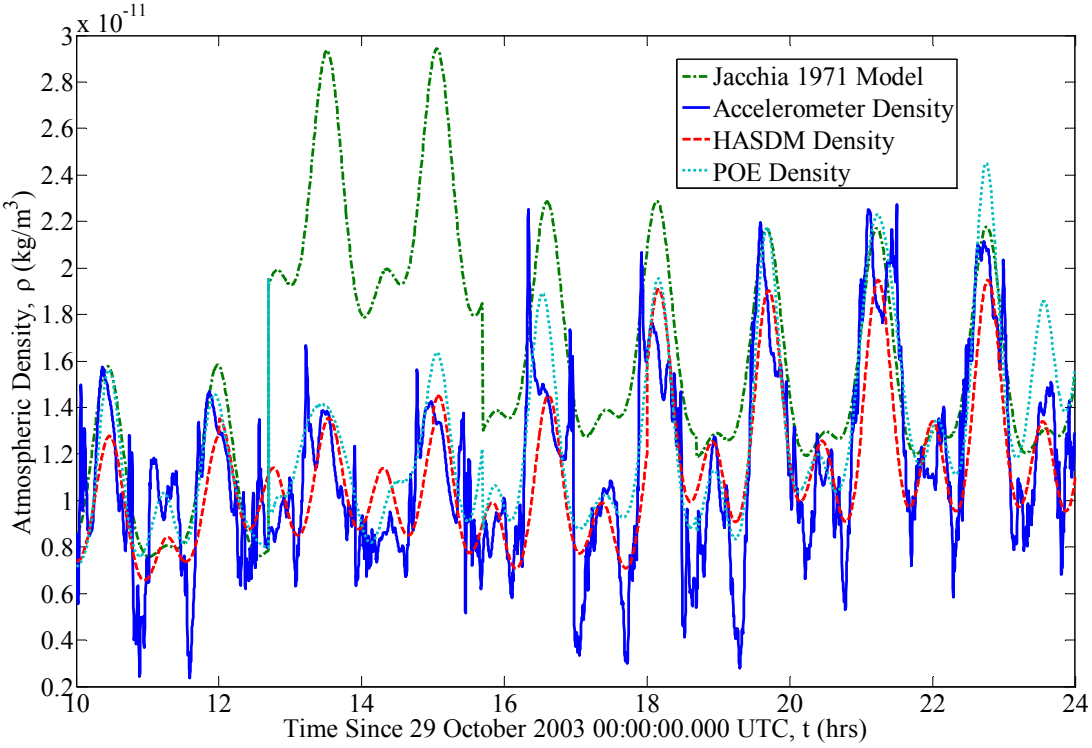

Figure 4.11 Comparison of Densities Obtained from Different Methods for 1000-2400 hours October 29, 2003. *POE density obtained using density and ballistic coefficient correlated half-lives of 18 minutes each and Jacchia-Roberts as the baseline density model.*

Figure 4.11 offers another comparison of the various methods for estimating density using the same four approaches mentioned previously. The same general trends are visible, especially the improvement of the POE and HASDM density over the Jacchia 1971 empirical model. Also, during periods of high solar and geomagnetic activity, the Jacchia 1971 empirical model has extreme difficulty in accurately estimating the density as seen by the large jump in its density estimate. HASDM and POE density estimates do not experience this problem and continue to have relatively good agreement with the accelerometer density. In particular, the POE estimated density might initially follow the baseline atmospheric model in an erroneous jump in density but quickly returns to a good match with the accelerometer density. The HASDM and POE density estimates provide comparable results. The Jacchia

1971 empirical model offers the least accurate estimate of density using the accelerometer density as truth. These observation are also supported by the cross correlation coefficients given previously where the coefficients for the POE and HASDM density estimates are higher than the coefficient for the Jacchia 1971 empirical model.

4.3.3 January 16, 2004 Covering Moderate Solar and Moderate Geomagnetic Activity

January 16, 2004 was presented and discussed in the previous chapter and the information will not be repeated here. The solution corresponding to these results is a 14 hour fit span beginning at 1000 hours and ending at 2400 hours that day. This day has solar activity classified as moderate with a $F_{10.7}$ equal to 120.3 SFUs and a moderate geomagnetic bin category with an A_p of 29. The cross correlation coefficients calculated for this day do not have their highest degree of correlation with the accelerometer density for the overall summary. This is another situation where the half-life combination and baseline atmospheric model predicted by the binned results do not turn out to be best.

The residuals fall well within the 3σ boundaries with amplitude of 5 to 7 cm, which are near the errors associated with the precision orbit ephemerides used to generate the POE density estimates. The position and velocity consistency tests are well satisfied for all times. The residual figure and position and velocity consistency test graphs show typical results for days that are characterized by moderate solar and moderate geomagnetic activity. The effects of varying the density and ballistic coefficient correlated half-lives and baseline atmospheric model on the POE density estimate are similar to the results obtained from the other days considered in this chapter. The HASDM and POE density estimates offer improvements over the Jacchia 1971 empirical model. Also, the HASDM and POE estimated densities are comparable with one another. The cross correlation coefficients obtained for this day and bin

support these observations. A more detailed discussion for January 16, 2004 including the associated tables and graphs are given in the previous chapter.

4.3.4 September 9, 2007 Covering Low Solar and Quiet Geomagnetic Activity

Table 4.19 Zero Delay Cross Correlation Coefficients for 1000-2400 Hours September 9, 2007. *The columns of density models are the baseline models used for the POE estimated density and not the actual models themselves. Yellow (or light gray) highlighted numbers indicate the largest value for the baseline model. The orange (or darker gray) highlighted number indicates the largest overall number. The cross correlation coefficient for the Jacchia 1971 empirical model is 0.9589. The cross correlation coefficient for the HASDM density is 0.9424.*

Half-Life Combinations, Density/Ballistic Coefficient (min)	*CIRA-1972*	*Jacchia 1971*	*Jacchia-Roberts*	*MSISE-1990*	*NRLMSISE-2000*
Case 1 1.8/1.8	0.9489	0.9500	0.9472	0.9414	0.9415
Case 2 18/1.8	0.9625	0.9626	0.9621	0.9600	0.9606
Case 3 180/1.8	0.9664	0.9662	0.9660	0.9660	0.9664
Case 7 1.8/18	0.9591	0.9598	0.9590	0.9552	0.9549
Case 8 18/18	0.9637	0.9638	0.9634	0.9618	0.9623
Case 9 180/18	0.9663	0.9658	0.9655	0.9669	0.9671
Case 13 1.8/180	0.9615	0.9618	0.9616	0.9600	0.9600
Case 14 18/180	0.9631	0.9630	0.9628	0.9630	0.9635
Case 15 180/180	0.9578	0.9569	0.9559	0.9632	0.9632

Table 4.20 Maximum Cross Correlation Coefficients for 1000-2400 Hours September 9, 2007. *The columns of density models are the baseline models used for the POE estimated density and not the actual models themselves. Yellow (or light gray) highlighted numbers indicate the largest value for the baseline model. The orange (or darker gray) highlighted number indicates the largest overall number. The cross correlation coefficient for the Jacchia 1971 empirical model is 0.9607with a -40 second delay. The cross correlation coefficient for the HASDM density is 0.9425 with a delay of -10 seconds. The values in parenthesis are the corresponding delays in seconds.*

Half-Life Combinations, Density/Ballistic Coefficient (min)	*CIRA-1972*	*Jacchia 1971*	*Jacchia-Roberts*	*MSISE-1990*	*NRLMSISE-2000*
Case 1 1.8/1.8	0.9605 (-110)	0.9613 (-110)	0.9597 (-120)	0.9535 (-120)	0.9530 (-120)
Case 2 18/1.8	0.9697 (-90)	0.9696 (-90)	0.9694 (-90)	0.9672 (-90)	0.9673 (-90)
Case 3 180/1.8	0.9702 (-60)	0.9700 (-60)	0.9699 (-60)	0.9699 (-60)	0.9702 (-60)
Case 7 1.8/18	0.9649 (-80)	0.9654 (-80)	0.9650 (-80)	0.9609 (-80)	0.9604 (-80)
Case 8 18/18	0.9699 (-80)	0.9698 (-80)	0.9697 (-80)	0.9680 (-80)	0.9681 (-80)
Case 9 180/18	0.9698 (-60)	0.9693 (-60)	0.9691 (-60)	0.9704 (-60)	0.9706 (-60)
Case 13 1.8/180	0.9649 (-60)	0.9651 (-60)	0.9650 (-60)	0.9632 (-60)	0.9630 (-60)
Case 14 18/180	0.9682 (-70)	0.9681 (-70)	0.9678 (-70)	0.9677 (-70)	0.9679 (-70)
Case 15 180/180	0.9607 (-60)	0.9598 (-60)	0.9588 (-60)	0.9661 (-60)	0.9659 (-50)

Tables 4.19 and 4.20 display the zero delay and maximum cross correlation coefficients, respectively, for September 9, 2007. The solution corresponding to these results is a 14 hour fit span beginning at 1000 hours and ending at 2400 hours that day. This day has solar activity classified as low with a $F_{10.7}$ equal to 66.7 SFUs and a quiet geomagnetic bin category

with an A_p of 3. The cross correlation coefficients calculated for this day do not have their highest degree of correlation with the accelerometer density for the overall summary.

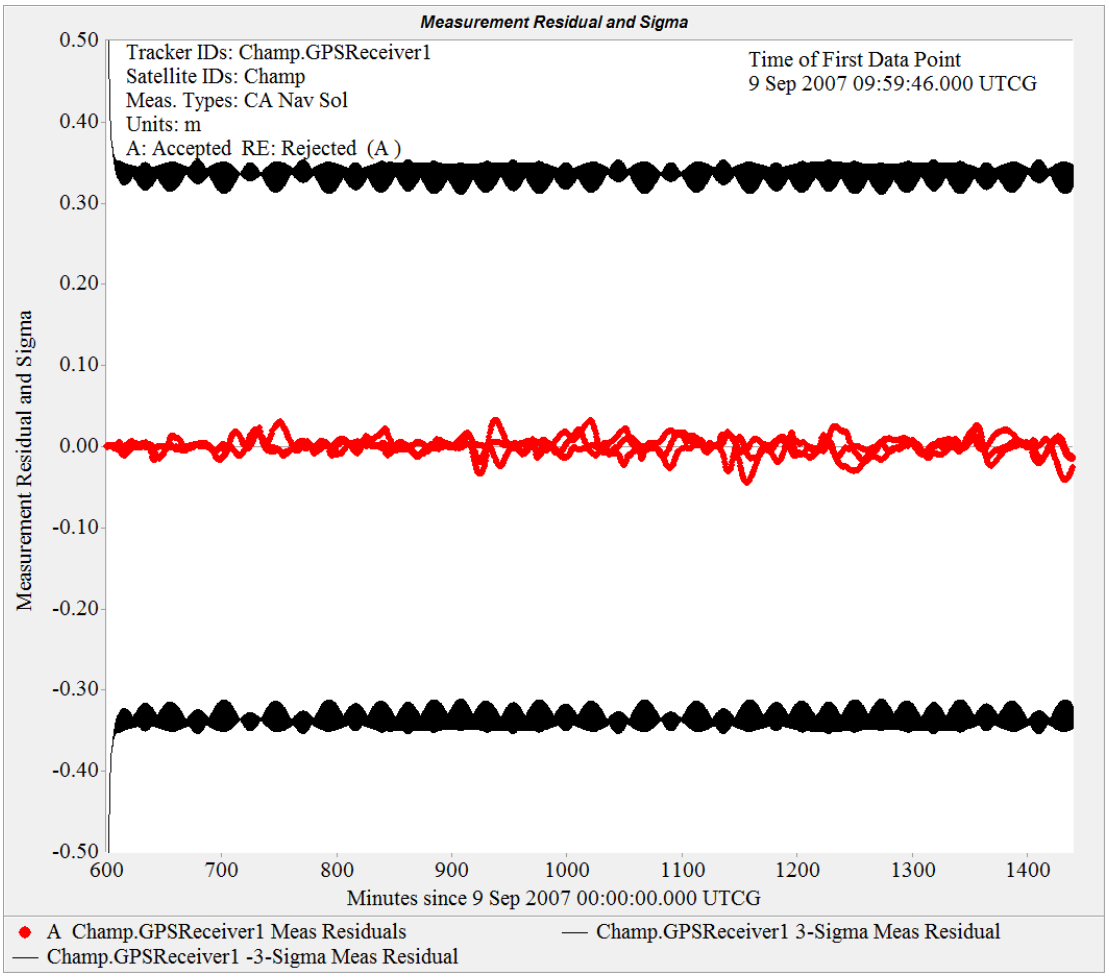

Figure 4.12 Filter Residuals for 1000-2400 Hours September 9, 2007. *Density and ballistic coefficient correlated half-lives are 180 and 18 minutes, respectively. The baseline density model is NRLMSISE-2000.*

Figure 4.12 displays the residuals for September 9, 2007. The 3σ boundary values are approximately 33 cm with the residual values falling to within about +4 to -4 cm. The residuals for this day are less than the error associated with the precision orbit ephemerides used to calculate the POE estimated density. The residuals tend to increase for increasing

solar or geomagnetic activity levels. These residuals are typical for most solutions that fall into the low solar or quiet geomagnetic bins.

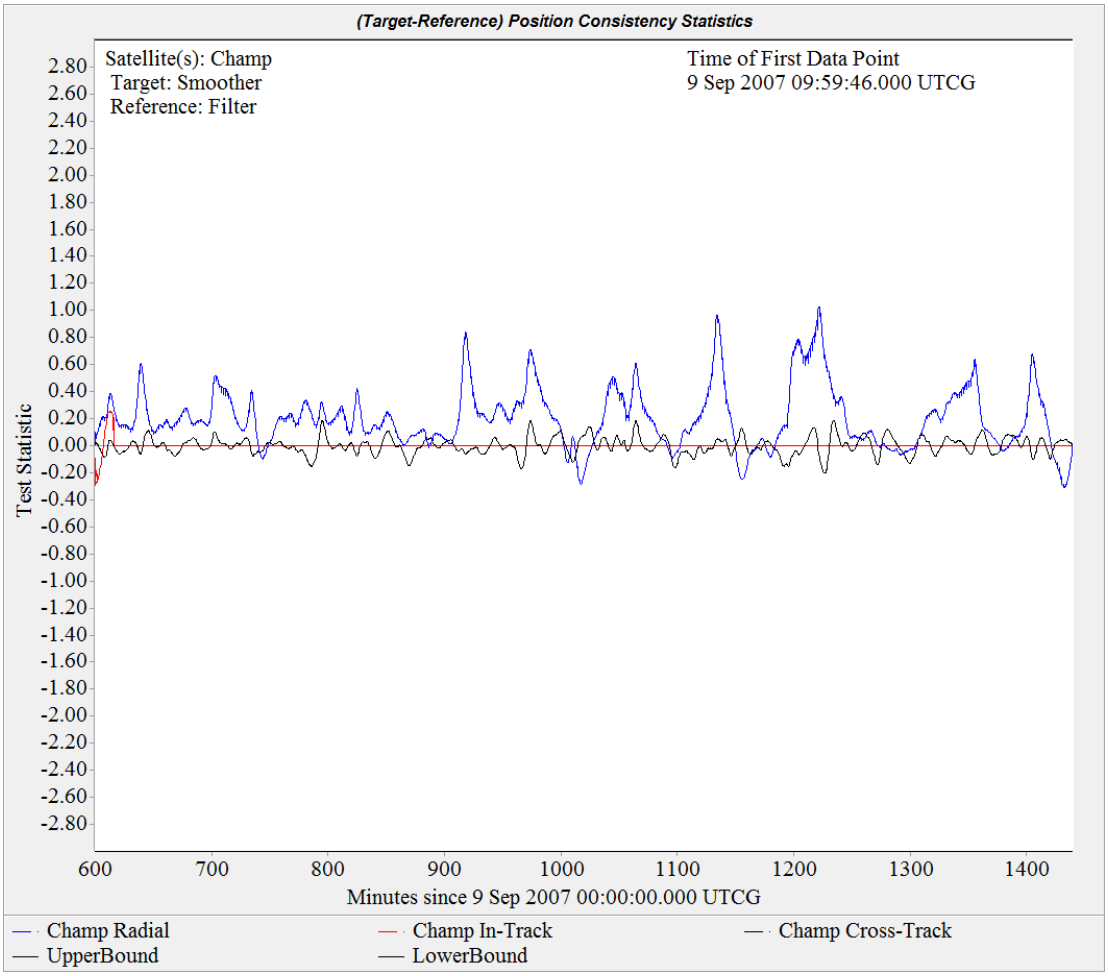

Figure 4.13 Position Consistency Test for 1000-2400 Hours September 9, 2007. *Density and ballistic coefficient correlated half-lives are 180 and 18 minutes, respectively. The baseline density model is NRLMSISE-2000.*

Figure 4.13 displays the position consistency test graph for September 9, 2007. The solution satisfies the position consistency test for all times. The position consistency test moves farther away from zero as the solar or geomagnetic activity levels increases. This is a typical graph of the position consistency test for solutions classified by low solar or quiet geomagnetic activity levels.

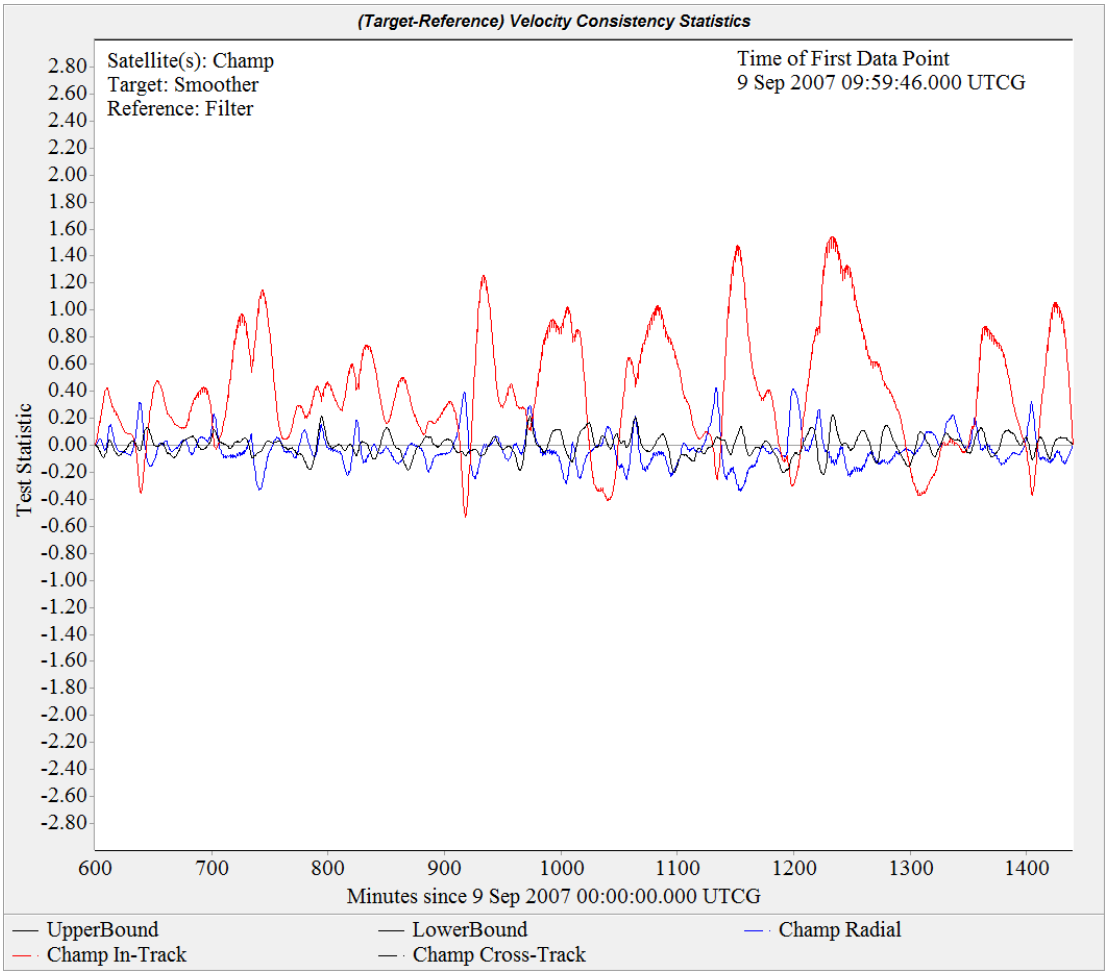

Figure 4.14 Velocity Consistency Test for 1000-2400 Hours September 9, 2007. *Density and ballistic coefficient correlated half-lives are 180 and 18 minutes, respectively. The baseline density model is NRLMSISE-2000.*

Figure 4.14 displays the velocity consistency test graph for September 9, 2007. The solution satisfies the velocity consistency test for all times. The velocity consistency test moves farther away from zero as the solar or geomagnetic activity levels increases. This is a typical graph of the velocity consistency test for solutions classified by low solar or quiet geomagnetic activity levels.

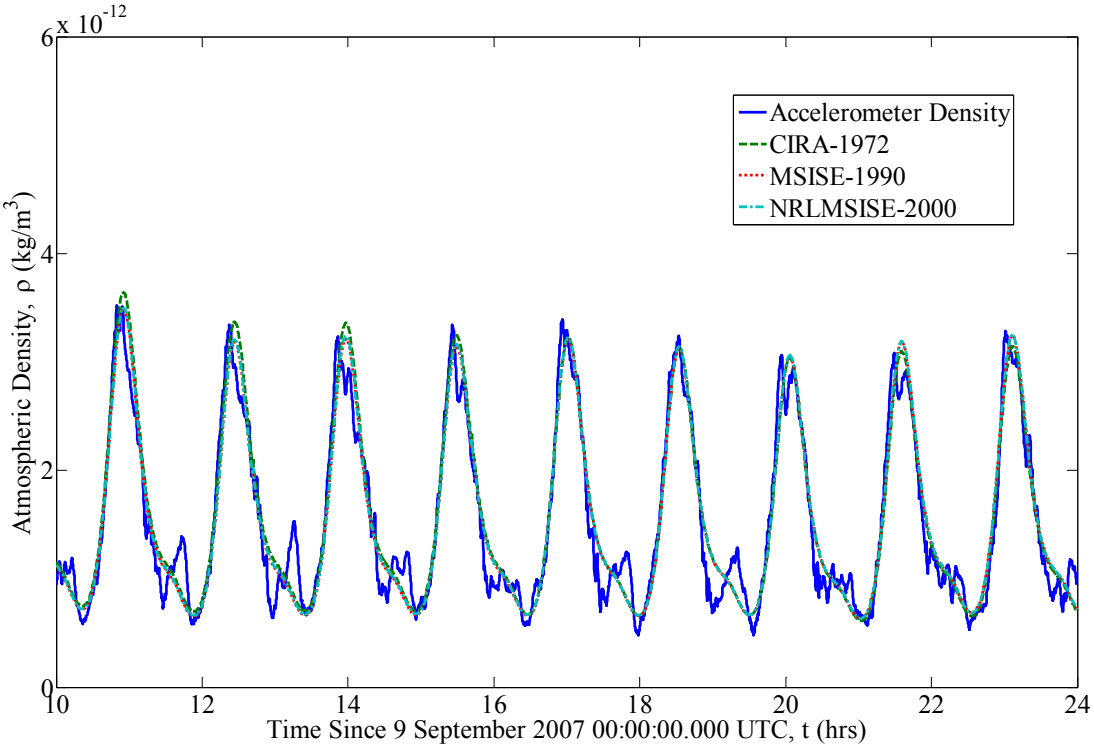

Figure 4.15 Effect of Varying the Baseline Atmospheric Model on the Estimated Density for 1000-2400 hours September 9, 2007. *Density and ballistic coefficient correlated half-lives are 180 and 18 minutes, respectively. The baseline density model is NRLMSISE-2000.*

Figure 4.15 demonstrates how varying the baseline atmospheric model affects the POE estimate density during periods of low solar and quiet geomagnetic activity. All three POE estimated density data sets using the stated baseline atmospheric model have very similar results with the CIRA-1972 baseline model POE density estimate having slightly better agreement with the accelerometer density. The MSISE-1990 and NRLMSISE-2000 POE density estimates are still very closely related to each other. However, the cross correlation coefficient results indicate that the POE density estimate using NRLMSISE-2000 as the baseline atmospheric model is the best choice. The similarity of all three POE density estimates is expected considering that the solar and geomagnetic activity levels are very low. Therefore, the Earth's atmosphere should be relatively calm with typically small variations in

density. Such a situation is the most ideal for the underlying atmospheric models and the subsequent POE orbit determination process to produce the most accurate density estimates.

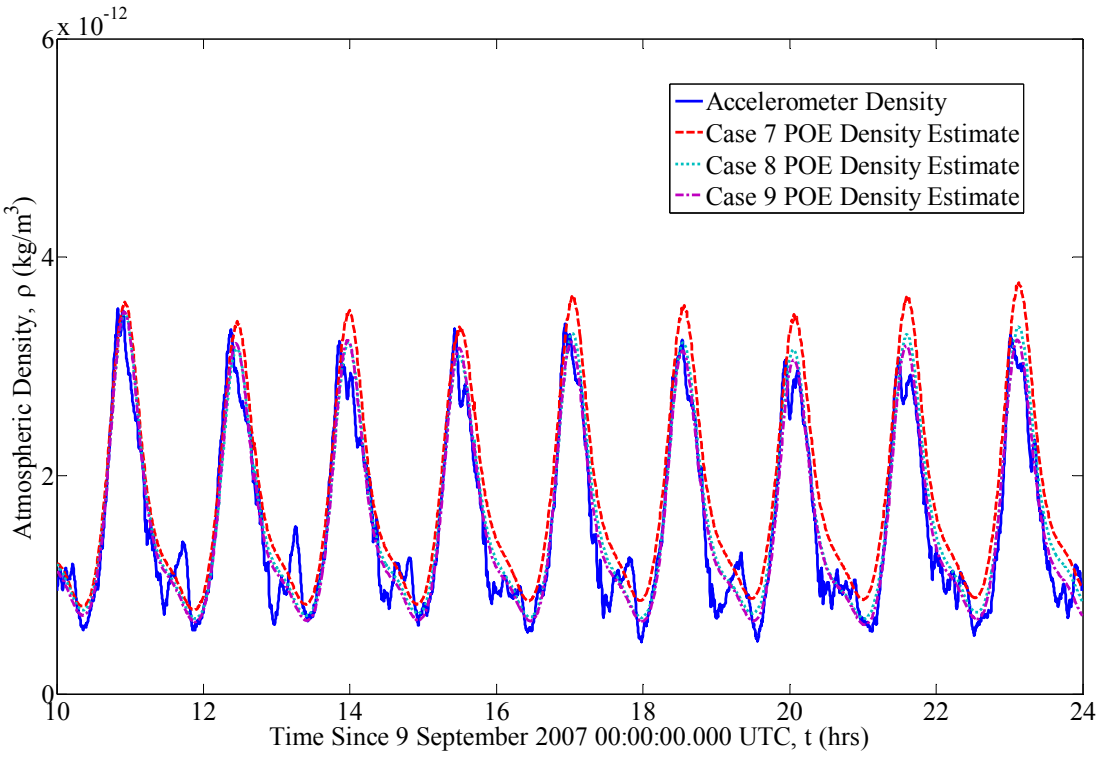

Figure 4.16 Effect of Varying the Density Correlated Half-Life on the Estimated Density for 1000-2400 hours September 9, 2007. *Ballistic coefficient correlated half-life is 18 minutes and the baseline density model is NRLMSISE-2000. Cases 7, 8, and 9 have density correlated half-lives of 1.8, 18, and 180 minutes, respectively.*

Figure 4.16 shows how varying the density correlated half-life affects the POE density estimate with a constant ballistic coefficient correlated half-life during days with low solar and quiet geomagnetic activity levels. The general effect is slightly mixed but an increase in the density half-life tends to decrease the estimated density. The results are slightly less pronounced for periods when less energy is being supplied to the atmosphere as indicated by the low solar and quiet geomagnetic activity levels. The cross correlation coefficient results indicate that the best of the three POE density estimates is the one with

density correlated half-life of 180 minutes and a ballistic coefficient correlated half-life of 18 minutes.

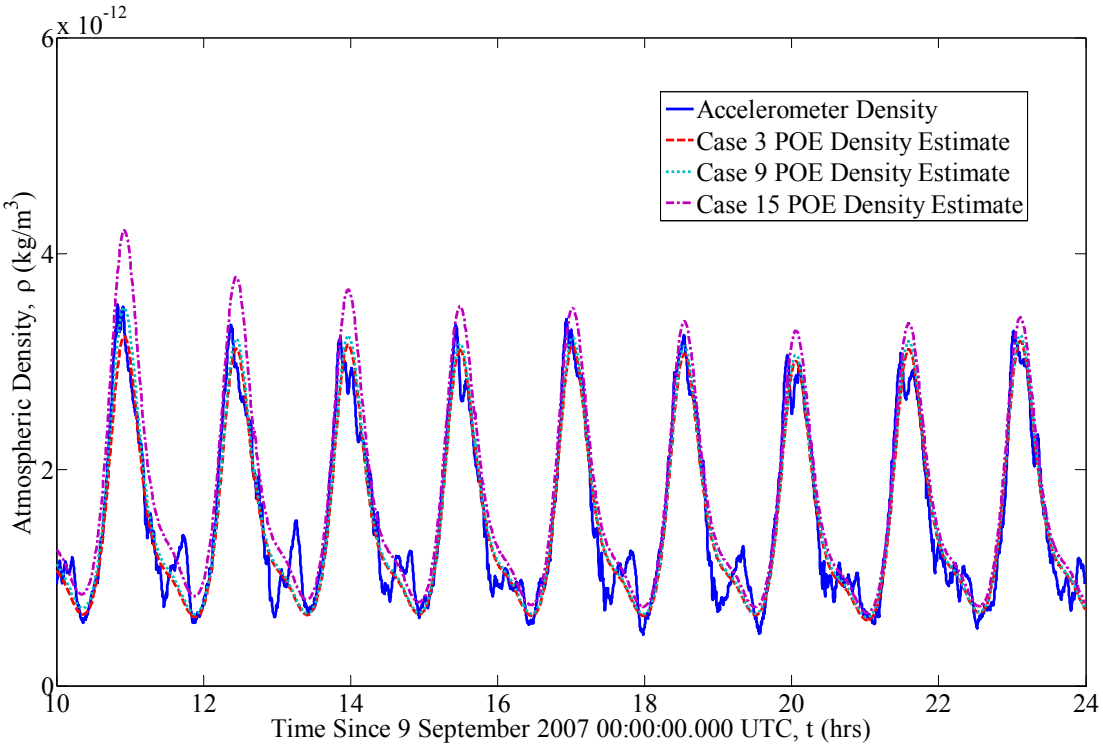

Figure 4.17 Effect of Varying the Ballistic Coefficient Correlated Half-Life on the Estimated Density for 1000-2400 hours September 9, 2007. *Density correlated half-life is 180 minutes and the baseline density model is NRLMSISE-2000. Cases 3, 9, and 15 have ballistic coefficient correlated half-lives of 1.8, 18, and 180 minutes, respectively.*

Figure 4.17 demonstrates the effect of varying the ballistic coefficient correlate half-life on the POE estimated density for a constant density half-life during periods of low solar and quiet geomagnetic activity levels. The observed effect is the opposite experienced for when the density correlated half-life is varied for a constant ballistic coefficient half-life. As the ballistic coefficient half-life is increased, the POE estimated density also increases. This effect is also slightly less pronounced during periods of low solar and quiet geomagnetic activity. Again, the cross correlation coefficient results indicate that the best of the three POE

density estimates is the one with density correlated half-life of 180 minutes and a ballistic coefficient correlated half-life of 18 minutes.

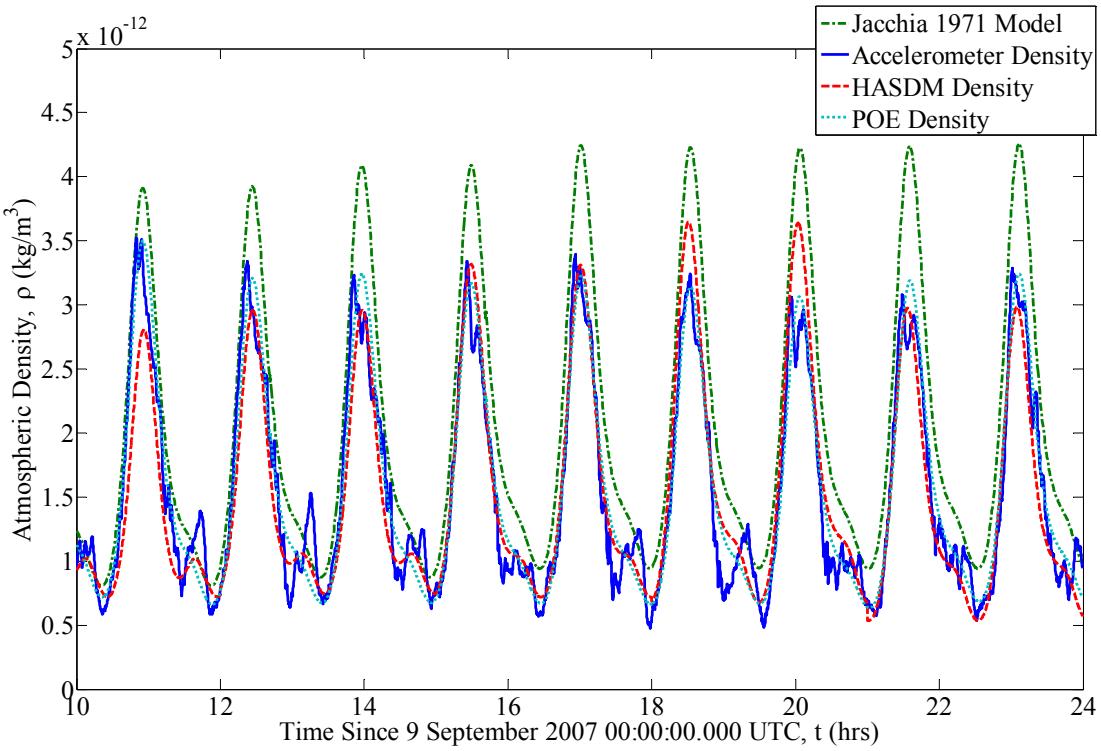

Figure 4.18 Comparison of Densities Obtained from Different Methods for 1000-2400 hours September 9, 2007. *POE density obtained using a density correlated half-life of 180 minutes and a ballistic coefficient correlated half-life of 18 minutes and NRLMSISE-2000 as the baseline density model.*

Figure 4.18 gives a comparison of the estimated densities obtained from four different approaches. The Jacchia 1971 empirical model gives the least agreement with the accelerometer density. The HASDM and POE density estimates give comparable results and both show relatively good agreement with the accelerometer density. HASDM and POE estimated densities provide improvements over the Jacchia 1971 empirical model. These observation are also supported by the cross correlation coefficients given previously where the coefficients for the POE and HASDM density estimates are higher than the coefficient for the Jacchia 1971 empirical model. The only exception is for the low solar activity bin where

the Jacchia 1971 empirical model has a slightly higher degree of correlation with the accelerometer density compared with the HASDM density. While the cross correlation coefficients for the Jacchia 1971 empirical model and the HASDM density are very close to each other, this situation highlights the importance of examining more than one set of results, because looking at only one source may not tell the whole story or necessarily give a good idea of the behavior of the results.

4.4 Chapter Summary

Cross correlation coefficients were generated that relate the POE density estimates with the accelerometer density. In particular, the days were organized and analyzed according to solar and geomagnetic activity levels or bins. The results indicate that determining which POE density estimate baseline atmospheric model and half-life combination is best is a function of the solar and geomagnetic bins. However, this dependence is greatly reduced once the solar activity reaches elevated levels or the geomagnetic activity becomes at least moderate. Even though the best baseline atmospheric model and half-life combination is primarily a function of solar and geomagnetic activity level, a general conclusion can be made. The CIRA-1972 baseline atmospheric model with a density correlated half-life of 18 minutes and a ballistic coefficient correlated half-life of 1.8 minutes are the recommended parameters to use in an orbit determination process to generate POE density estimates.

The dates examined demonstrated that the best baseline atmospheric model and half-life combination determined according to solar and geomagnetic activity bins do not hold true for every solution. Also, as the solar and geomagnetic activity levels increase, the residuals become larger, the consistency tests move farther from zero, and the cross correlation coefficients are generally reduced in magnitude. This would suggest that the density

estimates obtained from any approach will be less accurate as a function of increasing solar and geomagnetic activity. This conclusion is also supported by comparison of the density estimates with the accelerometer density, which is taken as truth. However, the POE and HASDM density estimates consistently showed improvement over the existing Jacchia 1971 empirical model. Also, the POE and HASDM density estimates have comparable results and at times the POE density estimate shows better agreement with the accelerometer density than the HASDM density.

5 ADDITIONAL CONSIDERATIONS FOR ATMOSPHERIC DENSITY ESTIMATES

This chapter examines additional considerations that have the potential to affect the atmospheric density estimates generated by an orbit determination process. In particular, the sensitivity of the density estimates to the initial ballistic coefficient, solution fit span length, and solution overlaps are considered. The effect of estimating the ballistic coefficient in orbit determination process on the POE density estimates is also addressed. Finally, an initial look at using GRACE-A POE data in an orbit determination process to generate POE density estimates is considered. These topics are covered briefly to give a general idea of the behavior of the density estimates for each situation.

5.1 Ballistic Coefficient Sensitivity

An important consideration in the orbit determination process used in this work to estimate atmospheric density is the nominal ballistic coefficient that initializes the process. The process estimates density in part by simultaneously estimating the ballistic coefficient. Therefore, the sensitivity of the density estimation process to the initial ballistic coefficient value is unknown. The ballistic coefficient is difficult to calculate mainly due to its dependence on the cross sectional area and drag coefficient, which are both difficult to calculate for a satellite. The cross sectional area of a satellite often changes continually thus requiring accurate attitude data or an attitude determination process. The required attitude data may not be readily available for a given satellite and an attitude determination process may require significant time and resources. The drag coefficient is typically approximated for satellites because its dependence on satellite configuration and altitude makes precise calculation very difficult. Therefore, the ballistic coefficient used to initialize the orbit

determination process will have some error associated with the underlying quantities. Determining how much error in the initial ballistic coefficient is acceptable and will still produce density estimates with the desired accuracy is of great importance. This section undertakes an initial investigation of the sensitivity of the atmospheric density estimates to variations in the initial ballistic coefficient used in an orbit determination process.

The investigation starts with a solution whose nominal ballistic coefficient is considered to be relatively well known and the resulting density estimates show good agreement with the accelerometer density. Also, the solution will satisfy the consistency tests to a satisfactory level and will not reject data as determined from the residuals. In essence, the solution used as the basis for comparison and nominal ballistic coefficient variation must have reasonably good results. March 12, 2005 was selected for this study because of the quiet geomagnetic and moderate solar flux activity for that day. October 28-29, 2003 was selected because of the active geomagnetic and high solar flux activity observed for this period. Therefore, the extremes of the solar and geomagnetic activity levels are covered by these two days.

The variations in the nominal ballistic coefficient considered were 1%, 10%, 25%, 50%, 75%, 90%, 110%, 150%, 200%, 300%, 600%, and 1100% of the initial value. The following example will help clarify the percentages. For October 28-29, 2003, the nominal ballistic coefficient is 0.00444 m^2/kg. Therefore, the variation in the nominal ballistic coefficient corresponding to 200% will have an initial ballistic coefficient of 0.00888 m^2/kg. For each variation the position and velocity consistency tests, residuals, and cross correlation coefficients were examined. Two sets of cross correlation coefficients were generated once using the accelerometer density as the basis for comparison and once where the original POE density estimate was used as the basis. The CIRA-1972 baseline atmospheric model was

used along with density and ballistic coefficient correlated half-lives of 1.8, 18, and 180 minutes each to generate the POE density estimates.

5.1.1 Examples of Rejected Data and Failed Consistency Tests

Examples of residual graphs that reject data and graphs showing failed consistency tests are useful in understanding the process of determining good solutions. For this work, if an orbit determination process rejects data, then the resulting solution is bad because the data used as measurements are known to be accurate. This may not always be true depending on the accuracy of the measurements used in the orbit determination process. However, regardless of the accuracy of the measurements, the filter residuals are still useful as a check on the orbit determination process and subsequent results. Accordingly, if the consistency tests are failed, then the orbit determination process is not performing well and is generating bad solutions. These test criteria for solutions are particularly useful when conducting the ballistic coefficient sensitivity study because they provide a quick and easy check on the results without spending time generating POE density estimate comparisons with accelerometer density. These test criteria are extremely crucial in estimating atmospheric density from an orbit determination process.

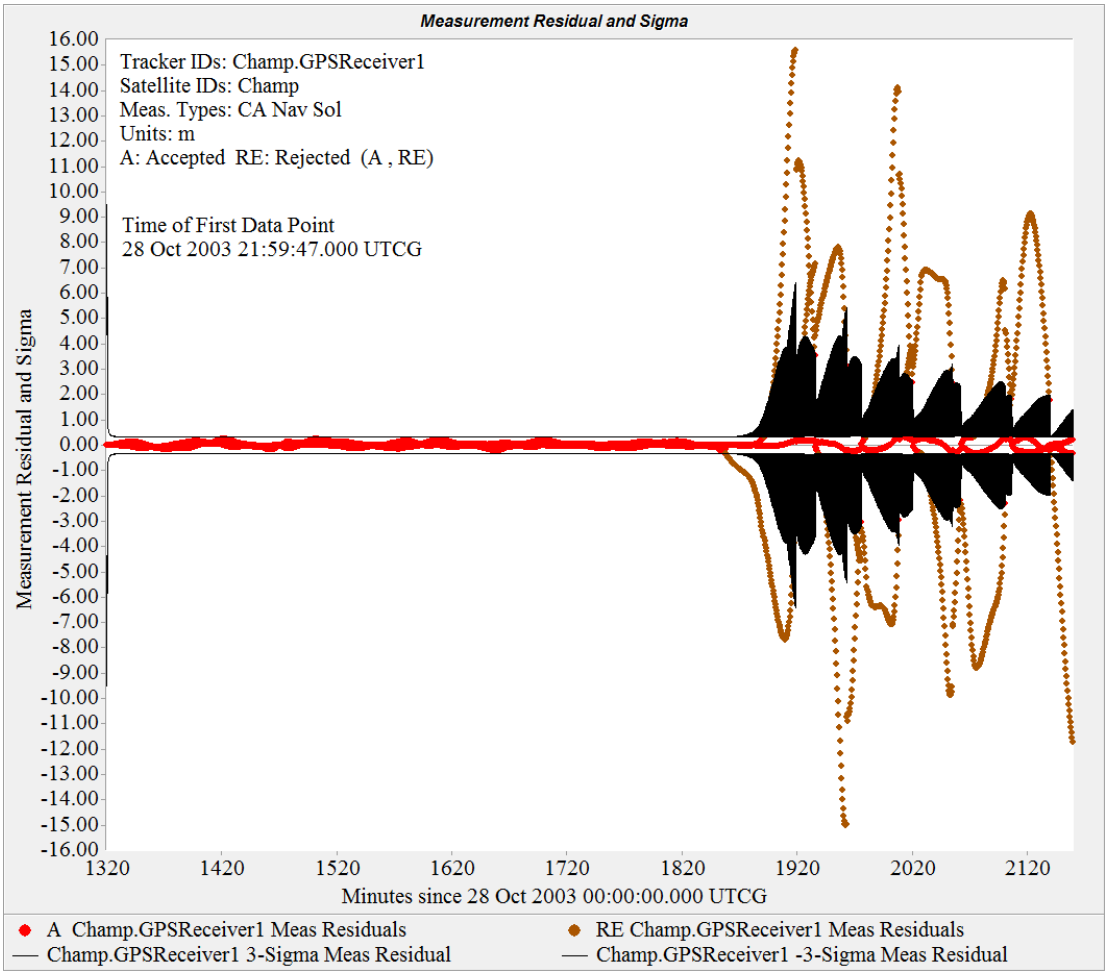

Figure 5.1 Example of Rejected Data from the Filter Residuals for 1000-2400 Hours October 29, 2003. *Density and ballistic coefficient correlated half-lives are 1.8 and 18 minutes, respectively. The baseline density model is CIRA-1972. The initial ballistic coefficient is 25% of the nominal ballistic coefficient for this day.*

Figure 5.1 shows rejected measurement data as seen from the residuals graph of the orbit determination process estimating density for an initial ballistic coefficient variation scenario of 25% of the nominal value. This figure is an extreme case of what can typically be observed from an orbit determination process generating a bad solution. However, the point is made that the residuals offer an excellent way to assess the performance of the determination process. In this figure, the rejected measurement data are the brown data

points, the accepted measurement data are the red data points, and the 3σ boundaries are the black lines that define rejection or acceptance of the residuals. The POE density estimates resulting from any solution containing rejected measurement data would not be used.

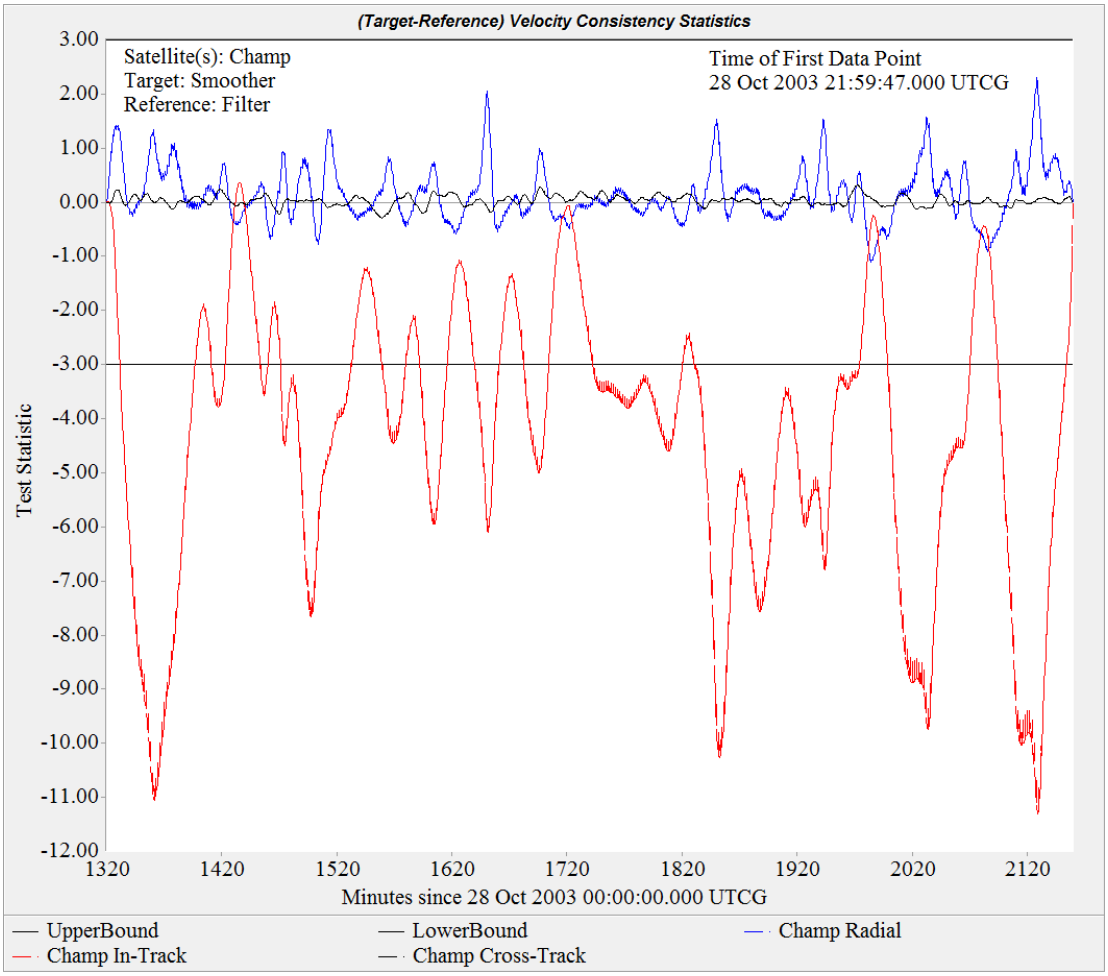

Figure 5.2 Example of a Failed Velocity Consistency Test for 1000-2400 Hours October 29, 2003. *Density and ballistic coefficient correlated half-lives are 180 minutes and the baseline density model is CIRA-1972. The initial ballistic coefficient is 10% of the nominal ballistic coefficient for this day.*

Figure 5.2 demonstrates a failed velocity consistency test graph of the orbit determination process estimating density for an initial ballistic coefficient variation scenario of 10% of the nominal value. In particular, the in-track components fail the consistency test while the radial and cross-track components satisfy the consistency test. This figure

illustrates the ease of using the consistency tests to determine how well the process is working. The POE density estimates resulting from any solution failing the consistency tests, including individual components, would not be used.

5.1.2 Ballistic Coefficient Sensitivity Study for March 12, 2005

The position consistency tests for this day were satisfied satisfactorily for variations in the initial ballistic coefficient of 75% to 300%. The velocity consistency test had satisfactory results for initial ballistic coefficient variations of 90% to 150%. The residuals did not reject any data for variations of 50% and up. The POE density estimates using initial ballistic coefficient variations less than 100% were more susceptible to failing the consistency tests and rejecting data than the POE density estimates whose initial ballistic coefficient was greater than 100%. Therefore, the results for the POE density estimates whose initial ballistic coefficient falls within 90-150% of the nominal value are given additional consideration.

Table 5.1 Zero Delay Cross Correlation Coefficients Using Accelerometer Density Data for the March 12, 2005 Solution with Variations in the Nominal Ballistic Coefficient. *The columns of percentages are the percentages of the nominal ballistic coefficient used to initialize the orbit determination process. Yellow (or light gray) highlighted numbers indicate the largest value for the specific variation. The tan (or darker gray) highlighted number indicates the largest overall number. The cross correlation coefficient for the Jacchia 1971 empirical model is 0.9768. The cross correlation coefficient for the HASDM density is 0.9838. The nominal ballistic coefficient is 0.00436 m^2/kg. CIRA-1972 is the baseline density model for all values.*

Half-Life Combinations, Density/Ballistic Coefficient (min)	*90%*	*100%*	*110%*	*150%*
Case 1 1.8/1.8	0.9824	0.9831	0.9831	0.9783
Case 2 18/1.8	0.9816	0.9827	0.9834	0.9836
Case 3 180/1.8	0.9813	0.9819	0.9825	0.9840
Case 7 1.8/18	0.9823	0.9822	0.9820	0.9794
Case 8 18/18	0.9813	0.9822	0.9828	0.9825
Case 9 180/18	0.9811	0.9815	0.9817	0.9822
Case 13 1.8/180	0.9800	0.9798	0.9795	0.9781
Case 14 18/180	0.9730	0.9735	0.9737	0.9728
Case 15 180/180	0.9746	0.9737	0.9726	0.9657

Table 5.1 shows the zero delay cross correlation coefficients using the accelerometer density data as the basis of comparison for March 12, 2005. CIRA-1972 is the baseline density model used to generate the POE density estimates for this day using a 14 hour fit span ranging 1000-2400 hours that day. These results show that a ballistic coefficient correlated half-life of 1.8 minutes has the highest degree of correlation with the accelerometer density for the full range of density correlated half-lives. Also, the Jacchia 1971 empirical model has a higher cross correlation coefficient for a minority of the POE density estimates. The HASDM density has a higher degree of correlation with the accelerometer density than all of the results except for the POE density estimate with a density and ballistic coefficient correlated half-life combination of 180 minutes and 1.8 minutes, respectively. The POE density estimates obtained from each initial ballistic coefficient variation show similar results. The highest degree of correlation with the accelerometer density occurs for the 150%

initial ballistic coefficient variation with a density correlated half-life of 180 minutes and a ballistic coefficient correlated half-life of 1.8 minutes.

Table 5.2 Maximum Cross Correlation Coefficients Using Accelerometer Density Data for the March 12, 2005 Solution with Variations in the Nominal Ballistic Coefficient. *The columns of percentages are the percentages of the nominal ballistic coefficient used to initialize the orbit determination process. Yellow (or light gray) highlighted numbers indicate the largest value for the specific variation. The tan (or darker gray) highlighted number indicates the largest overall number. The cross correlation coefficient for the Jacchia 1971 empirical model is 0.9769 with a 10 second delay. The cross correlation coefficient for the HASDM density is 0.9844 with a delay of -20 seconds. The nominal ballistic coefficient is 0.00436 m^2/kg. CIRA-1972 is the baseline density model for all values. The values in parenthesis are the corresponding delays in seconds.*

Half-Life Combinations, Density/Ballistic Coefficient (min)	*90%*	*100%*	*110%*	*150%*
Case 1 1.8/1.8	0.9829 (20)	0.9834 (20)	0.9833 (10)	0.9785 (-10)
Case 2 18/1.8	0.9819 (20)	0.9830 (20)	0.9836 (10)	0.9836 (10)
Case 3 180/1.8	0.9813 (10)	0.9820 (10)	0.9826 (10)	0.9843 (20)
Case 7 1.8/18	0.9826 (20)	0.9824 (10)	0.9821 (10)	0.9794 (0)
Case 8 18/18	0.9818 (20)	0.9825 (20)	0.9830 (20)	0.9827 (10)
Case 9 180/18	0.9811 (10)	0.9815 (10)	0.9819 (10)	0.9825 (20)
Case 13 1.8/180	0.9802 (20)	0.9800 (10)	0.9797 (10)	0.9781 (10)
Case 14 18/180	0.9735 (20)	0.9740 (20)	0.9742 (20)	0.9731 (20)
Case 15 180/180	0.9747 (10)	0.9739 (10)	0.9728 (20)	0.9662 (20)

Table 5.2 gives the maximum cross correlation coefficients using the accelerometer density as the basis for comparison for March 12, 2005 as previously defined. Many of the

same general trends are observed in these results as seen in the previous table of results. One notable difference is that the HASDM density data now has the highest degree of correlation with the accelerometer density compared with all of the results.

Table 5.3 Zero Delay Cross Correlation Coefficients Using the Nominal Ballistic Coefficient Solution for the March 12, 2005 Solution with Variations in the Nominal Ballistic Coefficient. *The columns of percentages are the percentages of the nominal ballistic coefficient used to initialize the orbit determination process. Yellow (or light gray) highlighted numbers indicate the largest value for the specific variation. The tan (or darker gray) highlighted number indicates the largest overall number. The nominal ballistic coefficient is 0.00436 m^2/kg. CIRA-1972 is the baseline density model for all values.*

Half-Life Combinations, Density/Ballistic Coefficient (min)	*90%*	*110%*	*150%*
Case 1 1.8/1.8	0.9997	0.9997	0.9943
Case 2 18/1.8	0.9999	0.9999	0.9974
Case 3 180/1.8	1.0000	1.0000	0.9992
Case 7 1.8/18	0.9999	0.9999	0.9981
Case 8 18/18	0.9999	0.9999	0.9975
Case 9 180/18	0.9999	0.9999	0.9989
Case 13 1.8/180	0.9999	0.9999	0.9990
Case 14 18/180	0.9999	0.9999	0.9980
Case 15 180/180	0.9999	0.9999	0.9974

Table 5.3 shows the zero delay cross correlation coefficients where the nominal ballistic coefficient or original solution was used as the basis of comparison. As expected, the results show that the variations are highly correlated to the nominal situation. Two of the cross correlation coefficients are shown having values 1.0000 with one indicating as being larger than the other. This ambiguity is a consequence of the limitations of available space to represent the results to the necessary decimal place resulting in the coefficients being rounded up. Because the cross correlation coefficients are so close in value to each other, there is little, real difference between the variations and half-life combinations. The highest degree of correlation with the nominal ballistic coefficient solution corresponds to the 110% variation

and a density and ballistic coefficient correlated half-lives of 180 minutes and 1.8 minutes, respectively. These results demonstrate that when the initial ballistic coefficient value is within ±10% of the nominal value, the orbit determination process generates sufficiently accurate POE density estimates.

Table 5.4 Maximum Cross Correlation Coefficients Using the Nominal Ballistic Coefficient Solution for the March 12, 2005 Solution with Variations in the Nominal Ballistic Coefficient. *The columns of percentages are the percentages of the nominal ballistic coefficient used to initialize the orbit determination process. Yellow (or light gray) highlighted numbers indicate the largest value for the specific variation. The tan (or darker gray) highlighted number indicates the largest overall number. The nominal ballistic coefficient is 0.00436 m^2/kg. CIRA-1972 is the baseline density model for all values. The values in parenthesis are the corresponding delays in seconds.*

Half-Life Combinations, Density/Ballistic Coefficient (min)	*90%*	*110%*	*150%*
Case 1 1.8/1.8	0.9997 (0)	0.9997 (0)	0.9951 (-13)
Case 2 18/1.8	0.9999 (0)	0.9999 (0)	0.9974 (0)
Case 3 180/1.8	1.0000 (0)	1.0000 (0)	0.9992 (0)
Case 7 1.8/18	0.9999 (0)	0.9999 (0)	0.9981 (-13)
Case 8 18/18	0.9999 (0)	0.9999 (0)	0.9975 (0)
Case 9 180/18	0.9999 (0)	0.9999 (0)	0.9989 (0)
Case 13 1.8/180	0.9999 (0)	0.9999 (0)	0.9990 (0)
Case 14 18/180	0.9999 (0)	0.9999 (0)	0.9980 (0)
Case 15 180/180	0.9999 (0)	0.9999 (0)	0.9974 (0)

Table 5.4 shows the maximum cross correlation coefficients where the nominal ballistic coefficient or original solution was used as the basis of comparison. As expected, the results show that the variations are highly correlated to the nominal situation. Two of the cross correlation coefficients are shown having values 1.0000 with one indicating as being larger than the other. This ambiguity is a consequence of the limitations of available space to represent the results to the necessary decimal place resulting in the coefficients being rounded up. Because the cross correlation coefficients are so close in value to each other, there is little, real difference between the variations and half-life combinations. The highest degree of correlation with the nominal ballistic coefficient solution corresponds to the 110% variation and a density and ballistic coefficient correlated half-lives of 180 minutes and 1.8 minutes, respectively. The zero delay and maximum cross correlation coefficient results in the previous two tables demonstrate that when the initial ballistic coefficient value is within ±10% of the nominal value, sufficiently accurate POE density estimates are obtained.

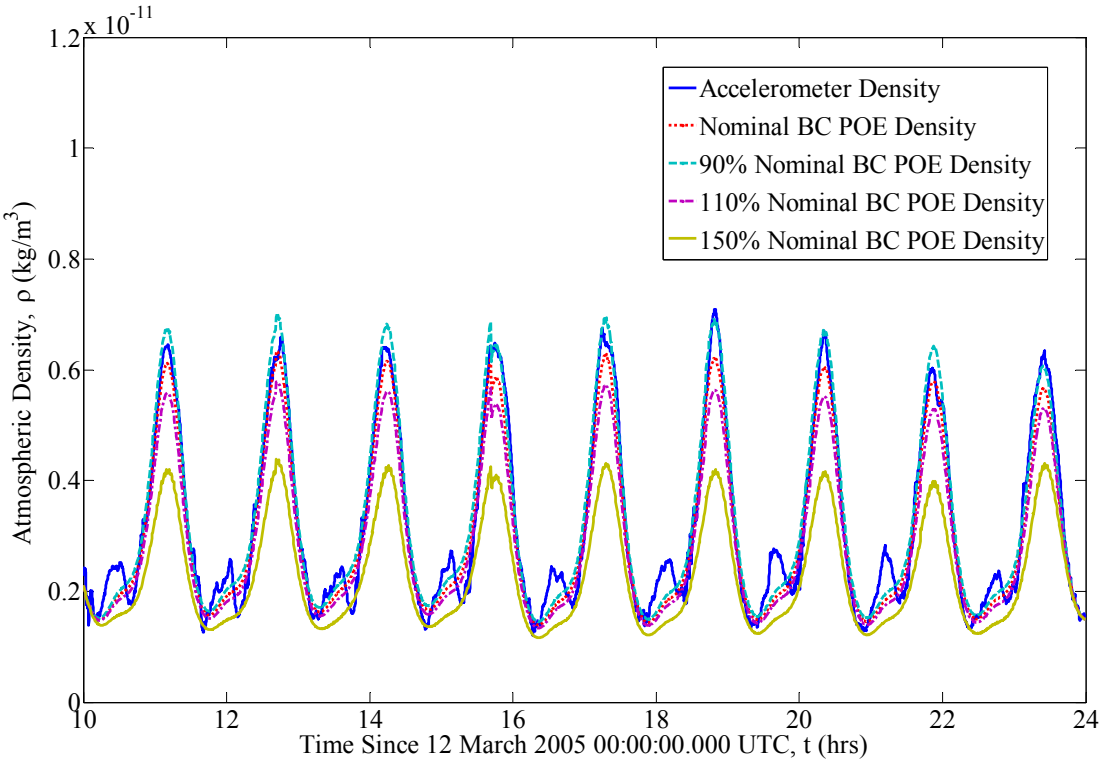

Figure 5.3 Effect of Varying the Initial Ballistic Coefficient on the POE Estimated Density for 1000-2400 hours March 12, 2005. *Density and ballistic coefficient correlated half-lives are 1.8 minutes and the baseline density model is CIRA-1972.*

Figure 5.3 shows the effect of varying the initial ballistic coefficient on the POE density estimates for March 12, 2005. As the initial ballistic coefficient value increases from 90 to 150% of the nominal value, the POE density estimates decrease with the most notable influence occurring at the density peaks. This result is expected given the relationship for the acceleration due to drag. The relationship states that for a constant acceleration the density will decrease as the ballistic coefficient increases. Also, the POE density estimates have the greatest agreement with the accelerometer density for the 90% initial ballistic coefficient variation.

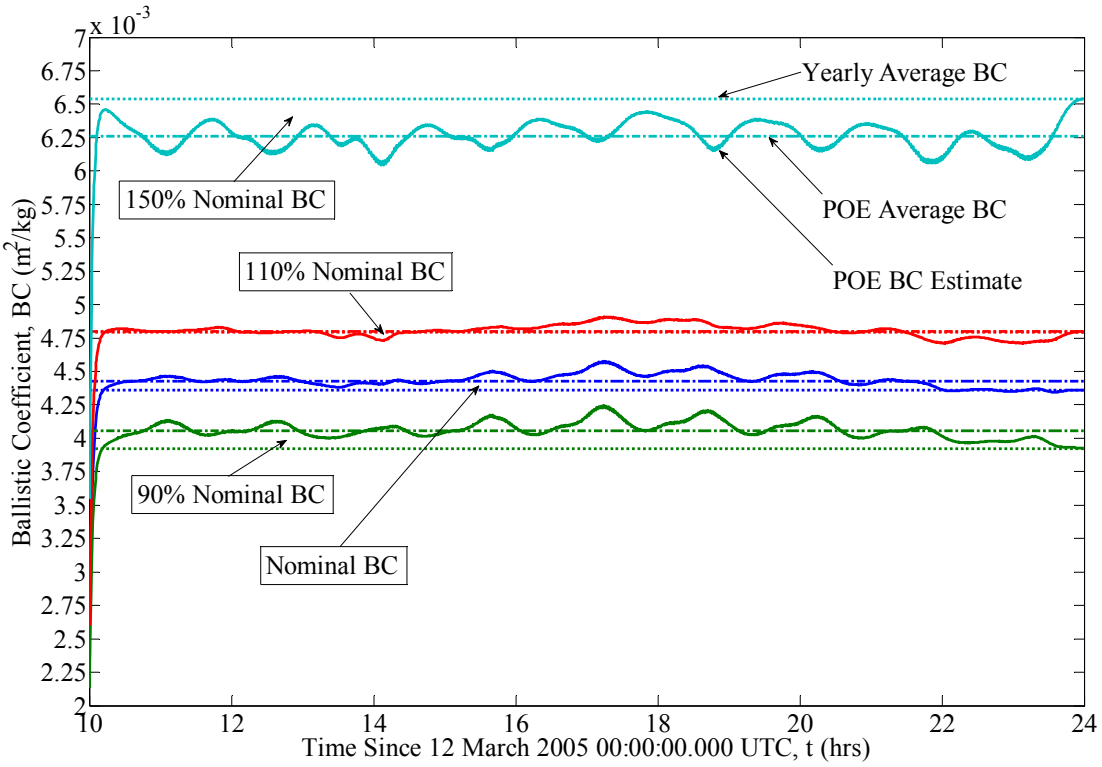

Figure 5.4 Effect of Varying the Initial Ballistic Coefficient on the POE Estimated Ballistic Coefficient for 1000-2400 hours March 12, 2005. *Density and ballistic coefficient correlated half-lives are 1.8 minutes and the baseline density model is CIRA-1972.*

Figure 5.4 shows the effect of varying the initial ballistic coefficient on the POE estimated ballistic coefficient for March 12, 2005. The ballistic coefficient is estimated as part of the orbit determination process. The initial value and the average estimated value are plotted along with the ballistic coefficients estimated for all given times. The first noticeable result is the extreme minimum values at the beginning of each solution. The cause of these extreme solutions is currently unknown and is something that needs to be addressed. Secondly, the POE ballistic coefficient estimates are fairly consistent and do not vary widely from their average value. This would indicate that the orbit determination process is performing well. Also, as the variation in the initial ballistic coefficient increases, the difference between the average POE estimated ballistic coefficient and the initial ballistic

coefficient value also increases. This would suggest that the orbit determination process is attempting to estimate a more accurate ballistic coefficient given the incorrect initial value, whether the value is too large or too small. Therefore, an orbit determination process might have the potential to be used in an iterative fashion to obtain a more accurate ballistic coefficient from a less accurate value. However, more research is required to verify such ability by the orbit determination process.

Table 5.5 Zero Delay Cross Correlation Coefficients Using Accelerometer Density Data for the March 12, 2005 Solution with Estimation and No Estimation of the Ballistic Coefficient. *The columns are for the POE density estimates when the ballistic coefficient is estimated and not estimated in the orbit determination process. Yellow (or light gray) highlighted numbers indicate the largest value for the specific method. If multiple values are highlighted, the multiple values are equal. The tan (or darker gray) highlighted number indicates the largest overall number. The cross correlation coefficient for the Jacchia 1971 empirical model is 0.9768. The cross correlation coefficient for the HASDM density is 0.9838. The nominal ballistic coefficient is 0.00436 m^2/kg. CIRA-1972 is the baseline density model for all values.*

Half-Life Combinations, Density/Ballistic Coefficient (min)	*BC Estimation*	*No BC Estimation*
Case 1 1.8/1.8	0.9831	0.9827
Case 2 18/1.8	0.9827	0.9825
Case 3 180/1.8	0.9819	0.9818
Case 7 1.8/18	0.9822	0.9827
Case 8 18/18	0.9822	0.9825
Case 9 180/18	0.9815	0.9818
Case 13 1.8/180	0.9798	0.9827
Case 14 18/180	0.9735	0.9825
Case 15 180/180	0.9737	0.9818

Table 5.5 gives the zero delay cross correlation coefficients using the accelerometer density as the basis for comparison for March 12, 2005 when the ballistic coefficient is both estimated and not estimated by the orbit determination process. These results demonstrate that regardless of whether the ballistic coefficient is estimated or not, the POE density estimates have similar results for most of the cases examined. However, the POE density

with the ballistic coefficient estimated as part of the orbit determination process with a density and ballistic coefficient correlated half-life of 1.8 minutes each and using the CIRA-1972 baseline atmospheric model does have the highest degree of correlation with the accelerometer density. When the ballistic coefficient is not estimated, the cross correlation coefficients are the same for constant density correlated half-lives and varying ballistic coefficient correlated half-lives. Also, the HASDM density has the highest degree of correlation with the accelerometer density compared with all of the results. The majority of the POE density estimates have a higher degree of correlation to the accelerometer density data compared with the Jacchia 1971 empirical model.

Table 5.6 Maximum Cross Correlation Coefficients Using Accelerometer Density Data for the March 12, 2005 Solution with Estimation and No Estimation of the Ballistic Coefficient. *The columns are for the POE density estimates when the ballistic coefficient is estimated and not estimated in the orbit determination process. Yellow (or light gray) highlighted numbers indicate the largest value for the specific method. If multiple values are highlighted, the multiple values are equal. The tan (or darker gray) highlighted number indicates the largest overall number. The cross correlation coefficient for the Jacchia 1971 empirical model is 0.9769 with a 10 second delay. The cross correlation coefficient for the HASDM density is 0.9844 with a delay of -20 seconds. The nominal ballistic coefficient is 0.00436 m^2/kg. CIRA-1972 is the baseline density model for all values. The values in parenthesis are the corresponding delays in seconds.*

Half-Life Combinations, Density/Ballistic Coefficient (min)	*BC Estimation*	*No BC Estimation*
Case 1 1.8/1.8	0.9834 (20)	0.9831 (20)
Case 2 18/1.8	0.9830 (20)	0.9828 (20)
Case 3 180/1.8	0.9820 (10)	0.9820 (10)
Case 7 1.8/18	0.9824 (10)	0.9831 (20)
Case 8 18/18	0.9825 (20)	0.9828 (20)
Case 9 180/18	0.9815 (10)	0.9820 (10)
Case 13 1.8/180	0.9800 (10)	0.9831 (20)
Case 14 18/180	0.9740 (20)	0.9828 (20)
Case 15 180/180	0.9739 (10)	0.9820 (10)

Table 5.6 displays the maximum cross correlation coefficients where the ballistic coefficient is both estimated and not estimated by the orbit determination process for March 12, 2005. The same general trends observed in the previous table of zero delay cross correlation coefficients are visible in these results.

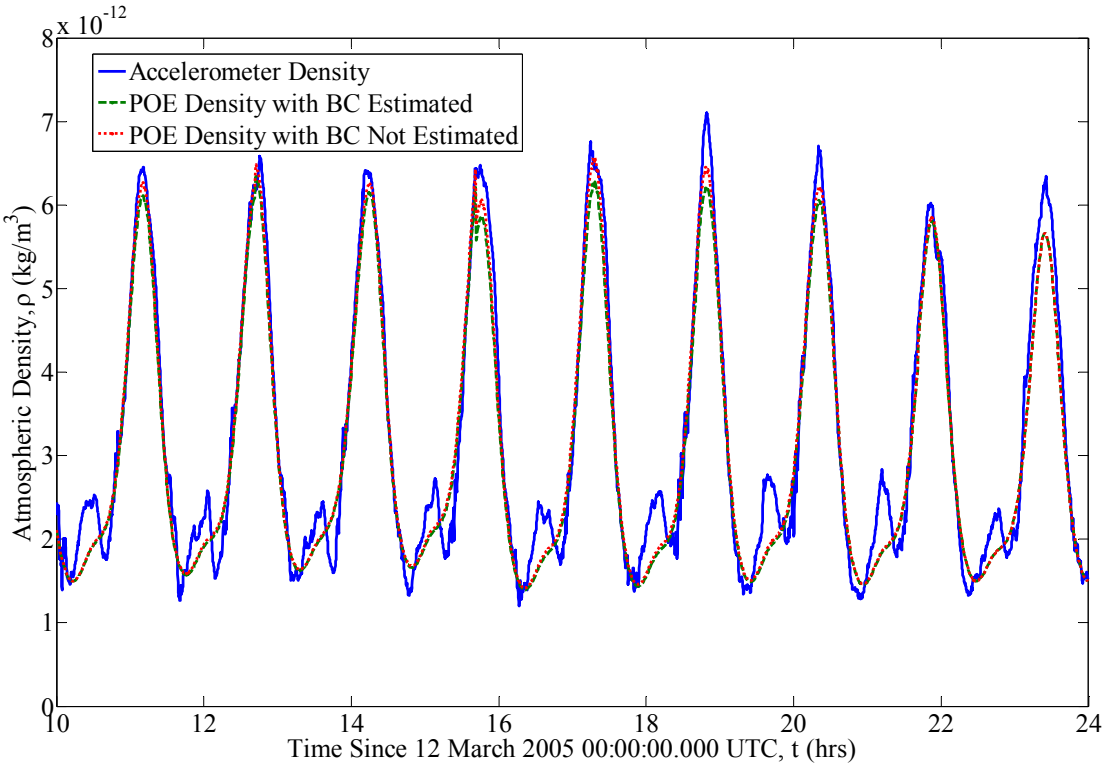

Figure 5.5 Effect of Estimating the Ballistic Coefficient on the POE Estimated Density for 1000-2400 hours March 12, 2005. *Density and ballistic coefficient correlated half-lives are 1.8 minutes and the baseline density model is CIRA-1972. The nominal ballistic coefficient is 0.00436 m^2/kg.*

Figure 5.5 shows the effect of estimating the ballistic coefficient on the POE density estimates for March 12, 2005. Notice that not estimating the ballistic coefficient generally produces a slight increase in the POE density estimates, primarily at the density peaks. The solution for March 12, 2005 is during a period of moderate solar and moderate geomagnetic activity. Therefore, the differences between these two POE density estimates are not as defined as for a period of high solar and active geomagnetic activity, which is given in the next subsection. However, regardless of whether or not the ballistic coefficient is estimated as part of the orbit determination process, the POE density estimates have very similar results. This similarity is demonstrated in the cross correlation coefficients for these two POE density estimates, which were shown in the previous tables to also be very similar.

5.1.3 Ballistic Coefficient Sensitivity Study for October 28-29, 2003

The position consistency tests for this day were satisfied satisfactorily for variations in the initial ballistic coefficient of 75% and up. The velocity consistency test had satisfactorily results for all cases considered only for the initial ballistic coefficient variation of 90%. The variations of initial ballistic coefficient of 110% and higher had velocity consistency tests with satisfactory results for all cases except for the in-track component for the case with a density and ballistic coefficient correlated half-life of 1.8 minutes each and the case with a density correlated half-life of 1.8 minutes and a ballistic coefficient correlated half-life of 18 minutes. The residuals did not reject any data for variations of 50% and up. The POE density estimates using initial ballistic coefficient variations less than 100% were more susceptible to failing the consistency tests and rejecting data than the POE density estimates whose initial ballistic coefficient was greater than 100%. October 28-29, 2003 scenarios with initial ballistic coefficient variations of 90%, 110%, and 150% were examined for comparison purposes with March 12, 2005 and to examine the behavior of the POE estimated density for ballistic coefficient variations above 100%.

Table 5.7 Zero Delay Cross Correlation Coefficients Using Accelerometer Density Data for the October 28-29, 2003 Solution with Variations in the Nominal Ballistic Coefficient. *The columns of percentages are the percentages of the nominal ballistic coefficient used to initialize the orbit determination process. Yellow (or light gray) highlighted numbers indicate the largest value for the specific variation. The tan (or darker gray) highlighted number indicates the largest overall number. The cross correlation coefficient for the Jacchia 1971 empirical model is 0.7041. The cross correlation coefficient for the HASDM density is 0.7884. The nominal ballistic coefficient is 0.00444 m^2/kg. CIRA-1972 is the baseline density model for all values.*

Half-Life Combinations, Density/Ballistic Coefficient (min)	*90%*	*100%*	*110%*	*150%*
Case 1 1.8/1.8	0.7666	0.7536	0.7401	0.6920
Case 2 18/1.8	0.7868	0.7779	0.7688	0.7327
Case 3 180/1.8	0.8032	0.8043	0.8050	0.8041
Case 7 1.8/18	0.7571	0.7458	0.7345	0.6939
Case 8 18/18	0.7881	0.7789	0.7692	0.7310
Case 9 180/18	0.8098	0.8112	0.8119	0.8103
Case 13 1.8/180	0.7284	0.7213	0.7145	0.6912
Case 14 18/180	0.7679	0.7607	0.7535	0.7262
Case 15 180/180	0.7920	0.7914	0.7905	0.7850

Table 5.7 shows the zero delay cross correlation coefficients from using the accelerometer density data as the basis for comparison for October 28-29, 2003. CIRA-1972 is the baseline density model used to generate the POE density estimates for this period using a 14 hour fit span ranging from 2200 hours October 28 to 1200 hours October 29. These results show that a density correlated half-life of 180 minutes and a ballistic coefficient correlated half-life of 1.8 minutes has the highest degree of correlation with the accelerometer density for the full range of initial ballistic coefficient variations. Also, the Jacchia 1971 empirical model has the lowest degree of correlation with the accelerometer density compared to all of the results. The HASDM density has a higher degree of correlation with the accelerometer density than the majority of the POE density estimates. The POE density estimates obtained from each initial ballistic coefficient variation show similar results. The highest degree of correlation with the accelerometer density occurs for the 110% initial

ballistic coefficient variation with a density correlated half-life of 180 minutes and a ballistic coefficient correlated half-life of 18 minutes.

Table 5.8 Maximum Cross Correlation Coefficients Using Accelerometer Density Data for the October 28-29, 2003 Solution with Variations in the Nominal Ballistic Coefficient. *The columns of percentages are the percentages of the nominal ballistic coefficient used to initialize the orbit determination process. Yellow (or light gray) highlighted numbers indicate the largest value for the specific variation. The tan (or darker gray) highlighted number indicates the largest overall number. The cross correlation coefficient for the Jacchia 1971 empirical model is 0.7150 with a -130 second delay. The cross correlation coefficient for the HASDM density is 0.8063 with a delay of -160 seconds. The nominal ballistic coefficient is 0.00444 m^2/kg. CIRA-1972 is the baseline density model for all values. The values in parenthesis are the corresponding delays in seconds.*

Half-Life Combinations, Density/Ballistic Coefficient (min)	*90%*	*100%*	*110%*	*150%*
Case 1 1.8/1.8	0.7714 (100)	0.7613 (120)	0.7510 (150)	0.7130 (220)
Case 2 18/1.8	0.7941 (110)	0.7883 (140)	0.7823 (160)	0.7570 (210)
Case 3 180/1.8	0.8034 (-20)	0.8044 (10)	0.8054 (30)	0.8070 (70)
Case 7 1.8/18	0.7588 (60)	0.7487 (70)	0.7386 (90)	0.7022 (130)
Case 8 18/18	0.7917 (80)	0.7844 (100)	0.7769 (120)	0.7464 (170)
Case 9 180/18	0.8111 (-50)	0.8118 (-30)	0.8121 (-20)	0.8110 (40)
Case 13 1.8/180	0.7300 (50)	0.7233 (60)	0.7169 (60)	0.6947 (80)
Case 14 18/180	0.7707 (70)	0.7646 (80)	0.7585 (90)	0.7350 (120)
Case 15 180/180	0.7932 (-50)	0.7921 (-30)	0.7909 (-20)	0.7850 (0)

Table 5.8 gives the maximum cross correlation coefficients using the accelerometer density as the basis for comparison for October 28-29, 2003. Many of the same general

trends are observed in these results as seen in the previous table of results. The highest degree of correlation with the accelerometer density still corresponds with the POE density estimates.

Table 5.9 Zero Delay Cross Correlation Coefficients Using the Nominal Ballistic Coefficient Solution for the October 28-29, 2003 Solution with Variations in the Nominal Ballistic Coefficient. *The columns of percentages are the percentages of the nominal ballistic coefficient used to initialize the orbit determination process. Yellow (or light gray) highlighted numbers indicate the largest value for the specific variation. The tan (or darker gray) highlighted number indicates the largest overall number. The nominal ballistic coefficient is 0.00444 m^2/kg. CIRA-1972 is the baseline density model for all values.*

Half-Life Combinations, Density/Ballistic Coefficient (min)	*90%*	*110%*	*150%*
Case 1 1.8/1.8	0.9982	0.9986	0.9786
Case 2 18/1.8	0.9993	0.9994	0.9888
Case 3 180/1.8	0.9996	0.9997	0.9939
Case 7 1.8/18	0.9988	0.9991	0.9853
Case 8 18/18	0.9992	0.9993	0.9879
Case 9 180/18	0.9996	0.9997	0.9929
Case 13 1.8/180	0.9996	0.9997	0.9952
Case 14 18/180	0.9995	0.9996	0.9928
Case 15 180/180	0.9997	0.9998	0.9953

Table 5.9 shows the zero delay cross correlation coefficients where the nominal ballistic coefficient or original solution was used as the basis of comparison. As expected, the results show that the variations are highly correlated to the nominal situation. Because the cross correlation coefficients are so close in value to each other, there is little, real difference between the variations and half-life combinations. The highest degree of correlation with the nominal ballistic coefficient solution corresponds to the 110% variation and a density and ballistic coefficient correlated half-lives of 180 minutes and 18 minutes, respectively.

Table 5.10 Maximum Cross Correlation Coefficients Using the Nominal Ballistic Coefficient Solution for the October 28-29, 2003 Solution with Variations in the Nominal Ballistic Coefficient. *The columns of percentages are the percentages of the nominal ballistic coefficient used to initialize the orbit determination process. Yellow (or light gray) highlighted numbers indicate the largest value for the specific variation. The tan (or darker gray) highlighted number indicates the largest overall number. The nominal ballistic coefficient is 0.00444 m^2/kg. CIRA-1972 is the baseline density model for all values. The values in parenthesis are the corresponding delays in seconds.*

Half-Life Combinations, Density/Ballistic Coefficient (min)	*90%*	*110%*	*150%*
Case 1 1.8/1.8	0.9982 (0)	0.9986 (0)	0.9796 (13)
Case 2 18/1.8	0.9993 (0)	0.9994 (0)	0.9891 (13)
Case 3 180/1.8	0.9996 (0)	0.9997 (0)	0.9939 (0)
Case 7 1.8/18	0.9988 (0)	0.9991 (0)	0.9866 (13)
Case 8 18/18	0.9992 (0)	0.9993 (0)	0.9888 (13)
Case 9 180/18	0.9996 (0)	0.9997 (0)	0.9933 (13)
Case 13 1.8/180	0.9996 (0)	0.9997 (0)	0.9952 (0)
Case 14 18/180	0.9995 (0)	0.9996 (0)	0.9932 (0)
Case 15 180/180	0.9997 (0)	0.9998 (0)	0.9957 (13)

Table 5.10 shows the maximum cross correlation coefficients where the nominal ballistic coefficient or original solution was used as the basis of comparison. As expected, the results show that the variations are highly correlated to the nominal situation. Because the cross correlation coefficients are so close in value to each other, there is little, real difference between the variations and half-life combinations. The highest degree of

correlation with the nominal ballistic coefficient solution corresponds to the 110% variation and a density and ballistic coefficient correlated half-lives of 180 minutes and 18 minutes, respectively. The zero delay and maximum cross correlation coefficient results in the previous two tables demonstrate that the initial ballistic coefficient value must be within ±10% of the nominal value to provide sufficient accuracy in the POE density estimates.

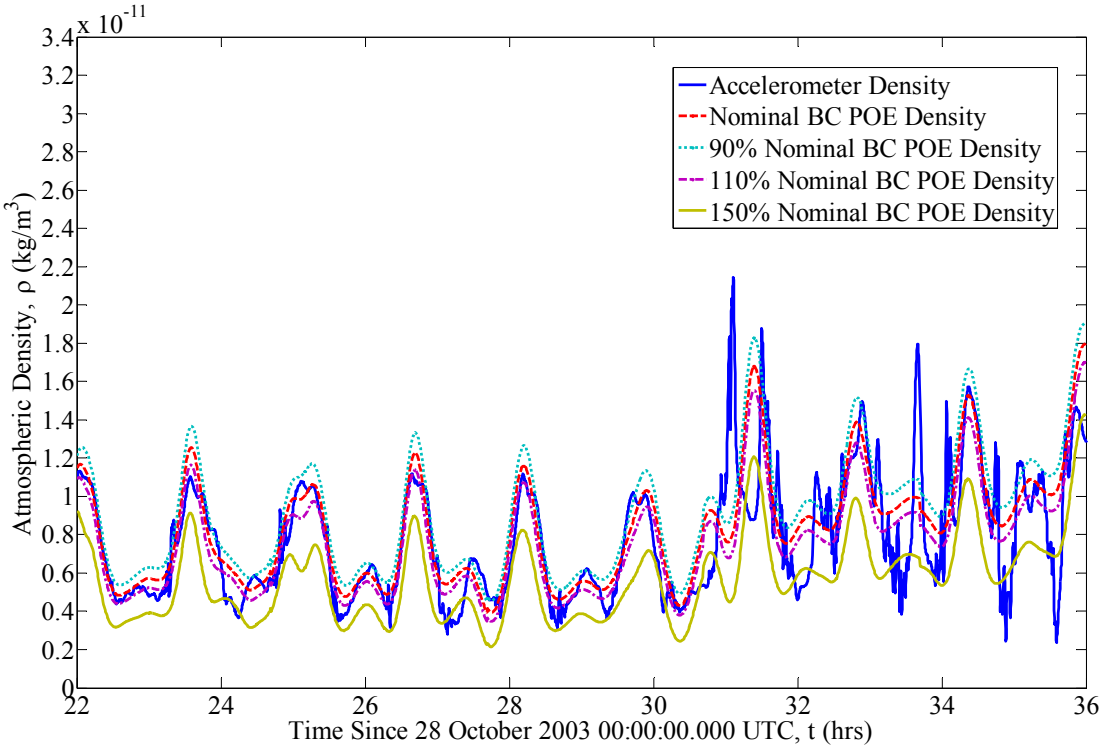

Figure 5.6 Effect of Varying the Initial Ballistic Coefficient on the POE Estimated Density for October 28-29, 2003. *Density and ballistic coefficient correlated half-lives are 18 minutes and 1.8 minutes, respectively. The baseline density model is CIRA-1972.*

Figure 5.6 shows the effect of varying the initial ballistic coefficient on the POE density estimates for October 28-29, 2003. As the initial ballistic coefficient value is increased from 90-150% of the nominal value, the POE density estimate decreases with the most notable influence occurring at the density peaks. Again, this result is expected given the relationship for the acceleration due to drag. The relationship states that for a constant

acceleration the density will decrease as the ballistic coefficient increases. Also, the POE density estimates agree well with the accelerometer density for the 90% initial ballistic coefficient variation and the nominal ballistic coefficient solution.

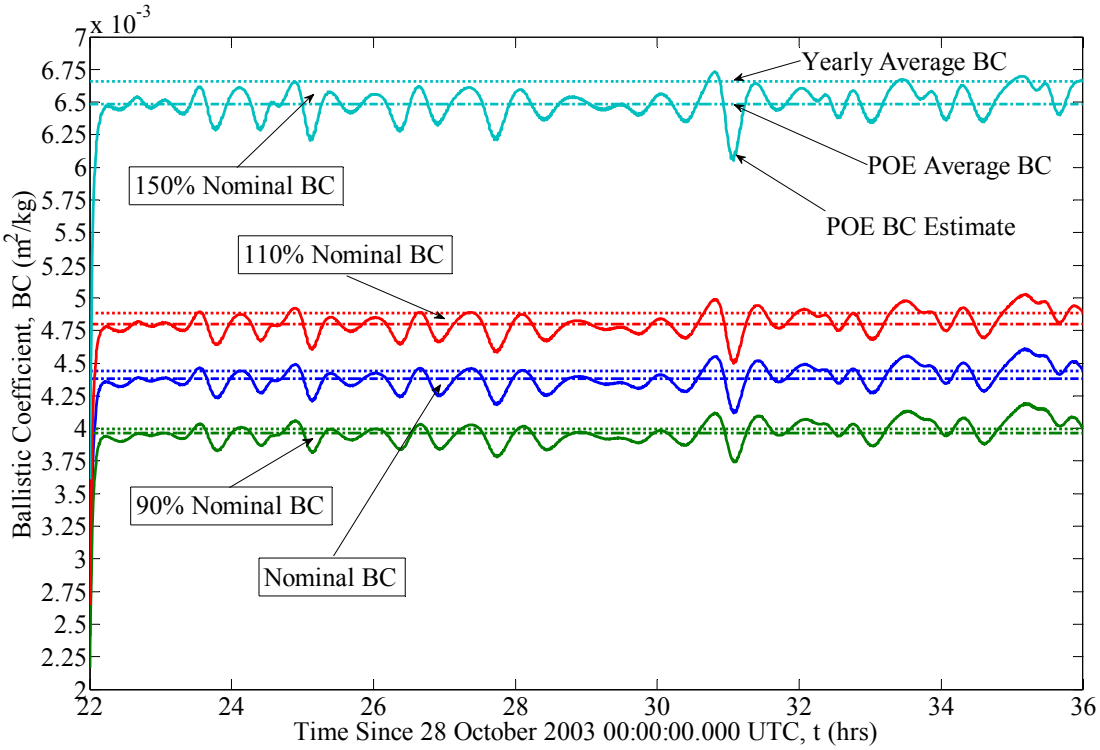

Figure 5.7 Effect of Varying the Initial Ballistic Coefficient on the POE Estimated Ballistic Coefficient for October 28-29, 2003. *Density and ballistic coefficient correlated half-lives are 18 minutes and 1.8 minutes, respectively. The baseline density model is CIRA-1972.*

Figure 5.7 shows the effect of varying the initial ballistic coefficient on the POE estimated ballistic coefficient for October 28-29, 2003. The ballistic coefficient is estimated as part of the orbit determination process. Notice that the spike in ballistic coefficient occurring a little after 31 hours corresponds to the large spike in the accelerometer density. The initial value and the average estimated value are graphed along with the ballistic coefficients estimated for all given times. Again, the extreme minimum values are present at the beginning of each solution. The POE ballistic coefficient estimates are fairly consistent

and do not vary widely from their average value. This would indicate that the orbit determination process is performing well. Also, as the variation in the initial ballistic coefficient increases, the difference between the average POE estimated ballistic coefficient and the initial ballistic coefficient value also increases. This would suggest that the orbit determination process is attempting to estimate a more accurate ballistic coefficient given the incorrect initial value, whether the value is too large or too small. As the orbit determination process estimates a more accurate ballistic coefficient, the resulting estimated density should also be more accurate given that ballistic coefficient and density are directly related to each other in the drag acceleration equation.

Table 5.11 Zero Delay Cross Correlation Coefficients Using Accelerometer Density Data for the October 28-29, 2003 Solution with Estimation and No Estimation of the Ballistic Coefficient. *The columns are for the POE density estimates when the ballistic coefficient is estimated and not estimated in the orbit determination process. Yellow (or light gray) highlighted numbers indicate the largest value for the specific variation. If multiple values are highlighted, the multiple values are equal. The tan (or darker gray) highlighted number indicates the largest overall number. The cross correlation coefficient for the Jacchia 1971 empirical model is 0.7041. The cross correlation coefficient for the HASDM density is 0.7884. The nominal ballistic coefficient is 0.00444 m^2/kg. CIRA-1972 is the baseline density model for all values.*

Half-Life Combinations, Density/Ballistic Coefficient (min)	*BC Estimation*	*No BC Estimation*
Case 1 1.8/1.8	0.7536	0.7443
Case 2 18/1.8	0.7779	0.7683
Case 3 180/1.8	0.8043	0.8043
Case 7 1.8/18	0.7458	0.7443
Case 8 18/18	0.7789	0.7683
Case 9 180/18	0.8112	0.8043
Case 13 1.8/180	0.7213	0.7443
Case 14 18/180	0.7607	0.7683
Case 15 180/180	0.7914	0.8043

Table 5.11 gives the zero delay cross correlation coefficients using the accelerometer density as the basis for comparison for October 28-29, 2003 when the ballistic coefficient is

both estimated and not estimated by the orbit determination process. These results demonstrate that regardless of whether the ballistic coefficient is estimated or not, the POE density estimates have similar results for most of the cases examined. However, the POE density estimate with the ballistic coefficient estimated as part of the orbit determination process with a density correlated half-life of 180 minutes and a ballistic coefficient correlated half-life of 18 minutes and using the CIRA-1972 baseline atmospheric model does have the highest degree of correlation with the accelerometer density. When the ballistic coefficient is not estimated, the cross correlation coefficients are the same for constant density correlated half-lives and varying ballistic coefficient correlated half-lives. Also, the HASDM density has a greater degree of correlation with the accelerometer density compared with the majority of the POE density estimates. All of the POE density estimates exhibit a greater degree of correlation with the accelerometer density data than the Jacchia 1971 empirical model.

Table 5.12 Maximum Cross Correlation Coefficients Using Accelerometer Density Data for the October 28-29, 2003 Solution with Estimation and No Estimation of the Ballistic Coefficient. *The columns are for the POE density estimates when the ballistic coefficient is estimated and not estimated in the orbit determination process. Yellow (or light gray) highlighted numbers indicate the largest value for the specific variation. If multiple values are highlighted, the multiple values are equal. The tan (or darker gray) highlighted number indicates the largest overall number. The cross correlation coefficient for the Jacchia 1971 empirical model is 0.7150 with a -130 second delay. The cross correlation coefficient for the HASDM density is 0.8063 with a delay of -160 seconds. The nominal ballistic coefficient is 0.00444 m^2/kg. CIRA-1972 is the baseline density model for all values. The values in parenthesis are the corresponding delays in seconds.*

Half-Life Combinations, Density/Ballistic Coefficient (min)	*BC Estimation*	*No BC Estimation*
Case 1 1.8/1.8	0.7613 (120)	0.7561 (160)
Case 2 18/1.8	0.7883 (140)	0.7821 (160)
Case 3 180/1.8	0.8044 (10)	0.8052 (40)
Case 7 1.8/18	0.7487 (70)	0.7561 (160)
Case 8 18/18	0.7844 (100)	0.7821 (160)
Case 9 180/18	0.8118 (-30)	0.8052 (40)
Case 13 1.8/180	0.7233 (60)	0.7561 (160)
Case 14 18/180	0.7646 (80)	0.7821 (160)
Case 15 180/180	0.7921 (-30)	0.8052 (40)

Table 5.12 displays the maximum cross correlation coefficients where the ballistic coefficient is both estimated and not estimated by the orbit determination process for October 28-29, 2003. The same general trends observed in the previous table of zero delay cross correlation coefficients are visible in these results.

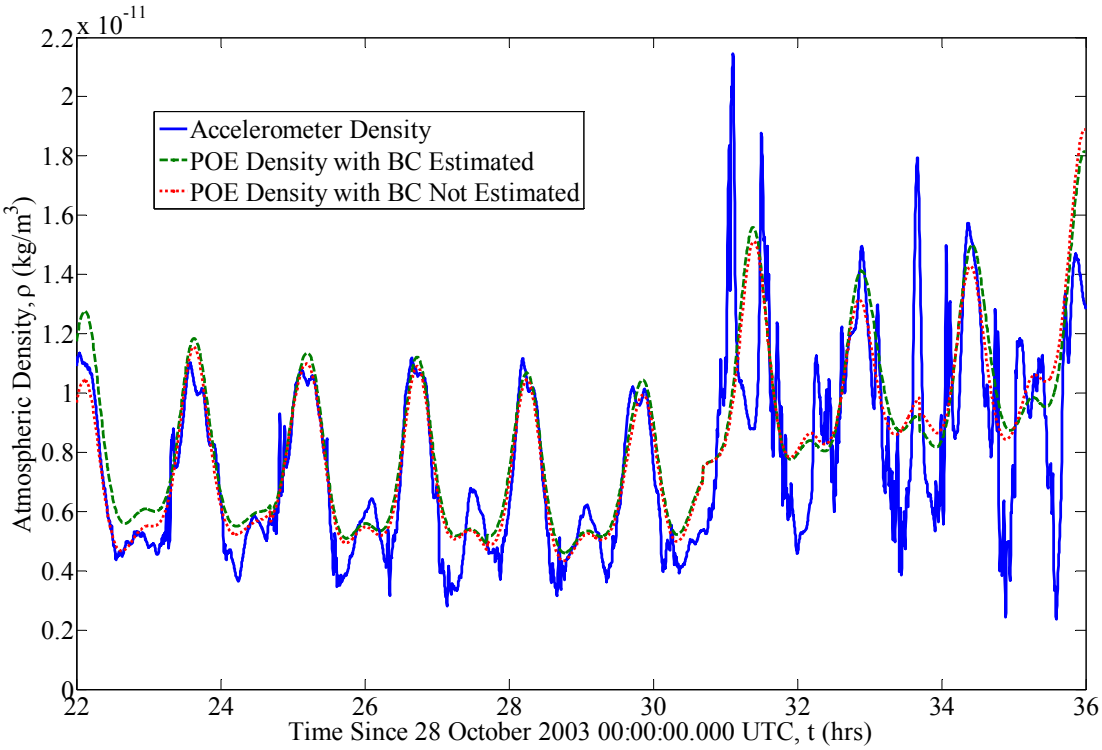

Figure 5.8 Effect of Estimating the Ballistic Coefficient on the POE Estimated Density for October 28-29, 2003. *Density and ballistic coefficient correlated half-lives are 180 minutes and 18 minutes, respectively. The baseline density model is CIRA-1972. The nominal ballistic coefficient is 0.00444 m^2/kg.*

Figure 5.8 shows the effect of estimating the ballistic coefficient on the POE density estimates for October 28-29, 2003. For this solution, the POE density estimates are generally reduced when the ballistic coefficient is not estimated in the orbit determination process. The influence of estimating the ballistic coefficient on the POE density estimate is more pronounced during this solution compared with the March 12, 2005 solution. October 28-29, 2003 is during a period of high solar and active geomagnetic activity. As expected, the observed differences between the two POE density estimates for this solution are more visible. However, whether or not the ballistic coefficient is estimated as part of the orbit determination process, the POE density estimates have similar results. This similarity can be seen in the previous two cross correlation coefficient tables.

5.1.4 Summary of the Ballistic Coefficient Sensitivity Study

The position and velocity consistency tests and the residuals define when the process satisfies predetermined test criteria and does not reject data. They are all important checks on the performance of the process and help to determine what scenarios to ignore or reject. However, they are not enough to definitively say that a given scenario provides accurate density estimates. In some instances, they may indicate a good solution when in fact the results may be less desirable than those obtained from another solution. The cross correlation coefficients using the accelerometer density as the basis for comparison also provides help in selecting the best scenarios but can not be the only data source from which to pick a scenario providing the desired accuracy. Cross correlation coefficients provide an indicator of precision but not necessarily accuracy. Other indicators of a successful solution must also be considered such as the residuals, consistency tests, and density comparisons. The POE estimated density must be compared with the accelerometer density data in conjunction with these other criteria to determine the success or failure of the orbit determination process in producing sufficiently accurate density estimates.

Based on these initial results, the orbit determination process produces relatively good POE density estimates for an initial ballistic coefficient that is ±10% (90-110%) of the nominal ballistic coefficient value regardless of the solar and geomagnetic activity level. For the period with moderate solar and quiet geomagnetic activity levels, the POE estimated density had the highest degree of correlation with the accelerometer density for a ballistic coefficient correlated half-life of 1.8 minutes and a density correlated half-life value of 1.8, 18, or 180 minutes. For the period of high solar and active geomagnetic activity, the POE density estimate had the highest degree of correlation with the accelerometer density for a density half-life of 180 minutes and a ballistic coefficient half-life of 18 minutes.

Also based on these initial results, the effect of estimating the ballistic coefficient in the orbit determination process has little influence on the resulting POE density estimate. The POE density estimate obtained for estimating the ballistic coefficient had very similar results compared with the POE density estimate where the ballistic coefficient was not estimated. The cross correlation coefficients for both situations demonstrated this similarity. However, the impact on the POE density estimate became more pronounced as the solar and geomagnetic activity level increased between the two separate solutions.

5.2 Dependence on Solution Fit Span Length

The solution fit span length chosen for a scenario must be considered carefully. The orbit determination process uses a smoother that takes into account all of the available data generated by the filter to create an estimated density of increased accuracy. Therefore, if the solution fit span is too short then the estimated density may not be as accurate as possible because insufficient data exists in the solution. In contrast, including too much data in a solution will significantly increase the time required to generate the solution with the resulting accuracy showing very little if any improvement over a more suitable and shorter solution fit span. A balance must then be struck to minimize the time and resources required to generate a solution with the desired accuracy while not limiting the amount of data available to the process thereby decreasing the accuracy. However, the definition of how long the fit span should be is not necessarily readily available.

This section examines the influence the fit span length has on the POE estimated density. A 36 hour fit span was generated for February 20-21, 2002 for the sake of comparison because a longer fit span should provide for a good comparison with shorter fit spans. Three different 6 hour fit spans were generated within the same period with successive fit spans possessing a small overlap region. These shorter fit spans were

compared to determine the performance of the orbit determination process in terms of how well they compare with the longer and presumably more accurate longer solution fit span.

Longer fit span lengths were examined but six hour fit span lengths are consider the worst case scenario. Accordingly, if the solutions obtained from a six hour fit span passed the consistency tests, did not reject any data, and compared well with the accelerometer density and 36 hour solution, then solutions obtained from longer fit spans could therefore be considered with confidence. Other fit span lengths examined include 12 hour and 24 hour lengths. The results were similar to those obtained from six hour fit span lengths. Solution fit span length was also examined for March 17, 2005. The results obtained for the March date are similar to the results present here for February 20-21, 2002.

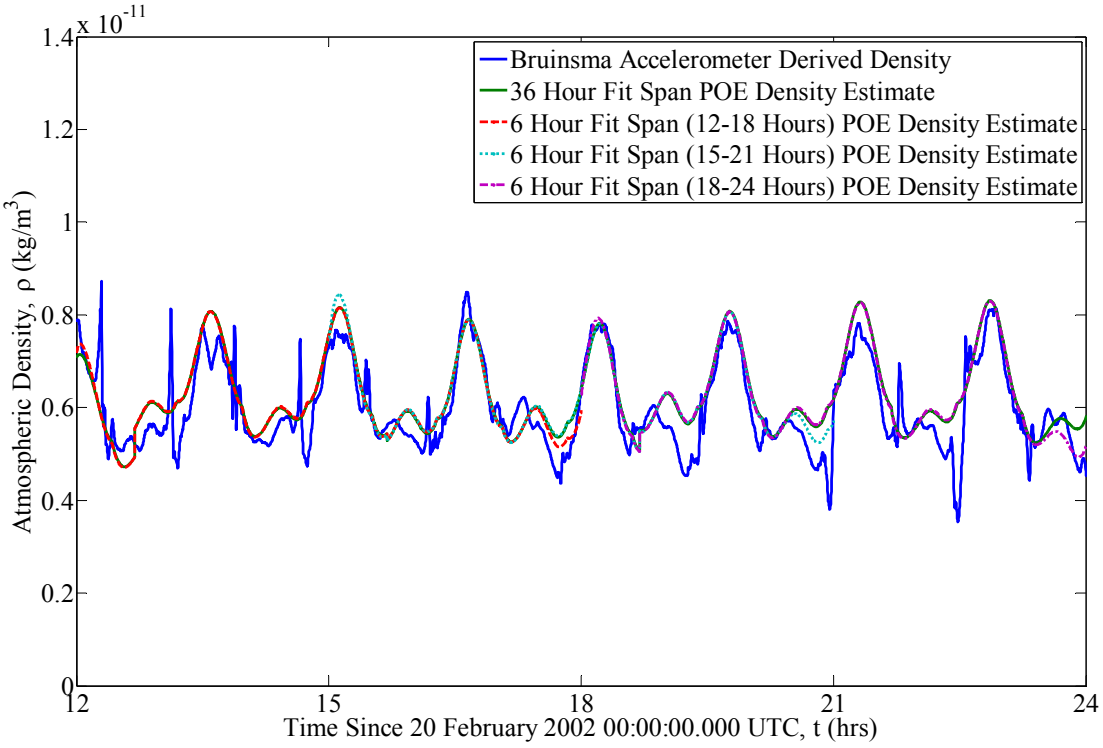

Figure 5.9 Effect of Solution Fit Span Length on the POE Estimated Density for February 20-21, 2002. *Density and ballistic coefficient correlated half-lives are 1.8 minutes each. The baseline density model is MRLMSISE-2000.*

Figure 5.9 shows how the solution fit span length influences the POE estimated density. The longer solution fit span shows relatively good agreement with the accelerometer density. The shorter fit spans essentially coincide with the longer solution fit span length and also show relatively good agreement with the accelerometer density. The only exception is the end effects observed for the 6 hour fit span length. The orbit determination process experiences difficultly producing good estimates of density at the ends of the solutions because of the diminishing amount of data available neighboring these locations.

This is a representative example showing that the orbit determination process is capable of generating relatively accurate estimates of atmospheric density even for short fit spans. The end effects seen in the above figure are experienced by all solutions regardless of the fit span length due to the lack of available data. The results would suggest that 6 hour fit spans are close to the minimum fit span length that produces sufficiently accurate density estimates. Any fit span length shorter than six hours also begins to become less practical. This section describes another approach to comparing the density estimates to ensure they are sufficiently accurate and that the orbit determination process is functioning well. Also, these results demonstrate that the 14 hour and longer POE data sets used in this work contain a sufficient amount of data to generate accurate POE density estimates. Therefore, stitching together successive POE data sets is not required to achieve the desired accuracy in the POE density estimates.

5.3 Overlap Regions

An orbit determination process generates density estimates using POE data for a fixed interval of time. For instance, the majority of solutions generated in this work are for 14 hour fit spans. The end effects for a given solution were clearly visible in the previous section and will exist for all solutions regardless of the fit span length. As mentioned

previously, this is a limitation inherent in the finite amount of data contained in the POE data files used in the orbit determination process. The overlaps provide an opportunity to analyze the estimated density in terms of how well the orbit determination process is functioning. The POE density estimates in the overlap regions will not be perfect but allow for a check in the consistency in the two solutions. If the orbit determination process is functioning properly, the two POE density estimates will closely agree with each other. However, the overlap regions should be considered carefully because they provide a check of the consistency between POE density estimates and not a comparison of accuracy to a benchmark density data set such as accelerometer density. For instance, two overlapping POE density data sets might have good agreement with each other but have a significant bias in both of the density estimates causing their accuracy to be poor compared with accelerometer density. Also, a satellite does not need to have an accelerometer to generate overlaps as a check on the consistency of the orbit determination solutions. The overlaps are created by the orbit determination process using POE data and not accelerometer data.

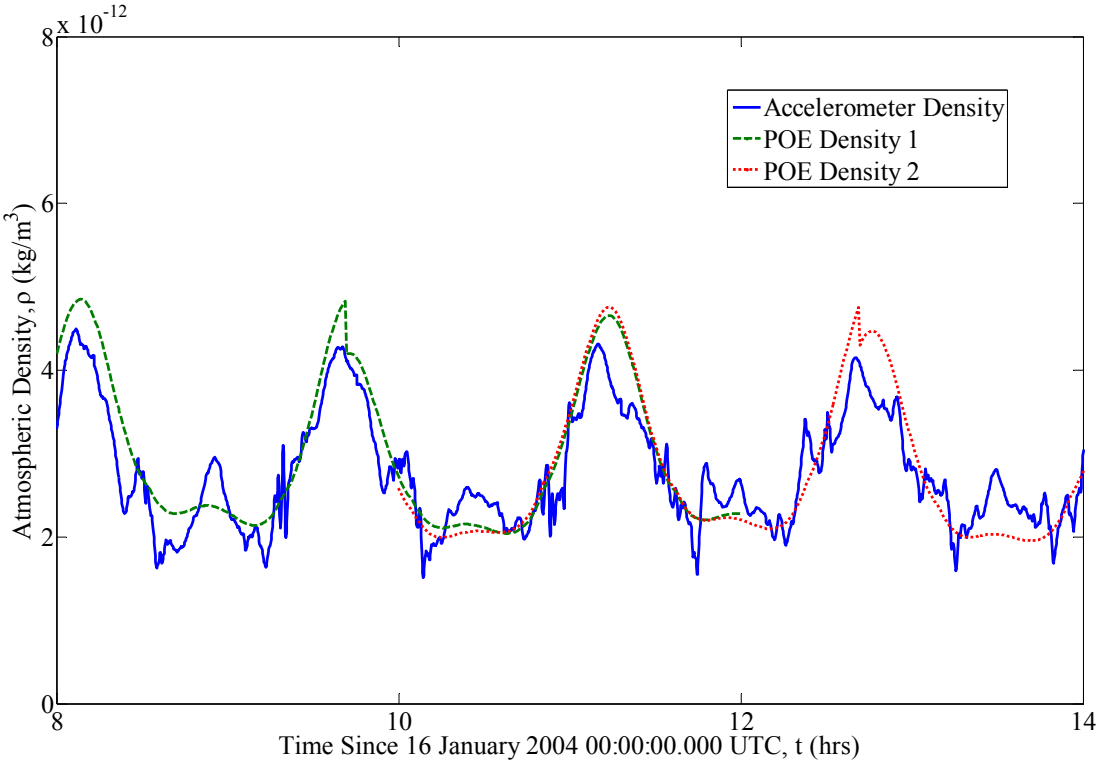

Figure 5.10 Accuracy of POE Density Estimates in an Overlap Region for January 16, 2004. *Density and ballistic coefficient correlated half-lives are 18 minutes each and the baseline density model is Jacchia 1971.*

Figure 5.10 demonstrates how an overlap region of two solutions can provide insight into the performance of the orbit determination process used to generate the density estimates. The two POE density estimates show relatively good agreement with one another indicating that the orbit determination process is generating consistent estimates of atmospheric density. The solutions within the overlap region also show good agreement with the accelerometer density indicating the orbit determination process is creating good density estimates. However, the orbit determination may generate consistent but poor estimates of the atmospheric density. As previously mentioned, a bias may exist in the density estimates causing them to have very poor agreement with the accelerometer density or some other benchmark density data set.

Table 5.13 Effect of Solar Activity on the Root Mean Square Error for Various Overlap Regions. *The dates considered for these results correspond to the POE density estimates using the best baseline atmospheric model and half-life combination for each respective day as previously defined. The overlap period is 2 hours for all dates except for February 19, 2002 that has an 18 hour overlap period. The POE density estimate for February 19, 2002 uses the Jacchia-Roberts baseline model with a density and ballistic coefficient correlated half-life of 18 and 1.8 minutes, respectively.*

Date	Solar Activity Level	Root Mean Square Error (kg/m^3)	Average Density (kg/m^3)	Error (%)
September 9, 2007	Low	7.4384e-014	1.4598e-012	5.10
January 16, 2004	Moderate	7.7909e-014	2.7751e-012	2.81
February 19, 2002	Elevated	7.7813e-014	5.8369e-012	1.33
October 29, 2003	High	1.6508e-012	1.0906e-011	15.14

Table 5.13 shows the effect of solar activity on the root mean square error for various overlap regions. The first observation readily available is that the root mean square errors are very small for all dates considered regardless of the level of solar activity. The second observation is that the root mean square error generally increases with increasing solar activity. The variation in the root mean square error is within a few percent among the days with low, moderate, and elevated solar activity. The largest increase of approximately 20% in the root mean square error occurs between the days with elevated and high solar activity. Also, the root mean square error for the elevated solar activity date shows a slight decrease in magnitude compared with the overlap region containing moderate solar activity. The likely cause of this difference is that the overlap region for February 19, 2002 is 18 hours compared with 2 hours for all other dates. Therefore, as the length of the overlap period increases, the two individual density estimates become more consistent with each other. The small values for the root mean square error indicate that the density estimates generated by the orbit determination process are consistent with each other for all solar activity levels. Also, the errors displayed in the far right column of the table represent the percentage of the root mean

square error of the average density or the difference compared to the average density. These errors range from approximately 1 to 15% indicating consistency of the solutions generated by the orbit determination process.

Table 5.14 Effect of Geomagnetic Activity on the Root Mean Square Error for Various Overlap Regions. *The dates considered for these results correspond to the POE density estimates using the best baseline atmospheric model and half-life combination for each respective date as previously defined. The overlap period is 2 hours for all dates.*

Date	Geomagnetic Activity Level	Root Mean Square Error (kg/m^3)	Average Density (kg/m^3)	Error (%)
September 9, 2007	Quiet	7.4384e-014	1.4598e-012	5.10
January 16, 2004	Moderate	7.7909e-014	2.7751e-012	2.81
October 29, 2003	Active	1.6508e-012	1.0906e-011	15.14

Table 5.14 demonstrates the effect of geomagnetic activity on the root mean square error for various overlap regions. The first observation readily available is that the root mean square errors are very small for all dates considered regardless of the level of geomagnetic activity. Also, the root mean square error increases with increasing geomagnetic activity. The variation in the root mean square error is within a few percent among the days with quiet and moderate geomagnetic activity. The largest increase of approximately 20% in the root mean square error occurs between the days with moderate and active geomagnetic activity. The small values for the root mean square error indicate that the density estimates generated by the orbit determination process are consistent with each other for all geomagnetic activity levels. As with the solar activity table, the errors in the far right column range from approximately 3 to 15% demonstrating the consistency of the solutions.

5.4 Using GRACE-A POE Data to Generate POE Density Estimates

The twin GRACE satellites are equipped with very sensitive accelerometers that can be used to generate accelerometer density data. They are also equipped with GPS receivers that generate POE data. Therefore, they provide an ability to check the results obtained thus far for CHAMP. The GRACE-A POE data were used to generate POE density estimates from an orbit determination process in a similar fashion done for CHAMP. The accelerometer density data obtained for GRACE-A are used as the comparison baseline data to which all of the resulting GRACE-A POE density estimates are compared. At 10 a.m. on September 9, 2007 GRACE-A was at an approximate altitude of 447 km with an inclination of 89 degrees in a near circular orbit. For this date and time, CHAMP was in a near circular orbit at an inclination of 87 degrees and an approximate altitude of 338 km.

Table 5.15 GRACE-A Zero Delay Cross Correlation Coefficients for 1000-2400 Hours September 9, 2007. *The columns of density models are the baseline models used for the POE estimated density and not the actual models themselves. Yellow (or light gray) highlighted numbers indicate the largest value for the baseline model. The orange (or darker gray) highlighted number indicates the largest overall number. The cross correlation coefficient for the Jacchia 1971 empirical model is 0.8674. The cross correlation coefficient for the HASDM density is 0.8757.*

Half-Life Combinations, Density/Ballistic Coefficient (min)	*CIRA-1972*	*Jacchia 1971*	*Jacchia-Roberts*	*MSISE-1990*	*NRLMSISE-2000*
Case 1 1.8/1.8	0.8685	0.8688	0.8683	0.8641	0.8603
Case 2 18/1.8	0.8618	0.8642	0.8602	0.8259	0.8290
Case 3 180/1.8	0.8718	0.8726	0.8713	0.8612	0.8623
Case 7 1.8/18	0.8687	0.8689	0.8686	0.8666	0.8633
Case 8 18/18	0.8642	0.8662	0.8628	0.8329	0.8356
Case 9 180/18	0.8719	0.8727	0.8714	0.8621	0.8633
Case 13 1.8/180	0.8692	0.8691	0.8693	0.8710	0.8692
Case 14 18/180	0.8710	0.8713	0.8707	0.8654	0.8655
Case 15 180/180	0.8655	0.8660	0.8652	0.8678	0.8692

Table 5.15 displays the zero delay cross correlations coefficients obtained for September 9, 2007 using GRACE-A POE data to generate the POE density estimates. This table of coefficients follows the same form and organization as for all of the previous coefficient tables. September 9, 2007 was selected for GRACE-A because the day was also previously considered for CHAMP allowing for comparison between the two sets of results. The first observation from comparing the GRACE-A and CHAMP results is that the cross correlation coefficients for GRACE-A are reduced in magnitude compared with the CHAMP coefficients. Also, the GRACE-A POE density estimate using a density correlated half-life of 180 minutes and a ballistic coefficient correlated half-life of 18 minutes along with the Jacchia 1971 baseline atmospheric model has the highest degree of correlation with the GRACE-A accelerometer density. For this day using the CHAMP POE data, the highest degree of correlation with the CHAMP accelerometer density data occurred for the same half-life combination as GRACE-A but for the NRLMSISE-2000 baseline atmospheric model.

The Jacchia family of baseline atmospheric models used to generate the GRACE-A POE density estimates has their highest degree of correlation for a density and ballistic coefficient correlated half-life of 180 and 18 minutes, respectively. This is also a change from the CHAMP results where a density and ballistic coefficient correlated half-life of 180 and 1.8 minutes, respectively, generated the POE density estimates with the highest degree of correlation when the Jacchia family of baseline models was used. However, both the GRACE-A and CHAMP results show little difference in the cross correlation coefficients for the aforementioned half-life combinations. In fact, the cross correlation coefficients are very close in magnitude regardless of half-life combination for both the GRACE-A and CHAMP results. Also, the coefficients for the CIRA-1972, Jacchia 1971, and Jacchia-Roberts baseline atmospheric models used to generate the POE density estimates all show similar results as the

half-life combinations are varied. This result is consistent between the GRACE-A and CHAMP cross correlation coefficients. A similar discussion can be made for the MSIS family of baseline atmospheric models used to generate the POE density estimates. However, the zero delay cross correlation coefficients demonstrate that the MSISE-1990 and NRLMSISE-2000 baseline atmospheric models used to create the GRACE-A POE density estimates have their highest degree of correlation for a half-life combination different than for the CHAMP results.

One noticeable difference between the GRACE-A and CHAMP results is that the HASDM density has the highest degree of correlation for the GRACE-A results compared with the POE density estimates having the greatest degree of correlation for the CHAMP results. However, the difference between the HASDM and POE density estimates for the GRACE-A results is very small. Also, the GRACE-A POE density estimates have a higher degree of correlation with the accelerometer density compared with the Jacchia-1971 empirical model. This result is mirrored in the CHAMP cross correlation coefficient results.

Table 5.16 GRACE-A Maximum Cross Correlation Coefficients for 1000-2400 Hours September 9, 2007. *The columns of density models are the baseline models used for the POE estimated density and not the actual models themselves. Yellow (or light gray) highlighted numbers indicate the largest value for the baseline model. The orange (or darker gray) highlighted number indicates the largest overall number. The cross correlation coefficient for the Jacchia 1971 empirical model is0.8767 with a 120 second delay. The cross correlation coefficient for the HASDM density is 0.8788 with a delay of 60 seconds. The values in parenthesis are the corresponding delays in seconds.*

Half-Life Combinations, Density/Ballistic Coefficient (min)	*CIRA-1972*	*Jacchia 1971*	*Jacchia-Roberts*	*MSISE-1990*	*NRLMSISE-2000*
Case 1 1.8/1.8	0.8781 (125)	0.8785 (125)	0.8779 (125)	0.8708 (95)	0.8697 (120)
Case 2 18/1.8	0.8731 (130)	0.8754 (130)	0.8716 (130)	0.8356 (125)	0.8403 (135)
Case 3 180/1.8	0.8813 (120)	0.8821 (120)	0.8808 (120)	0.8708 (120)	0.8720 (120)
Case 7 1.8/18	0.8783 (120)	0.8785 (125)	0.8781 (120)	0.8738 (100)	0.8726 (120)
Case 8 18/18	0.8751 (130)	0.8771 (130)	0.8738 (130)	0.8422 (120)	0.8463 (130)
Case 9 180/18	0.8813 (120)	0.8821 (120)	0.8808 (120)	0.8714 (120)	0.8728 (120)
Case 13 1.8/180	0.8788 (125)	0.8787 (125)	0.8789 (125)	0.8797 (115)	0.8788 (120)
Case 14 18/180	0.8815 (125)	0.8817 (125)	0.8812 (130)	0.8753 (125)	0.8763 (130)
Case 15 180/180	0.8747 (120)	0.8752 (120)	0.8743 (120)	0.8769 (120)	0.8784 (120)

Table 5.16 shows the maximum cross correlation coefficients obtained for September 9, 2007 using GRACE-A POE data to generate the POE density estimates. Many of the general trends observed in the previous table are visible in these results. The first observation for these results is the change in half-life combination for a few of the baseline atmospheric model used to generate the GRACE-A POE density data. Also, the GRACE-A POE density

estimate using the Jacchia 1971 baseline atmospheric model and a density correlated half-life of 180 minutes and a ballistic coefficient correlated half-life of 18 minutes now has the highest degree of correlation with the accelerometer density compared with the coefficient for the HASDM density. A majority of the GRACE-A POE density estimates have cross correlation coefficients greater the coefficient for the Jacchia 1971 empirical model. The results displayed in this table of cross correlation coefficients are consistent with the trends observed for the CHAMP results. The main exception is that the half-life combinations for the baseline atmospheric models used to generate the GRACE-A POE density estimates with the highest degree of correlation are different for the GRACE-A results compared to the CHAMP results. However, the differences between the GRACE-A half-life combinations for each baseline atmospheric model are very small such that the results would be only slightly influenced from using any of the half-life combinations other than what has the highest cross correlation coefficient. Also, notice the relatively large delays for the POE density estimates and the Jacchia 1971 empirical model.

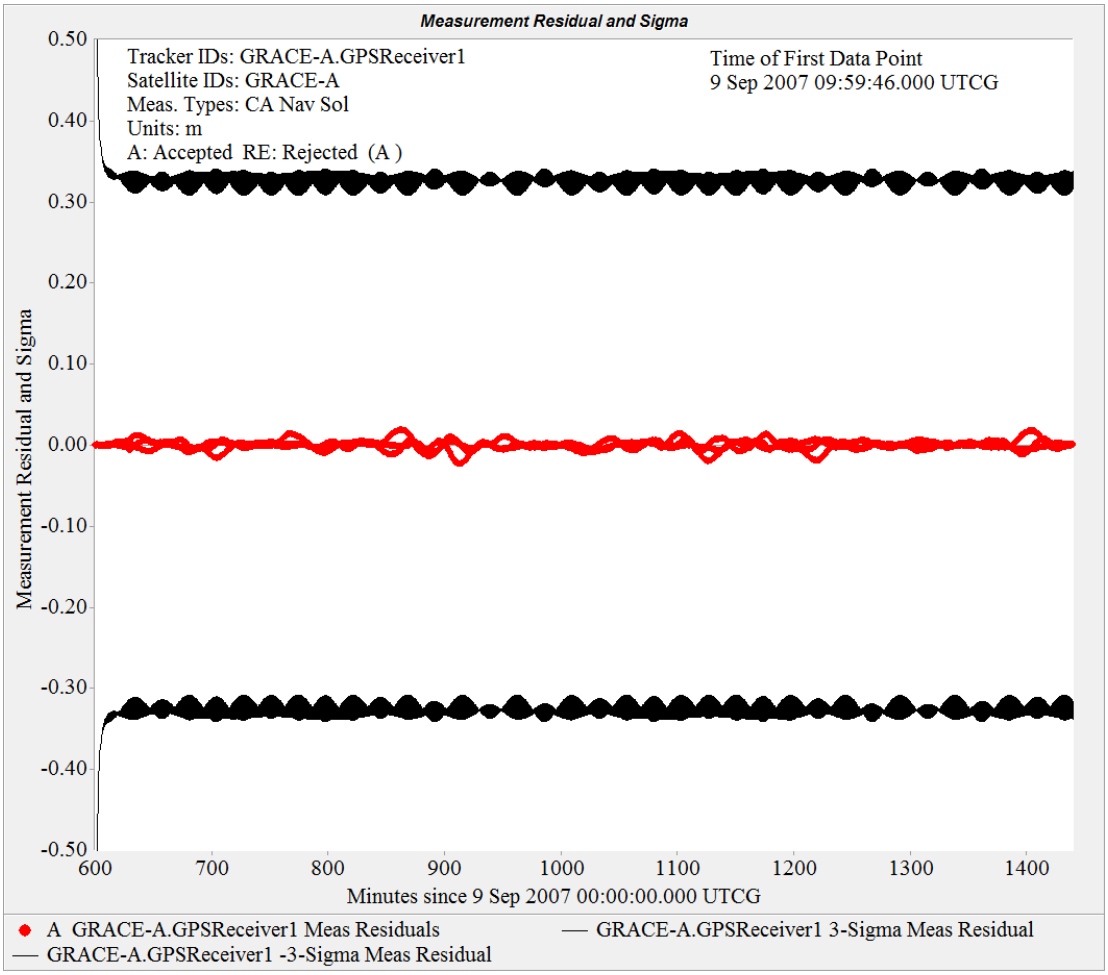

Figure 5.11 GRACE-A Filter Residuals for 1000-2400 Hours September 9, 2007. *Density and ballistic coefficient correlated half-lives are 180 and 18 minutes, respectively. The baseline density model is Jacchia 1971.*

Figure 5.11 shows the filter residuals obtained for the GRACE-A solution for September 9, 2007. The filter residuals fall within ±3 cm with a 3σ boundary of about 33 cm. This range of values for the residuals is expected given that the measurement data are also expected to be very accurate because they are processed in a similar fashion as the CHAMP measurement data. Also, September 9, 2007 is a period of low solar and quiet geomagnetic activity so the residuals should be small compared with more active periods.

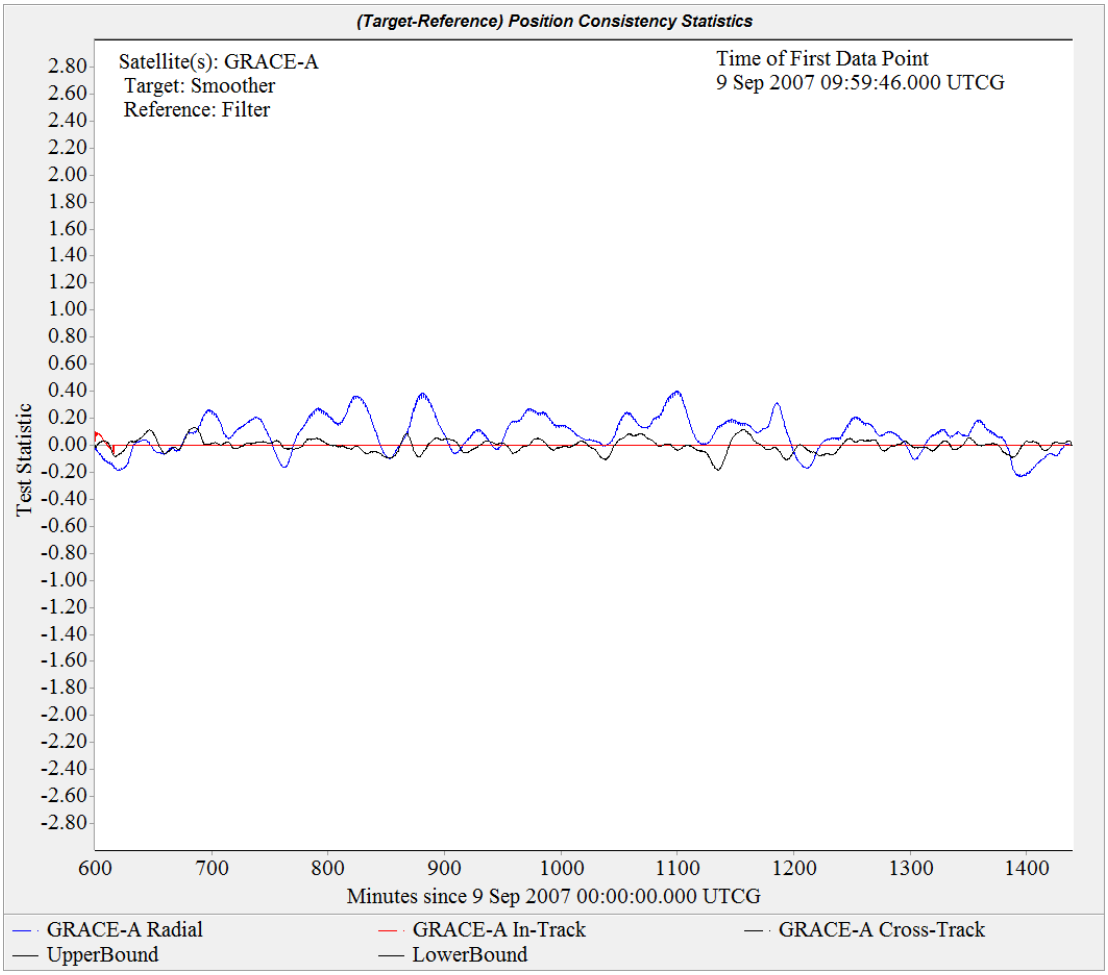

Figure 5.12 GRACE-A Position Consistency Test for 1000-2400 Hours September 9, 2007. *Density and ballistic coefficient correlated half-lives are 180 and 18 minutes, respectively. The baseline density model is Jacchia 1971.*

Figure 5.12 displays the position consistency test graph for the September 9, 2007 solution for the GRACE-A satellite. The consistency test for the in-track, cross-track, and radial direction is well satisfied at all times. This is also expected given the expected accuracy of the measurement data and the low solar and quiet geomagnetic activity levels for this day.

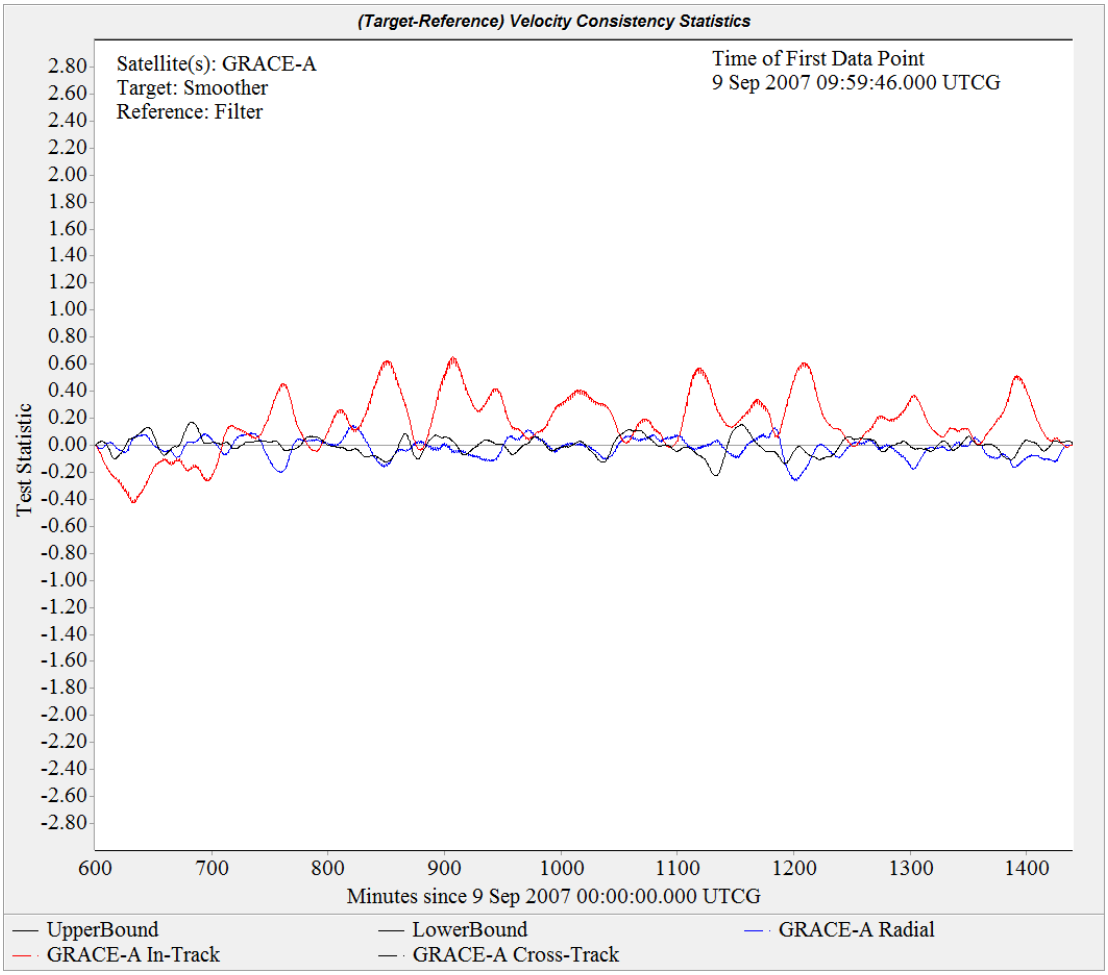

Figure 5.13 GRACE-A Velocity Consistency Test for 1000-2400 Hours September 9, 2007. *Density and ballistic coefficient correlated half-lives are 180 and 18 minutes, respectively. The baseline density model is Jacchia 1971.*

Figure 5.13 displays the velocity consistency test graph for the September 9, 2007 solution for the GRACE-A satellite. The consistency test for the in-track, cross-track, and radial direction is well satisfied at all times. As for the position consistency test, this is also expected given the expected accuracy of the measurement data and the low solar and quiet geomagnetic activity levels.

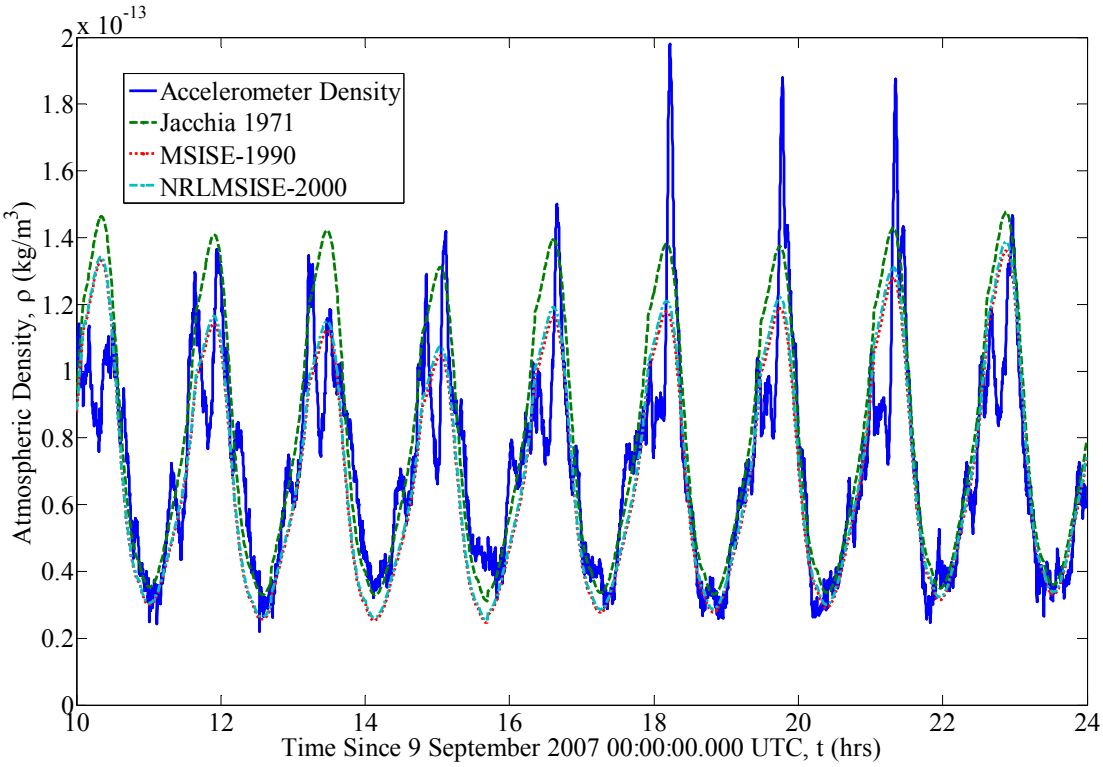

Figure 5.14 Effect of Varying the Baseline Atmospheric Model on the Estimated Density for GRACE-A for 1000-2400 hours September 9, 2007. *Density and ballistic coefficient correlated half-lives are 180 and 18 minutes, respectively. The baseline density model is Jacchia 1971.*

Figure 5.14 demonstrates the effect of varying the baseline atmospheric model on the POE density data for the GRACE-A solution for September 9, 2007. As seen in previous graphs depicting similar effects, the MSISE-1990 and NRLMSISE-2000 baseline atmospheric model used to generate the GRACE-A POE density data sets have very similar results. The GRACE-A POE density data set using Jacchia 1971 as the baseline atmospheric model shows the best agreement with the accelerometer density data. The cross correlation coefficient tables support these results. In particular, the GRACE-A POE density estimate using the Jacchia 1971 baseline atmospheric model had the highest degree of correlation with the accelerometer density data. These results for the GRACE-A POE density estimates are similar to those obtained for the CHAMP POE density estimates.

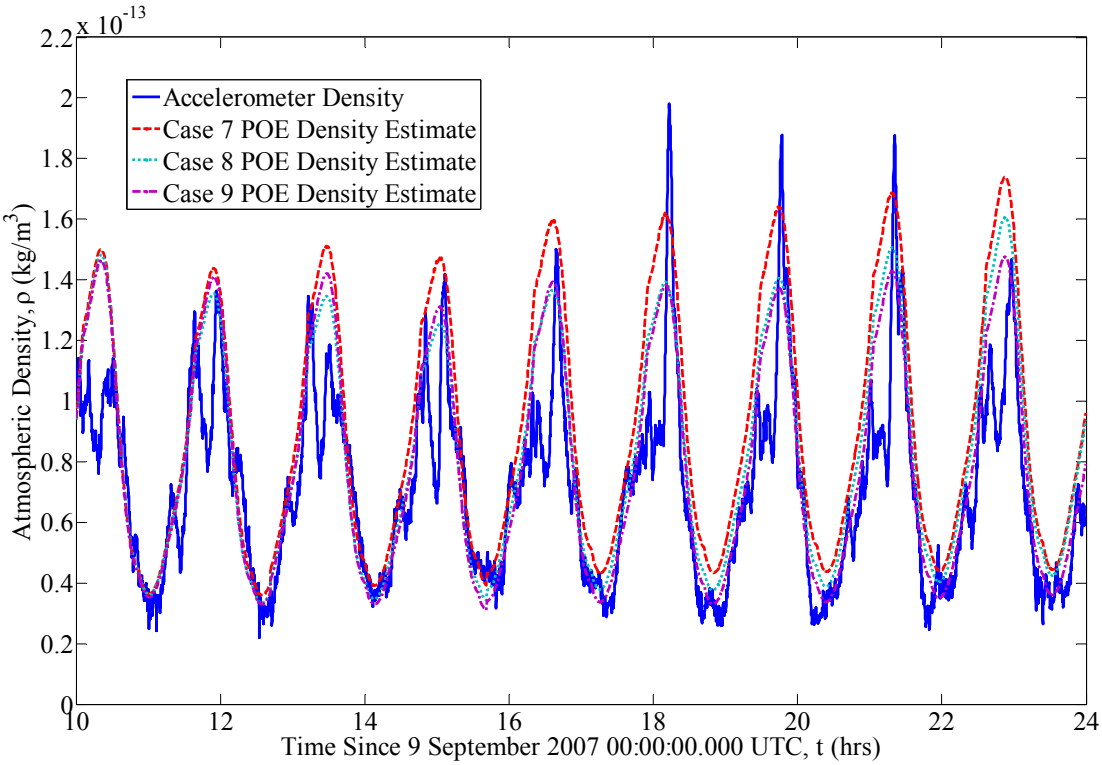

Figure 5.15 Effect of Varying the Density Correlated Half-Life on the Estimated Density for GRACE-A for 1000-2400 hours September 9, 2007. *Ballistic coefficient correlated half-life is 18 minutes and the baseline density model is Jacchia 1971. Cases 7, 8, and 9 have density correlated half-lives of 1.8, 18, and 180 minutes, respectively.*

Figure 5.15 demonstrates the effect of varying the density correlated half-life for a constant ballistic coefficient correlated half-life on the GRACE-A POE density estimates for September 9, 2007. Generally, as the density correlated half-life is increased, the GRACE-A POE density estimate is decreased. This effect was also observed for the CHAMP POE density estimates. The cross correlation coefficients indicate that a value of 180 minutes is the best density correlated half-life for this particular ballistic coefficient correlated half-life of 18 minutes.

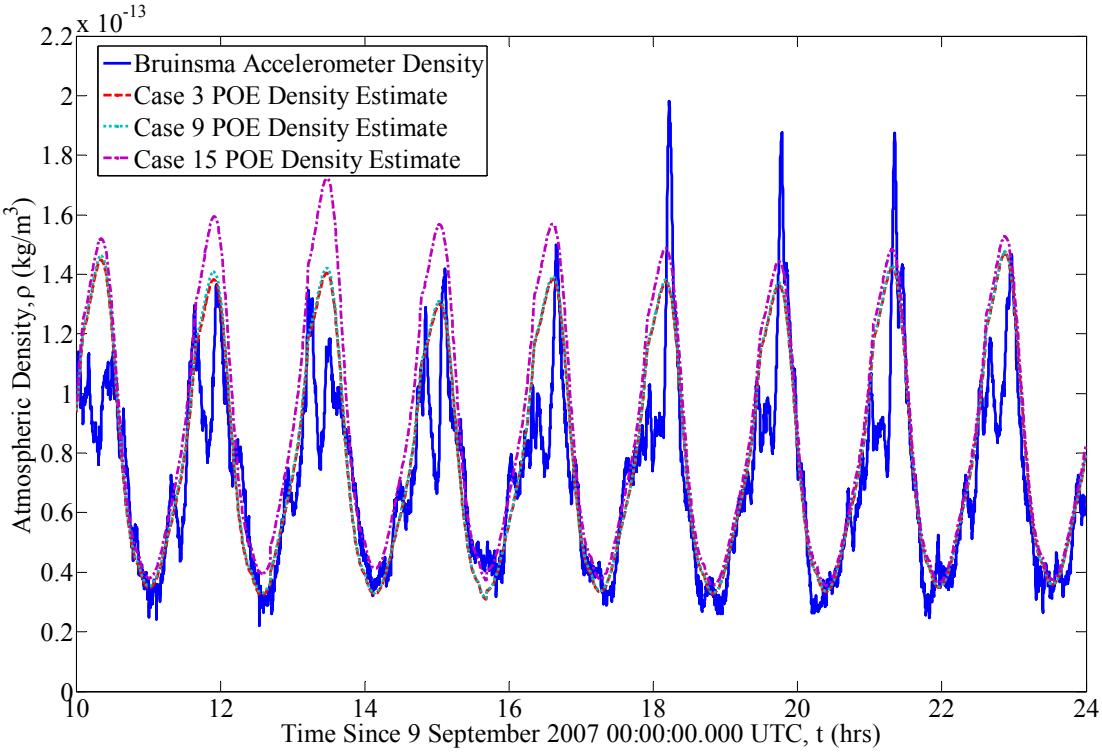

Figure 5.16 Effect of Varying the Ballistic Coefficient Correlated Half-Life on the Estimated Density for GRACE-A for 1000-2400 hours September 9, 2007. *Density correlated half-life is 180 minutes and the baseline density model is Jacchia 1971. Cases 3, 9, and 15 have ballistic coefficient correlated half-lives of 1.8, 18, and 180 minutes, respectively.*

Figure 5.16 shows the effect on the GRACE-A POE density estimates of varying the ballistic coefficient correlated half-life while holding the density correlated half-life constant. As the ballistic coefficient correlated half-life is increased, the GRACE-A POE density estimate values tend to decrease in magnitude. The same trend is seen for the CHAMP POE density estimates. The cross correlation coefficients for the GRACE-A POE density estimates show that when the density correlated half-life is held constant at 180 minutes, a ballistic coefficient correlated half-life of 18 minutes has the highest degree of correlation with the accelerometer density.

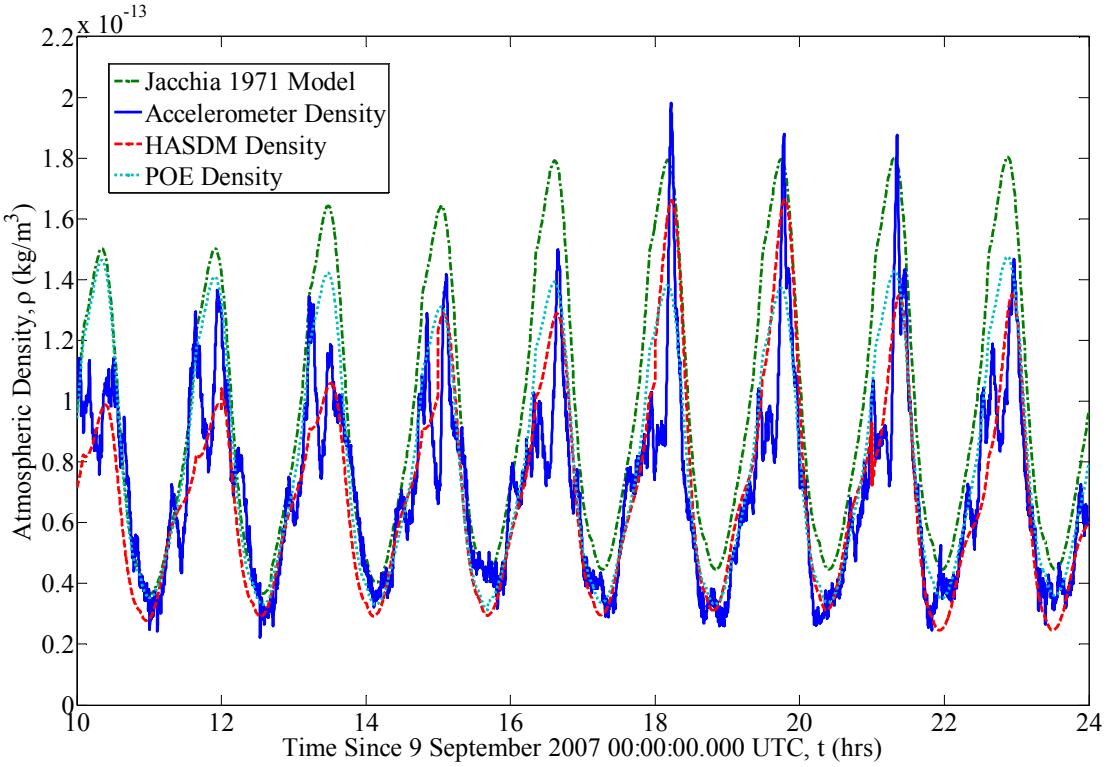

Figure 5.17 Comparison of Densities Obtained from Different Methods for GRACE-A for 1000-2400 hours September 9, 2007. *POE density obtained using a density correlated half-life of 180 minutes and a ballistic coefficient correlated half-life of 18 minutes and Jacchia 1971 as the baseline density model.*

Figure 5.17 displays a comparison of the estimated densities obtained from the Jacchia 1971 empirical model, the GRACE-A accelerometer, HASDM, and the GRACE-A POE density estimate. The Jacchia 1971 empirical demonstrates the least agreement with the accelerometer density, which is also visible in the cross correlation coefficient value. Both the HASDM and GRACE-A POE density estimates show improvement over the existing baseline atmospheric model such as the Jacchia 1971 empirical model. Examination of the cross correlation coefficient tables provides some support for this observation. Also, the GRACE-A POE density estimate appears to have better agreement with the accelerometer density compare with the HASDM density. However, the cross correlation coefficient tables

have conflicting results in terms of whether the GRACE-A POE density estimate or the HASDM density correlates best with the accelerometer density. Examining the zero delay cross correlation coefficient table, the HASDM density has the higher value compared with the GRACE-A POE density estimate. In contrast, the maximum cross correlation coefficient table shows the opposite where the GRACE-A POE density estimate has a higher degree of correlation with the accelerometer density compared with the HASDM density. The general conclusions and trends seen in this graph are also exhibited in the CHAMP POE density estimate results and comparisons.

The results obtained from looking at one solution using the GRACE-A POE data in an orbit determination process to generate POE density estimates demonstrates very similar results for the CHAMP POE data. There are some differences in the GRACE-A results with those differences mainly being in the cross correlation coefficient tables in terms of the half-life combinations and baseline atmospheric model to use to generate the GRACE-A POE density estimates with the best correlation with the accelerometer density. However, as with the CHAMP results, the differences observed in the cross correlation coefficients among the various half-life combinations for a given baseline atmospheric model is so small that most of the half-life combinations can be used with little effect on the resulting GRACE-A POE density estimates. Also, the baseline atmospheric model producing the POE density estimate with the highest degree of correlation with the accelerometer is different for the GRACE-A satellite compared with the CHAMP satellite. While many of the same general trends and conclusions are available for the GRACE-A POE density estimates as were found for the CHAMP results, much research needs to be conducted using the GRACE-A POE data to expand on these initial results and confirm the results obtained in this work for the CHAMP POE data.

6 SUMMARY, CONCLUSIONS, AND FUTURE WORK

6.1 Summary

Current atmospheric models are incapable of accurately predicting the majority of density variations observed in the Earth's atmosphere. In particular, the thermosphere and exosphere are far more variable than predicted by existing models. These unmodeled or misrepresented density variations directly affect the orbit of satellites in low Earth orbit. Consequently, predicting or determining a satellite's orbit becomes extremely difficult, particularly during periods of increased solar and geomagnetic activity when the Earth's upper atmosphere experiences the greatest variations.

The research conducted for this work showed the potential for using precision orbit data to generate density corrections to an existing atmospheric model resulting in density estimates of increased accuracy. These improved density estimates can be used to create enhanced atmospheric drag calculations, improve orbit determination and prediction, and provide a better understanding and measurement of the density and density variations observed in the thermosphere and exosphere.

This work examined numerous dates selected to consist of days from every year ranging from 2001 to 2007 sampling all twelve calendar months and all four seasons. The dates were distributed to ensure that the various solar and geomagnetic bins were covered and sufficiently sampled. The solar activity bins, with units of SFUs, are labeled as low solar flux ($F_{10.7} < 75$), moderate solar flux ($75 \leq F_{10.7} < 150$), elevated solar flux ($150 \leq F_{10.7} < 190$), and high solar flux ($F_{10.7} \geq 190$). The geomagnetic activity bins are grouped as quiet geomagnetic ($A_p \leq 10$), moderate geomagnetic ($10 < A_p < 50$), and active geomagnetic ($A_p \geq 50$).

This research used precision orbit ephemerides consisting of position and velocity vectors for the Challenging Minisatellite Payload (CHAMP) in an orbit determination process

to generate improved density estimates based on density corrections applied to existing atmospheric models. The orbit determination scheme utilized a sequential Kalman filter/smoother to process the measurements. The baseline atmospheric models currently available in the Orbit Determination Tool Kit (ODTK) software package are Jacchia 1971, Jacchia-Roberts, CIRA-1972, MSISE-1990, and NRLMSISE-2000. Particular attention was given to the effects on the density estimates caused by varying the baseline atmospheric model and the density and ballistic coefficient correlated half-lives. The density and ballistic coefficient correlated half-lives are a user controlled parameter in ODTK that affects the way the unmodeled or inaccurately modeled drag forces influence a satellite's motion and therefore the atmospheric density and ballistic coefficient estimates. The values of the density and ballistic coefficient correlated half-lives primarily used in this study were 1.8, 18, and 180 minutes. Therefore, 9 possible half-life combinations were created using these values. Solutions were generated covering the complete range of solar and geomagnetic activity levels to observe the effect on the atmospheric density and density variations. The solutions included all combinations of the baseline atmospheric model and all density and ballistic coefficient correlated half-life combinations. The resulting atmospheric density estimates were compared with the accelerometer derived density as calculated by Sean Bruinsma at the Centre National d'Études Spatiales (CNES). The precision orbit ephemerides (POE) atmospheric density estimates were also compared to the estimated density from the High Accuracy Satellite Drag Model (HASDM) as obtained from Bruce Bowman of the U.S. Air Force Space Command.

The POE density estimates were also evaluated by examining the position and velocity consistency test graphs generated by the orbit determination process. The consistency tests offer an easy way to view how well the orbit determination process is

functioning. The test statistic incorporates the difference between the filter and smoother divided by the root variance obtained from the error covariance matrices of the filter and smoother. The orbit determination scheme also calculates the residuals, which is the difference between the estimated and measured position of the satellite. The residuals provide another check on the accuracy of the solution generated by the orbit determination process by stating when any measurements are rejected. The measurements used in this work for the orbit determination process are very accurate so if the orbit determination process rejects measurements than this indicates a problem within the determination scheme. However, concluding that an orbit determination scheme has a problem based on data measurements rejected by the filter is limited to the situation where the input data is known to be accurate. Often an orbit determination process using observation data will frequently throw out or reject data because that particular data point might be an outlier not previously removed. This is a common occurrence for many orbit determination processes that must be kept in mind. Therefore, knowing the accuracy of the input measurement data is important when using the filter residuals for evaluation of a particular orbit determination process.

A cross correlation coefficient was also calculated indicating how well the POE density estimates correlate to the accelerometer density data, which is taken as truth for comparison purposes. The cross correlation coefficients were calculated as zero delay and maximum cross correlation coefficients, including the delays, for each specific solution. The resulting cross correlation coefficients were organized as an overall summary and according to the solar and geomagnetic activity bins. The time averaged values were then calculated for the overall summary and activity bins. Similar cross correlation coefficients were calculated for the Jacchia 1971 empirical model and HASDM density estimates correlated to the

accelerometer density for each solution and grouped in an overall summary and according to activity bins.

The sensitivity of the POE density estimates on variations in the initial ballistic coefficient was also examined for two time periods. The first was a 14 hour fit span for October 28-29, 2003 using CIRA-1972 as the baseline atmospheric model and a density and ballistic coefficient correlated half-life of 18 and 1.8 minutes, respectively. The second time period was a 14 hour fit span using CIRA-1972 as the baseline atmospheric model for March 12, 2005 with a density and ballistic coefficient correlated half-life of 1.8 minutes each. The ballistic coefficient may not be well known due to difficulties in the way the cross sectional area and the drag coefficient are calculated. The cross sectional area typically changes constantly and the drag coefficient depends heavily on the configuration of the satellite. Therefore, errors in the ballistic coefficient directly affect the density estimates. A ballistic coefficient study was done to determine how much the ballistic coefficient could vary from the initial value and still give sufficiently accurate estimates of atmospheric density. Residuals and position and velocity consistency tests were used as a check on the performance of the orbit determination process generating the density estimates. Cross correlation coefficients were calculated relating the POE density estimates obtained from the various scenarios of varying initial ballistic coefficient with the accelerometer density to help determine which variation provides the best results. The POE density estimates were compared with the accelerometer density to determine the level of agreement with the accelerometer density. Also, the POE estimated ballistic coefficient was compared with the initial value and the average estimated ballistic coefficient. The POE estimated ballistic coefficient should be close to the initial value if the orbit determination process is estimating density and ballistic coefficient properly.

Variations in the solution fit span length were also considered for February 20-21, 2002 and March 17, 2005. This study was conducted to determine the effects of fit span length on the POE density estimates. A longer fit span possesses more data making the resulting density estimate more accurate. However, a shorter fit span length can be generated much faster and requires fewer resources. The goal of varying the fit span length was to determine how short the fit span could be and still generate sufficiently accurate density estimates. Fit span lengths of 6, 12, and 24 hours were generated for March 12, 2005. Fit spans of 6, 12, 24, and 36 hours were created for February 20-21, 2002. Particular attention was paid to the 6 hour fit spans because they were considered the worst case for fit span length. Therefore, if the 6 hour fit spans generated sufficiently accurate POE density estimates, then the longer fit spans would also have at least sufficiently accurate POE density estimates because of the increase in available data for longer fit spans.

Overlap regions between two POE density estimates were also considered as a check on the consistency of the estimates generated by the orbit determination process. If the two POE density estimates showed good agreement with each other, then the orbit determination process was functioning properly and generating consistent results. Use of the overlap regions must be used carefully, because they describe the consistency between POE density data sets and not accuracy of the estimates with a benchmark such as accelerometer density data.

6.2 Conclusions

The results obtained from the research conducted for this work allow the following conclusions to be made.

1. When all solutions are considered regardless of solar and geomagnetic activity levels, the POE density estimates using CIRA-1972 as the baseline atmospheric

model with a density correlated half-life of 18 minutes and a ballistic coefficient correlated half-life of 1.8 minutes provides the overall highest degree of correlation with the accelerometer derived density.

2. During periods of low solar activity, the POE density estimates from an orbit determination process using the CIRA-1972 baseline model with a density correlated half-life of 180 minutes and a ballistic coefficient correlated half-life of 18 minutes provides the overall highest degree of correlation with the accelerometer derived density.
3. For periods with moderate solar activity, the POE density estimates found using the Jacchia 1971 baseline model with a density correlated half-life of 180 minutes and a ballistic coefficient correlated half-life of 1.8 minutes provides the overall highest degree of correlation with the accelerometer derived density.
4. During periods of elevated and high solar activity, POE density estimates created using CIRA-1972 as the baseline atmospheric model with a density correlated half-life of 18 minutes and a ballistic coefficient correlated half-life of 1.8 minutes provides the overall highest degree of correlation with the accelerometer derived density.
5. During times of quiet geomagnetic activity, the POE density estimates found using the Jacchia 1971 baseline model with a density and ballistic coefficient correlated half-life of 1.8 and 18 minutes, respectively, provides the overall highest degree of correlation with the accelerometer derived density.
6. For periods of moderate and active geomagnetic activity, POE density estimates generated using CIRA-1972 as the baseline atmospheric model with a density correlated half-life of 18 minutes and a ballistic coefficient correlated half-life of

1.8 minutes provides the overall highest degree of correlation with the accelerometer derived density.

7. The conclusions found for the overall summary and binned results do not hold true for every solution. The best baseline atmospheric model and half-life combination for a specific day may not be the same as the conclusions according to the overall summary or solar and geomagnetic activity bins.
8. The POE density estimates show consistent improvement over the Jacchia 1971 empirical model density estimates as compared to the accelerometer density.
9. The POE density estimates have similar results whether the CIRA-1972, Jacchia 1971, or Jacchia-Roberts baseline atmospheric model is used. This result is expected given that these three baseline models are derived from the same atmospheric model.
10. The POE density estimates have similar results whether the MSISE-1990 or NRLMSISE-2000 baseline atmospheric model is used. This result is expected given that these two baseline models are derived from the same atmospheric model.
11. The POE density estimates using the Jacchia family of baseline models typically have a higher degree of correlation with the accelerometer density compared with the POE density estimates using the MSIS family of baseline models.
12. The POE density estimates are always comparable to the HASDM density.
13. The POE density estimates typically have a higher degree of correlation with the accelerometer density than the HASDM density.
14. The general effect of increasing the density correlated half-life is a reduction in the POE estimated density.

15. The general effect of increasing the ballistic coefficient correlated half-life is an increase in the POE estimated density.
16. The POE density estimates are capable of matching the general structure of the accelerometer density but are unable to observe the rapid changes in density. This is a limitation inherent to the underlying baseline atmospheric model.
17. The POE density estimates appear to be somewhat sensitive to variations or errors in the nominal ballistic coefficient used to initialize the orbit determination process that generates the POE density estimates. The extent of this sensitivity remains unclear and requires additional study.
18. Variations or errors of ±10% in the nominal ballistic coefficient used to initialize the determination process still provide sufficiently accurate POE density estimates as compared with the accelerometer density. Supporting evidence includes the position and velocity consistency test being satisfactorily satisfied. Also, no measurement data is rejected as seen in the residuals graphs. Most importantly, the cross correlation coefficients of the POE density estimate to the accelerometer density indicate a high degree of correlation.
19. As the initial ballistic coefficient value used in the orbit determination process increases, the POE density estimate decreases as expected.
20. The orbit determination process appears to attempt to achieve a better estimate of the ballistic coefficient if the initial value is incorrect. More study on this topic is required to gain more information on the behavior of the ballistic coefficient in the orbit determination process.
21. Estimation of the ballistic coefficient within the orbit determination process has little effect on the resulting POE density estimates obtained from the two

solutions examined in this work. Additional research is required to determine more precisely the effects of ballistic coefficient estimation on the POE density estimates.

22. The dependence of the POE density estimate on the solution fit span length is very low. Six hour fit span lengths were shown to provide good agreement with the accelerometer density and POE density estimates with longer fit span lengths. However, the end effects must be considered for all solutions, especially when dealing with short fit spans.
23. Regions of overlap between successive solutions have differences compared to the average density of 5.10%, 2.81%, 1.33%, and 15.14% for low, moderate, elevated, and high solar activity, respectively. For quiet, moderate, and active geomagnetic activity levels, the overlap regions between successive solutions have differences compared to the average density of 5.10%, 2.81%, and 15.14%, respectively. These results indicate good agreement between the overlapping solutions and that the orbit determination process is generating consistent solutions, including POE density estimates.
24. Use of GRACE-A POE data in an orbit determination process to generate POE density estimates shows initial results consistent with those obtained for the CHAMP POE data. Additional research needs to be conducted with GRACE-A POE data to expand and confirm these initial results.
25. The residuals for the orbits used in estimating density have worst case values of ±8 cm for high solar and active geomagnetic activity levels. The residuals are reduced for periods of low solar and quiet geomagnetic activity levels. The residuals for all orbits used in estimating density are comparable to the reported

errors of the precision orbit ephemerides used as measurements in the orbit determination process used to generate the POE density estimates.

26. The position and velocity consistency tests are satisfied for the best combinations of baseline atmospheric model and half-life combinations examined in this work. The position and velocity consistency test move farther away from zero as the solar and geomagnetic activity level increases.
27. The cross correlation coefficients, residuals, and position and velocity consistency tests are insufficient evidence supporting a preference of one baseline atmospheric model and half-life combination for use in an orbit determination process to generate POE density estimates. A comparison of the POE density estimates with the accelerometer density and root mean square error values are required in conjunction with these data sources to make such a determination.

Using precision orbit ephemerides in an orbit determination process to generate atmospheric density estimates was demonstrated to have significant improvements over existing atmospheric models such as the Jacchia 1971 empirical model. The POE density estimates were shown to have comparable and often superior results compared with HASDM density. These conclusions were supported by the cross correlation coefficients demonstrating a high degree of correlation with the accelerometer density primarily for the POE density estimates. However, the POE estimated density was shown to be affected by the level of solar and geomagnetic activity. Selecting which baseline atmospheric model and half-life combination to use to generate POE density estimates with the best agreement and correlation with the accelerometer density proved to primarily be a function of the solar and

geomagnetic activity. However, some general conclusions can be made regardless of the level of solar and geomagnetic activity.

Table 6.1 Summary of Select POE Density Estimate Orbit Determination Parameters Resulting in the Best Correlation with Accelerometer Density.

Activity Level	Baseline Atmospheric Model	Density Correlated Half-Life (min)	Ballistic Coefficient Correlated Half-Life (min)
Overall	CIRA-1972	18	1.8
Low Solar	CIRA-1972	180	18
Moderate Solar	Jacchia 1971	180	1.8
Elevated Solar	CIRA-1972	18	1.8
High Solar	CIRA-1972	18	1.8
Quiet Geomagnetic	Jacchia 1971	1.8	18
Moderate Geomagnetic	CIRA-1972	18	1.8
Active Geomagnetic	CIRA-1972	18	1.8

Table 6.1 gives a summary of the baseline atmospheric model, density correlated half-life, and ballistic coefficient correlated half-life used in an orbit determination process to generate a POE density estimate with the highest degree of correlation with the accelerometer density. The results in the table are organized according to an overall summary and by solar and geomagnetic activity levels. This table presents some of the conclusions previously listed and allows for some additional discussion. First, the POE density estimates using the Jacchia family of baseline atmospheric models generally produced the best results compared with the accelerometer data. In particular, the CIRA-1972 baseline model was frequently the best choice regardless of solar and geomagnetic activity level. Second, all of the baseline models in the Jacchia family produced POE density estimates having very similar results. Therefore, choosing one model over the other out of the Jacchia family will have little effect on the POE density estimate as their cross correlation coefficients are typically very close in magnitude. Thirdly, the half-life combinations displayed in the above table all correspond to

POE density estimates whose cross correlation coefficients are very similar. Selection of any of the half-life combinations in this table will provide POE density estimates with similar degrees of correlation to the accelerometer density. However, a density correlated half-life of 18 minutes and a ballistic coefficient correlated half-life of 1.8 minutes most frequently provide POE density estimates with the best correlation with accelerometer density data. Consequently, using CIRA-1972 as the baseline atmospheric model with a density correlated half-life of 18 minutes and a ballistic coefficient correlated half-life of 1.8 minutes is the recommended combination for use in an orbit determination process generating POE density estimates with the best correlation to the "true" atmospheric density.

An additional consideration is the accuracy of the initial ballistic coefficient used in the orbit determination process. The results showed that the POE density estimates are sensitive to the initial ballistic coefficient value. However, a window of ±10% of the nominal ballistic coefficient value exists where the orbit determination process generates sufficiently accurate density estimates. Additional research is necessary to better understand the effects on the POE density estimate caused by variations in the initial ballistic coefficient.

6.3 Future Work

6.3.1 Additional Days Complimenting Existing Research

This work examined days from 2001 to 2007 with a total selection including days from each calendar month and season. The density variations have many driving factors so a wide range of days must be considered to ensure the sampling size is sufficiently large. Proposed future work would be an expansion of the current research to encompass at least one week from every month of available CHAMP POE data. Additionally, the distribution of examined days within the solar and geomagnetic activity bins should be representative of the

distribution of the total days within the corresponding bins. The resulting temporal coverage would cover all seasons and properly account for all time-varying effects on atmospheric density.

6.3.2 Considering Gravity Recovery and Climate Experiment (GRACE) Accelerometer Derived Density Data

The work completed so far is limited to one specific satellite. The results obtained from this research demonstrate general improvement over existing atmospheric models and a promising potential for using POE data in an orbit determination process to estimate atmospheric density. However, an additional check on the results obtained from this research is required and would lend further support to the conclusions seen in this work. Proposed future work includes expanding this research to other satellites with precision orbit data and that are also equipped with very sensitive accelerometers. This would allow the results obtained for CHAMP to be validated prior to expanding to satellites that have precision orbit data but no accelerometer. The GRACE satellites are an excellent choice because their precision orbit data is available online and their accelerometers are very sensitive.

6.3.3 A More Detailed Examination of the Density and Ballistic Coefficient Correlated Half-Lives

The research conducted thus far concerns varying the density and ballistic coefficient correlated half-lives in order of magnitude increments. The overall summary of the cross correlation coefficients presented in this work suggests that smaller half-lives provide the highest degree of correlation between the POE density estimates and the accelerometer density. The solar and geomagnetic activity bins also show that smaller half-lives possess the highest degree of correlation between the POE and accelerometer densities. Proposed future

work would include looking at increments of 1 minute to both the density and ballistic coefficient correlated half-lives ranging from 1 to 20 minutes. A smaller increment in the half-life values would give greater resolution to the observed effects on the POE estimated density.

6.3.4 Using the Jacchia-Bowman 2008 Atmospheric Model as a Baseline Model

All of the baseline atmospheric models currently available in the ODTK software package consider the solar and geomagnetic indices in a similar fashion. In particular, they all rely primarily on $F_{10.7}$ and a_p as inputs into the baseline models to represent the energy input from solar heating and geomagnetic activity. Use of such indices has been shown to be insufficient and severely limited, especially in terms of temporal resolution. Satellites now exist that directly measure the extreme ultraviolet and many other solar flux wavelengths responsible for the direct heating of the Earth's atmosphere resulting in the observed density variations. This data now offers a more complete index list for use in atmospheric models. While few models currently exist capable of using these indices, the Jacchia-Bowman 2008 atmospheric model utilizes these new indices providing a more complete account of the solar flux responsible for the observed density variations. Proposed future work would use the Jacchia-Bowman 2008 atmospheric model as a new baseline model in the orbit determination process to generate POE density estimates. Because the Jacchia-Bowman 2008 model possesses a more complete model of the solar flux heating, the POE density estimates should have increased accuracy over what is achieved in the current research. The results presented in this work demonstrated that the accuracy of the POE density estimate is directly related to the accuracy of the underlying baseline atmospheric model used in the orbit determination process.

6.3.5 Additional Satellites with Precision Orbit Ephemerides

Additional satellites with precision orbit ephemerides will need to be examined to support the results obtained in this work and to expand the research to include different orbits and altitudes. By using additional satellites in different orbits, the spatial resolution of POE density estimates can be increased. Also, using precision orbit ephemerides from satellites in different altitudes will provide a more complete understanding of the Earth's atmosphere, including density. In particular, satellites equipped with Global Positioning System (GPS) receivers are capable of producing very accurate position and velocity vectors. Other systems providing precision orbit ephemerides include satellite laser ranging (SLR) and the Doppler Orbitography by Radiopositioning Integrated on Satellite (DORIS) instrument. However, these systems either do not provide complete coverage of the satellite's orbit or are not as accurate compared with GPS receivers. The use of GPS data provides constant coverage of the satellite's orbit thereby enabling the atmospheric density to be determined throughout the entire orbit. This precision orbit data can be used in an orbit determination scheme similar to the one used in this work to estimate atmospheric density. Other satellites that have precision orbit ephemerides, especially accurate ephemerides obtained from GPS data, include the Ice, Cloud, and Land Elevation Satellite (ICESat), Jason-1, TerraSAR-X, and other Earth observing satellites. The ultimate goal is to utilize the large number of satellites capable of generating precision orbit ephemerides to create atmospheric density estimates with good spatial and temporal resolution.

REFERENCES

1. D. A. Vallado, *Fundamentals of Astrodynamics and Applications*, Microcosm Press, El Segundo, CA, 3rd Edition, 2007, Chap. 8, App. B.
2. A. C. Tribble, *The Space Environment: Implications for Spacecraft Design*, Princeton University Press, Princeton, New Jersey, 2003.
3. C. A. McLaughlin, "Upper Atmospheric Phenomena and Satellite Drag," *Advances in the Astronautical Sciences*, Vol. 123, AAS 05-315, Univelt, 2005, pp. 989-996.
4. J. K. Hargreaves, *The Solar-Terrestrial Environment*, Cambridge University Press, Cambridge, 1992.
5. C. Sabol and K. K. Luu, "Atmospheric Density Dynamics and the Motion of Satellites," *AMOS Technical Conference*, Wailea, HI, September 2002.
6. J. T. Emmert, J. M. Picone, J. L. Lean, and S. H. Knowles, "Global Change in the Thermosphere: Compelling Evidence of a Secular Decrease in Density," *Journal of Geophysical Research*, v. 109, 2004.
7. L. G. Jacchia, *Revised Static Models for the Thermosphere and Exosphere with Empirical Temperature Profiles*, SAO Special Report No. 332, Smithsonian Institution Astrophysical Observatory, Cambridge, MA, 1971.
8. C. E. Roberts, Jr., "An Analytic Model for Upper Atmosphere Densities Based upon Jacchia's 1970 Models," *Celestial Mechanics*, Vol. 4, Issue 3-4, December 1971, pp. 368-377.
9. COSPAR Working Group IV, *COSPAR International Reference Atmosphere*, Akademie-Verlag, Berlin, 1972.
10. A. E. Hedin, "Extension of the MSIS Thermosphere Model into the Middle and Lower Atmosphere," *Journal of Geophysical Research*, Vol. 96, 1991, pp. 1159-1172.
11. J.M. Picone, A. E. Hedin, D. P. Drob, "NRLMSISE-00 Empirical Model of the Atmosphere: Statistical Comparisons and Scientific Issues," *Journal of Geophysical Research*, Vol. 107, No. A12, 2002.
12. D. H. Oza and R. J. Friertag, "Assessment of Semi-empirical Atmospheric Density Models for Orbit Determination," *Advances in the Astronautical Sciences*, Vol. 89, AAS 95-101, Univelt, 1995, pp. 21-42.
13. B. R. Bowman, W. K. Tobiska, F. A. Marcos, C. Y. Huang, C. S. Lin, W. J. Burke, "A New Empirical Thermospheric Density Model JB2008 Using New Solar and Geomagnetic Indices," AIAA 2008-6438, AIAA/AAS Astrodynamics Specialist Conference, Honolulu, HI, August 2008.
14. F. O. Marcos, J. O. Wise, M. J. Kendra, and N. J. Grossbard, "Satellite Drag Research: Past, Present, and Future," *Advances in the Astronautical Sciences*, Vol. 116, AAS 03-620, Univelt, 2003, pp. 1865-1878.
15. National Geophysical Data Center, *Solar Indices Bulletin*, Boulder, CO: National Geophysical Data Center, http://www.ngdc.noaa.gov/ and ftp://ftp.ngdc.noaa.gov/STP/SOLAR_DATA/SOLAR_RADIO/FLUX.
16. National Geophysical Data Center, *Solar Indices Bulletin*, Boulder, CO: National Geophysical Data Center, http://www.ngdc.noaa.gov/ and ftp://ftp.ngdc.noaa.gov/STP/GEOMAGNETIC_DATA/INDICES/KP_AP/.

17. S. Tanygin and J. R. Wright, "Removal of Arbitrary Discontinuities in Atmospheric Density Modeling," *Advances in the Astronautical Sciences*, Vol. 119, AAS 04-176, Univelt, 2004, pp. 1185-1196.
18. M. F. Storz, B. R. Bowman, Major J. I. Branson, S. J. Casali, and W. K. Tobiska, "High Accuracy Satellite Drag Model (HASDM)," *Advances in Space Research*, Vol. 36, Issue 12, 2005, pp. 2497-2505.
19. B. Bowman, F. A. Marcos, and M. J. Kendra, "A Method for Computing Accurate Atmospheric Density Values from Satellite Drag Data," *Advances in the Astronautical Sciences*, Vol. 119, AAS 04-173, Univelt, 2004, pp. 1117-1134.
20. B. Bowman, "The Semiannual Thermospheric Density Variation from 1970 to 2002 Between 200-1100 km," *Advances in the Astronautical Sciences*, Vol. 119, AAS 04-174, Univelt, 2004, pp. 1135-1154.
21. P. J. Cefola, R. J. Proulx, A. I. Nazarenko, and V. S. Yurasov, "Atmospheric Density Correction Using Two Line Element Sets as the Observation Data," *Advances in the Astronautical Sciences*, Vol. 116, AAS 03-626, Univelt, 2003, pp. 1953-1978.
22. V. S. Yurasov, A. I. Nazarenko, P. J. Cefola, and K. T. Alfriend, "Results and Issues of Atmospheric Density Correction," *Journal of the Astronautical Sciences*, Vol. 52, No. 3, July-September 2004, pp. 281-300.
23. V. S. Yurasov, A. I. Nazarenko, K. T. Alfriend, and P. J. Cefola, "Reentry Time Prediction Using Atmospheric Density Corrections," *Journal of Guidance, Control, and Dynamics*, Vol. 31, No. 2, March-April 2008, pp. 282-289.
24. M. P. Wilkins, C. A. Sabol, P. J. Cefola, and K. T. Alfriend, "Improving Dynamic Calibration of the Atmosphere," *Advances in the Astronautical Sciences*, Vol. 127, AAS 07-185, Univelt, 2007, pp. 1257-1272.
25. M. P. Wilkins, C. A. Sabol, P. J. Cefola, and K. T. Alfriend, "Validation and Application of Corrections to the NRLMSISE-00 Atmospheric Density Model," *Advances in the Astronautical Sciences*, Vol. 127, AAS 07-189, Univelt, 2007, pp. 1285-1304.
26. M. P. Wilkins, C. A. Sabol, P. J. Cefola, and K. T. Alfriend, "Practical Challenges in Implementing Atmospheric Density Corrections to the NRLMSISE-00 Model," *Advances in the Astronautical Sciences*, Vol. 124, AAS 06-170, Univelt 2006, pp. 1113-1130.
27. S. R. Mance, C. A. McLaughlin, F. G. Lemoine, D. D. Rowlands, and P. J. Cefola, "GEOSAT Follow-On Precision Orbit Improvement Through Drag Model Update," AAS 09-105, AAS/AIAA Spaceflight Mechanics Conference, Savannah, GA, February 2009.
28. E. Doornbos, H. Klinkrad, and P. Visser, "Use of Two-Line Element Data for Thermosphere Neutral Density Model Calibration," *Advances in Space Research*, Vol. 41, 2008, pp. 1115-1122.
29. E. A. Rhoden, J. M. Forbes, and F. A. Marcos, "The Influence of Geomagnetic and Solar Variability on Lower Thermospheric Density," *Journal of Atmospheric and Solar-Terrestrial Physics*, Vol. 62, 2000, pp. 999-1013.
30. R. Konig and K. H. Neumayer, "Thermospheric Events in CHAMP Precise Orbit Determination," *First CHAMP Mission Results for Gravity, Magnetic and Atmospheric Studies*, eds. C. Reigber, H. Luhr, P. Schwintzer, Springer, Berlin, 2003, pp. 112-119.

31. S. Bruinsma and R. Biancale, "Total Density Retrieval with STAR," *First CHAMP Mission Results for Gravity, Magnetic and Atmospheric Studies*, eds. C. Reigber, H. Luhr, P. Schwintzer, Springer, Berlin, 2003, pp. 192-199.
32. S. Bruinsma and R. Biancale, "Total Densities Derived from Accelerometer Data," *Journal of Spacecraft and Rockets*, Vol. 40, No. 2, March-April 2003, pp. 230-236.
33. S. Bruinsma, S. D. Tamagnan and R. Biancale, "Atmospheric Densities Derived from CHAMP/STAR Accelerometer Observations," *Planetary and Space Science*, Vol. 52, 2004, pp. 297-312.
34. R. S. Nerem, J. M. Forbes, E. K. Sutton, and S. Bruinsma, "Atmospheric Density Measurements Derived from CHAMP/STAR Accelerometer Data," *Advances in the Astronautical Sciences*, Vol. 116, AAS 03-621, Univelt, 2003, pp. 1879-1898.
35. K. Schlegel, H. Luhr, J. P. St. Maurice, G. Crowley, and C. Hackert, "Thermospheric Density Structures over the Polar Regions Observed with CHAMP," *Annales Geophysicae*, Vol. 23, 2005, pp. 1659-1672.
36. E. K. Sutton, R. S. Nerem, and J. M. Forbes, "Global Thermospheric Neutral Density and Wind Response to the Severe 2003 Geomagnetic Storms from CHAMP Accelerometer Data," *Journal of Geophysical Research*, Vol. 110, 2005.
37. J. M. Forbes, G. Lu, S. Bruinsma, S. Nerem, and X. Zhang, "Thermospheric Density Variations Due to the 15-24 April 2002 Solar Events from CHAMP/STAR Accelerometer Measurements," *Journal of Geophysical Research*, Vol. 110, 2005, pp. 1-9.
38. E. K. Sutton, J. M. Forbes, R. S. Nerem, and T. N. Woods, "Neutral Density Response to the Solar Flares of October and November, 2003," *Geophysical Research Letters*, Vol. 33, 2006.
39. S. Bruinsma, J. M. Forbes, R. S. Nerem, and X. Zhang, "Thermospheric Density Response to the 20-21 November 2003 Solar and Geomagnetic Storm from CHAMP and GRACE Accelerometer Data," *Journal of Geophysical Research*, Vol. 111, No. AO6303, 2006, pp. 1-14.
40. S. L. Bruinsma and J. M. Forbes, "Storm-Time Equatorial Density Enhancements Observed by CHAMP and GRACE," *Journal of Spacecraft and Rockets*, Vol. 44, No. 6, 2007, pp. 1154-1159.
41. E. K. Sutton, R. S. Nerem, and J. M. Forbes, "Density and Winds in the Thermosphere Deduced from Accelerometer Data," *Journal of Spacecraft and Rockets*, Vol. 44, No. 6, 2007, pp. 1210-1219.
42. B. D. Tapley, J. C. Ries, S. Bettadpur, and M. Cheng, "Neutral Density Measurements for the Gravity Recovery and Climate Experiment Accelerometers," *Journal of Spacecraft and Rockets*, Vol. 44, No. 6, 2007, pp. 1220-1225.
43. S. L. Bruinsma and J. M. Forbes, "Medium- to Large-Scale Density Variability as Observed by CHAMP," *Space Weather*, Vol. 6, S08002, doi:10.1029/2008SW000411, 2008.
44. S. L. Bruinsma and J. M. Forbes, "Properties of Traveling Atmospheric Disturbances (TADs) Inferred from CHAMP Accelerometer Observations," *Advances in Space Research*, Vol. 43, 2009, pp. 369-376.
45. Y. L. Zhou, S. Y. Ma, H. Lühr, C. Xiong, and C. Reigber, "An Empirical Relation to Correct Storm-Time Thermospheric Mass Density Modeled by NRLMSISE-00 with CHAMP Satellite Air Drag Data," *Advances in Space Research*, Vol. 43, 2009, pp. 819-828.

46. E. Doornbos, H. Klinkrad, and P. Visser, "Atmospheric Density Calibration Using Satellite Drag Observations," *Advances in Space Research*, Vol. 36, 2005, pp. 515-521.
47. J. van den IJssel and P. Visser, "Performance of GPS Accelerometry: CHAMP and GRACE," *Advances in Space Research*, Vol. 39, 2007, pp. 1597-1603.
48. J. van den Ijssel, P. Visser, and R. Haagmans, "Determination of Non-Conservative Accelerations from Orbit Analysis," *Earth Observation with CHAMP Results from Three Years in Orbit*, eds. C. Reigber, H. Luhr, P. Schwintzer, J. Wickert, Springer, Berlin, 2005, pp. 95-100.
49. J. van den IJssel and P. Visser, "Determination of Non-Gravitational Accelerations from GPS Satellite-to-Satellite Tracking of CHAMP," *Advances in Space Research*, Vol. 36, 2005, pp. 418-423.
50. O. Montenbruck, T. van Helleputte, R. Kroes, and E. Gill, "Reduced Dynamic Orbit Determination Using GPS Code and Carrier Measurements," *Aerospace Science and Technology*, Vol. 9, 2005, pp. 261-271.
51. P. Willis, F. Deleflie, F. Barlier, Y. E. Bar-Sever, and L. J. Romans, "Effects of Thermosphere Total Density Perturbations on LEO Orbits During Severe Geomagnetic Conditions (Oct-Nov 2003) Using DORIS and SLR Data," *Advances in Space Research*, Vol. 36, 2005, pp. 522-533.
52. C. A. McLaughlin and B. S. Bieber, "Neutral Density Determined from CHAMP Precision Orbits," *Advances in the Astronautical Sciences*, Vol. 129, AAS 07-260, Univelt, 2008, pp. 167-186.
53. C. A. McLaughlin, A. Hiatt, and B. S. Bieber, "Comparison of Total Density Derived from CHAMP Precision Orbits and CHAMP Accelerometer," *Advances in the Astronautical Sciences*, Vol. 130, AAS 08-177, Univelt, 2008, pp. 1193-1206.
54. C. A. McLaughlin, A. Hiatt, T. Lechtenberg, "Calibrating Precision Orbit Derived Total Density," AIAA 2008-6951, *2008 AIAA/AAS Astrodynamics Specialist Conference and Exhibit*, Honolulu, HI, August 2008.
55. A. Hiatt, C. A. McLaughlin, and T. Lechtenberg, "Deriving Density Estimates Using CHAMP Precision Orbit Data for Periods of High Solar Activity," AAS 09-104, 19th AAS/AIAA *Spaceflight Mechanics Meetings*, Savannah, GA, February 2009.
56. B. D. Tapley, B. E. Schutz, and G. H. Born, *Statistical Orbit Determination*, Elsevier Academic Press, Amsterdam, 2004.
57. J. R. Wright, "Real-Time Estimation of Local Atmospheric Density," *Advances in the Astronautical Sciences*, Vol. 114, AAS 03-164, Univelt, 2003, pp. 927-950.
58. J. R. Wright and J. Woodburn, "Simultaneous Real-Time Estimation of Atmospheric Density and Ballistic Coefficient," *Advances in the Astronautical Sciences*, Vol. 119, AAS 04-175, Univelt, 2004, pp. 1155-1184.
59. R. Konig, S. Zhu, C. Reigber, K. H. Neumayer, H. Meixner, R. Galas, G. Baustert, "CHAMP Rapid Orbit Determination for GPS Atmospheric Limb Sounding," *Advances in Space Research*, Vol. 30, No. 2, 2002, pp. 289-293.
60. G. Michalak, G. Baustert, R. Konig, C. Reigber, "CHAMP Rapid Science Orbit Determination: Status and Future Prospects," *First CHAMP Mission Results for Gravity, Magnetic and Atmospheric Studies*, eds. C. Reigber, H. Luhr, P. Schwintzer, Springer, Berlin, 2003, pp. 98-103.
61. R. Konig, G. Michalak, K. H. Neumayer, S. Y. Zhu, H. Meixner, C. Reigber, "Recent Developments in CHAMP Orbit Determination at GFZ," *Earth Observation with*

CHAMP Results from Three Years in Orbit, eds. C. Reigber, H. Luhr, P. Schwintzer, J. Wickert, Springer, Berlin, 2005, pp. 65-70.

62. R. Konig, G. Michalak, K. H. Neumayer, S. Zhu, "Remarks on CHAMP Orbit Products," *Observation of the Earth System from Space*, eds. J. Flury, R. Rummel, C. Reigber, M. Rothacher, G. Boedecker, U. Schreiber, Springer, Berlin, 2006, pp. 17-26.
63. O. Montenbruck and E. Gill, *Satellite Orbits: Models, Methods, and Applications*, Springer-Verlag, Berlin, 2001.
64. J. R. Wright, "Optimal Orbit Determination," *Advances in the Astronautical Sciences*, Vol. 112, AAS 02-192, Univelt, 2002, pp. 1123-1134, http://www.agi.com/downloads/support/productSupport/literature/pdfs/whitePapers/optimal_od.pdf.
65. Analytical Graphics, Inc., "Orbit Determination Tool Kit Help," *Orbit Determination Tool Kit*, Version 5.1.3.
66. J. R. Wright, "Orbit Determination Tool Kit Theorems and Algorithms," *Analytical Graphics, Inc.*, 2007.
67. B. R. Bowman, F. A. Marcos, K. Moe, M. M. Moe, "Determination of Drag Coefficient Values for CHAMP and GRACE Satellites Using Orbit Drag Analysis," *Advances in the Astronautical Sciences*, Vol. 129, AAS 07-259, Univelt, 2008, pp. 147-166.
68. P. Bourke, "Cross Correlation," August 1996, Last Accessed: April 6, 2009, http://local.wasp.uwa.edu.au/~pbourke/miscellaneous/correlate/.